

Discovery of a novel antibiotic, Transitmycin, from *Streptomyces* sp unveils highly efficient activities against tuberculosis and human immunodeficiency virus

Vanaja Kumar^{*1,4}, Balagurunathan Ramasamy², Mukesh Doble^{§3,5}, Radhakrishnan Manikkam⁴, Luke Elizabeth Hanna¹, Gandarvakottai Senthilkumar Arumugam^{3,7}, Kannan Damodharan³, Suresh Ganesan³, Azger Dusthakeer¹, Precilla Lucia¹, Shainaba A Saadhali¹, Shanthi John², Poongothai Eswaran², Selvakumar Nagamiah¹, Jaleel UCA⁶, Rakhila M⁶, Ayisha Safeeda⁶ and Sathish S⁶

¹National Institute for Research in Tuberculosis, Chennai – 600031, Tamilnadu, India

²Department of Microbiology, Periyar University, Salem – 636011, Tamilnadu, India

³Department of Biotechnology, Indian Institute of Technology, Madras – 600036, Tamilnadu, India

⁴Centre for Drug Discovery and Development, Sathyabama Institute of Science and Technology (Deemed to be University), Chennai – 600119, Tamilnadu, India

⁵ Saveetha Dental College and Hospitals, 62, Poonamallee High Rd, Chennai, 600077, India

⁶Open Source Pharma Foundation-National Institute of Advanced Studies Drug Discovery Lab, NIAS, IISc Campus, Bangalore, Karnataka, India

⁷SSS International Drug Discovery & Development Research Private Limited, Innovation & Entrepreneurship, Sudha & Shankar innovation hub, IIT Madras, Chennai-600036, India

Email: *vanaja_kumar51@yahoo.co.in; § mukeshdoble.sdc@saveetha.com

Abstract

HIV is identified as a factor that aggravates tuberculosis disease pathogenesis and its progression to latent TB. While, TB is declared as one of the major causes for AIDS-associated mortality. So there is a dire need for new drugs to combat such ailments that have a synergistic interaction. This has led us to study a novel antibiotic purified from a marine *Streptomyces* sp isolated from the coral reef ecosystem of South Indian coast. *Streptomyces* sp. R2 (MTCC 5597; DSM 26035), isolated from the marine water was grown on agar plates and the crude yellowish orange pigment secreted was extracted using various solvents. The antibiotic, named as Transitmycin, was purified and tested against *M. tuberculosis*, drug resistant strains, and *M. tuberculosis* biofilm. The compound was also tested against HIV-1 viruses belonging to six subtypes. Several characterisation tools were used to elucidate the structure of this novel antibiotic. Transitmycin was derivitaised to elucidate the absolute configurations of the amino acids present in it. Tr, unlike actinomycin D, has L-valine in both the rings instead of D-valine (found in the latter). Also, one of the proline in Tr is in D-configuration while in actinomycin D, the configuration is in L-configuration. This is a novel

36 compound and is not reported so far. It exhibits dual activities against the standard H37Rv,
37 49 drug sensitive clinical isolates, and MtB biofilm as well as standard and 20 clinical
38 isolates of HIV. This is the first paper that reports the isolation of a new antibiotic from
39 marine actinobacteria exhibiting unusual anti-TB and HIV activities which could be exploited
40 further as a lead molecule in the quest for the design of drug with dual activities.

41

42 Highlights

- 43 • A novel antibiotic was purified from a marine *Streptomyces* sp isolated from the coral
44 reef of S. India
- 45 • Presence of L-valine, not observed in actinomycin D, and one of the proline in D
46 configuration suggest that it is a novel structure not reported before
- 47 • It exhibits activity against standard MtB strain as well as clinical isolates and drug
48 resistance ones
- 49 • It exhibits anti-HIV activity against several clinical isolates

50 Key words: Antibiotic, *Streptomyces* sp., Actinomycin, Transitmycin, Tuberculosis, HIV,

51

52 Introduction

53 Despite, the history of infectious diseases is time immemorial, an urgent need for protection
54 against infectious diseases has one of the major health concerns. Antibiotics have
55 revolutionized the diagnostic factor in various aspects and the drug discovery is considered as
56 a hallmark in human history. However, the concomitant development of resistance against
57 diseases is the most serious consequence [1]. In 2020, an overall rate of 1.5 million people
58 pretentious from TB. In fact, TB is one of the leading sources of death, wherein occupied the
59 13th position and moreover the second foremost infective destroyer after COVID-19 (above
60 HIV/AIDS). Since it is an airborne infectious disease caused by *M tuberculosis*, continues to
61 be a major cause of mortality and morbidity worldwide [2].

62 An upsurge of multi drug resistance (MDR) and extensively drug resistance (XDR) is
63 an additional perturbing factor in tuberculosis chemotherapy. Comprehensively, the existing
64 treatment for TB based on half yearly quadruple therapy containing rifampicin, isoniazid,
65 ethambutol and pyrazinamide results the cure rate of 90-95% [3] for drug-sensitive TB at
66 global level. Nevertheless, this regimen is inadequate to treat MDR and XDR-TB infections,
67 sometimes the second line antibiotics are employed to treat MDR-TB infections for
68 prolonged time whereas XDR infections are almost untreatable. Different TB drugs with
69 unique mode of action are desperately necessary to fight against drug resistant tuberculosis.

70 For example, bedaquiline and delamanid are approved for drug resistant TB, however due to
71 the reported toxicity issues, they may employ only on last resort [4]. In addition, the second
72 line drugs used to treat MDR-TB with several disadvantages such as less efficacious, more
73 toxic, and more expensive than the first-line drugs [5]. At presently progressing anti TB drugs
74 should partake essential properties like succeed a short therapy period (sterilizing effect), a
75 simpler regimen, capable of act on MDR/XDR-TB, concurrent treatment of TB/HIV and
76 advanced safety level than the existing drugs [6]. Alike the human immunodeficiency virus
77 (HIV) leads to destruction of the immune system resulting a condition termed as Acquired
78 Immuno Deficiency Syndrome (AIDS). After its finding AIDS becomes a great risk to
79 humans, reflected to be pandemic and it is the greatest public health crisis in globally. As of
80 2021, millions of people living with HIV were rescuing antiretroviral therapy [7]. Several
81 researches have been developed the drugs against HIV disease, such as the growth of many
82 antiretroviral drugs (ARVs), including the atazanavir, ibalizumab, darunavir, abacavir,
83 zidovudine, lamivudine, efavirenz, tenofovir disoproxil fumarate, tenofovir alafenamide,
84 emtricitabine, bictegravir, cabotegravir, rilpivirine etc. nevertheless, the competency of HIV
85 intensive to mutate rapidly leads to the upsurge of drug resistance to existing anti-retrovirals
86 [8]. Since the finding of penicillin, many of the microbial natural products tends to the new
87 paradigm for novel drug discovery development [9,10].

88 Over the past 60 years, [11] the microbial bioprospecting has gained a remarkable
89 quantity of medicinal components, including actinobacteria, the major bacterial phylum
90 group of Gram-positive bacteria with guanine and cytosine (G+C) rich content in their
91 genomic sequence, which are the important prokaryotes in economic and ecological manner.
92 Significantly the existence of actinobacterial multiplicity in several rare ecosystems liable for
93 prolific producers of many biologically active natural compounds with different potential
94 activities [12-15]. Some of the pharmaceutical companies have dramatically declined in the
95 result of novel wide range antibiotics in the past few decades [16]. Obviously, this critical
96 state has caused in the surplus of such antibiotics with distinct mode of activity targeting the
97 arcade, wherein this precluded the assessment of usual terrestrial sources in particular for
98 actinobacteria and led scientists to pursuit unique habitats on the marine family for novel
99 bioactive molecules [12,17,18]. Indeed, actinobacteria are ubiquitous in the marine
100 environment, which are occupying a substantial ecological characteristic in the recycling and
101 production of novel natural products with huge pharmaceutical applications [19].

102 Generally, the 16S rRNA gene sequencing has concomitantly employed to identify,
103 classify and quantitation of microbes in multifaceted biological molecules. It is obvious from

104 the 16S rRNA sequencing that marine microbial species as bacteria and archae have an
105 extreme different taxonomy. Even the 16S rRNA sequences of more than ten thousand
106 actinomycetes had been isolated hitherto from marine outsources. The discovery of novel
107 secondary metabolites from marine actinobacteria has just surpassed that of their terrestrial
108 counterparts [15]. According to the review of Blunt et al., [20] shown that there are 179 new
109 natural products isolated during 2016, in which the actinobacterial genus *Streptomyces*
110 remains to be the dominant source. An extensive study on typical marine actinobacterial
111 genera like *Salinispora* and *Verrucosispora* produces salinosporamide and abyssomycin
112 respectively, which suggest that actinobacteria improves significant feature towards marine
113 drug discovery research [21]. Further, marine based antibiotics are more ingenious in combat
114 infections due to the terrestrial bacteria do not have chance to develop resistance against them
115 [22]. During the microbial bioprospecting process, the actinobacterial extracts isolated from
116 various less-explored ecosystems were screened for anti-TB and anti-HIV activity. The
117 isolation, characterization and potential bioactivities against TB and HIV of an antibiotic
118 obtained from a marine *Streptomyces* sp. R2 is being reported herewith.

119

120 **Results and Discussion**

121 *Description of the actinobacterial strain*

122 *Transitmycin* is a depsipeptide (bicyclic) molecule produced by actinobacterial strain R2,
123 which was isolated from the sediment samples from Rameswaram coral reef ecosystem (Lat.
124 9.2876° N; Long. 79.3129° E), Tamil Nadu, South India using Starch Casein Agar (SCA)
125 supplemented with nalidixic acid (20µg/ml) and nystatin (100µg/ml). Viability of strain was
126 maintained in International Streptomyces Project-2 (ISP2) agar slants, 30% glycerol broth
127 followed by lyophilisation. It was also deposited in Microbial Type Culture Collection
128 (MTCC), India and in DSMZ – German Collection of Microorganisms and Cell Cultures,
129 Germany. (R2 = MTCC5597; DSM26035).

130 *Characterization and taxonomy*

131 The characterization of a strain is the key element in classification of prokaryotes including
132 actinobacteria [23]. Actinobacterial classification was initially based mainly on
133 morphological and physiological characteristics [24-25]. The onset of chemotaxonomic
134 standards has provided reproducible and reliable data to identify the genera at genus level
135 [26]. This microbial strain R2 under microscopic observation showed the presence of dense
136 aerial and substrate mycelia with long, un-fragmented spore chains with hairy structures
137 (Supplementary Fig. 1a-b). The physiological and biochemical characteristics of the strain R2

138 are given in Supplementary S-Table 1. Strain R2 showed good growth in various ISP media
139 and utilized a wide range of carbon and nitrogen sources. In addition, good growth was also
140 observed at different physiological conditions. Notably, the extracellular yellow pigment
141 production was greatly influenced by nitrogen substrates, pH, temperature and NaCl. Strain
142 R2 produced lipase and amylase. High sensitivity was observed for most of the antibiotics
143 tested (Supplementary S-Table 1). The cell wall analysis revealed that the strain R2 is rich in
144 LL-2,6-Diaminopimelic acid (L-DAP) and glycine. No diagnostic sugars were found in the
145 cell wall constituents. In our present study, the results of phenotypic characterization and cell
146 wall analysis indicated that the actinobacterial strain R2 belongs to the genus *Streptomyces*,
147 however it is not adequate for differentiation at species level.

148 Furthermore, the PCR (Polymerase Chain Reaction) amplification of 16S rRNA gene
149 of strain R2 formed around 1400 base pair sequence and the BLAST (Basic Local Alignment
150 Search Tool) analysis have shown 99% similarity to the 16S rRNA gene sequence of
151 *Streptomyces variabilis* (EU570414) and other closely related species submitted in GenBank.
152 Phylogenetic relationship of the strain R2 and related taxa are given in Supplementary S-Fig.
153 1c.

154
155 The 16S rRNA gene sequence of strain R2 has the accession number HQ012501 at GenBank,
156 but this gene provides limited resolution for species level identification, since it discloses
157 more extensive genotypic differences. At this stage, the average nucleotide identity (ANI)
158 [27] of all preserved genes between any two genomes shows likely to reform taxonomy,
159 because it also correlates with the best DNA: DNA Hybridization (DDH) values. The most
160 often used standards for species delineation *i.e.* the 70% DDH [28] which is closely
161 equivalent to 95% ANI (Average Nucleotide Identity) values. Moreover, no organisms have
162 been defined hitherto that has shown <98.7% identity in their 16s rRNA gene and shown <95%
163 ANI or 70% DDH. These results supported the substitution of cumbersome DDH and related
164 procedures with simple sequence-based standards. Significantly the metabolic property of
165 transitmycin production had not been reported before from any other meticulously associated
166 *Streptomyces* species. Based on the aforesaid facts, the actinobacterial strain R2 is identified
167 to be a novel strain of *Streptomyces variabilis*, but still it showed 99% similarity with its
168 associated proximity neighbors. It is very important to mention here that there is no literature
169 evidence on any commercially available antibiotic, in particular anti-TB and/or anti-HIV
170 compounds from *Streptomyces variabilis*.

171 ***Transitmycin production***

172 The growth of *Streptomyces* sp. R2 is simultaneously observed with grey colour aerial
173 mycelia and soluble yellow orange pigment in good yield. The crude compound is extracted
174 well in several solvents namely, methanol, chloroform and dichloromethane, followed by
175 diethyl ether and ethyl acetate (Supplementary Table 2). The extracts in the former solvents
176 were intensely coloured when compared to the extracts from the latter solvents. Salts and
177 debris were present in the extracts while using former solvents, so ultimately ethyl acetate
178 was chosen for extracting the bioactive pigment.

179 The activity of the crude extract was also tested on different strains of *M. tuberculosis*. More
180 than 95% reduction in Relative Light Units (RLU) was observed through Luciferase Reporter
181 Phage Assay against all three *M. tuberculosis* strains. When 1.0 L of YEME agar was used
182 for production it yielded 800 mg crude antibiotic extract in ethyl acetate. Major antibiotics
183 reported from actinobacteria are extracellular in nature [29-30]. Industrial production of many
184 antibiotics from *Streptomyces* is achieved through submerged fermentation process [31]. In
185 contrast, some actinobacterial strains are found to produce antibiotics only on solid media and
186 very little reason is reported as to why activity is restricted to solid culture and not observed
187 in submerged cultures. Shomura *et al* reported [32] that about 1300 out of 6500
188 actinomycetes showed antimicrobial activity against one or more of the test organisms when
189 tested by agar plug method. In the secondary screening, about 25 (1.9%) of the 1300 strains
190 were found to be non-producers in submerged cultures. So, we conclude that the reports of
191 antibiotics isolated from only agar cultures of actinomycetes are very rare.

192 According to Mayurama *et al.* [33] fumaridamycin was detected with much difficulty
193 in submerged cultures, because the mycelium of the producing strain inactivate the antibiotic
194 more readily in liquid than in agar culture. Similarly, Shomura *et al* [32] demonstrated that the
195 antibiotic produced by *Streptomyces halstedii* has shown activity against Gram negative
196 bacteria only in agar dishes, which correlates well with its mycelial morphology. The aerial
197 mycelium was filamentous during antibiotic production in solid cultures, but fragmented in
198 non-producing liquid cultures. Similar to report from Shomura *et al.* [32] the bioactive
199 pigment production by the *Streptomyces* strain R2 was observed only in agar culture, where
200 the vegetative mycelium was filamentous. While decreasing the concentration of YEME
201 broth from 2X to 1/10X the mycelia filamentation was found to increase. However, none of
202 the five concentrations of YEME broth produced the pigment (unpublished data). This
203 outcome evidenced that the filamentous mycelial structure does not influence pigment
204 production by the strain R2 in broth while the bioactive pigment production was observed in
205 all the concentrations of YEME agar when filamentous mycelia was formed. In accordance to

206 Ohnishi *et al.* [34] who reported that 2-aminophenoxazin-3-one containing grixazone A and
 207 B, afford yellow pigments during phosphate depletion by *Streptomyces griseus*. By adopting
 208 these strategies, it was concluded that optimizing the medium components may trigger the
 209 pigmented bioactive compound production by our isolated *Streptomyces* sp. R2 in liquid
 210 cultures.

211

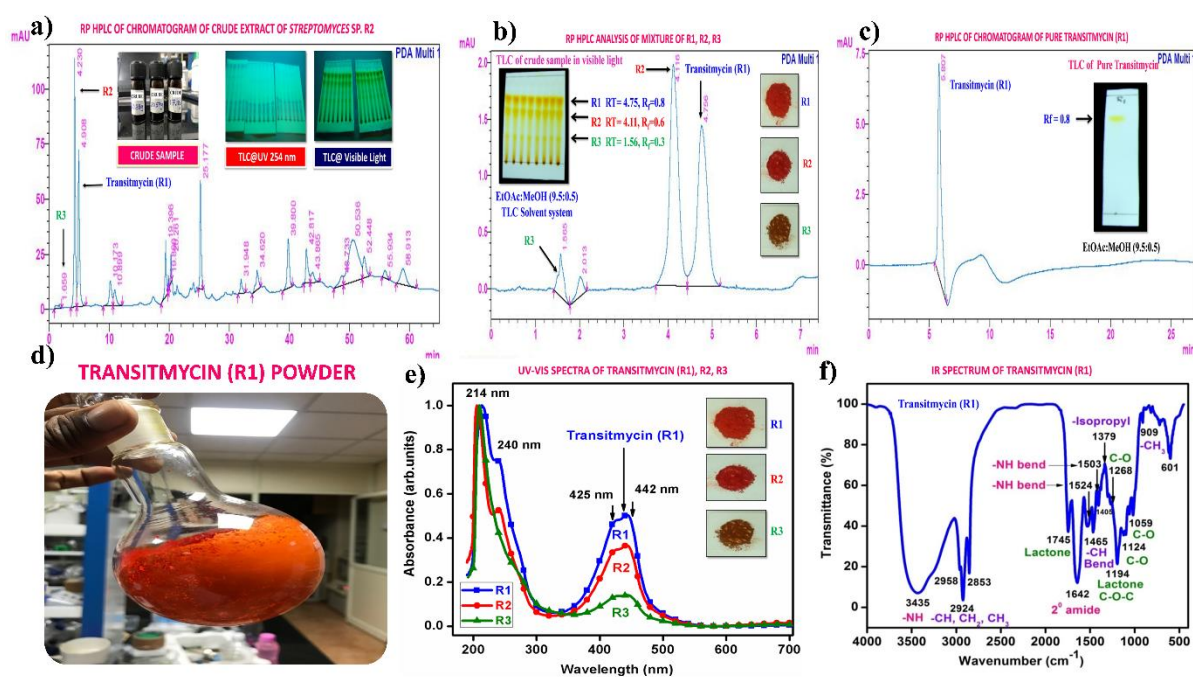
212 Transitmycin purification, characterization and structure elucidation

213

214 The *Streptomyces* sp. R2 was found to produce 800 mg of crude pigment per litre of yeast
 215 extract malt extract medium in agar surface fermentation. The yellow-orange pigment was
 216 separated from the crude ethyl acetate extract by TLC and column chromatography and its
 217 purity was confirmed by HPLC analysis (Supplementary Fig S13-S17).

218 Primarily the three well separated spots *viz.* R1, R2 and R3 with R_f values of 0.8, 0.6, 0.3,
 219 respectively were observed on analytical TLC using EtOAc:MeOH (9.5:0.5) solvent system.

220 In bioassay directed isolation, fraction R1 (named as Transitmycin) showed more than 95%
 221 inhibition against *M. tuberculosis* strain H37Rv in LRP assay. It was isolated as an orange
 222 colour amorphous powder with $[\alpha]_D^{25}$: -106° ($c = 0.2$, MeOH). The R1, R2, R3 in crude
 223 extract and as purified compounds R1, R2, R3 showed similar retention time in RP-HPLC
 224 chromatograph (Fig. 1a-d). A single peak of transitmycin at a RT of 5.8 minutes confirmed
 225 its purity (Fig. 1c).



226

227 **Fig. 1.** Representative HPLC chromatogram of crude and isolated samples R1, R2 and R3. **a**
228 RP HPLC of Chromatogram of crude extract of *Streptomyces* sp. R2. **b** RP HPLC analysis of
229 mixture of R1, R2, R3. **c** RP HPLC of Chromatogram of pure Transitmycin R1. **d**
230 Transitmycin R1 obtained after column chromatographic purification. **e** UV-Vis spectra of
231 Transitmycin R1, R2 and R3. **f** IR Spectrum of Transitmycin R1.

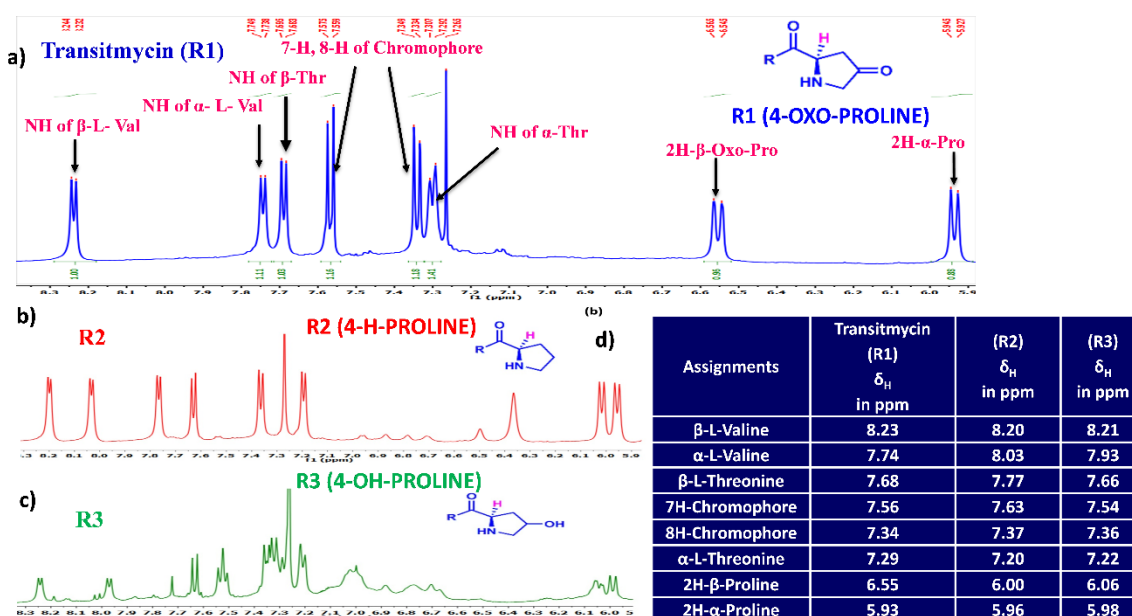
232 The chemical structures of these molecules (R1, R2 and R3) were elucidated by UV-Visible,
233 IR, CD, ^1H , ^{13}C , DEPT 135 NMR, 2D NMR (^1H - ^1H COSY, ^1H - ^1H DQF-COSY, ^1H - ^1H
234 TOCSY, ^1H - ^{13}C HSQC, ^1H - ^{13}C HMBC, NOSEY, ROESY) and MALDI-TOF-MS, HR-
235 ESIMS, HR-EIMS, HR-LCMS, and 3200 QTRAP-LC/MS/MS analyses and also compared
236 with the previously reported NMR and Mass data of actinomycins (Supplementary
237 Information) [35-57]. Advances in spectroscopic techniques have mainly utilized for
238 compound identification and immensely accelerated the unambiguous representation of
239 compound characterization and structural elucidations. The UV-Vis spectrum of
240 Transitmycin showed a strong absorption band around (λ_{max} 214, 240, 425, 442 nm (in
241 MeOH) (Fig. 1e). The colour and absorption peak in UV-Vis analysis revealed the presence
242 of phenoxazinone chromophore. Singh *et al.* [58] and Maskey *et al.* [59] detected the
243 presence of phenoxazinone chromophore in bioactive metabolites from *Streptomyces* sp. and
244 *Actinomadura* sp. The absolute configuration of the amino acids were supposed to be
245 identical to that of actinomycin D, as indicated by the negative optical rotation values and the
246 strong cotton effect at about 210 nm in the CD spectra. The CD values of Transitmycin (R1)
247 are: [MeOH, [nm], (mdeg)] $\lambda_{\text{max}}(\Delta\epsilon)$ 195 (+24.0), 210 (-21.5), 241 (+1.7).

248 In the IR spectrum, a strong absorption broad band appears at around 3435 cm^{-1} , an
249 intense strong peak at 1746 cm^{-1} and a band around 1099 cm^{-1} are assignable to be amino (or
250 hydroxyl), lactone ring and alicyclic 6-membered ether type (C-O) groups, respectively. IR
251 data of transitmycin (R1) (KBr cm^{-1}), 3435 cm^{-1} for NH, $2958, 2924\text{ cm}^{-1}$ (m, -CH str, asym,
252 CH_3 and CH_2), $2872\text{ cm}^{-1}, 2853\text{ cm}^{-1}$ (m, -CH str, sym, CH_3 and CH_2), 1746 cm^{-1} (s, C=O str,
253 lactone ring), 1642 cm^{-1} (s, -C=O str, 2° amide), $1524, 1503$ (m, -NH bend, 2° amide), 1466
254 (m, CH bend (scissoring), CH_2), 1379 cm^{-1} (s, -CH bend, isopropyl group), 1268 (s, C-O str,
255 ester), 1194 (C-O-C of lactone) $1099, 1059, 1017$ (s, C-O or C-N), $720, 712, 694, 689$ (s, -
256 CH bend, oop, aromatic ring), 909 (w, CH_3 rocking) [48] (Fig. 1f).

257 The ^1H and ^{13}C NMR spectra exhibited the typical features of two (alpha and beta
258 ring) pentapeptido lactone ring attached with phenoxazinone chromophore, i.e., each ring

259 contained four amide carbonyl resonances and one ester carbonyl in one ring (δ_C 168.8,
 260 173.4, 173.1, 166.2, 167.4 (α -ring) and 168.9, 173.9, 172.7, 166.4, 167.4 (β -ring), together
 261 with phenoxazinone chromophore (101.8 (C-1), 147.3 (C-2), 179.0 (C-3), 113.4 (C-4), 144.9
 262 (C-4a), 140.3 (C-5a), 127.6 (C-6), 130.2 (C-7), 126.0 (C-8), 132.1 (C-9), 128.4 (C-9a), 14.9
 263 (C-11), 7.6 (C-12), 166.0 (C-13), 165.8 C-14). One of the amino acid proline in the β -ring
 264 contained a keto group (208.0 in the ^{13}C NMR). From 1H NMR spectrum, NH of amino acids
 265 (δ_H 8.23, β -L-Valine), (δ_H 7.74, α -L-Valine), (δ_H 7.69, β -L-Threonine), (δ_H 7.2, α -L-
 266 Threonine), (δ_H 6.55, 2H of β -proline) (δ_H 5.93 2H of α -proline) and four N-methyl groups
 267 (δ_H 2.91, 2.88, 2.89, 2.87) (Fig. 2 a-d). In addition, the 1H NMR spectra of Transitmycin
 268 indicated the presence of eight methyl groups arising from four isopropyls.

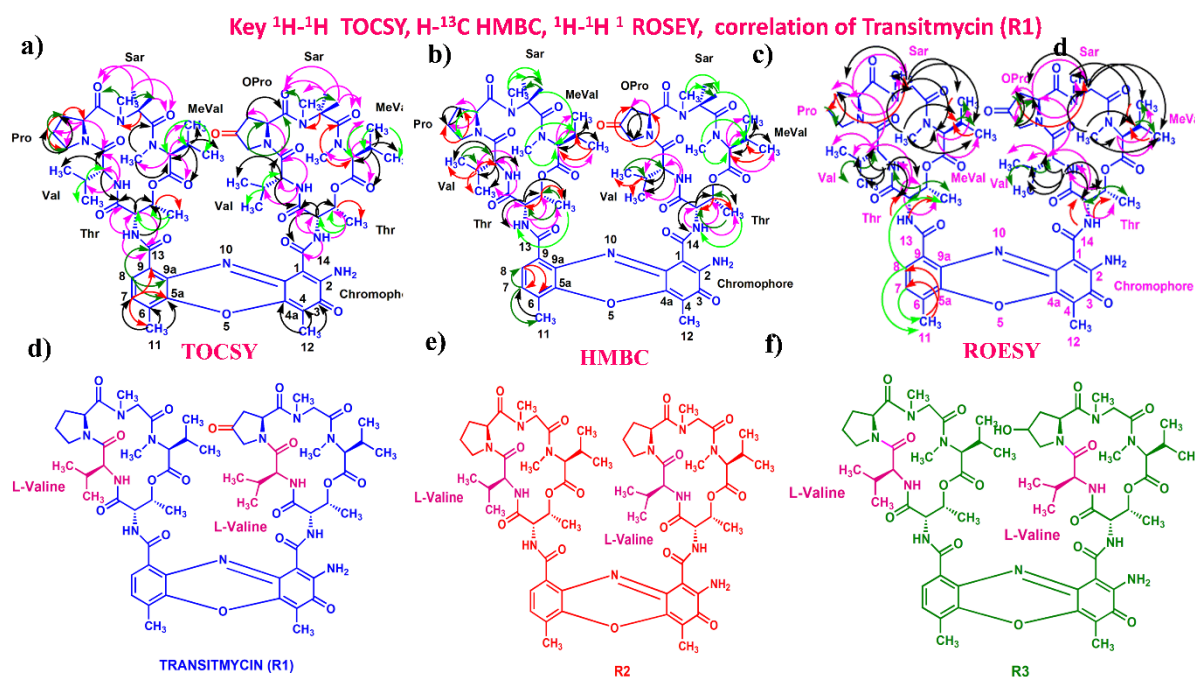
NOTABLE CHARACTERISTIC 1H NMR SPECTRA OF DIFFERENT PROLINE UNITS OF TRANSITMYCIN (R1), R2, R3



269
 270 **Fig. 2** Notable characteristic 1H NMR spectra of different proline units of Transitmycin as
 271 **a** R1 (4-oxoproline). **b** R2 (proline) and **c** R3 (4-OH proline). **d** Comparative studies for 1H
 272 NMR (500 MHz, $CDCl_3$) chemical shift value of NH containing amino acid residue and
 273 chromophore motifs of Transitmycin (R1), R2 and R3.

274 The UV/Vis absorption spectra with maximal absorbance at 240 nm and 442 nm support
 275 the presence of an amino phenoxazinone chromophore in its structure. From 1H - 1H COSY
 276 and TOCSY experiments, five amino acid systems namely Pro, Thr, Val, N-Methyl Val, and
 277 Sar were identified. The assignments of the protonated carbons were obtained from the
 278 HSQC spectrum, in combination with inspection of the HMBC spectrum. By comparison of

279 the UV spectrum (λ_{max} 442 nm, in MeOH) of Transitmycin with that of actinomycin series
 280 (λ_{max} 440 nm, in MeOH) (Fig. 1e) it was concluded that the former contained an
 281 aminophenoxazinone chromophore residue. In ^1H NMR, two *ortho* coupled protons at 7-H,
 282 8-H; δ_{H} 7.56 and 7.34 corresponding to 1,2,3,4-tetrasubstituted aromatic ring, and two 3H
 283 singlet at δ_{H} 2.52 (11- CH_3) and 1.95 (12- CH_3) of methyl groups in peri-position of the
 284 aromatic system were identified. This is the characteristics of phenoxazinone chromophore
 285 found in various actinomycins.



286 **Fig. 3. a** Key ^1H - ^1H COSY correlation of Transitmycin (R1). **b** Key ^1H - ^1H TOCSY
 287 correlation of Transitmycin (R1). **c** Key ^1H - ^{13}C HMBC connectivity for Transitmycin (R1). **c**
 288 ^1H - ^1H ROESY correlation of Transitmycin (R1). **d** Chemical structure of isolated compounds
 289 Transitmycin (R1). **e** R2. **f** R3.

290 The result was further confirmed by HMBC correlations between the 7-H (δ_{H} 7.59) and 8-H
 291 (δ_{H} 7.34) of the tetra substituted double bond and the carbonyl resonances at δ_{C} 166.0. The
 292 carbonyl carbons of Pro, Thr, Sar, Val, and N-methyl Val, were clearly assigned to (δ_{C} 179.0,
 293 174.0, 173.1, 169.02, 198.8, 167.5, 166.5, 166.56, 166.3, 166.1 and 165.9) on the basis of
 294 the observed correlations between carbonyl groups protons of the same amino acid residue in
 295 the HMBC spectrum. All the residues were connected on the basis of DQF-COSY, TOCSY,
 296 HMBC, ROESY and NOESY correlations (Fig. 3a-c), thus establishing the amino acid
 297 sequences and overall constitution. (Supplementary Fig. S14-65, S-Table 5). The detailed
 298 analysis of ^1H - ^1H COSY, ^1H - ^1H DQF-COSY, ^1H - ^{13}C HMBC, and ^1H - ^{13}C HSQC, ^1H - ^1H

299 TOCSY, ^1H - ^1H NOESY, ^1H - ^1H ROESY NMR spectra [35-51] (Supplementary Information
300 Fig. S14-65, S-Table S5) and MALDI-TOF-MS (Fig. 4a-m and Fig. 5) and HR-ESIMS, HR-
301 LCMS, ESI-MS, QTRAP LC-MS/MS [52-57] (Fig. 5, S-Table S6), (Supplementary
302 Information Fig. S14-115, S-Table S7a-b) spectral fragmentation pattern revealed ten amino
303 acids in Transitmycin (Fig. 3d), which is identical to those present in actinomycin X2 [35-57]
304 (2 X MeVal, 2 X Thr, 2 X Sar, 2 X Val, proline and ketoproline). OPro was identified by the
305 ketone moiety (δ_{C} 208.6 ppm) and the altered chemical shifts and coupling patterns of the
306 neighbouring methylene groups (Table 1).

307 **Table 1.** ^1H NMR (500 MHz, CDCl_3)/ ^{13}C NMR (125 MHz, CDCl_3) and 2D NMR (500 MHz,
308 CDCl_3) correlation spectral data of Transitmycin (R1) ^1H - ^1H COSY, ^1H - ^1H TOCSY ^1H - ^{13}C
309 HMBC, ^1H - ^1H ROESY

α - ring	Position	δ_C	δ_H	J (Hz)	COSY	TOCSY	HMBC	ROSEY
Thr	1	168.8	-	-	-	-	-	-
	2	54.6	4.60	d, 10.0	3, 4, -NH	3, 4	1, 3, 13	3, 4, 2-Val, Val-NH
	3	74.7	5.13	m	2, 4, -NH	2, 4,	4	2, 4, Val-NH
	4	17.0	1.10	d, 6.5	2, 3	2, 3, -NH	2, 3	2, 3, Val-NH
	NH	-	7.29	d, 7.0	2, 3, 4	2, 3, 4	1, 3, 13	2, 4
L-Val	1	173.4	-	-	-	-	-	-
	2	58.7	3.58	dd, 10.5,6.5	3, 4, 5, -NH	3, 4, 5, -NH	1, 5, 1-Thr	3, 4, 5, 2-Pro
	3	31.7	2.08	m	2, 4, 5	2, 4, 5	2,5	4, 5, 4-Thr
	4	19.0	0.89	d, 7.0	2, 3	2, 3, -NH	2,3,5	2, 3, 5
	5	18.9	1.13	d, 6.5	2, 3	2, 3, -NH	2,3,4	2, 3, 2-Val, Val-NH
	NH	-	7.74	d, 5.5	2, 3, 4, 5	2, 3, 4, 5	2, 3, 1-Thr	2, 3, 4, 5, 2- Thr, 3-Thr
Pro	1	173.1	-	-	-	-	-	-
	2	56.4	5.93	d, 9.5	3a,3b,4a,4b	3a,3b 4a, 4b	3, 4, 5, 1-Val	3a, 3b, 2a-Sar,2b-Sar, Sar-NMe
	3	31.6	2.73 1.84	dd, 17.5,7.0 dd, 19.5, 6.5	3b, 4a, 4b 3a, 4a,	3b, 4a, 4b 3a, 4a,	1, 2, 4 1, 4, 5	3b, 2a-Sar, 2b-Sar 3a, 4a, 4b
	4	23.3	2.26 2.01	d, 16.5 d, 8.0	3a, 3b, 4b 3b, 4a	3a, 3b, 4b 3b, 4a	3, 5 3, 5	4b, 5a, 5b 4a, 5a
	5a 5b	47.8	3.86 3.67	d, 18.5 d, 18.5	3a, 4a, 4b 3a, 4a, 4b	3a, 4a, 4b 3a, 4a, 4b	4, 1-Val	5b
Sar	1	166.2	-	-	-	-	-	-
	2	51.2	2a, 4.70 2b, 3.64	d, 17.5 d, 17.5	2b 2a	2b, NMe 2a, NMe	1, NMe,1-pro 1, NMe,1-Pro	2b, NMe, 2-Pro 4-MeVal, 5-MeVal, NMe
	N-Me	34.9	2.87	s		2a, 2b	2, 1-Pro	2b, 3-MeVal
Me-Val	1	167.4	-	-	-	-	-	-
	2	71.3	2.70	d, 9.0	3, 4, 5	3, 4, 5	1, 3,4,NMe	4, 5
	3	26.9	2.62	d, 7.0	2, 4, 5	2, 4, 5	1, 3, 4, 5, NMe	4, 5
	4	21.6	0.96	d, 6.0	2, 3	2, 3, 5	2, 3, 5	3
	5	19.2	0.72	d, 6.5	2, 3	2, 3, 4	2, 3, 4	3
	N-Me	39.2	2.89	s	-	2, 3	2, 1-Sar	2, 3, 5, 2a-Sar, 2b-Sar

β -ring	position	δ_C	δ_H	J (Hz)	COSY	TOCSY	HMBC	NOESY
Thr	1	168.9	-	-	-	-	-	-
	2	54.9	4.50	d, 9.0	3,4, -NH	3, 4	1, 3, 14	3, 4, 2-Val, Val-NH
	3	74.6	5.23	m	2,4,- NH	2, 4	4	2,4, Val-NH
	4	17.6	1.20	d, 6.0	2, 3	2, 3, - NH	2, 3	2,3, Val-NH
	NH	-	7.68	d, 6.0	2, 3, 4	2, 3, 4	1, 3, 14	2, 4
L-Val	1	173.9	-	-	-	-	-	-
	2	57.1	3.71	dd, 10.5, 6.5	3, 4, 5, - NH	3, 4, 5, -NH	1, 3, 5, 1- Thr,	3, 4, 5, 2-Oxo pro
	3	31.8	2.20	m	2, 4, 5	2, 4, 5	2, 5	4, 5, 4-Thr
	4	19.0	0.86	d, 7.0	2, 3	2, 3, -NH	2, 3, 5	2, 3, 5
	5	18.8	1.14	d, 7.0	2, 3	2, 3, -NH	2, 3, 4	2, 3, 2-Val, Val-NH
	NH	-	8.23	d, 6.0	2, 3, 4, 5	2, 3, 4, 5	2, 3, 1-Thr	2, 3, 4, 5, 2-Thr, 3- Thr
Oxo-Pro	1	172.7	-	-	-	-	-	-
	2	54.2	6.55	dd, 10.0, 2.0	3, 5	3, 5	3, 1-Val	3, 5, 2a-Sar, 2b-sar- NMe
	3	41.8	2.32 2.13	d, 18.5 d, 13.0	2, 5 2, 5	2, 5 2, 5	1 1	2, 5 2, 5
	4	208.0	-	-	-	-	-	-
	5	53.7	3.83 3.90	d, 18.5 dd, 18.5, 12.0	2, 3 2, 3	2, 3 2, 3	1, 2 1, 2	2, 3 2, 3
	Sar	1	166.4	-	-	-	-	-
	2	51.28	2a, 4.54 2b, 3.95	d, 19.5 d, 19.0	2b 2a	2b, NMe 2a, NMe	1, NMe, 1- Pro 1, NMe, 1- Pro	2b, NMe, 2-oxo-pro 4-MeVal, 5-MeVal, NMe
	N-Me	34.7	2.88	s	-	2a, 2b	2, 1-Pro	2b, 2MeVal
Me-Val	1	167.4	-	-	-	-	-	-
	2	71.1	2.67	d, 8.5	3, 4, 5	3, 4, 5	1, 3, 4, 5, NMe	4, 5
	3	26.8	2.60	d, 8.0	2, 4, 5	2, 4, 5	1, 3, 4, 5, NMe	4, 5
	4	21.5	0.93	d, 6.0	2, 3	2, 3, 5	2, 3, 5	3
	5	19.1	0.73	d, 6.0	2, 3	2, 3, 4	2, 3, 4	3
	N-Me	39.0	2.91	s	-	2, 3	2, 1- Sar	2, 5, 2a-Sar, 2b-Sar

310
311
312
313
314

Chromophore

315

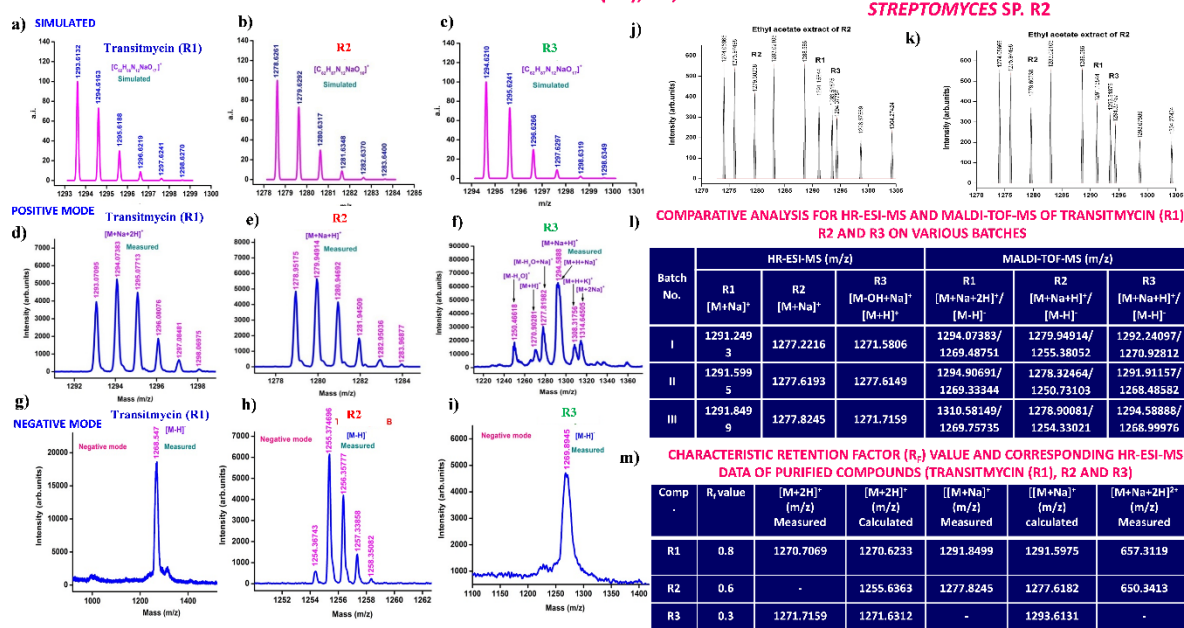
Position	δ_C	δ_H	J (Hz)	COSY	TOCSY	HMBC	NOESY
1	101.8	-	-	-	-	-	-
2	147.3	-	-	-	-	-	-
3	179.0	-	-	-	-	-	-
4	113.4	-	-	-	-	-	-
4a	144.9	-	-	-	-	-	-
5	-	-	-	-	-	-	-
5a	140.3	-	-	-	-	-	-
6	127.6	-	-	-	-	-	-
7	130.2	7.34	d, 8.0	8, 11	8, 11	5a, 9, 11-Me	11
8	126.0	7.56	d, 7.5	7, 11	7, 11	9a, 5a, 13	11
9	132.1	-	-	-	-	-	-
9a	128.4	-	-	-	-	-	-
10	-	-	-	-	-	-	-
11	14.9	2.52	s	7, 8	7, 8	5a, 6, 7	7, 8
12	7.6	2.18	s	-	-	3, 4, 4a	-
13	166.0	-	-	-	-	-	-
14	165.8	-	-	-	-	-	-

316

317

MALDI-TOF-MS FOR MOLECULAR ION PEAK OF TRANSITMYCIN (R1), R2, R3

MALDI-TOF-MS SPECTRA OF CRUDE EXTRACT OF STREPTOMYCES SP. R2



318

339 (β -Ring-Thr-Val-Oxo-Pro-Sar), 371(β -Ring-Thr-Val-Oxo-Pro-Sar), 294 (β -Ring-Thr-Val-
340 Oxo-Pro).

341

342 The MALDI-TOF-MS spectrum of crude extract of *Streptomyces* sp. R2 (Fig. 4j-k) and
343 measured, calculated mass of purified compounds Transitmycin (R1), R2, R3 were given in
344 (Fig. 4a-i, Supplementary Figure S70-115). The molecular formula was established as
345 $C_{62}H_{84}N_{12}NaO_{17}$ based on Positive HRESI-MS, which showed protonated pseudo molecular
346 ion peak $[M+H]^+$ at m/z 1270.7069 (Fig. 4a-m). It also showed intense peaks, due to Na and
347 K adducts, at m/z 1291.8307 $[M+Na]^+$ and 1307.8124. $[M+K]^+$ respectively (Calcd. for
348 $C_{62}H_{84}N_{12}NaO_{17}$: 1291.5975: Found: 1291.8307). Fig. 4a-i Similarly, the MALDI TOF MS
349 spectrum of transitmycin showed intense peak in positive mode at m/z 1293.61316
350 $[M+Na+2H]^{+3}$ and at m/z 1309.93062 $[M+K]^+$ and in negative mode at m/z 1269.33344
351 $[M-H]^-$ (Fig. 4a-m, Fig. 4-5, Supplementary Information Fig. S115a-b). The compound R2
352 was isolated as orange red powder and its molecular formula was established as
353 $C_{62}H_{86}N_{12}O_{16}$ $[M+Na]^+$ by positive HRESIMS. The MALDI TOF molecular ion of R2
354 showed peak at m/z 1278.95175 $[M+Na+H]^+$ and negative ion mode at m/z 1255.38052 $[M-$
355 $H]^-$ For a molecular formula of $C_{62}H_{87}N_{12}O_{16}Na$ its molecular weight is calculated as
356 1278.6261 $[M+Na+H]^+$ which matches with 1278.95175, that is similar to that of
357 actinomycin D (Fig. 3e). The compound R3 was obtained as an oranges red powder and the
358 molecular formula of R3 was determined to be $C_{62}H_{87}N_{12}O_{17}$ from HR-ESIMS peak at m/z
359 1271.7159z $[M+H]^+$ and when calculated for the molecular formula, $C_{62}H_{87}N_{12}O_{17}$
360 1271.6312, found to be 1271.7159 and 1277.6149 $[M-OH-Na]^+$. The molecular formula of
361 R3 was established as $C_{62}H_{87}N_{12}O_{17}$ by positive MALDI-TOF 1294.5888 $[M+H+Na]^+$ and
362 negative mode 1268.4852 $[M-H]^-$ (Fig. 4f) which is identical to that of actinomycin 0 β
363 (Supplementary Information Fig. S70-115, S-Table S7a-b) [52-57].

364 The differences between compounds R1, R2, R3 were because of the variation in proline at
365 4th position. Transitmycin (R1) has keto group in the 4th position, R2 does not have keto
366 group and compound R3 has hydroxyl group in the 4th position (Fig. 3a-c).

367

368

369

370 HPLC Analysis of L-FDAA Derivatives of Transitmycin (R1)

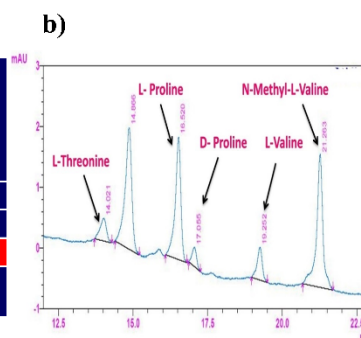
371

372 HPLC experiment was used to determine the absolute configuration of isolated compounds.
373 The absolute configurations of the amino acids were assumed to be identical to that of
374 actinomycin X₂, as indicated by the negative optical rotation values and the strong cotton
375 effect at about 210 nm in the CD spectra. The assignment of the amino acids was carried out
376 primarily by the analysis of the ¹H-¹³C HSQC and ¹H-¹H-COSY correlations, MALDI-TOF-
377 MS (Fig. 4 a-m, S-Table S6), QTRAP LC-MS/MS (Supplementary Information Fig. S14-
378 114, S115a-b, S-Table S7a-b), and completed with the help of HMBC spectrum (Fig. 3a-c).
379 Additionally, a small amount of compound Transitmycin and R3 were hydrolyzed and the
380 free amino acid were analyzed by HPLC, HR-LCMS, HR-ESIMS after chiral derivatization
381 with Marfey's reagent. Altered proline and sarcosine were not available as reference.
382 Although neither the altered proline and threonine moieties nor N-methylated alanine were
383 available as references, they can be assumed to possess L-configurations due to the fact that
384 the exchange of a single amino acid with its enantiomer leads to significant conformational
385 changes of the respective peptidolactone ring, resulting in reduced biological activities as
386 well as chemical shift deviations that have not been observed. The absolute configuration of
387 the threonine, valine, methyl valine, proline in Transitmycin (R1) was clarified by Marfey's
388 method applied for the acid hydrolysate of Transitmycin (R1) in comparison with standard
389 amino acid analysis [60-64]. Retention times of the standard N^α-(5-fluoro-2,4-di-nitrophenyl)-
390 L-alanamide (FDAA) derivatives were as follows: D-threonine, 15.682 min; L-threonine,
391 13.987 min; D-proline, 17.035 min; L-proline, 16.519 min; D-valine, 21.244 min; L-valine,
392 19.248 min; D-N-methyl valine, 22.089 min; L-Methyl valine 20.814 min. The
393 chromatogram of the FDAA derivatives of acid hydrolysate Transitmycin (R1) showed
394 peaks corresponding to L-Threonine (14.021 min), L-proline (16.520 min), L-valine
395 (19.252), L-N-methyl valine (21.263 min) were obtained in the hydrolysate. The above same
396 mentioned procedure for compound R3 was also done and similar results was obtained.
397 (Supplementary Information Fig. S116-125, Table S-8a-b) [60-64]. Comparison, with
398 authentic standards, revealed the presence of L-MeVal, L-Thr and D-Val as expected,
399 however the D-Valine is in L-configuration as well as one of the proline is in D-proline
400 instead of L-configuration. (Fig. 6a-c).

HPLC data analysis for L-FDAA derivatives to hydrolysates of Transitmycin (R1) and standard amino acids

a)

Amino acids	HPLC retention time of Marfey's derivatives for standard amino acids		HPLC retention time of Marfey's derivatives for acid hydrolysate of Transitmycin R1	Assignment
	D	L		
Threonine	15.682	13.987	14.021	L
Proline	17.035	16.519	17.055 & 16.520	D & L
Valine	21.244	19.248	19.252	L
N-methyl valine	22.089	20.814	21.263	L



HR-LCMS data analysis for L-FDAA derivatives to hydrolysates of Transitmycin (R1) and standard amino acids

c)

Amino acids	LCMS retention times of Marfey's derivatives for standard amino acids		HPLC retention time of Marfey's derivatives for acid hydrolysate of Transitmycin R1	[M+H] ⁺ m/z	[M-H] ⁻ m/z	Assignment
	D	L				
Threonine	9.90	13.50	13.73	372.13	370.13	L
Proline	15.16	14.31	14.23 & 15.36	366.13	363.07	D&L
Valine	19.65	17.65	18.02	370.13	368.07	L
N-methyl valine	20.33	19.25	19.96	384.20	382.20	L

401

402

403

404

405

406

407

408

409

410

411

412

413

414

415

416

417

418

419

420

421

422

Fig. 6. a HPLC data analysis for L-FDAA derivatives to hydrolysates of Transitmycin R1 and standard amino acids. **b** Graphical representation for RP-HPLC chromatogram of L-FDAA (Marfey's) derivatives of hydrolyzed Transitmycin (R1). **c** HR-LCMS data analysis for L-FDAA derivatives to hydrolysates of Transitmycin R1 and standard amino acids.

LC-MS Analysis of L-FDAA Derivatives of Transitmycin (R1)

The retention times of the D- and L-FDAA derivatives of standard amino acid, respectively, were as follows: Pro: 14.35, 14.97, min, m/z 366.13 $[M+H]^+$, m/z 363.07 $[M-H]^-$; Val: 19.63, 17.52 min, m/z 370.13 $[M+H]^+$, 368.13 $[M-H]^-$; Thr: 9.90, 13.50 min, m/z 372.07 $[M+H]^+$, 370.13 $[M-H]^-$; NMeVal: 20.33, 19.23 min, m/z 384.20 $[M+H]^+$, 382.20 $[M-H]^-$. The L-FDAA was used to derivatize the acid hydrolysates of Transitmycin (R1), R3 and eight standard amino acids (D-Val, L-Val, D-Thr, L-Thr, D-N-MeVal, L-N-MeVal, D-Pro and L-Pro). The reaction with L-FDAA was performed with the same procedure as above. [63-64]. The retention times of the L-FDAA derivatives were as follows: D-Pro: 15.16 min, L-Pro: 14.31 min, m/z 366.13 $[M+H]^+$, 363.07 $[M-H]^-$; D-Val: 19.65 min, L-Val 17.65 min, m/z 370.13 $[M+H]^+$, 368.07 $[M-H]^-$; D-Thr: 9.90 min, L-Thr, 13.50 min, m/z 372.13 $[M+H]^+$, 370.13 $[M-H]^-$; D-N-MeVal 20.33 min, L-N-MeVal 19.25 min, m/z 384.20 $[M+H]^+$, 382.20 $[M-H]^-$. The retention time of L-FLDA derivatives of acid hydrolysates Transitmycin (R1) were as follows: L-threonine (13.73 min), L-Proline (14.23 min), D-Proline or keto-proline (15.36 min), L-valine (18.02 min), N-Methyl valine (19.96 min) as illustrated in Fig. 6 a-b. The retention time of L-FLDA derivatives of acid

423 hydrolysates (R3) (Supplementary Information Fig. S-128-161, S-Table S9 a and b) were as
 424 follows: to L-threonine (12.45 min) or D-threonine (9.36 min), L-Proline (14.25 min), D-
 425 Proline or keto-proline (15.21 min), L-valine (17.49 min), N-Methyl valine (19.93).
 426 Comparison with authentic standards revealed the presence of L-MeVal, L-Thr, L-Proline,
 427 L-Valine and one of the Proline as in D-configuration (Fig. 6c). Hence, we named the
 428 unusual newly found compound as Transitmycin (Fig. 3d, Table 1& 2), a member of the X-
 429 type [35-64].

430 **Table 2.** Physico-chemical properties of Transitmycin

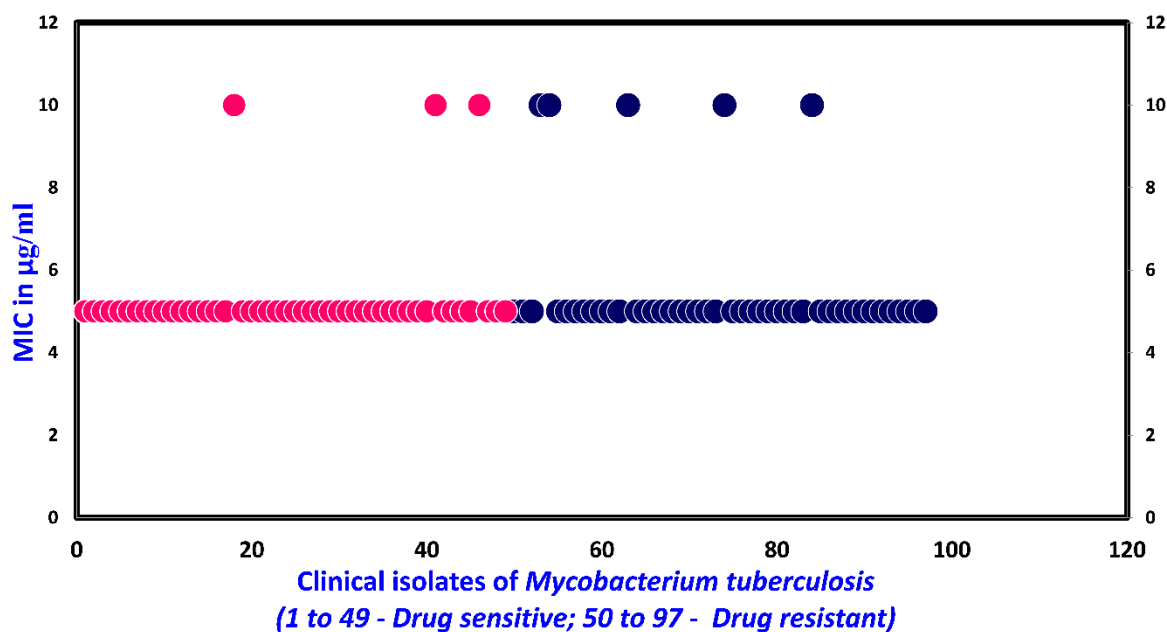
Transitmycin (R1)	Properties
TLC	Single yellow spot with R _f value 0.8 (EtOAc:MeOH (9.5:0.5))
Color and consistency	Orange color amorphous powder
Yield	200 mg, 20%
Melting point (mp)	240-242°C
[α]_D²⁵	-106 ° (c = 0.2, MeOH)
Solubility	Soluble in chloroform, dichloromethane, ethyl acetate, methanol, ethanol, acetonitrile, DMSO and water; Insoluble in Hexane
UV	(MeOH) λ _{max} (log ε) 214 (3.07), 240 (2.30), 425 (1.44), 442 (1.51) nm
CD	[MeOH, [nm], (mdeg)]: λ _{max} (Δε) 195 (+11.1), 210 (-21.0), 242 (+4.7)
IR (KBr), ν_{max}	3435, 2958, 2924, 2853, 1745, 1642, 1524, 1465, 1379, 1194, 1099, 1059 cm ⁻¹
¹H NMR (500MHz)	Table 2
¹³C NMR (125MHz, CDCl₃):	179.0, 174.0, 173.5, 173.17, 169.0, 168.8, 167.5, 167.5, 166.5, 166.3, 166.1, 165.9, 144.34, 145.93, 145.04, 140.5, 132.19, 130.3, 129.2, 127.8, 126.1, 113.6, 101.8, 76.7, 74.76, 74.67, 71.4, 71.2, 58.5, 57.2, 56.4, 54.9, 54.7, 54.3, 51.3, 29.6, 29.6, 29.3, 22.6, 21.7, 21.6, 19.2, 19.2, 19.09, 19.06, 18.8, 17.14, 14.11, 7.77.
HRESI-MS	<i>m/z</i> (pos.ions) 656.9243 [M+2H] ²⁺ , 1270.7069 [M+ H] ⁺ , 1291.8449 [M + Na] ⁺ 1307.9286 [M + K] ⁺ C ₆₂ H ₈₄ N ₁₂ O ₁₇ Na [M + Na] ⁺ calc. 1291.5975, found. 1291.8449
MALDI-TOF-MS	<i>m/z</i> (pos.ions) 1293.61316 [M + Na+2H] ⁺ , 1309.93062 [M+K] ⁺ <i>m/z</i> (neg.ions) 1269.33344 [M-H] ⁻ C ₆₂ H ₈₄ N ₁₂ O ₁₇ Na [M+Na+2H] ⁺ calc. 1293.61950, found. 1291.61316
EI-MS: (70 ev)	<i>m/z</i> (pos.ions) 1348.1437, 1291.4173 [M+Na] ⁺ , 1224.7363, 1191.8994, 1023.6241, 886.0243, 743.2058, 614.8185, 347.6111, 202.5464, 138.5079
LCESI-MS	<i>m/z</i> (pos.ions) 1291.5995 [M + Na] ⁺ C ₆₂ H ₈₄ N ₁₂ O ₁₇ Na [M+Na] ⁺ calc. 1291.5975, found. 1291.5995
CHN	Anal. calcd for C ₆₂ H ₈₄ N ₁₂ O ₁₇ : C, 58.66; H, 6.67; N, 13.24. Found: C, 59.71; H, 7.28; N, 10.19.

431

432 **Determination of anti TB and anti-HIV activity**

433 *Activity against planktonic cultures of M. tuberculosis*

434 Despite the introduction of new anti TB drugs, emergence of antibiotic resistance among *M.*
435 *tuberculosis* strains remains a major challenge in tuberculosis therapy. According to WHO
436 Global Tuberculosis report - 2022, there is a 3.1% increase in incidence of multi drug
437 resistant and rifampicin resistant TB cases from 2020 to 2021[65]. Thus, there is a burning
438 need for more new antitubercular drugs to tackle drug resistant tuberculosis [66]. Since
439 1940s, secondary metabolites and their associated derivatives have played a key role in anti-
440 TB drugs development. This is best exemplified by an extremely active aminoglycoside,
441 namely streptomycin, the first clinical drug that was made available against TB [67]. In a
442 previous study, Streptocytosines A, Bamitecin and Amitecin isolated from sea water
443 *Streptomyces* in Japan showed activity against *M. smegmatis* at 32, 16 and 8 µg/ml
444 concentrations, respectively [68]. In another study, actinomycin X2 and actinomycin D
445 isolated from marine *Streptomyces* sp. MS449 in China showed activity against *M.*
446 *tuberculosis* H37Rv at 1.92mg/ml and 1.77 mg/ml, respectively [69]. In the present study
447 Transitmycin, a novel molecule isolated from a marine *Streptomyces* sp. R2 picked up from
448 coral reef ecosystem showed activity notably against drug sensitive, multi drug resistant
449 (MDR) and mono resistant strains of *M. tuberculosis* at concentrations of 5 and 10 µg/ml
450 (Fig. 7). Based on the preliminary experiment on laboratory strain, *M. tuberculosis* H37Rv,
451 minimum inhibitory concentration for transitmycin was determined on clinical isolates
452 which included 49 drug sensitive strains and 48 drug resistant strains. The drug resistant
453 profile of the clinical isolates are given in (supplementary S-table 12). Out of 97 clinical
454 isolates, MIC at 5 µg/ml was seen in 89 isolates and MIC at 10 µg/ml was seen in 8 isolates
455 for transitmycin based on LRP assay.



456

457 **Fig. 7.** MIC of Transitmycin in micrograms per millilitre for *Mycobacterium tuberculosis*
458 isolates susceptible to anti-TB drugs (n=49) and drug resistant to one or more anti-TB drugs
459 (n=48) as determined by LRP assay. Sensitive strains are represented in blue colour and
460 resistant strains are represented in brown colour.

461 *Activity against M. tuberculosis biofilm*

462 Bacteria can persist for extended periods of time inside the biofilm due to their ability to
463 resist the immune system, display increased virulence and become phenotypically more
464 resistant to antibiotics. Moreover, antibiotic concentrations required to control bacteria
465 within a biofilm are estimated to be 100–1,000 fold greater than that is needed to treat
466 planktonic forms. As planktonically-grown *M. tuberculosis* are unlikely to be entirely
467 representing the bacterial load during human infection, we set out to determine how
468 effective transitmycin can be against *M. tuberculosis* growing as a biofilm, a bacterial
469 phenotype known to be more resistant to antibiotic treatment [70]. In the present study, *M.*
470 *tuberculosis* culture showed biofilm formation in the control wells alone which could be
471 observed by the naked eye. The wells with cells and transitmycin failed to produce biofilm.
472 CFU determined prior to the addition of transitmycin was 1.9×10^6 to 2.3×10^6 /ml. After 4
473 days of exposure with the compound, the CFU dropped to 9×10^4 to 10×10^4 ml. Addition of
474 transitmycin completely killed all the cells at the end of 5 weeks (Table 3).

475

476

477

478 Table – 3. Activity of transitmycin on biofilm formation

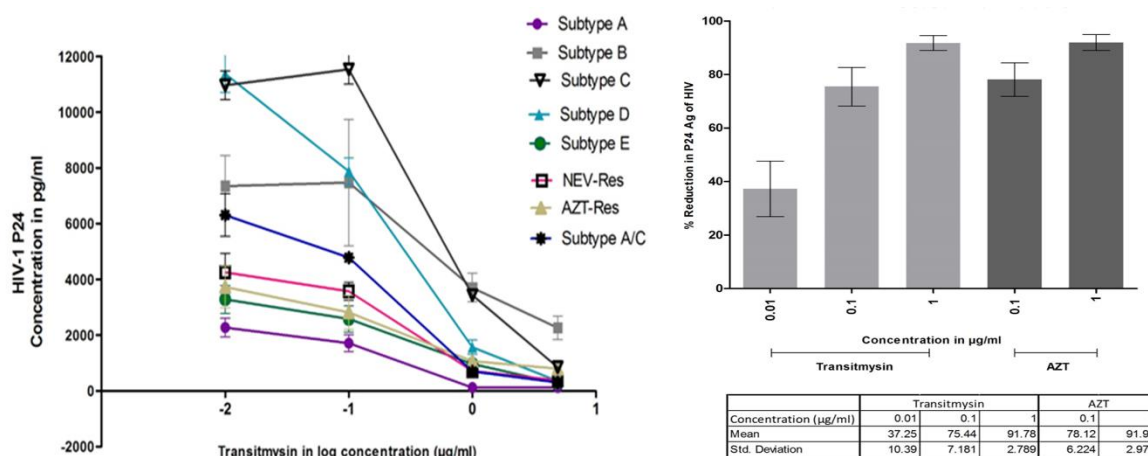
Culture	Zero days		After 4 days		Biofilm formation after 5 weeks
	10 ⁵ x CFU/ml		10 ⁵ x CFU/ml		
<i>M. tuberculosis</i> alone	1.1	1.8	6.6	3.6	Present
<i>M. tuberculosis</i> + Transitmycin (10 µg/ml)	19.0	23.0	0.9	1.0	0.0

479

480 *Anti-HIV activity*

481 The symbiotic association of TB and HIV poses a challenge to human survival in which HIV
482 complicates the treatment and diagnosis of TB. Besides, HIV–TB patients encounter other
483 unique problems such as cumulative toxicity, immune reconstitution inflammatory syndrome
484 (IRIS), drug-drug interactions, lower plasma drug levels, and the emergence of drug
485 resistance during treatment [71]. The currently available therapy for treating patients co-
486 infected with HIV and TB requires a very high pill load. Therefore, a class of drugs that can
487 be used to treat TB and HIV would be a real breakthrough in TB and AIDS Research.
488 Hence, the present study also evaluated the anti-HIV activity of transitmycin. A dose-
489 dependent reduction was observed in HIV-1 p24 levels in viral culture indicating that
490 transitmycin possessed significant anti-HIV activity. Transitmycin demonstrated good anti-
491 viral activity against the different subtypes of HIV-1 as well as clinical isolates obtained
492 directly from HIV-infected persons. In addition, transitmycin was also active against HIV-1
493 viruses resistant to nevirapine and AZT (Fig. 8a). The estimated IC₅₀ value ranged between
494 0.19 and 0.65µg/ml for the viruses tested. There was a >50% inhibition at a concentration of
495 0.1µg/ml and 80-95% inhibition at a concentration of 1µg/ml in the clinical isolates (Fig.
496 10b). The compound demonstrated a remarkable inhibitory effect on primary isolates
497 belonging to various subtypes as well as to clinical isolates obtained from HIV-infected
498 individuals. IC₅₀ values calculated for the various strains tested indicate that transitmycin is
499 a potent inhibitor of HIV-1 under *in vitro* experimental conditions. Importantly, transitmycin
500 also inhibited drug resistant forms of the virus, in a dose-dependent manner. These findings
501 suggest that transitmycin holds promise as the first potent compound that can be used to

502 treat TB and HIV infections when they occur singly, as well as in combination as HIV/TB
 503 co-infection. (Supplementary S-table 13).



504
 505
 506 **Fig. 8 a** Activity of Transitmycin against different HIV-1 clades. Various concentrations of
 507 Transitmycin were tested using 100 TCID₅₀ of virus belonging to 6 different HIV-1 clades as
 508 well as two drug-resistant strains. Each concentration was tested in triplicate on all the
 509 indicated viruses and mean \pm SEM values are shown in the graph. Log₁₀ -2 in the figure
 510 equals 0.01 µg/ml, Log₁₀ -1 equals 0.1 µg/ml, Log₁₀ 0 equals 1 µg/ml and Log₁₀ 1 equals 10
 511 µg/ml. **b** Activity of Transitmycin on clinical isolates obtained from HIV-1 infected
 512 individuals. Three concentrations of Transitmycin and two concentrations of AZT were
 513 tested against 20 clinical isolates and mean \pm SD values are shown on the graph. This
 514 experiment was performed on two different occasions.

515
 516 **R1, R2 and R3 intercalates with the genomic DNA of Mycobacterium tuberculosis**

517 Actinomycin D is the structurally similar compound for R1, R2 and R3. Actinomycin D and
 518 its derivatives are reported to intercalate with the DNA and exhibits fluorescence. So, we
 519 tested R1, R2 and R3 for its properties of DNA intercalation and fluorescence. Ethidium
 520 bromide 0.5 µg/ml is used as a positive control. The relative fluorescence unit (RFU) of R1,
 521 R2 and R3 with the DNA is compared with the RFU of R1, R2 and R3 without DNA. The
 522 average RFU of Ethidium bromide was 8561429. From the experiment, it was observed that
 523 all the three compounds, R1, R2 and R3 have DNA intercalating property and exhibits
 524 fluorescence (Fig. 9).

525
 526

527

528

529

530

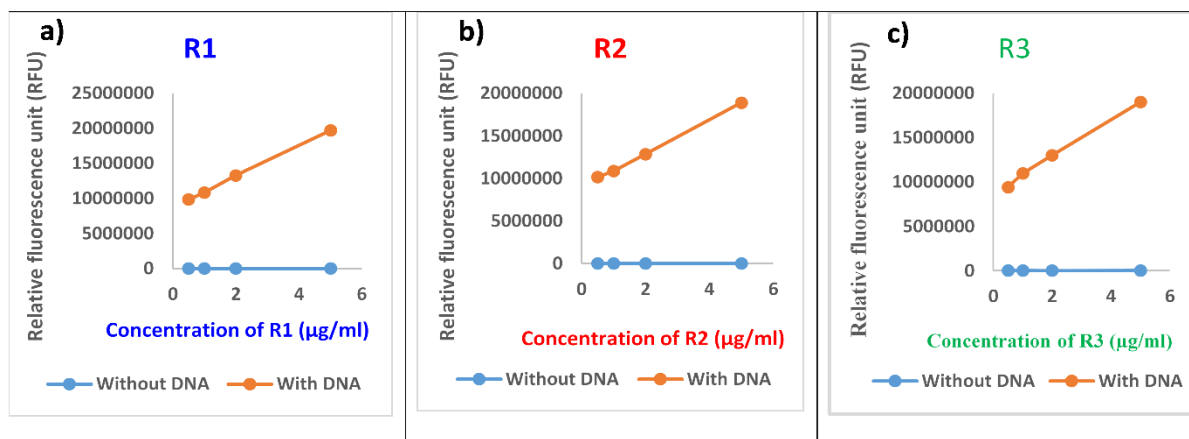
531

532

533

534

535



536 Fig. 9 a) R1, b) R2 and c) R3 binds with the DNA and emit fluorescence in a dose dependent
537 manner. The concentrations of R1, R2 and R3 tested were 0.5 µg/ml, 1 µg/ml, 2 µg/ml and 5
538 µg/ml. As the concentration increases, the Relative fluorescence unit (RFU) also increases.

539 Docking and molecular dynamics studies

540 The concept behind docking was to assess the potential interaction between the transitymycin
541 Fig. 10a or its derivative molecules and various DNA/Protein targets of interest. Through
542 docking studies, we aimed to validate the anticipated interactions, even though
543 comprehensive molecular dynamics studies were restricted, particularly for the entire
544 transitymycin or its derivatives. Nevertheless, the chromophore part Fig. 10b molecular
545 dynamics dynamics displayed enhanced stability, indicating promising outcomes in our
546 research

547 We performed docking and molecular docking experiments with a specific target and three
548 ligands: R1, R2, and R3. Our analysis showed that 1MNV displayed favorable interactions
549 with R2, whereas 3PKE exhibited superior binding with R3 Fig. 10c. The docking score data
550 is presented in Table 4.

551 Docking Score: docking scores were determined using the knowledge-based iterative
552 scoring functions ITScorePP or ITScorePR. A more negative docking score implies a higher
553 likelihood of a binding model. However, it's important to note that the score doesn't
554 represent the true binding affinity, as it hasn't been calibrated against experimental data.

555 Confidence Score: To gauge the likelihood of binding between two molecules, we
556 introduced a confidence score based on docking scores. The formula for the confidence
557 score is:

558 Confidence_score=1.01.0+e0.02×(Docking_Score+150)Confidence_score=1.0+e0.02×(Doc
559 king_Score+150)1.0

560 In this context, when the confidence score surpasses 0.7, it suggests a high probability of
561 binding. Scores between 0.5 and 0.7 indicate a possible binding, whereas scores below 0.5
562 imply an unlikely binding.

563 **Ligand RMSD:** Ligand RMSD values were computed by comparing ligands in the docking
564 models with the input or modelled structures.

565 **Table 4.** The docking score data of specific target (1MNV, 3PKE, 1MO3, 3IU8) and three
566 ligands: R1, R2, and R3

Name of the Molecule	Docking Score	Confidence Score	Ligand RMSD (Å)
1MNV with R1	-489.71	0.9989	22.52
1MNV with R2	-518.80	0.9994	17.61
1MNV with R3	-532.55	0.9995	25.15
1MO3 with R1	-397.33	0.9929	83.36
1MO3 with R2	-424.84	0.9959	83.95
1MO3 with R3	-420.99	0.9956	83.36
3PKE with R1	-391.53	0.9921	52.95
3PKE with R2	-493.89	0.9990	50.96
3PKE with R3	-503.74	0.9992	57.70
3IU8 with R1	-337.77	0.9771	37.59
3IU8 with R2	-418.79	0.9954	47.58
3IU8 with R3	-437.87	0.9969	50.75

567

568

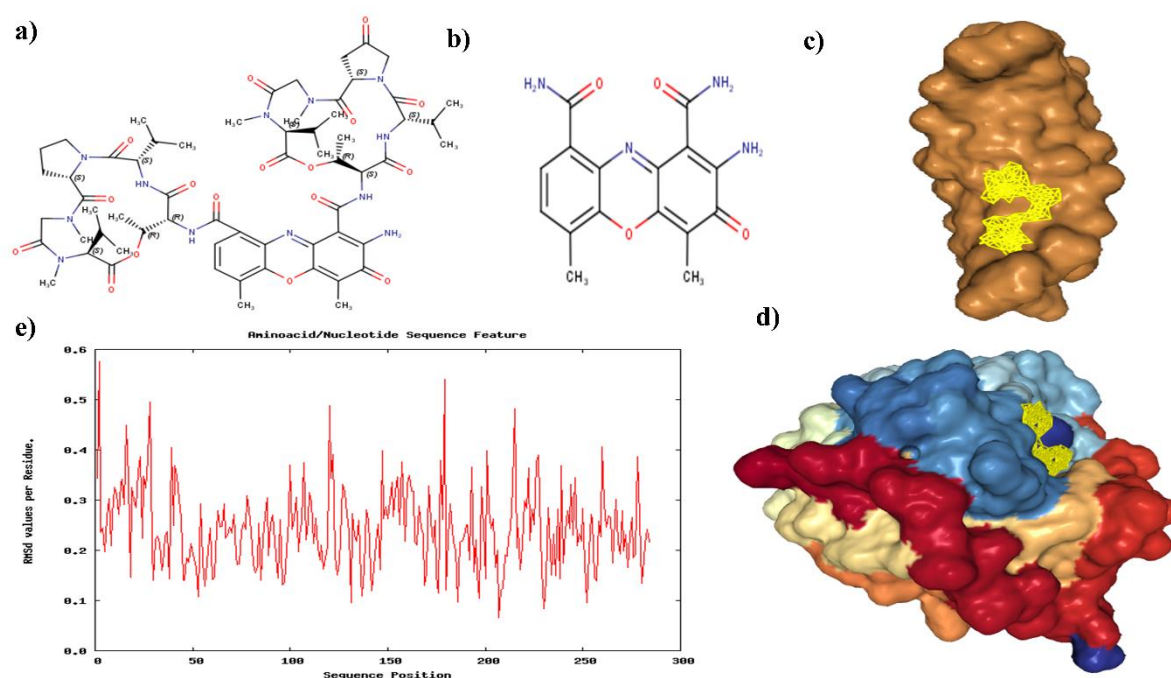
569

570 We conducted Molecular Dynamics (MD) simulations for the complex 1MNV with R2 and
571 R3. Unfortunately, MD simulations for R2 and R3 couldn't be performed due to the large
572 size of their peptide side chains, preventing accommodation into the minor groove of DNA
573 (1MNV). However, we successfully carried out simulations with the chromophores of R2
574 and R3. The RMSD of the residues remained within acceptable limits during these
575 simulations.

576 Additionally, MD simulations were conducted for the complex 3PKE with R3. Similar
577 challenges were encountered with the peptide side chains, leading to simulations being
578 performed with the chromophore, as illustrated in Figure 10b. The RMSD values plotted
579 against residues are presented in Figure 10e.

580 The results of the MD simulations indicate the stability of the protein backbone throughout
581 the simulation period. However, it is noteworthy that the simulations faced computational
582 challenges, primarily due to the size of the peptide side chains. Despite these difficulties, the
583 obtained data provides valuable insights into the behavior of the complexes during the
584 simulations.

585



586

587

588 **Fig 10.** a) Transitmycin structure b) Chromophore part of transitmycin or its derivatives,
589 c) 1 MNV R2 Docking Pose d) 3PKE with R3 Docking pose e) RMSD values of Residues
590 during the simulation Plot (3PKE with R3).

591

592 **Methods**

593 **Characterization and taxonomy of *Streptomyces* sp. R2**

594 Micromorphology of potential *Streptomyces* sp. R2 was studied by adopting Transplantation
595 Embedding Technique [72]. Briefly, a rectangular trough was dug out of an ISP2 agar plate
596 using sterile knife. Then the spores of *Streptomyces* strain were inoculated on the edges of
597 the trough under aseptic condition. A sterile cover-slip was placed over the agar, touching
598 the inoculated area on the ISP2 agar plate. The plate was incubated at 28°C for 7-14 days.
599 The cover-slip was aseptically removed using sterile forceps and placed over clean
600 microscopic slide fixing the same using cellophane tape. Micromorphology of *Streptomyces*
601 sp. R2 was observed under bright field microscope (Olympus) under 10x and 40x
602 magnifications. Spore structure and spore surface morphology were recorded using a
603 scanning electron microscope (JEOL model JSM5600LV). Media and procedures used for
604 determination of cultural characteristics and carbon and nitrogen source utilization were
605 those described originally by Shirling and Gottlieb [24]. Effect of pH, temperature, NaCl
606 concentration and anaerobic condition were studied using modified ISP2 medium. Antibiotic
607 susceptibility pattern was determined by disc diffusion method using standard antibiotic
608 discs (Hi media) following the standard protocol [73]. Biomass for cell wall analysis was
609 prepared by growing *Streptomyces* sp. R2 in shake flasks (120 rpm) containing ISP2 broth at
610 28 °C for 5 days. Amino acid and sugar content analyses of whole cell hydrolysates were
611 performed according to the original procedure described by Stanek and Roberts [74].

612

613 **Molecular characterization and phylogenetic analysis**

614 *Streptomyces* sp. R2 was grown in 50 ml of ISP2 broth at 28°C for 48 h. The genomic DNA
615 was extracted using Chromous genomic DNA isolation kit. Polymerase chain reaction
616 (PCR) was performed for the amplification of 16S rRNA gene using the primers 5' –
617 AGAGTRTGATCMTYGCTWAC – 3' and 5' – CGYTAMCTTWTTACGRCT – 3' on a
618 ABI12720 thermal cycler (Applied Biosystems). The conditions used for thermal cycling
619 were as follows: initial denaturation at 94°C for 4 min, followed by 35 cycles consisting of
620 denaturation at 94°C for 30 sec, primer annealing at 55°C for 30 sec and primer extension at
621 72°C for 2 min, followed by a final extension at 72°C for 5 min. The amplified 16s rRNA
622 gene fragment (~ 1.4 kb) was separated by agarose gel electrophoresis and the purified
623 fragment was used for sequencing in an ABI3130 genetic analyser. The nearly complete 16s
624 rRNA gene sequence of strain R2 (1400 nt) was subjected to BLAST comparison against the
625 16s rRNA sequences given in GenBank/DDBJ/EMBL databases.

626 Phylogenetic analysis was performed using CLUSTAL-W and MEGA version 3.1.
627 Evolutionary distances (Kimura's two parameter model) [75] and clustering were calculated
628 employing the neighbour-joining method. The topology of phylogenetic tree was evaluated
629 by the bootstrap re-sampling method with 1000 replicates.

630

631 **Production of Transitmycin**

632 Hundred microliters of *Streptomyces* sp. R2 spore suspension was transferred into 10 YEME
633 agar plates and spread using sterile L- rods. The plates were incubated at 28°C for 10 days.
634 After every 24 hours of fermentation, the mycelial growth was scrapped out and the crude
635 pigment secreted into the agar medium was extracted using equal volume (1:1) of different
636 organic solvents such as n-hexane, dichloromethane, chloroform, ethyl acetate and methanol
637 for 24 hours. The solvent portion was collected and dried at 40°C using Concentrator plus
638 (Eppendorf) [76]. Anti TB activity of crude extracts were tested against *M. tuberculosis*
639 H37Rv at 100µg concentration adopting LRP assay [77].

640 *Streptomyces* sp. R2 was cultured for 10 days at 28°C on YEME agar plates (2000 ml of
641 medium in 100 petriplates of 90 mm diameter) to produce the culture extract in bulk. After
642 the incubation period, the cell material was aseptically removed and discarded after
643 autoclaving. The yellow pigmented antibiotic containing agar medium was cut in to pieces
644 and extracted twice with equal volume (1:1 ratio) of ethyl acetate for 24 hours.

645

646 **Purification of transitmycin**

647 Transitmycin was purified by preparative thin layer chromatography (TLC) using Merck
648 silica gel 60 (GF254) pre coated aluminium (6x8 cm size) plates. The extract was separated
649 using different solvents in different proportions. After running, the 200 sheets were kept at
650 room temperature for complete drying of the plate. Spots on TLC were detected through
651 naked eye as well as under UV light (254 and 365 nm). After drying, three major yellow
652 colour spots (R1, R2 and R3) were scrapped, mixed with ethyl acetate and filtered using a
653 funnel fitted with Whatman filter paper. Ethyl acetate was evaporated to dryness under
654 vacuum to obtain the compounds as dry amorphous powder. (Supplementary Fig. S2).

655 All three compounds were tested against *M. tuberculosis* H37Rv at 100 µg
656 concentration by LRP assay. All three compounds from the ethyl acetate extract was purified
657 using column chromatography packed with neutral alumina using a gradient of 1%
658 methanol/chloroform mixture (CH₃OH/ CHCl₃) as the eluent. Fractions were collected and

659 concentrated under vacuum to obtain pure transitmycin. The product was visualized in a
660 silica gel coated TLC sheet (Supplementary Fig. S2 and S3).

661 The compound R1 (named as transitmycin) that showed maximum activity was taken
662 for characterization and other studies testing its biological activity. Purity of transitmycin
663 (Fig. 2c). was analysed by HPLC using Shimadzu (Japan) RID-10A gradient high-
664 performance liquid chromatographic instrument, equipped with two LC-20AD pumps
665 controlled by a CBM-10 inter-face module. Refractive index Detector RID 10A (Shimadzu)
666 was used for the peak. Analysis was performed on a Luna 5u C₁₈ (2) reversed-phase column,
667 100 (150X4.6mm). The analytical parameters were selected after screening a number of
668 solvent systems and gradient profiles. Separation was achieved using a two-pump gradient
669 program for pump A (0.1% Acetic acid in CH₃CN) and pump B (0.1% Acetic acid in H₂O)
670 in a linear gradient of acetonitrile and water from 0:100 to 65:35 in 65 minutes at a flow rate
671 of 2 ml/min. Detection was done at 254 nm, the absorption maxima close to that of majority
672 of the compounds. Injection size for sample was 20 µl. Column temperature was 30°C.
673 (Supplementary Fig. S4 and S5).

674

675 **Characterization and structure elucidation**

676 Colour and consistency of the purified antibiotic was visually observed. Solubility
677 was tested in water, methanol, acetone, ethyl acetate, diethyl ether, dichloromethane,
678 chloroform, and n-hexane by dissolving 1 mg of purified antibiotic. Optical rotations were
679 measured with a Autopol IV Automatic polarimeter, and the $[\alpha]_D$ values are given in deg
680 cm² g⁻¹. Melting point was analysed using Mettler Toledo Model FP62 [78]. Ultraviolet
681 (UV) spectrum was determined using Shimadzu UV-1700 series. One milligram of sample
682 was dissolved in 10ml of methanol and the spectra were recorded at wavelength between
683 190 – 900 nm. The Infrared (IR) spectrum of the purified antibiotic was determined on
684 Perkin Elmer Spectrum One FT-IR. The spectrum was obtained using potassium bromide
685 (KBr) pellet technique in the range of 450 to 4000 cm⁻¹ at a resolution of 1.0 cm⁻¹.
686 Potassium bromide (AR grade) was dried under vacuum at 100°C and 100 mg of KBr with
687 1mg of purified antibiotic was used to prepare KBr pellet. The spectrum was plotted as
688 intensity versus wave number [79]. ¹H and ¹³C NMR spectra were recorded on a Bruker
689 Advance 500 NMR spectrometer in CDCl₃ with TMS as internal Standard and with
690 chemical shifts (δ) reported in ppm. Two-dimensional ¹H–¹H COSY, DQF-COSY, NOESY,
691 ROESY, ¹H–¹³C HSQC, HMBC, and spectra were recorded on a Bruker Advance 500 NMR
692 spectrometer. MALDI-TOF MS analyses were performed using an Applied Biosystems

693 ABI4700 TOF mass spectrometer in reflector mode with an accelerating voltage of 20 kV.
694 HRESIMS were measured on a Q-TOF micro mass spectrometer (Waters USA) in positive
695 ion mode with methanol as solvent. QTOF- MS was recorded on an Agilent 6520-QTOF
696 LCMS having an ESI source in positive mode.

697

698 **HPLC Analysis of L-FDAA Derivatives of Transitmycin**

699 Transitmycin (3.0 mg) was dissolved in 1 ml of 6NHCl and heated in a sealed glass
700 tube at 110°C for 24 h. After removing the solvents, the hydrolysate mixture (3 mg) and the
701 amino acid standards (0.5 mg) were separately dissolved in 0.1 mL of water and treated with
702 0.2 mL of 1% 1-fluoro-2,4-dinitrophenyl-5-L-alaninamide (FDAA) (Marfey's reagent) in
703 acetone (10 mg/mL in acetone) and 0.04 mL of 1.0 M sodium bicarbonate. The vials were
704 heated at 50°C for 90 min, and the contents after cooling at room temperature were
705 neutralized with 1N HCl. After degassing, an aliquot of the FDAA derivative was diluted in
706 CH₃CN, Water (1:1) and analysed by reversed phase HPLC column Luna 5u C₁₈ (2) 100
707 (150X4.6mm) and a linear gradient of acetonitrile and water containing 0.05%
708 trifluoroacetic acid from 10:90 to 50:50 in 20 min and then isocratic. The flow rate was
709 adjusted to 1 mL/min and the absorbance detection was at 340 nm. The chromatogram was
710 compared with those of amino acid standards treated in the same conditions [60-61].

711

712 **LC-MS Analysis of L-FDAA Derivatives of Transitmycin**

713 The analysis of the L- and D-FDLA derivatives of Transitmycin was performed on a
714 Waters Acquity UPLC coupled with a Thermo LCQ Deca XP MAX. QTOF- MS was
715 recorded on an Agilent 6520-QTOF LCMS having a ESI source in Positive mode and
716 employing a linear gradient of from 25% to 70% CH₃CN in 0.01 M formic acid at 0.5
717 mL/min over 60 min [62-64].

718

719 **Transitmycin (R1)**. R1 was obtained as an orange red solid; $[\alpha]_D^{25}$ -106 ° (c 0.2, MeOH);
720 UV (MeOH) λ_{max} (log ϵ) 214 (3.07), 240 (2.30), 425 (1.44), 442 (1.51) nm; CD
721 [(MeOH),(mdeg)] $\lambda_{max}(\Delta\epsilon)$ 195 (+11.1), 210 (-21.0), 242 (+4.7) nm; IR (KBr), ν_{max} 3435,
722 2958, 2924, 2853, 1745, 1642, 1524, 1465, 1379, 1194, 1099, 1059 cm⁻¹; HRESI-MS
723 (pos.ions): m/z 1270.7069 [M+2H]⁺, 1291.8449 [M+Na]⁺, 1307.9286 [M+K]⁺, 657.3119
724 [M+2H]²⁺; MALDI-TOF-MS (pos.ions): m/z 1293.07095 [M+Na+2H]⁺, 1309.93062

725 [M+K]⁺ MALDI-TOF-MS (neg.ions) 1269.33344 [M-H]⁻ ¹HNMR, ¹³NMR and 2DNMR
726 details (Supplementary Fig. S14-52, S-Table 5).

727

728 **Compound (R2).** R2 was obtained as a red solid; [α]_D²⁵: -24° (c 0.2, MeOH); UV(MeOH) λ
729 max, (log ε) 205(1.25),240(0.63),425 (0.39), 442 (0.42) nm; CD [MeOH, (mdeg)] λ_{max}, (Δε)
730 195 (+8.8), 210 (-22.0), 240 (+4.3) nm;IR (KBr), ν_{max}3436, 2961, 2924, 2853, 1744, 1650,
731 1565, 1415, 1204, 1140, 1045, 1019 cm⁻¹; HRESI-MS (pos. ions) :1277.8245 [M +
732 Na]⁺1293.8735 [M + K]⁺m/z 650.3413 [M+2H]⁺²; MALDI-TOF-MS m/z (pos.ions)
733 1278.95175 [M+Na+H]⁺; MALDI-TOF-MS (neg.ions) m/z 1255.38052 [M-H]⁻, ¹HNMR,
734 ¹³NMR and 2D NMR details (Supplementary Fig. S53-63).

735

736 **Compound (R3):** R3 was obtained as orange solid; [α]_D²⁵:-27 ° (c 0.2, MeOH); UV
737 (MeOH) λ max (log ε) 206 (1.90), 240 (0.69) 424 (0.191), 442.2 (0.19) nm; CD [MeOH,
738 (mdeg)] λ_{max} (Δε) 195 (+24.0), 210 (-21.5), 241 (+1.7) nm; IR (KBr), ν_{max} 3415, 2957, 2924,
739 2853, 1745, 1642, 1583, 1464, 1384, 1193, 1093, 1078 cm⁻¹; HRESI-MS
740 (pos.ions):1271.7159 [M +H]⁺ m/z1277.6149 [M-OH+Na]⁺; MALDI-TOF-MS (pos.ions)
741 m/z 1294.5888 [M + Na]⁺ MALDI-TOF-MS (neg. ions) m/z 1268.48582 [M-H]⁻, ¹HNMR,
742 ¹³CNMR and 2D NMR details, (Supplementary Fig. S64-69).

743

744 **Determination of anti TB and anti-HIV activity**

745 Anti-TB activity was determined by adopting Luciferase Reporter Phage (LRP) assay
746 against the standard laboratory strain, *Mycobacterium tuberculosis* H₃₇Rv, and 97 clinical *M.*
747 *tuberculosis* isolates including drug sensitive and cultures exhibiting different drug resistant
748 patterns. Different concentrations (5 – 50 μg/ml) of purified antibiotic – transitmycin were
749 prepared using 10% dimethyl sulfoxide (DMSO). About 50μl of antibiotic solution was
750 added to 350 μl of glycerol 7H9 broth in cryo vials. Effect of DMSO was also tested by
751 adding 50 μl of 10% DMSO instead of the antibiotic. Mycobacterial cell suspension
752 equivalent of 2 McFarland units was prepared from log phase culture and 100 μl of the same
753 was added to all the vials before incubating at 37°C for 72 hours. After incubation, 50 μl of
754 high titre luciferase reporter phage phAE129 and 40 μl of 0.1M CaCl₂ were added to test
755 and control vials. All the vials were incubated at 37°C for 4 hours. After incubation 100 μl
756 of suspension from each vial was transferred to a luminometer cuvette. 100 μL of D-
757 luciferin was added and relative light unit (RLU) was measured in a luminometer [77].

758 Percentage of inhibition was calculated using the RLU of control and test and MIC was
759 determined. [81,82]

760

761

762 **Activity against *M. tuberculosis* biofilm**

763 Cell suspensions of *M. tuberculosis* H37Rv were prepared using 7H9 broth. Biofilms of *M.*
764 *tuberculosis* were developed on 6 well tissue culture plates by adding 2 ml of Sautons
765 medium (without Tween 80) and inoculating 20 µL of saturated planktonic culture of *M.*
766 *tuberculosis* H₃₇Rv. The plate was wrapped with parafilm and incubated without shaking at
767 37°C in humidified conditions for 7 to 14 days. The plate was observed regularly after 7
768 days for biofilm formation by *M. tuberculosis* which can be visibly seen. When the biofilm
769 was formed, 10 µg/ml of transitmycin was added to the transitmycin test wells leaving the
770 controls and considered as zero day. The viable counts of tubercle bacilli were determined
771 from the wells on zero day, 4th day and after 5 weeks and expressed in cfu/ml [80].

772 **Anti-HIV activity**

773 **Viruses:** HIV-1 viruses belonging to subtypes A, B, C, D, E and A/C (Subtype A:
774 92RW020, Subtype B: JR-FL, Subtype C: 92BR025, Subtype D: 92UG001, Subtype E:
775 92TH021 and Subtype A/C: 92RW009), were obtained from the NIH AIDS Repository
776 (Germantown, MD, USA). Clinical isolates of HIV-1 were produced in our laboratory by
777 co-culture of HIV-infected peripheral blood mononuclear cells (PBMC) with activated
778 donor PBMC.

779

780 **Testing for anti-HIV activity**

781 Anti-HIV activity of Transitmycin was determined using the HIV-1 gag p24 inhibition
782 assay. Initially, testing was performed on a lab-adapted HIV-1 subtype B isolate, HIV-1
783 IIB. Donor PBMC were obtained from healthy volunteers after obtaining the approval of
784 the Institutional Ethics Committee of the National Institute for Research in Tuberculosis as
785 well as the informed consent of the participants. Donor PBMC were stimulated with PHA
786 (Phytohemagglutinin) for 72 hours and incubated with 100 TCID₅₀ of the virus per 1 x 10⁶
787 cells for 4 h at 37°C. The cells were washed to remove the un-adsorbed virus and plated at a
788 concentration of 10,000 cells/well in a 96-well tissue culture plate. Varying concentrations
789 of Transitmycin (0.01µg/ml, 0.1µg/ml, 1.0µg/ml and 5.0µg/ml) were added to triplicate

790 wells. Control cultures were set up without the addition of the compound. AZT was used as
791 the reference compound. Cultures were maintained for 7 days at 37°C in a CO₂ incubator.
792 On day 7, HIV-1 gag p24 antigen production was determined as an indirect measure of viral
793 replication in the culture supernatants using the Alliance HIV-1 p24 ELISA kit (Perkin
794 Elmer, USA).

795 **Testing of Transitmycin against different HIV-1 subtypes**

796 Anti-viral activity of Transitmycin was also tested on primary HIV-1 isolates belonging to
797 different subtypes - Subtype A: 92RW020, Subtype B: JR-FL, Subtype C: 92BR025,
798 Subtype D: 92UG001, Subtype E: 92TH021 and Subtype A/C: 92RW009, as well as a
799 Nevirapine resistant and AZT resistant strain, using the method described above. The
800 activity of Transitmycin on different viruses was determined by measuring HIV-1 p24
801 antigen in 7-day culture supernatants. The IC₅₀ value (concentration of compound required to
802 inhibit 50% of virus replication) of Transitmycin for the different HIV-1 subtypes was
803 calculated by fitting a dose response curve using a non-linear regression analysis to generate
804 a sigmoidal three parameter dose response curve (GraphPad Prism, version 6).

805 **Activity against clinical strains of HIV**

806 Anti-viral activity of Transitmycin was further evaluated on 20 clinical isolates of HIV-1
807 obtained by co-culture of patient PBMC with PHA-stimulated donor PBMC in the
808 laboratory. For this analysis, only three concentrations (0.01 µg/ml, 0.1 µg/ml and 1 µg/ml)
809 of transitmycin was used based on the results of the above experiment.

810 **DNA binding and Fluorescence assay**

811 0.5 µg/ml, 1 µg/ml, 2 µg/ml and 5 µg/ml of R1, R2 and R3 were separately added to 100 µl
812 of PBS in triplicates in 96 well plate. *Mycobacterium tuberculosis* genomic DNA was
813 extracted and 200 ng of DNA is added to each test wells. DNA was not added to the control
814 wells of R1, R2 and R3. For the positive control, 0.5 µg/ml of Ethidium bromide is taken in
815 PBS and 200 ng of DNA is added to it. After 15 mins, the plate is read in Multimode - plate
816 reader, Spinco Biotech, with excitation 546 nm and emission 595 nm. The relative
817 fluorescence unit is recorded. Average of RFU for each concentration of R1, R2 and R3 was
818 taken and plotted as graph.

819

820

821 **Conclusion:**

822 Globally, the general public has latent or active tuberculosis, and this is expected to
823 increase in the future, causing the medical system a major challenge. The need of the hour is
824 to identify novel antibiotics to support the current regimens with reduced side effects,
825 duration and cost of treatment. Transitmycin is a novel antibiotic isolated from a novel
826 *Streptomyces* sp. MTCC from the coral reef soil from Rameshwaram waters in India. It has
827 the unique property of killing latent and active forms of TB bacilli irrespective of the
828 resistance they have towards major antiTB drugs and also sterilising the different resistant
829 and recombinant clades of standard and clinical HIV virus. When brought into the market
830 for human use, transitmycin can strategize treating TB and HIV simultaneously, which could
831 be a major breakthrough, none the less. Of course, preclinical trials and toxicity studies need
832 to be performed before it can be tested on human volunteers which will require sufficient
833 resources. Countries which are burdened with this dual ailment may have to take
834 considerable interest in this direction. Structural modifications to the parent compound can
835 further improve its activity.

836

837 **Acknowledgement**

838

839 Professor Balasubramanian Kalpattu Kuppusami, INSA Senior Scientist, Department of
840 Chemistry, IIT Madras Chennai 600 036, India and Professor Krishna Kumari Gadepalli
841 Narasi, Department of Medicinal Chemistry, Sri Ramachandra University, Chennai 600 116,
842 India, acknowledged for discussion of structure elucidation of Transitmycin. Technical
843 assistance of Dr. S. Balaji and Dr. A. S. Shainaba of National Institute for Research in
844 Tuberculosis is acknowledged in fine tuning and uploading the manuscript.

845 **Supplementary materials**

846 The comprehensive characterization of the anticipated products have been subjected
847 through UV/Vis, IR, CD, CHNS analyses, whilst, followed by $^1\text{H-NMR}$ $^{13}\text{C-NMR}$, $^1\text{H-}^1\text{H}$
848 COSY, $^1\text{H-}^1\text{H}$ DQF-COSY, $^1\text{H-}^{13}\text{C}$ HMBC, and $^1\text{H-}^{13}\text{C}$ HSQC, $^1\text{H-}^1\text{H}$ TOCSY, $^1\text{H-}^1\text{H}$
849 NOESY, $^1\text{H-}^1\text{H}$ NOESY 2D NMR spectra and MALDI-TOF-MS, HR-ESIMS, HR-LCMS,
850 ESI-MS, QTRAP LC-MS/MS, RP-HPLC and LCMS analyses respectively. The following
851 L-FDAA derivatives of R1, R2, R3 spectral information on all compounds of this article can
852 be found in the online version.

853

854

855 **Funding Received for this study**

856 1) Potential Tuberculosis Drugs from Marine Actinomycetes, Funded by Department of
857 Science and Technology, New Delhi (November, 2007 to November, 2009).

858 2) Study to evaluate the baseline anti TB and anti-HIV properties of novel antibiotic
859 transitmycin (Tr) isolated from novel *Streptomyces* Sp. R2 funded by Indian Council of
860 medical Research (2009-2012).

861 3) Purity and in vitro efficacy studies on transitmycin funded by Indian Council of Medical
862 Research (2015-2016).

863

864 **Authors' individual contributions**

865 Vanaja Kumar – Principal Investigator, planning, supervision, coordination and data
866 compilation, manuscript writing and editing.

867 Balagurunthan Ramasamy–Facilitating Growing of producer strain, coordination in crude
868 extract preparation as lab head.

869 Mukesh Doble – Purification of compound from crude extract, structure analysis and
870 chemical characterisation and report preparation as lab head.

871 Gandarvakottai Senthilkumar Arumugam – Isolation, purification, characterization,
872 complete structural elucidation and a key role in Innovation Of Transitmycin drug discovery
873 development and manuscript writing and editing.

874 Kannan Damodharan - Isolation, purification, characterization, structural elucidation of
875 Transitmycin compounds and final manuscript drafting.

876 Radhakrishnan Manikkam- Isolation and characterisation of producer strain, biological and
877 biochemical characterisation, testing biological activities, data compilation, manuscript
878 writing.

879 Hanna Luke Elizabeth - Testing crude extract and purified compound on HIV standard and
880 clinical clades. Preparation of write up.

881 Suresh Ganesan – Isolation, purification, characterization, structural elucidation of
882 Transitmycin compounds and final manuscript drafting

883 Azger Dusthacker- Testing biological activities against latent bacilli and biofilms,
884 preparing the write up.

885 Precilla Lucia – Laboratory work for testing the compound on HIV clades.

886 Shainaba A Saadhali- Testing biological activities against latent bacilli and biofilms,
887 preparing the write up.

888 Shanthi John – laboratory work with respect to growing the producer strain and preparation
889 of crude extract.

890 Poongothai Eswaran - laboratory work with respect to growing the producer strain and
891 preparation of crude extract.

892 Selvakumar Nagamiah– supervision of laboratory work on testing biological activities,
893 editing manuscript.

894 Soumya Swaminathan – Facilitating coordinated activity for fund release, conduct of
895 experiments against HIV clades as Head of the laboratory and the Institute.

896 Jaleel UCA-Provided the overall conceptualization of theoretical study, and offered
897 guidance throughout the research process and reviewed and edited the manuscript to ensure
898 clarity, consistency, and scientific accuracy.

899 Rakhila M-Conducted the data analysis, molecular docking simulations, and statistical
900 interpretation of the results and edited the manuscript to ensure clarity, consistency, and
901 scientific accuracy.

902 Ayisha Safeeda- Conducted the data analysis, molecular docking simulations, and statistical
903 interpretation of the results and edited the manuscript to ensure clarity, consistency, and
904 scientific accuracy.

905 Satheesh S -was responsible for creating and editing the figures and tables that visually
906 represented the key findings.

907

908 **Additional Information**

909 **Competing Interests**

910 The authors declare no competing interests.

911

912 **Figure Legends**

913

914 **Fig. 1.** Representative HPLC chromatogram of crude and isolated samples R1, R2 and R3. **a**
915 RP HPLC of Chromatogram of crude extract of *Streptomyces* sp. R2. **b** RP HPLC analysis
916 of mixture of R1, R2, R3. **c** RP HPLC of Chromatogram of pure Transitmycin R1. **d**
917 Transitmycin R1 obtained after column chromatographic purification. **e** UV-Vis spectra of
918 Transitmycin R1, R2 and R3. **f** IR Spectrum of Transitmycin R1.

919 **Fig. 2** Notable characteristic ^1H NMR spectra of different proline units of Transitmycin as **a**
920 **R1** (4-oxoproline). **b** **R2** (proline) and **c** **R3** (4-OH proline). **d** Comparative studies for ^1H
921 NMR (500 MHz, CDCl_3) chemical shift value of NH containing amino acid residue and
922 chromophore motifs of Transitmycin (**R1**), **R2** and **R3**.

923 **Fig. 3. a** Key ^1H - ^1H COSY correlation of Transitmycin (**R1**). **b** Key ^1H - ^1H TOCSY
924 correlation of Transitmycin (**R1**). **c** Key ^1H - ^{13}C HMBC connectivity for Transitmycin (**R1**).
925 **c** ^1H - ^1H ROESY correlation of Transitmycin (**R1**). **d** Chemical structure of isolated
926 compounds Transitmycin (**R1**). **e** **R2**. **f** **R3**.

927 **Fig. 4 a-m.** Comparative analysis of MALDI-TOF-MS for molecular ion peak of
928 Transitmycin (**R1**), **R2**, **R3**. **a** **R1** (Simulated). **b** **R2** (Simulated). **c** **R3** (Simulated). **d** **R1**
929 (Measured, positive mode. **e** **R2** (Measured, Positive mode). **f** **R3** (Measured, Positive
930 mode). **g** **R1** (Measured, Negative mode). **h** **R2** (Measured, Negative mode). **i** **R3**
931 (Measured, Negative mode), MALDI-TOF-MS spectra of crude extract of *Streptomyces* sp.
932 **R2**. **j** positive mode. **k** negative mode **l** Comparative analysis for HR-ESI-MS and MALDI-
933 TOF-MS of Transitmycin (**R1**), **R2** and **R3** on various batches. **m** Characteristic retention
934 factor (R_f) value and corresponding HR-ESI-MS data of purified compounds (Transitmycin
935 (**R1**), **R2** and **R3**).

936 **Fig. 5. a** Mass spectral fragmentation of Transitmycin (**R1**) obtained by MALDI-TOF-MS,
937 **b** MALDI-TOF-MS spectrum of Transitmycin (**R1**). **c** Mass spectral fragmentation of
938 Transitmycin (**R1**) obtained by MALDI-TOF-MS, 211- β -Ring-Val-Oxo-Pro, 233- α -Ring-
939 Val-Pro, 294- β -Ring-Oxo-Pro-Sar-NMeVal, 295-Chromophore, 297- β -Ring-Thr-Val-Oxo-
940 Pro, 357- α -Ring-Val-Pro-Sar-MeVal, 371- β -Ring-Val-Oxo-Pro-Sar-MeVal, 412- β -Ring-
941 Val-Oxo-Pro-Sar-NMeVal, 412- α -Ring-Val-Pro-Sar-NMeVal+859 (Y ion), 495- β -Ring-
942 Thr-Val-Oxo-Pro-Sar-NMeVal, 496- α -Ring-Thr-Val-Pro-Sar-NMeVal, 464 α -Ring-Thr-
943 Val-Oxo-Pro-Sar-NMeVal, 746-Y-113 (MeVal), 747- α -Ring-Val-Pro-Sar-NMeVal+Y-
944 MeVal+545.6, 495= β -Ring-Thr-Val-Oxo-Pro-Sar-NMeVal, 495-371=124-23=101 MeVal
945 (β -Ring-Thr-Val-Oxo-Pro-Sar), 371(β -Ring-Thr-Val-Oxo-Pro-Sar), 294 (β -Ring-Thr-Val-
946 Oxo-Pro).

947

948 **Fig. 6. a** HPLC data analysis for L-FDAA derivatives to hydrolysates of Transitmycin **R1**
949 and standard amino acids. **b** Graphical representation for RP-HPLC chromatogram of L-

950 FDAA (Marfey's) derivatives of hydrosylated Transitmycin (R1). **c** HR-LCMS data analysis
951 for L-FDAA derivatives to hydrolysates of Transitmycin R1 and standard amino acids.

952

953 **Fig. 7.** MIC of Transitmycin in micrograms per millilitre for *Mycobacterium tuberculosis*
954 isolates susceptible to anti-TB drugs (n=49) and drug resistant to one or more anti-TB drugs
955 (n=48) as determined by LRP assay. Sensitive strains are represented in blue colour and
956 resistant strains are represented in brown colour.

957

958 **Fig. 8 a** Activity of Transitmycin against different HIV-1 clades. Various concentrations of
959 Transitmycin were tested using 100 TCID₅₀ of virus belonging to 6 different HIV-1 clades as
960 well as two drug-resistant strains. Each concentration was tested in triplicate on all the
961 indicated viruses and mean \pm SEM values are shown in the graph. Log₁₀ -2 in the figure
962 equals 0.01 μ g/ml, Log₁₀ -1 equals 0.1 μ g/ml, Log₁₀ 0 equals 1 μ g/ml and Log₁₀ 1 equals 10
963 μ g/ml. **b** Activity of Transitmycin on clinical isolates obtained from HIV-1 infected
964 individuals. Three concentrations of Transitmycin and two concentrations of AZT were
965 tested against 20 clinical isolates and mean \pm SD values are shown on the graph. This
966 experiment was performed on two different occasions.

967

968 **Fig. 9** a) R1, b) R2 and c) R3 binds with the DNA and emit fluorescence in a dose
969 dependent manner. The concentrations of R1, R2 and R3 tested were 0.5 μ g/ml, 1 μ g/ml, 2
970 μ g/ml and 5 μ g/ml. As the concentration increases, the Relative fluorescence unit (RFU)
971 also increases.

972

973 **Fig 10.** a) Transitmycin structure b) Chromophore part of transitmycin or its derivatives,
974 c) 1MNV R2 Docking Pose d) 3PKE with R3 Docking pose e) RMSD values of Residues
975 during the simulation Plot (3PKE with R3).

976

977 Table Legends

978

979 **Table 1.** ¹H NMR (500 MHz, CDCl₃)/¹³C NMR (125 MHz, CDCl₃) and 2D NMR (500
980 MHz, CDCl₃) correlation spectral data of Transitmycin (R1) ¹H-¹H COSY, ¹H-¹H TOCSY
981 ¹H-¹³C HMBC, ¹H-¹H ROESY

982 **Table 2.** Physico-chemical properties of Transitmycin.

983 **Table 3.** Activity of transitmycin on biofilm formation.

984 **Table 4.** The docking score data of specific target (1MNV, 3PKE, 1MO3, 3IU8) and three
985 ligands: R1, R2, and R3

986 **References**

- 987 1. Abdelmohsen UR, Potential of marine natural products against drug-resistant fungal, viral,
988 and parasitic infections. *Lancet Infect. Dis.* 2017;17: e30–e41.
989
- 990 2. Quan D, et al. New tuberculosis drug leads from naturally occurring compounds. *Int. J.*
Infect. Dis. 2017;56:212-220.
- 991 3. Shin HJ, Kwon JS. Treatment of Drug Susceptible Pulmonary Tuberculosis. *Tuberc. Respir.*
992 *Dis.* 2015; 78:161-167.
993
- 994 4. Tran T, et al. Sansanmycin natural product analogues as potent and selective anti-
995 mycobacterials that inhibit lipid I biosynthesis. *Nature Commun.* 2017; 8:14414.
- 996 5. Sotgiu G. *et al.* Tuberculosis Treatment and Drug Regimens. *Cold Spring Harb Perspect*
Med 2015;5: a017822.
- 997 6. Igarashi M, et al. New antituberculous drugs derived from natural products: current
998 perspectives and issues in antituberculous drug development. *J. Antibiot.* 2018;71:15–25.
- 999 7. UNAIDS Report, (2017)
- 1000 8. Schader SM, Wainberg MA. Insights into HIV-1 pathogenesis through drug discovery: 30
1001 years of basic research and concerns for the future. *HIV AIDS Rev.* 2011; 10:91–98.
- 1002 9. Parveen M, et al. Anti-HIV Drug Discovery Struggle: From Natural Products to Drug
1003 Prototypes. In *Natural Products in Clinical Trials*. Publisher: Bentham Science Publishers
1004 (2018).
- 1005 10. Huang T, Lin S, Microbial Natural Products: A Promising Source for Drug Discovery. *J.*
1006 *Appl. Microbiol. Biochem.* 2017;1:5.
- 1007 11. Barka EA, *et al.* Taxonomy, physiology, and natural products of *Actinobacteria*. *Microbiol.*
1008 *Mol. Biol. Rev.* 2016;80;1–43.
- 1009 12. Berdy J, Thoughts and facts about antibiotics: Where we are now and where we are heading.
1010 *J. Antibiot.* 2012;65:385-395.
1011
- 1012 13. Velho-Pereira, SKamat, NM. Actinobacteriological research in India. *Indian J. Exp. Biol.*
2013; 51:573–596.
14. Balagurunathan R, et al. Extremophilic and extremotolerant Actinomycetes: Distribution
and Importance. In: *Recent Trends in Microbial Diversity and Bioprospecting*. Westville
Publishing House, New Delhi (ISBN: 978-93-83491-14-8); 2014: pp. 114-128.

- 1013
1014 15. Dhakal D, et al. Marine Rare Actinobacteria: Isolation, Characterization, and Strategies for
1015 Harnessing Bioactive Compounds. *Front Microbiol.* 2017;8;1106.
- 1016 16. Genilloud O, Actinomycetes: still a source of novel antibiotics. *Nat. Prod. Rep.* 2017;34:
1017 1203-1232.
- 1018 17. Lam, KS. Discovery of novel metabolites from marine actinomycetes. *Curr. Opin.*
1019 *Microbiol.* 2006;9;245-251.
- 1020 18. Raveh A, et al. Discovery of potent broad-spectrum antivirals derived from marine
1021 actinobacteria. *PLoS ONE.* 2013;8: e82318.
- 1022 19. Valliappan K, et al. Marine actinobacteria associated with marine organisms and their
1023 potentials in producing pharmaceutical natural products. *Appl. Microbiol.*
1024 *Biotechnol.* 2014;98;7365–7377.
- 1025 20. Blunt JW, et al. Marine natural products. *Nat. Prod. Rep.* 2018;35:8-53.
- 1026 21. Sarkar S, et al. Enhanced production of antimicrobial compounds by three salt-tolerant
1027 actinobacterial strains isolated from the Sundarbans in a niche-mimic bioreactor. *Mar.*
1028 *Biotechnol.* 2008;10:518-526.
- 1029 22. Saha M, et al. Production and purification of a bioactive substance inhibiting multiple drug
1030 resistant bacteria and human leukemia cells from a salt-tolerant
1031 marine *Actinobacterium* sp. isolated from the Bay of Bengal. *Biotechnol. Lett.* 2006;
1032 28:1083–1088.
- 1033 23. Tindall BJ, et al. Notes on the characterization of prokaryote strains for taxonomic purposes.
1034 *Int. J. Syst. Evol. Microbiol.* 2010; 60:249e266.
- 1035 24. Shirling EB, & Gottlieb D. Methods for characterization of *Streptomyces* species. *Int. J.*
1036 *Syst. Bacteriol.* 16, 313-340 (1966).
- 1037 25. Nonomura H. Key for classification and identification of 458 species of the *Streptomyces*
1038 included in ISP. *J. Ferment. Technol.* 1974; 52:78-92.
- 1039 26. Labeda DP, Shearer MC. Isolation of actinomycetes for biotechnological applications. In
1040 Isolation of Biotechnological Organisms from Nature, D.P. Labeda, Ed., 1990;19:1–19,
1041 McGraw-Hill, New York, NY, USA.
- 1042 27. Konstantinidis KT, Tiedje JM. Genomic insights that advance the species definition for
1043 prokaryotes. *Proc. Natl. Acad. Sci.* 2005; 102:2567-2572.
- 1044 28. Stackebrandt E, et al. Report of the ad hoc committee for the reevaluation of the species
1045 definition in bacteriology. *Int. J. Syst. Evol. Microbiol.* 2002;52:1043-1047.

104529. Gopikrishnan V, et al. Quercetin from marine derived *Streptomyces fradiae* PE7:
1046 Taxonomy, fermentation, antifouling activity and characterization. *Environ. Sci. Pollut. Res.*
1047 *Int.* 2016; 23:13832-13842.
104830. Pazhanimurugan R, et al. Terpenoid bioactive compound from *Streptomyces rochei* (M32):
1049 Taxonomy, fermentation and biological activities. *World. J. Microbiol. Biotechnol.* 2016;31:
1050 161.
105131. Manteca A, et al. Mycelium differentiation and antibiotic production in submerged cultures
1052 of *Streptomyces coelicolor*. *Appl. Environ. Microbiol.* 2008;74:3877-3886.
105332. Shomura T, et al. Studies on actinomycetales producing antibiotics only on agar culture I.
1054 Screening, taxonomy and morphological productivity relationship of *Streptomyces halstedii*
1055 strain SF-1993. *J. Antibiot.* 1979; 32:427-435.
105633. Mayurama HB, et al. A new antibiotic, fumaridmycin. I. Production, biological properties
1057 and characterization of producer strain. *J. Antibiot.* 1975;28:636-647.
105834. Ohnishi Y, et al. Structures of Grixazone A and B, A-factor dependent yellow pigments
1059 produced under phosphate depletion by *Streptomyces griseus*. *J. Antibiot.* 2004;57:218-223.
106035. Conti F, De Santis P. Conformation of Actinomycin D. *Nature.* 1970; 227:191239-1241.
1061
106236. Ulrich Hollstein, Actinomycin. Chemistry and Mechanism of Action, Chemical Reviews,
1063 1974, 74;6.625-652.
1064
106537. AB. Mauger, WA. Thomas, NMR Studies of Actinomycins Varying at the Proline Sites,
1066 ORGANIC MAGNETIC RESONANCE, 1981;17:3,1981.
1067
106838. Yu C, Tseng YY. NMR study of the solution conformation of actinomycin D. *Eur. J.*
1069 *Biochem.* 1992; 209:181-187. <https://doi.org/10.1111/j.1432-1033.1992.tb17275.x>.
1070
107139. Shigehiro K, Fusao T. Multiple Binding Modes of Anticancer Drug Actinomycin D: X-ray,
1072 Molecular Modeling, and Spectroscopic Studies of d (GAAGCTTC)₂-Actinomycin D
1073 Complexes and Its Host DNA, *J. Am. Chem. Soc.* 1994;116:41544-165.
1074
107540. Helmut L, Isabel B, Nobuharu S, Lewis KP, Anthony B. Mauger. Structures of Five
1076 Components of the Actinomycin Z Complex from *Streptomyces fradiae*, Two of Which
1077 Contain 4-Chlorothreonine. *J. Nat. Prod.* 2000; 63:352-356.
1078
107941. Jens B, Victoria G, Axel Z, Actinomycins with Altered Threonine Units in the $\hat{\alpha}$ -
1080 Peptidolactone, *J. Nat. Prod.* 2006;69:1153-1157.
1081

108242. Bitzer J, Streibel M, Langer, HJ, Grond S. First Y-type actinomycins from *Streptomyces*
1083 with divergent structure-activity relationships for antibacterial and cytotoxic properties. *Org.*
1084 *Biomol. Chem.* 2009; 7:444–450.
1085
108643. Lackner H, Bahner I, Shigematsu N, Pannell LK, Mauger, AB. Structures of five
1087 components of the actinomycin Z complex from *Streptomyces fradiae*, two of which contain
1088 4-chlorothreonine. *J. Nat. Prod.* 2000; 63:352–356. <https://doi.org/10.1021/np990416u>.
1089
109044. Caixia C, Fuhang S, Qian W, Wael M, Abdel M, HuiGuo, Chengzh F, Weiyuan H,
1091 Huanqin D, Xueting L, Na Yang, FengXie, Ke Yu, Ruxian Chen, Lixin Zhang, A marine-
1092 derived *Streptomyces* sp. MS449 produces high yield of actinomycin X2 and actinomycin D
1093 with potent anti-tuberculosis activity. *Appl Microbiol Biotechnol.* 2012; 95:919–927.
1094
109545. Xiaoling W, Jioji Tabudravu Mostafa Ezzat Rateb, Krystal JA, Zhiwei Q, Marcel J, Zixin D,
1096 Yi Yband, Hai D, Identification and characterization of the actinomycin G gene cluster in
1097 *Streptomyces iakyrus*. *Mol. BioSyst.* 2013; 9:1286—1289.
1098
109946. Xiufang Zhang, Xuwei Ye, Weiyun Chai, Xiao-Yuan Lian, and Zhizhen Zhang, New
1100
110147. Metabolites and Bioactive Actinomycins from Marine-Derived *Streptomyces* sp. ZZ338,
1102 *Mar. Drugs* 2016;14:181.
110348. Machushynets, NV, Elsayed, SS, Du C. et al. Discovery of actinomycin L, a new member
1104 of the actinomycin family of antibiotics. *Sci Rep* 2022; 12:2813.
1105 <https://doi.org/10.1038/s41598-022-06736-0>.
1106
110749. Wang Q, Zhang Y, Wang M. et al. Neo-actinomycins A and B, natural actinomycins
1108 bearing the 5H-oxazolo[4,5-b] phenoxazine chromophore, from the marine-derived
1109 *Streptomyces* sp. IMB094. *Sci Rep.* 2017; 7: 3591. [https://doi.org/10.1038/s41598-017-](https://doi.org/10.1038/s41598-017-03769-8)
1110 03769-8.
1111
111250. Qureshi KA, Bholay, AD, Rai PK. et al. Isolation, characterization, anti-MRSA evaluation,
1113 and in-silico multi-target anti-microbial validations of actinomycin X2 and actinomycin D
1114 produced by novel *Streptomyces smyrnaeus* UKAQ_23. *Sci Rep.* 2021; 11:14539.
1115 <https://doi.org/10.1038/s41598-021-93285-7>.
1116
111751. Zhang Z, Peng G, Yang G, Xiao CL, Hao XQ (2009) Isolation, purification, identification
1118of structures and study of bioactivity of anti-TB active component 9005B. *Chin J Antibiot*
111934:399–402.
1120
112152. Roboz, J Nieves E, Holland JF. McCamish, M, Smith C. Collisional Activation
1122 Decomposition of Actinomycins Using Tandem Mass Spectrometry *BIOMEDICAL AND*
1123 *ENVIRONMENTAL MASS SPECTROMETRY*, 1988;16:67-70.
1124

112553. Darren T, Michael M, Jonathan M. Curtis R, K. Boyd K, Fragmentation Mechanisms of
1126 Protonated Actinomycins and Their Use in Structural Determination of Unknown
1127 Analogues, *JOURNAL OF MASS SPECTROMETRY*.1995;30:1111-1125.
- 1128 54. Rebecca H. Wills, Peter BO. Connor Structural Characterization of Actinomycin D
1129 Using Multiple Ion Isolation and Electron Induced Dissociation *J. Am. Soc. Mass Spectrom.*
1130 2014; 25:186Y195.
- 1131 55. Benzel J, Bajraktari-Sylejmani, G. Uhl, P. Davis A, Nair S, Pfister SM, Haefeli WE,
1132 Weiss J, Burhenne J, Pajtler, KW. Sauter M. Investigating the Central Nervous System
1133 Disposition of Actinomycin D: Implementation and Evaluation of Cerebral Microdialysis and
1134 Brain Tissue Measurements Supported by UPLC-MS/MS Quantification. *Pharmaceutics*
1135 2021; 13:1498. <https://doi.org/10.3390/pharmaceutics13091498>.
- 1136 56. Vater J, Crnovčić I, Semsary S, Keller U. MALDI-TOF mass spectrometry, an efficient
1137 technique for in situ detection and characterization of actinomycins. *J Mass Spectrom.* 2014
1138 ;49(3):210-22. doi: 10.1002/jms.3329. PMID: 24619547.
- 1139 57. Crnovčić I, Vater, J. Keller, U. Occurrence and biosynthesis of C-demethylactinomycins
1140 in actinomycin-producing *Streptomyces chrysomallus* and *Streptomyces parvulus*. *J Antibiot,*
1141 2013;66:211–218. <https://doi.org/10.1038/ja.2012.120>.
114258. Singh, M. P. *et al.* Mannopectimycins, new cyclic glycopeptide antibiotics produced by
1143 *Streptomyces hygroscopicus*LL-AC98: Antibacterial and mechanistic activities. *Antimicrob.*
1144 *Agents Chemother.*2003;47:62-69.
114559. Maskey. R. P. *et al.* Chandranainmycins A-C: Production of novel anticancer antibiotics
1146 from a marine *Actinomadura sp.* Isolate M)-48 by variation of medium composition and
1147 growth conditions. *J. Antibiot.* 2003; 57:1-7.
114860. Marfey, P. Determination of D-amino acids. II. Use of a bifunctional reagent, 1,5-difluoro-
11492,4-dinitrobenzene. *Carlsberg Res. Commun.* 1984; 49:59. <https://doi.org/10.1007/BF02908688>.
1150
115161. Kochhar S. and Christen P. Amino acid analysis by high-performance liquid
1152chromatography after derivatization with 1-fluoro-2, 4-dinitrophenyl-5-L-ala-nine amide. *Anal.*
1153*Biochem.* 1989; 178:17–21.
1154
115562. Goodlett DR, Abuaf PA, Savage PA, Kowalski K.A, Mukherjee TK. Tolan JW., et al.
1156Peptide chiral purity determination: hydrolysis in deuter-ated acid derivatization with Marfey's
1157reagent and analysis using high-performance liquid chromatography-electrospray ionization-
1158mass spectrometry. *J. Chromatog.* 1995; A707:233–244.
1159
116063. Ken-ichi H, Kiyonaga F, Tsuyoshi M, Yasuko H, Makoto S, Yoshitomo I, Hisao O, A
1161method usingL/CMS for determination of absolute configuration of constituent amino acids in
1162peptide --- advanced Marfey's method.,*Tetrahedron Letters*, 1995;36:9,1515-1518.
1163

116464. Ayon NJ, Sharma AD, Gutheil WG. LC-MS/MS-Based Separation and Quantification of
1165Marfey's Reagent Derivatized Proteinogenic Amino Acid DL-Stereoisomers. *J Am Soc Mass*
1166*Spectrom.* 2019;30(3):448-458.
1167
116865. Global tuberculosis report 2022. Geneva: World Health Organization; 2022. Licence: CC
1169 BY-NC-SA 3.0 IGO.
117066. Chiarelli, L. R. *et al.* A multi target approach to drug discovery inhibiting *Mycobacterium*
1171 *tuberculosis* PyrG and PanK. *Nature Sci. Rep.* 2018;8;3187.
117267. Heo, J. *et al.* High-content screening of raw actinomycete extracts for the identification of
1173 antituberculosis activities. *SLAS Discovery.* 2017; 22:144-154.
117468. Bu Y. Y. *et al.* Anti-mycobacterial nucleoside antibiotics from a marine-derived
1175 *Streptomyces* sp. TPU1236A. *Mar. Drugs.* 2014;12: 6102-6112.
1176
117769. Chen, C. *et al.* A marine-derived *Streptomyces* sp. MS449 produces high yield of
1177 actinomycin X2 and actinomycin D with potent anti-tuberculosis activity. *Appl. Microbiol.*
1178 *Biotechnol.* 2012;**95**:
117970. Dalton JP, *et al.* Effect of common and experimental anti-tuberculosis treatments on
1180 *Mycobacterium tuberculosis* growing as biofilms. *Peer J.* 2016;4: e2717.
118171. Narendran G, Swaminathan, S. TB–HIV co-infection: a catastrophic comradeship. *Oral*
1182 *Dis.*2016; 22:46–52.
118372. Xu LH, *et al.* Actinomycete Systematics – Principles, Methods, and Practice. Science Press:
1184 Beijing (2007).
118573. Bauer AW, Kirby, WMM. Antibiotic susceptibility testing by a standardized single disc
1186 method. *American J. Clin. Pathol.* 1966; 45:493-496.
118774. Stanek JL, Roberts GD. Simplified Approach to Identification of Aerobic Actinomycetes
1188 by Thin-Layer Chromatography. *Appl. Microbiol.*1974;28:226-231.
118975. Kimura MA, simple method for estimating evolutionary rates of base substitutions through
1190 comparative studies of nucleotide sequences. *J. Mol. Evol.*1980;16:111–120.
119176. Eccleston GP, *et al.* The occurrence of bioactive micromonosporae in aquatic habitats of the
1192 Sunshine Coast in Australia. *Mar. Drugs.*2008;6: 243–261.
119377. Radhakrishnan M, *et al.* Preliminary screening for antibacterial and antimycobacterial
1194 activity of actinomycetes from less explored ecosystems. *World J. Microbiol.*
1195 *Biotechnol.*2010;26:561-566.

119678. Harindran J, et al. HA-1-92, A new antifungal antibiotic produced by *Streptomyces* CDRIL-
1197 312: fermentation, isolation, purification and biological activity. *World J. Microbiol.*
1198 *Biotechnol.*1999;15:425-430.

119979. Augustine SK, et al. A non-polyene antifungal antibiotic from *Streptomyces albidoflavus* PU
1200 23. *J. Biosciences.* 2005:30201-211.

120180. Ojha AK, et al. Growth of *Mycobacterium tuberculosis* biofilms containing free mycolic
1202 acids and harbouring drug-tolerant bacteria. *Mol. Microbiol.*2008;69:164–174.

120381. Arumugam, G.S., et al. Significant perspectives on various viral infections targeted antiviral
1204 drugs and vaccines including COVID-19 pandemicity. *Mol Biomed* **3**, 21 (2022).
1205 <https://doi.org/10.1186/s43556-022-00078-z>

120682. Mondal R, et al. (2023) In-vivo studies on Transitmycin, a potent *Mycobacterium*
1207 *tuberculosis* inhibitor. PLoS ONE 18(3): e0282454.
1208 <https://doi.org/10.1371/journal.pone.0282454>.

1209

1210

1211

1212

1213

1214

1215

1216

1217

1218

1219

1220

1221

1222

1223

1224

1225

Discovery of a novel antibiotic, Transitmycin, from *Streptomyces* sp unveils highly efficient activities against tuberculosis and human immunodeficiency virus

Vanaja Kumar*^{1,4}, Balagurunathan Ramasamy², Mukesh Doble ^{§3,5}, Radhakrishnan Manikkam⁴, Luke Elizabeth Hanna¹, Gandarvakottai Senthilkumar Arumugam^{3,7}, Kannan Damodharan³, Suresh Ganesan³, Azger Dusthakeer¹, Precilla Lucia¹, Shainaba A Saadhali¹, Shanthi John², Poongothai Eswaran², Selvakumar Nagamiah¹, Jaleel UCA⁶, Rakhila M⁶, Ayisha Safeeda⁶ and Sathish S⁶

¹National Institute for Research in Tuberculosis, Chennai – 600031, Tamilnadu, India

²Department of Microbiology, Periyar University, Salem – 636011, Tamilnadu, India

³Department of Biotechnology, Indian Institute of Technology, Madras – 600036, Tamilnadu, India

⁴Centre for Drug Discovery and Development, Sathyabama Institute of Science and Technology

(Deemed to be University), Chennai – 600119, Tamilnadu. India

⁵ Saveetha Dental College and Hospitals, 62, Poonamallee High Rd, Chennai, 600077, India

⁶ Open Source Pharma Foundation-National Institute of Advanced Studies Drug Discovery Lab, NIAS, IISc Campus, Bangalore, Karnataka, India

⁷SSS International Drug Discovery & Development Research Private Limited, Innovation & Entrepreneurship, Sudha & Shankar innovation hub, IIT Madras,-600036
Chennai, India

Email: *vanaja_kumar51@yahoo.co.in; § mukeshdoble.sdc@saveetha.com

Corresponding Author:

Dr. Vanaja Kumar

Former Scientist G & Head

Department of Bacteriology

¹National Institute for Research in Tuberculosis,

Chennai – 600 031. Tamil Nadu. India

Email: vanaja_kumar51@yahoo.co.in

Supplementary Information

	Title	Page Number
S-Table 1.	Phenotypic characteristics of Streptomyces sp. R2	S10
S-Table 2.	Effect of solvents on the extraction of Transitmycin	S11
Figure S1	Characteristic microbial strain and its morphological arrangement	S12
Figure S1a	(a) TLC of Ethyl acetate extract of Streptomyces sp R2 in UV light (b) Long UV (c) Short UV	S13
Figure S2.	Purification of EA extract of Streptomyces sp. R2 by Preparative Thin-Layer Chromatography	S14
Figure S3.	Scheme of purification of EA extract of Streptomyces sp. R2 by Column Chromatograph	S15
Figure S4.	RP HPLC of the ethyl acetate extract of Streptomyces sp. R2 (Batch II)	S16
Figure S5.	Purity of Transitmycin R1, R2, R3 were checked by RP HPLC method	S17
S-Table 3.	HPLC Retention time of R1, R2, R3	S17
Figure S6.	UV/Vis Spectrum of R2 in methanol	S18
Figure S7.	UV/Vis Spectrum of R3 in methanol	S19
Figure S8.	Circular Dichroism Spectrum of Transitmycin (R1) in methanol	S20
Figure S9.	Circular Dichroism Spectrum of R2 in methanol	S21
Figure S10.	Circular Dichroism Spectrum of R3 in methanol	S22
Figure S11.	FT-IR Spectrum of Transitmycin (R1), R2, R3	S23
Figure S12.	FT-IR Spectrum of R2	S24
Figure S13.	FT-IR Spectrum of R3	S25
Table S4.	IR Absorption Frequencies of Functional Groups Present in R1, R2, R3	S26
Figure S14.	¹ H-NMR (500 MHz, CDCl ₃) Spectrum of Transitmycin (R1)	S27
Figure S15.	Expansion of ¹ H-NMR (500 MHz, CDCl ₃) Spectrum of Transitmycin (R1)	S28
Figure S16.	Expansion of ¹ H-NMR (500 MHz, CDCl ₃) Spectrum of Transitmycin (R1)	S29
Figure S17.	Expansion of ¹ H-NMR (500 MHz, CDCl ₃) Spectrum of Transitmycin (R1)	S30
Figure S18.	Expansion of ¹ H-NMR (500 MHz, CDCl ₃) Spectrum of Transitmycin (R1)	S31

Figure S19.	^{13}C -NMR (125 MHz, CDCl_3) Spectrum of Transitmycin (R1)	S32
Figure S20.	^{13}C -NMR (125 MHz, CDCl_3) Spectrum of Transitmycin (R1)	S33
Figure S21.	^{13}C -NMR (125 MHz, CDCl_3) Spectrum of Transitmycin (R1)	S34
Figure S22.	^{13}C -NMR (125 MHz, CDCl_3) Spectrum of Transitmycin (R1)	S35
Figure S23.	^{13}C -NMR (125 MHz, CDCl_3) Spectrum of Transitmycin (R1)	S36
Figure S24.	^{13}C -NMR (125 MHz, CDCl_3) Spectrum of Transitmycin (R1)	S37
Figure S25.	^{13}C -NMR (125 MHz, CDCl_3) Spectrum of Transitmycin (R1)	S38
Figure S26.	DEPT135 (125 MHz CDCl_3) Spectrum of Transitmycin (R1)	S39
Figure S27.	COSY (500 MHz) Spectrum of Transitmycin (R1)	S40
Figure S28.	DQF-COSY (500 MHz) Spectrum of Transitmycin (R1)	S41
Figure S29.	Expansion of DQF-COSY (500 MHz) Spectrum of Transitmycin (R1)	S42
Figure S30.	Expansion of DQF-COSY (500 MHz) Spectrum of Transitmycin (R1)	S43
Figure S31.	Expansion of DQF-COSY (500 MHz) Spectrum of Transitmycin (R1)	S44
Figure S32.	Expansion of DQF-COSY (500 MHz) Spectrum of Transitmycin (R1)	S45
Figure S33.	HMBC (500 MHz) Spectrum of Transitmycin (R1)	S46
Figure S34.	Expansion of HMBC (500 MHz, CDCl_3) Spectrum of Transitmycin (R1)	S47
Figure S35.	Expansion of HMBC (500 MHz, CDCl_3) Spectrum of Transitmycin (R1)	S48
Figure S36.	Expansion of HMBC (500 MHz, CDCl_3) Spectrum of Transitmycin (R1)	S49
Figure S37.	Expansion of HMBC (500 MHz, CDCl_3) Spectrum of Transitmycin (R1)	S50
Figure S38.	Expansion of HMBC (500 MHz, CDCl_3) Spectrum of Transitmycin (R1)	S51
Figure S39.	Expansion of HMBC (500 MHz, CDCl_3) Spectrum of Transitmycin (R1)	S52
Figure S40.	Expansion of HMBC (500 MHz, CDCl_3) Spectrum of Transitmycin (R1)	S53
Figure S41.	HSQC (500 MHz, CDCl_3) Spectrum of Transitmycin (R1)	S54
Figure S42.	TOCSY (500 MHz) Spectrum of Transitmycin (R1)	S55
Figure S43.	Expansion of TOCSY (500 MHz, CDCl_3) Spectrum of Transitmycin (R1)	S56

Figure S44.	Expansion of TOCSY (500 MHz, CDCl ₃) Spectrum of Transitmycin (R1)	S57
Figure S45.	Expansion of TOCSY (500 MHz, CDCl ₃) Spectrum of Transitmycin (R1)	S58
Figure S46.	NOESY (500 MHz, CDCl ₃) Spectrum of Transitmycin (R1)	S59
Figure S47.	Expansion of NOESY (500 MHz, CDCl ₃) Spectrum of Transitmycin (R1)	S60
Figure S48.	Expansion of NOESY (500 MHz, CDCl ₃) Spectrum of Transitmycin (R1)	S61
Figure S49.	Expansion of NOESY (500 MHz, CDCl ₃) Spectrum of Transitmycin (R1)	S62
Figure S50.	Expansion of NOESY (500 MHz, CDCl ₃) Spectrum of Transitmycin (R1)	S63
Figure S51.	Expansion of NOESY (500 MHz, CDCl ₃) Spectrum of Transitmycin (R1)	S64
Figure S52.	ROESY (500 MHz) Spectrum of Transitmycin (R1)	S65
Table S5.	NMR data of Transitmycin (R1) in CDCl ₃ (¹ H: 500 MHz ¹³ C: 125 MHz)	S66-72
Figure S53.	¹ H-NMR (500 MHz, CDCl ₃) Spectrum of Compound R2	S73
Figure S54.	¹³ C NMR (125 MHz, CDCl ₃) Spectrum of Compound R 2	S74
Figure S55.	DEPT135&90 (125 MHz CDCl ₃) Spectrum of Compound R2	S75
Figure S56.	Expansion of DEPT135 & 90 (125 MHz, CDCl ₃) Spectrum of Compound R2	S76
Figure S57.	Expansion of DEPT135 & 90 (125 MHz, CDCl ₃) Spectrum of Compound R2	S77
Figure S58.	COSY (500 MHz) Spectrum of Compound R2	S78
Figure S59.	DQF-COSY (500 MHz) Spectrum of Compound R2	S79
Figure S60.	HMBC (500 MHz) Spectrum Compound of R2	S80
Figure S61.	HSQC (500 MHz) Spectrum of Compound R2	S81
Figure S62.	TOCSY (500 MHz) Spectrum of Compound R2	S82
Figure S63.	NOESY (500 MHz) Spectrum of Compound R2	S83
Figure S64.	¹ H-NMR (500 MHz, CDCl ₃) Spectrum of Compound R3	S84
Figure S65.	DQF-COSY (500 MHz) Spectrum of Compound R ₃	S85
Figure S66.	HMBC (500 MHz) Spectrum of Compound R3	S86
Figure S67.	HSQC (500 MHz) Spectrum of Compound R3	S87

Figure S68.	TOCSY (500 MHz) Spectrum of Compound R3	S88
Figure S69.	NOESY (500 MHz) Spectrum of Compound R3	S89
Figure S70.	MALDI-TOF MS Spectrum of Transitmycin (R1) (Molecular ion peak) (positive mode)	S90
Figure S71.	Expansion of MALDI-TOF MS Spectrum of Transitmycin (R1) (Molecular ion peak)	S91
Figure S72.	Expansion of MALDI-TOF MS Spectrum of Transitmycin (R1) (Molecular ion peak)	S92
Figure S73.	MALDI-TOF MS Spectrum of R2 (Molecular ion peak) (positive mode)	S93
Figure S74.	Expansion of MALDI-TOF MS Spectrum of R2 (Molecular ion peak) (positive mode)	S94
Figure S75.	Expansion of MALDI-TOF MS Spectrum of R2 (Molecular ion peak) (Negative mode)	S95
Figure S76.	MALDI-TOF MS Spectrum of R3 (Molecular ion peak) (positive mode)	S96
Figure S77.	MALDI-TOF MS Spectrum of R3 (Molecular ion peak) (Negative mode)	S97
Figure S78.	MALDI-TOF MS Spectrum of Transitmycin (R1) (Positive mode)	S98
Figure S79.	MALDI-TOF MS Spectrum of Transitmycin A (Negative mode)	S99
Table S6.	MALDI-TOF MS Spectral Fragmentation of Transitmycin (R1) (Positive mode)	S100
Figure S80.	MALDI-TOF MS Spectrum of R2 (Positive mode)	S101
Figure S81.	MALDI-TOF MS Spectrum of R2 (Negative mode)	S102
Figure S82.	MALDI-TOF MS Spectrum of R3 (Positive mode)	S103
Figure S83.	MALDI-TOF MS Spectrum of R3 (Negative mode)	S104
Figure S84.	QTRAP MS/MS Transitmycin (R1) (Molecular ion peak) (Positive mode)	S105
Figure S85.	QTRAP MS/MS Transitmycin (R1) (Molecular ion peak $[M+H]^{2+}$) (Positive mode)	S106
Figure S86.	QTRAP MS/MS of Transitmycin (R1) (Molecular ion peak) (Negative mode)	S107
Figure S87.	QTRAP MS/MS of R2 (Molecular ion peak) ((Positive mode)	S108
Figure S88.	QTRAP MS/MS of R2 $[M+H]^{2+}$ ion peak (Positive mode)	S109
Figure S89.	QTRAP MS/MS of R2 (Molecular ion peak) (Positive mode)	S100
Figure S90.	QTRAP MS/MS of R3 Molecular ion peak (Positive mode)	S111
Figure S91.	QTRAP MS/MS of R3 (Molecular ion peak) (Negative mode)	S112
Figure S92.	HR-ESI-MS Spectrum of Transitmycin (R1) (Positive mode)	S113
Figure S93.	HR-ESI-MS Spectrum of Transitmycin (R1) (Molecular ion Peak) (Positive mode)	S114

Figure S94.	HR-ESI-MS Spectrum of R2 (Positive mode)	S115
Figure S95.	HR-ESI-MS Spectrum of R2 (Molecular ion Peak) (Positive mode)	S116
Figure S96.	HR-ESI-MS Spectrum of R3 (Positive mode)	S117
Figure S97.	HR-ESI-MS Spectrum of R3 (Molecular ion Peak) (Positive mode)	S118
Figure S98.	LC-ESI-MS Spectrum of Transitmycin (R1) (Molecular ion peak) (Positive mode)	S119
Figure S99.	LC-ESI-MS Spectrum of Transitmycin (R1) (Positive mode).	S120
Figure S100.	LC-ESI-MS Spectrum of Trasitmycin (R1) (Positive mode)	S121
Figure S101.	LC-ESI-MS Spectrum of Trasitmycin (R1) (Positive mode)	S122
Figure S102.	LC-ESI-MS Spectrum of R2 (Positive mode)	S123
Figure S103.	LC-ESI-MS Spectrum of R2 (Molecular ion) (Positive mode)	S124
Figure S104.	LC-ESI-MS Spectrum of R3 (Positive mode).	S125
Figure S105.	LC-ESI-MS Spectrum of R3 (Positive mode)	S126
Figure S106.	EI-MS Spectrum of Transitmycin (R1) (Positive mode)	S127
Figure S107.	EI-MS Spectrum of (R1) (molecular ion peak) (Positive mode)	S128
Figure S108.	EI-MS Spectrum of (R2) (Positive mode)	S129
Figure S109.	EI-MS Spectrum of (R3) (Positive mode)	S130
Figure S110.	CHN analysis data of Transitmycin (R1), R2, R3	S131
Figure S111.	3200 QTRAP LC/MS/MS Spectrum of Transitmycin (R1) (Negative mode)	S132
Figure S112.	3200 QTRAP LC/MS/MS Spectrum of Transitmycin (R1) (positive mode)	S133
Figure S113.	3200 QTRAP LC/MS/MS Spectrum of Transitmycin (R1) (positive mode)	S134
Figure S114.	3200 QTRAP LC/MS/MS Spectrum of Transitmycin (R1) (positive mode)	S135
Figure S115.	3200 QTRAP LC/MS/MS Spectrum of Transitmycin (R1) (positive mode)	S136
Figure S115 a, b	Structural characterisation of Transitmycin (R1) obtained by QTRAP LC-MS/MS	S137
Table S7a.	Structural characterisation of Transitmycin (R1) [M+H] ⁺ obtained by QTRAP LCMS/MS	S138
Table S7b.	Structural characterisation of Transitmycin (R1) [M+Na] ⁺ obtained by QTRAP LCMS/MS	S139
Figure S116.	Hydrolysis of amino acid residue of Transitmycin (R1), R2, R3	S140
Figure S117a.	HPLC analysis of standard L-FDAA-D/L-Valine	S141a

Figure S117b.	HPLC analysis of standard L-FDAA-D-Valine	S141b
Figure S117c.	HPLC analysis of standard L-FDAA-L-Valine	S141c
Figure S118 a.	HPLC analysis of standard L-FDAA-D/L-Proline	S142a
Figure S118 b.	HPLC analysis of standard L-FDAA-D-Proline	S142b
Figure S118c.	HPLC analysis of standard L-FDAA-L-Proline	S142c
Figure S119a.	HPLC analysis of standard L-FDAA-D/L-Threonine	S143a
Figure S119b.	HPLC analysis of standard L-FDAA-D-Threonine	S143b
Figure S119c.	HPLC analysis of standard L-FDAA-D-Threonine	S143c
Figure S120a.	HPLC analysis of standard L-FDAA-D/L-N-Methyl Valine	S144a
Figure S120b.	HPLC analysis of standard L-FDAA-D-N-Methyl Valine	S144b
Figure S120c.	HPLC analysis of standard L-FDAA-D-N-Methyl Valine	S144c
Figure S121a.	HPLC analysis of standard L-FDAA-D-Valine	S145a
Figure S121b.	HPLC analysis of standard L-FDAA-L-Valine	S145b
Figure S121c.	HPLC Analysis of L-FDAA Derivatives of acid hydrolysates of Transitmycin (R1)	S143a
Figure 122a.	HPLC analysis of standard L-FDAA-D-Valine	S143b
Figure S122b.	HPLC analysis of standard L-FDAA-L-Valine	S143c
Figure S122c.	HPLC Analysis of L-FDAA Derivatives of acid hydrolysates of R2	S144a
Figure S123a.	HPLC analysis of standard L-FDAA-D-Valine	S144b
Figure S123b.	HPLC analysis of standard L-FDAA-L-Valine	S144c
Figure S123c.	HPLC Analysis of L-FDAA Derivatives of acid hydrolysates of R3	S145
Figure S124.	HPLC Analysis of L-FDAA Derivatives of acid hydrolysates of R2	S148
Figure S125.	HPLC Analysis of L-FDAA Derivatives of acid hydrolysates of R3	S149
Table 8a.	Analysis of L-FDAA derivates of acid hydrolysate of R2 by HPLC	S150
Table 8b.	Analysis of L-FDAA derivatives of acid hydrolysate of R3 by HPLC	S150
Figure S126.	ESI- MS Spectrum of Marfey's Derivatives of Transitmycin (R1) (Positive mode)	S151
Figure S127.	ESI- MS Spectrum of Marfey's Derivatives of Transitmycin (R1) (Positive mode)	S152
Figure S128.	LCMS analysis of Standard L-FDAA-D-Proline (Positive mode)	S153

Figure S129.	LCMS analysis of Standard L-FDAA-D-Proline (Negative mode)	S154
Figure S130.	LCMS analysis of Standard L-FDAA-L-Proline (Positive mode)	S155
Figure S131.	LCMS analysis of Standard L-FDAA-L-Proline (Negative mode)	S156
Figure S132.	LCMS analysis of Standard L-FDAA-D/L-Proline (Positive mode)	S157
Figure S133.	LCMS analysis of Standard L-FDAA-D/L-Proline (Negative mode)	S158
Figure S134.	LCMS analysis of Standard L-FDAA-D-Valine (Positive mode)	S159
Figure S135.	LCMS analysis of Standard L-FDAA-D-Valine (Negative mode)	S160
Figure S136.	LCMS analysis of Standard L-FDAA-L-Valine (Positive mode)	S161
Figure S137.	LCMS analysis of Standard L-FDAA-L-Valine (Negative mode)	S162
Figure S138.	LCMS analysis of Standard L-FDAA-D/L-Valine (Positive mode)	S163
Figure S139.	LCMS analysis of Standard L-FDAA-D/L-Valine (Negative mode)	S164
Figure S140.	LCMS analysis of Standard L-FDAA-D/L-Valine (Positive mode)	S165
Figure S141.	LCMS analysis of Standard L-FDAA-D/L-Valine (Negative mode)	S166
Figure S142.	LCMS analysis of Standard L-FDAA-D-Threonine (Positive mode)	S167
Figure S143.	LCMS analysis of Standard L-FDAA-D-Threonine (Negative mode)	S168
Figure S144.	LCMS analysis of Standard L-FDAA-D/L Threonine (Positive mode)	S169
Figure S 145.	LCMS analysis of Standard L-FDAA-D/L Threonine (Negative mode)	S170
Figure S146.	LCMS analysis of Standard L-FDAA-D/L N-Methyl valine (Positive mode).	S171
Figure S147.	LCMS analysis of Standard L-FDAA-D/L N-Methyl Valine (Positive mode)	S172
Figure S148.	LCMS analysis of Standard L-FDAA-L N-Methyl valine (Positive mode)	S173
Figure S149.	LCMS analysis of Standard L-FDAA-L- N-Methyl valine (Positive mode)	S174
Figure S150.	LCMS analysis of Standard L-FDAA-L N-Methyl Valine (Positive mode)	S175
Figure S151.	LCMS analysis of Standard L-FDAA-L N-Methyl Valine (Positive mode)	S176
Figure S152.	LCMS analysis of Standard L-FDAA-L N-Methyl Valine (Negative mode)	S177
Figure S153.	LCMS analysis of Standard L-FDAA-D/L N-Methyl Valine (Positive mode)	S178
Figure S154.	LCMS analysis of Standard L-FDAA-L N-Methyl Valine (Positive mode)	S179
Figure S155.	LCMS analysis of Standard L-FDAA-D/L N-Methyl Valine (Positive mode)	S180

Figure S156.	LCMS analysis of Standard L-FDAA-D/L N-Methyl Valine (Negative mode).	S181
Figure S157.	LCMS analysis of Standard L-FDAA-D/L N-Methyl Valine (Negative mode)	S182
Figure S158.	LCMS analysis of Standard L-FDAA-D/L N-Methyl Valine (Negative mode).	S183
Figure S159.	LCMS analysis of L-FDAA derivatives of Transitmycin (R1) (Positive mode)	S184
Figure S160.	LCMS analysis of L-FDAA derivatives of Transitmycin (R1) (Negative mode)	S185
Figure S161.	LCMS analysis of L-FDAA derivatives of R3 (Positive mode)	S186
Table S9a.	Analysis of L-FDAA derivates of acid hydrolysate of Transitmycin R1 by HPLC-MS	S187
Table S9b.	Analysis of L-FDAA derivates of acid hydrolysate of R3 by HPLCMS	S187
Table S10.	Physico-chemical properties of R2	S188-89
Table S11.	Physico-chemical properties of R3	S190-91
Table S12	Drug resistant profile of the clinical isolates of <i>Mycobacterium tuberculosis</i> used to determine the anti TB activity of Transitmycin	S192-194
Table S13	Anti-HIV activity of Transitmycin on various HIV-1 subtypes	S195

S-Table 1. Phenotypic characteristics of *Streptomyces* sp. R2

Characteristics	Results
Micromorphology	
Aerial mycelium	Present
Substrate mycelium	Present
Spore chain morphology	Rectus flexibile, non fragmented
Spore surface	Hairy
Cultural characteristics	
Colony consistency	Powdery
Aerial mass colour	Ash white
Reverse side pigment	Yellow
Soluble pigment	Yellow
Melanoid pigment	Absent
Growth on Different media	
ISP1	Moderate
ISP2	Good
ISP3	Good
ISP4	Good
ISP5	Moderate
ISP6	Moderate
ISP7	Good
Carbon utilization	
Glucose	Good
Arabinose	Poor
Sucrose	Poor
Xylose	Moderate
Inositol	Poor
Mannitol	Good

Fructose	Moderate
Rhamnose	Moderate
Raffinose	No Growth
Cellulose	No Growth
pH tolerance	
5	No growth
7	Good
9	Good
11	Moderate
Growth at	
20 ⁰ C	Poor
30 ⁰ C	Good
40 ⁰ C	Good
50 ⁰ C	Moderate
NaCl tolerance (%)	
0	Poor
1	Good
2.5	Good
5	Good
7.5	Poor
10	No growth
Susceptibility to	Tetracycline, chloramphenicol, erythromycin, gentamicin, vancomycin
Resistant to	Penicillin, nystatin, nalidixic acid

S-Table 2. Effect of solvents on the extraction of Transitmycin

Solvents	Quantity of extracts	Antibacterial activity against <i>S. aureus</i> MTCC 96	Anti TB activity (% reduction in RLU)
Methanol	40	14	58.31
Chloroform	41	9	18.07
Dichloromethane	40	13	22.71
Diethyl ether	10	14	74.23
Ethyl acetate	9	19	83.40
n-hexane	-	-	-

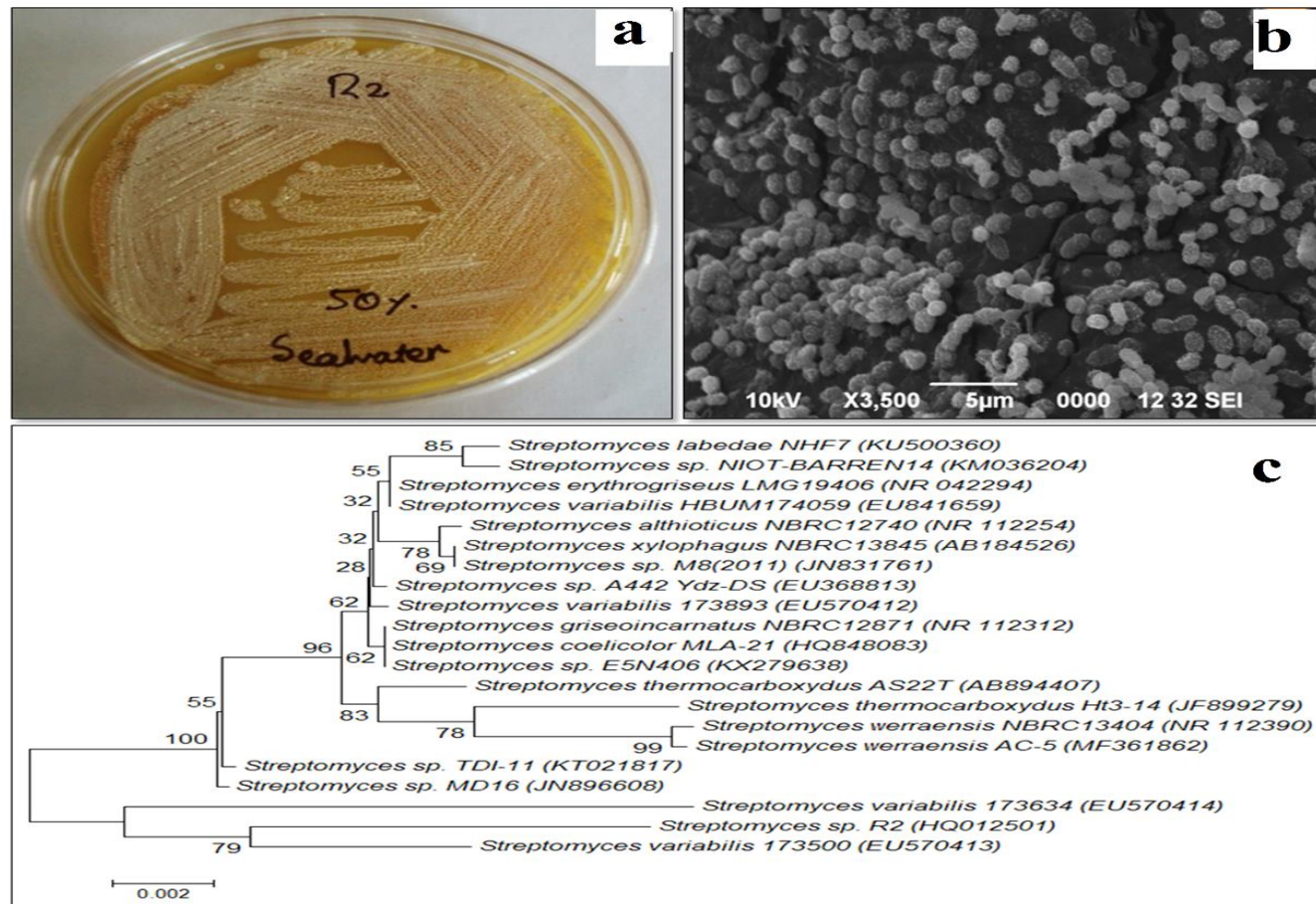
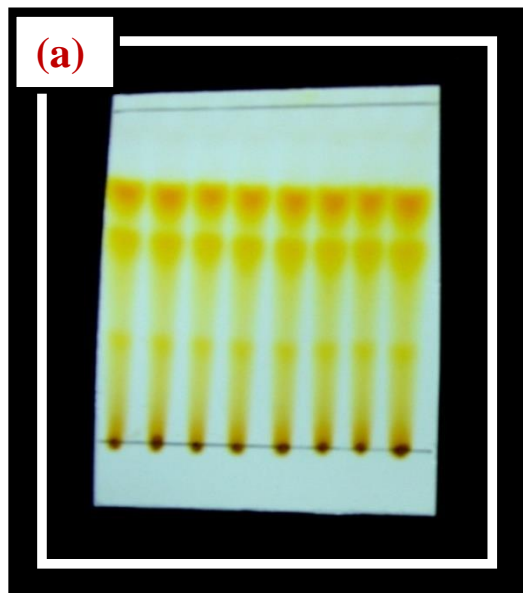
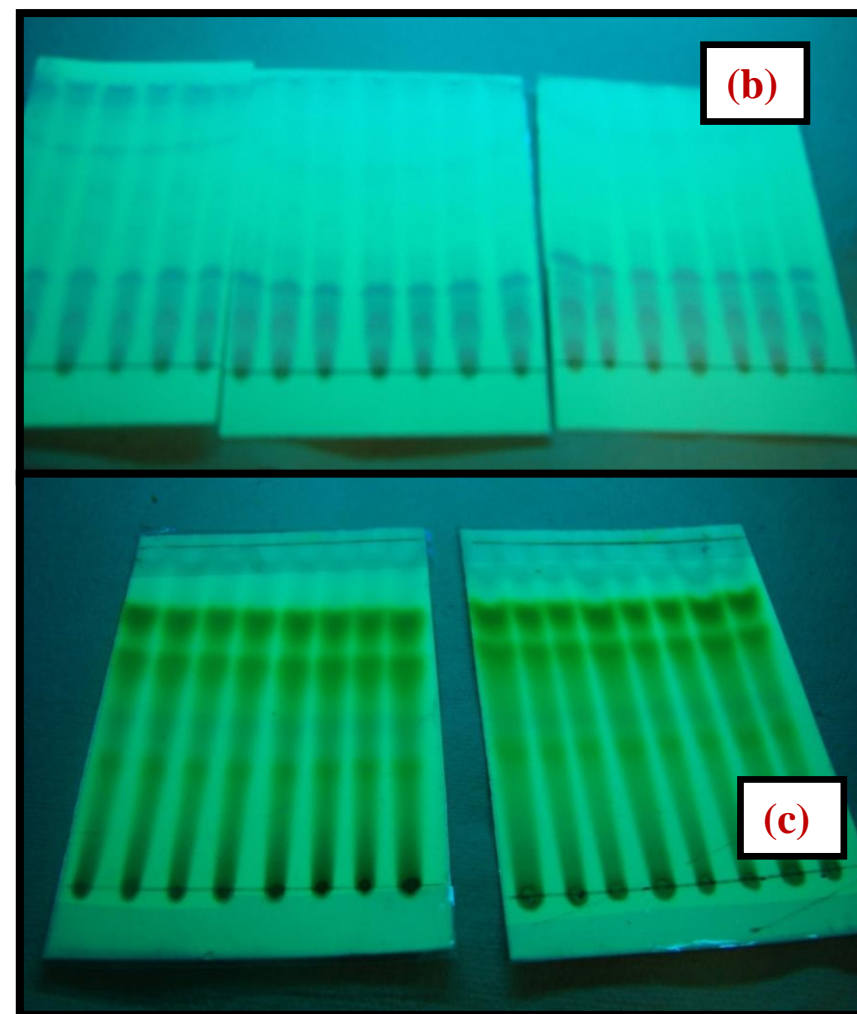


Fig. S1. Characteristic microbial strain and its morphological arrangement. **a** Cultural morphology and microscopic visualization. **b** SEM image (3,500X) of *Streptomyces variabilis* R2 on ISP2 agar medium. **c** Phylogenetic dendrogram obtained by distance matrix analysis of 16s rRNA gene sequences, showing the position of strain R2 among its phylogenetic neighbours.



Transitmycin (R1)
R2
R3



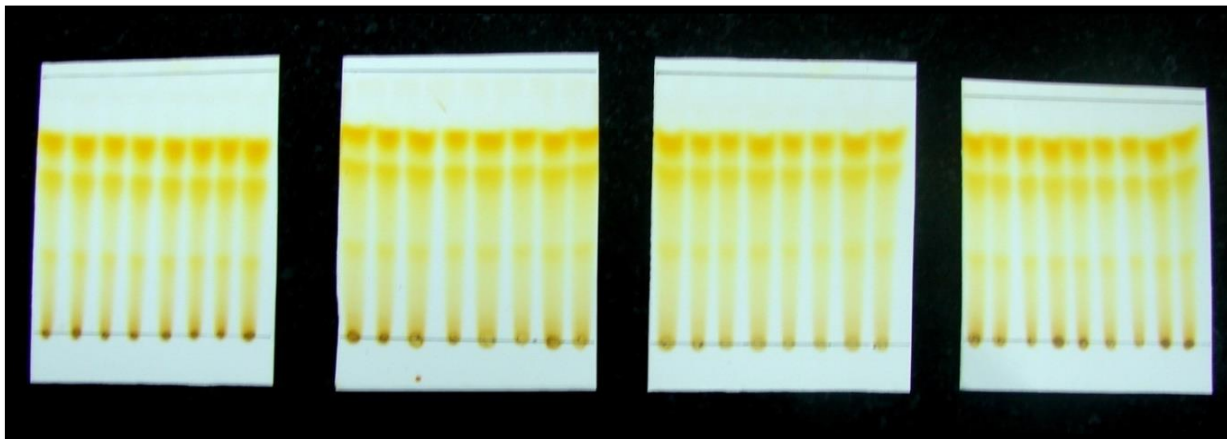
Solvent system for TLC: Ethyl acetate /Methanol, (9.5:0.5)

Rf value of Transitmycin (R1) = 0.8

Rf value of R2 = 0.6

Rf value of R3 = 0.3

Solvent system for TLC: Ethyl acetate/Methanol, (9.5:0.5) (a) TLC of Ethyl acetate extract of Streptomyces sp. R2 in UV light (b) Long UV (c) Short UV

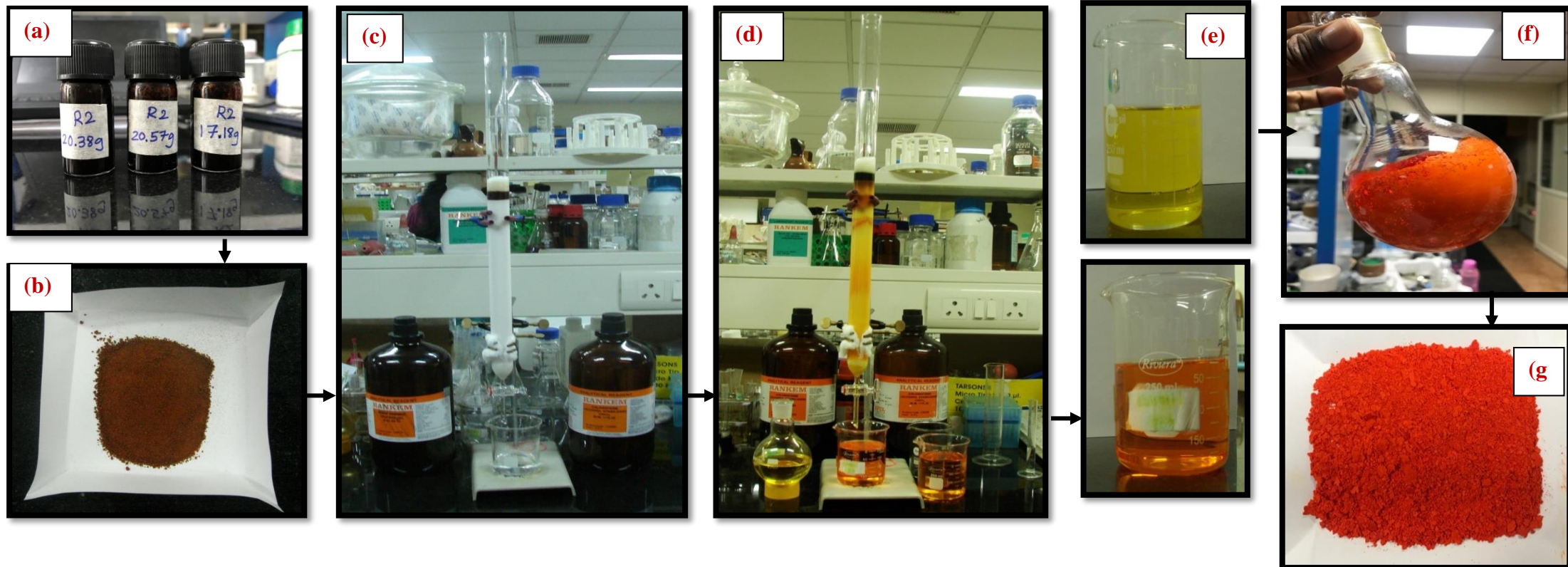


Solvent used for Preparative TLC: Ethylacetate:methanol, (9.5:0.5)

Figure S2. Purification of EA extract of *Streptomyces* sp. R2 by Preparative Thin-Layer Chromatography

Extraction and Isolation

Purification of compounds were performed by preparative thin layer chromatography (TLC) using Merck silica gel 60 (GF254) pre coated aluminium (6x8 cm size) plates. The crude pigment was purified by using preparative thin layer chromatography commercially available pre coated silica gel chromatography sheets (6x8 cm size) were used. To find out the best solvent system to separate the crude compound, the solvents were used in different proportions, among all solvent systems used, Ethylacetate: methanol (9.5:0.5) showed good separation. The crude pigment (2 g) was dissolved in 5 mL of ethyl acetate. With the help of capillary tube, the sample was spotted at the bottom of silica gel coated sheet (6 x 8 cm) and then it was placed in the developing 100 mL beaker containing mobile phase (Ethyl acetate/ Methanol, 9.5:0.5) 5 mL, covered with the watch glass in order to prevent the evaporation of the solvents. The solvent was allowed to run till it reaches about half a centimetre below the top of the plate. After running, the 200 sheets were kept at room temperature for the complete drying of the plate. Spots on TLC were detected under UV light (254 and 365 nm) and by spraying with concentrated H₂SO₄ followed by heating at 105 °C for 5 min. After drying, the yellow pigment spot was scrapped, mixed with ethyl acetate and filtered using funnel fitted with what man filtered paper and Ethyl acetate was evaporated to dryness under vacuum to afford the pure compound Transitmucin R1 (10 mg), R 2 (10 mg), R3 (5 mg). R_f value of the spot separated on the TLC plate was determined. The solvent system Ethyl acetate: methanol (9.5:0.5) was found to have good separation with single spot when compared to all the solvent systems used for TLC.



Column chromatography was carried out on Neutral Alumina (230-400 mesh) and Column size: (id 30m × 90 cm). The crude ethyl acetate extract *Streptomyces* sp (R2) was purified using column chromatography packed with neutral alumina using a gradient of 1% Methanol/Chloroform mixture (CH₃OH/ CHCl₃) was used as the eluent. Fractions were collected and concentrated under vacuum to afford pure compounds. The desired product was monitored in a TLC with pre coated alumina sheet silica. The isolated compounds were obtained Transimycin (R1) (200 mg), R2 (100 mg), R3 (50 mg).

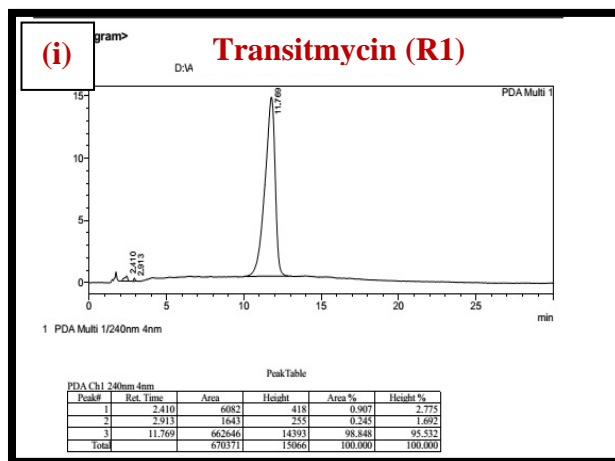


Figure S3 (a) Crude (b) Crude with alumina (c) Before elution (d) After elution (e) solution form (f) solid form (g) After drying (h) TLC (i) RP-HPLC

S61

Figure S3. Scheme of purification of EA extract of *Streptomyces* sp. R2 by column chromatography

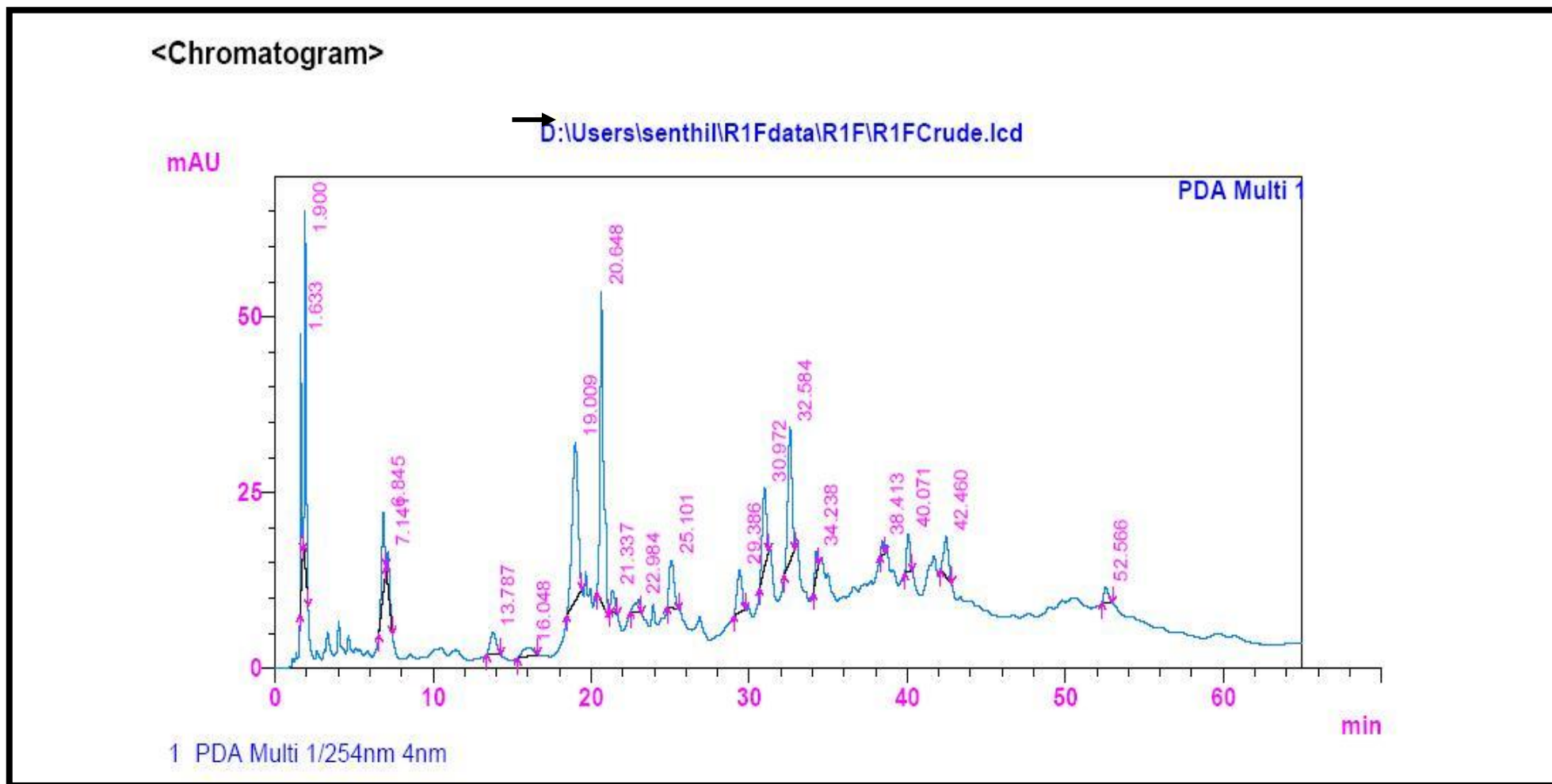
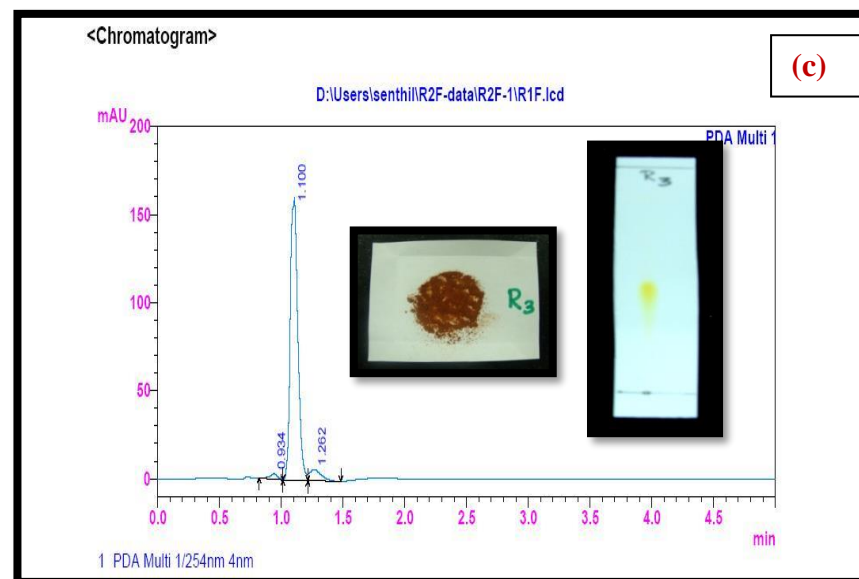
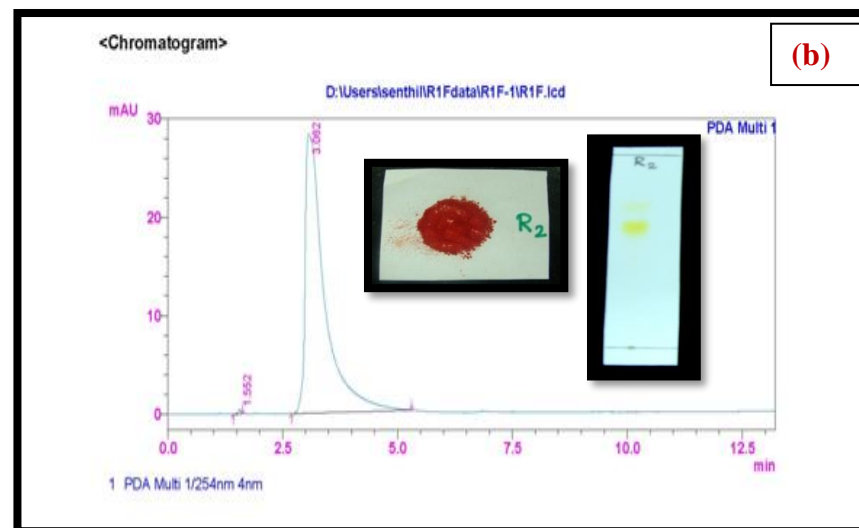
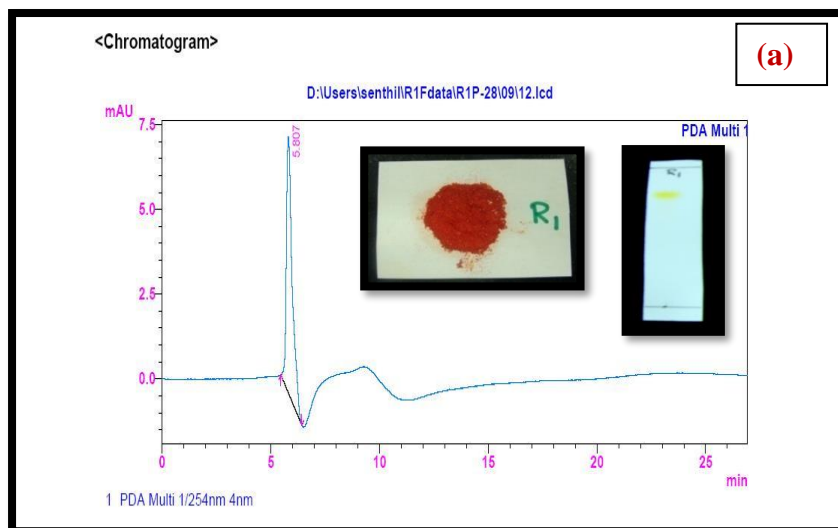


Figure S4. RP HPLC of the crude ethyl acetate extract of *Streptomyces sp. R2 (Batch II)* Analytical HPLC condition: Luna 5u C₁₈ (2) 100 (150 X 4.6 mm) Solvent system: A: B (35: 65 v/v); flow rate 2 ml/min, 254 nm Solvent A: Acetonitrile; Solvent B: Water, Detection: PDA, Injection volume: 20µl, Column Temperature: 30 °C



S-Table 3. RP-HPLC Retention time of R1, R2, R3

a	Ret. Time of R1	5.807 min
b	Ret. Time of R1	3.062 min
c	Ret. Time of R2	1.100 min

Figure S5. Purity of Transitmycin R1, R2, R3 were checked by RP HPLC method

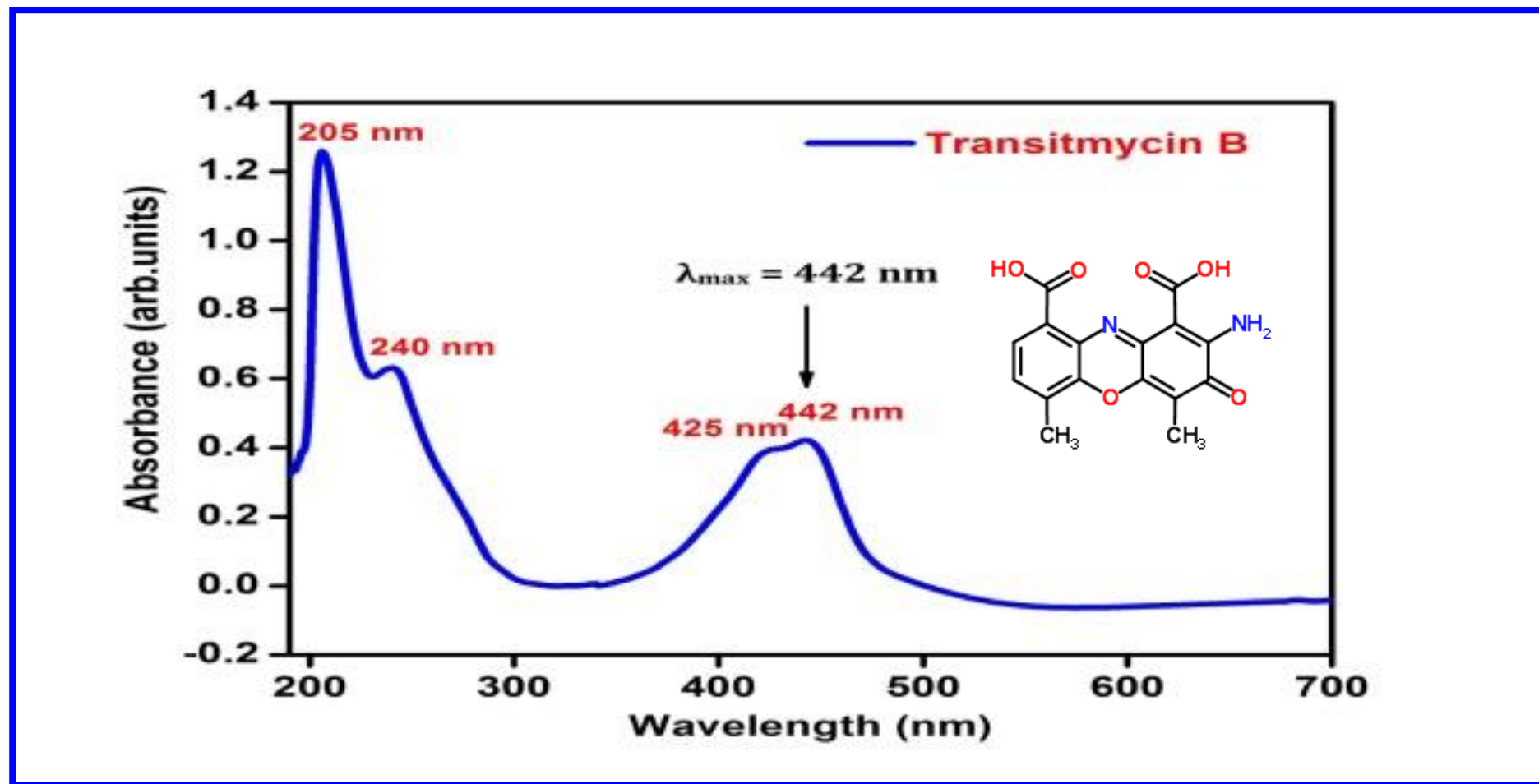


Figure S6: UV/Vis Spectrum of R2 in methanol [UV: (MeOH) λ_{\max} , (log ϵ) 205, (1.25), 240 (0.63), 425 (0.39), 442(0.42) nm]

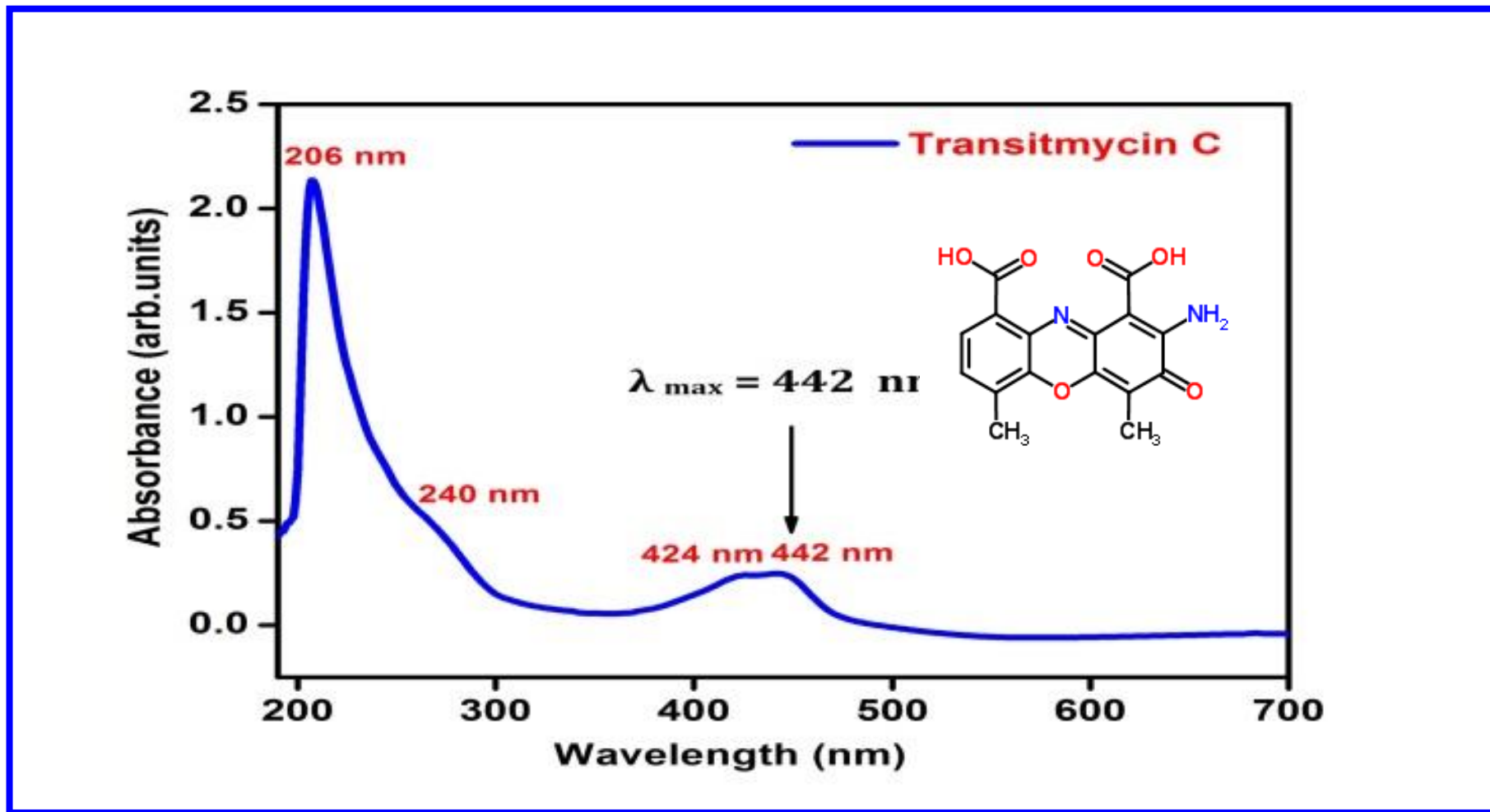


Figure S7. UV/Vis Spectrum of R3 in methanol [UV (MeOH) λ_{\max} (log ϵ) 206 (1.90), 240 (0.69) 424 (0.191), 442.2 (0.19) nm]

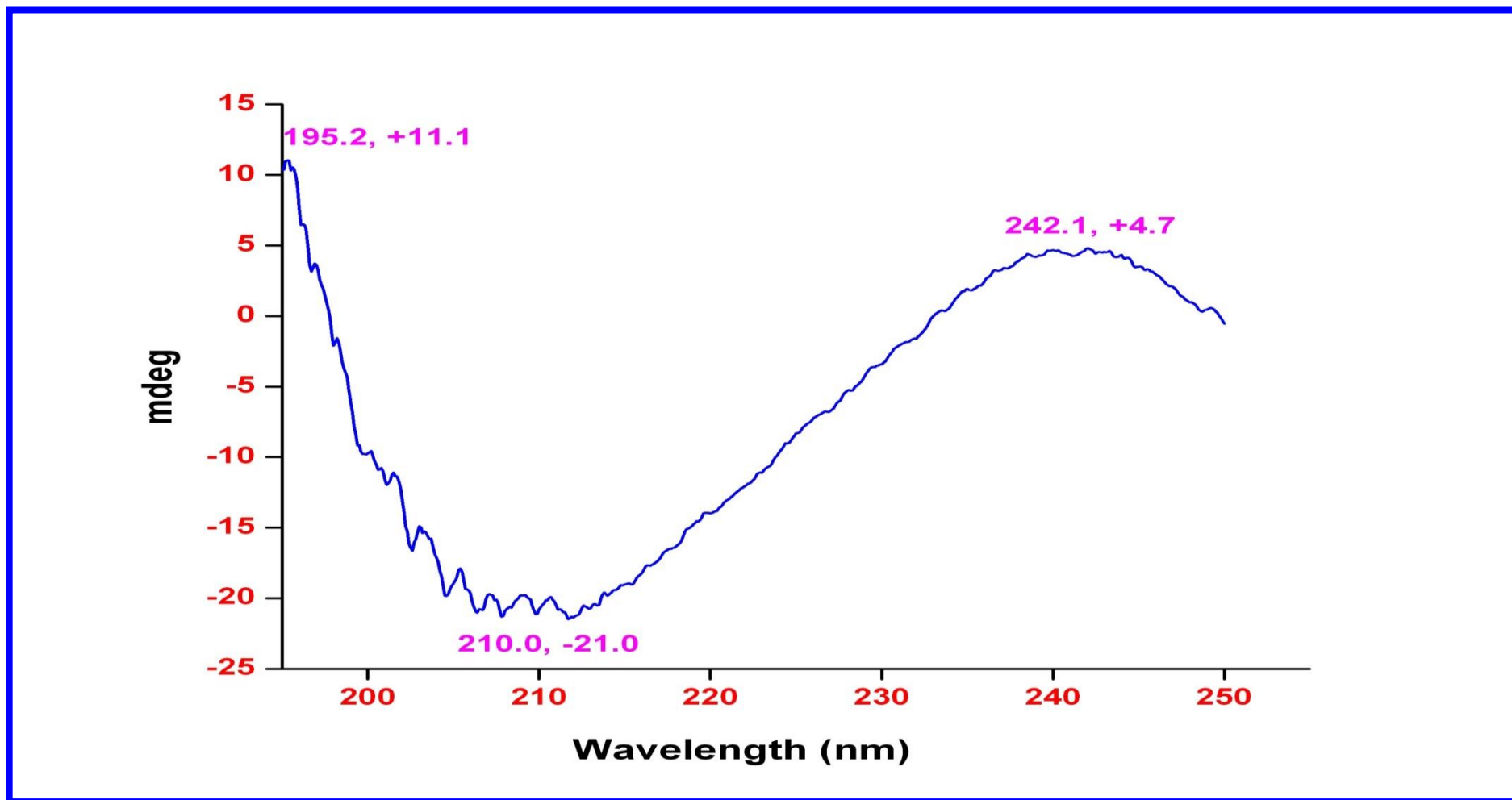


Figure S8. Circular Dichroism Spectrum of Transitmycin (R1) in methanol CD: [MeOH, [nm], (mdeg)]: $\lambda_{\max}(\Delta\epsilon)$ 195 (+11.1), 210 (-21.0), 242 (+4.7)

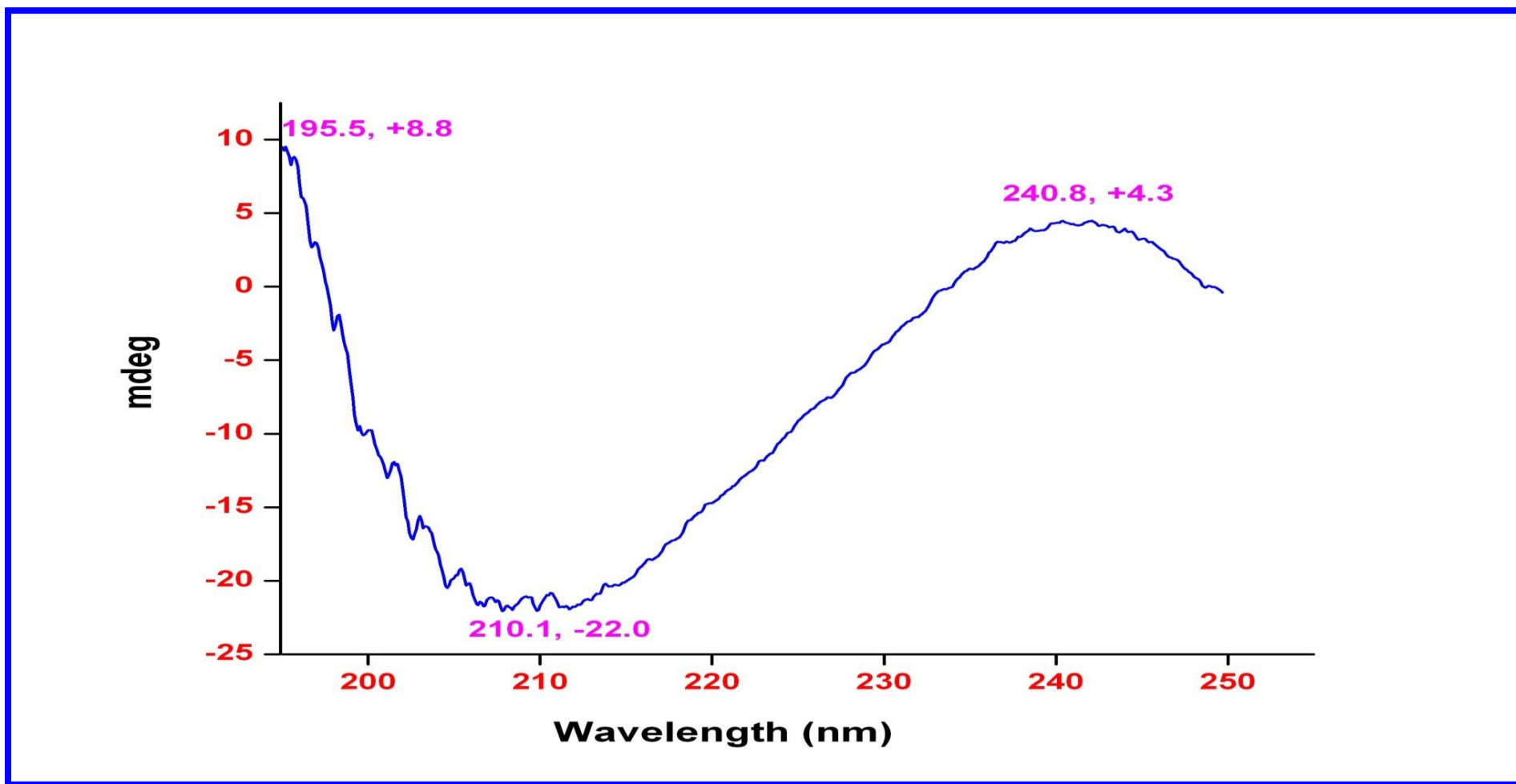


Figure S9. Circular Dichroism Spectrum of R2 in methanol CD: [MeOH, [nm], (mdeg)]: λ_{\max} , ($\Delta\epsilon$) 195 (+8.8), 210 (-22.0), 240 (+4.3) nm

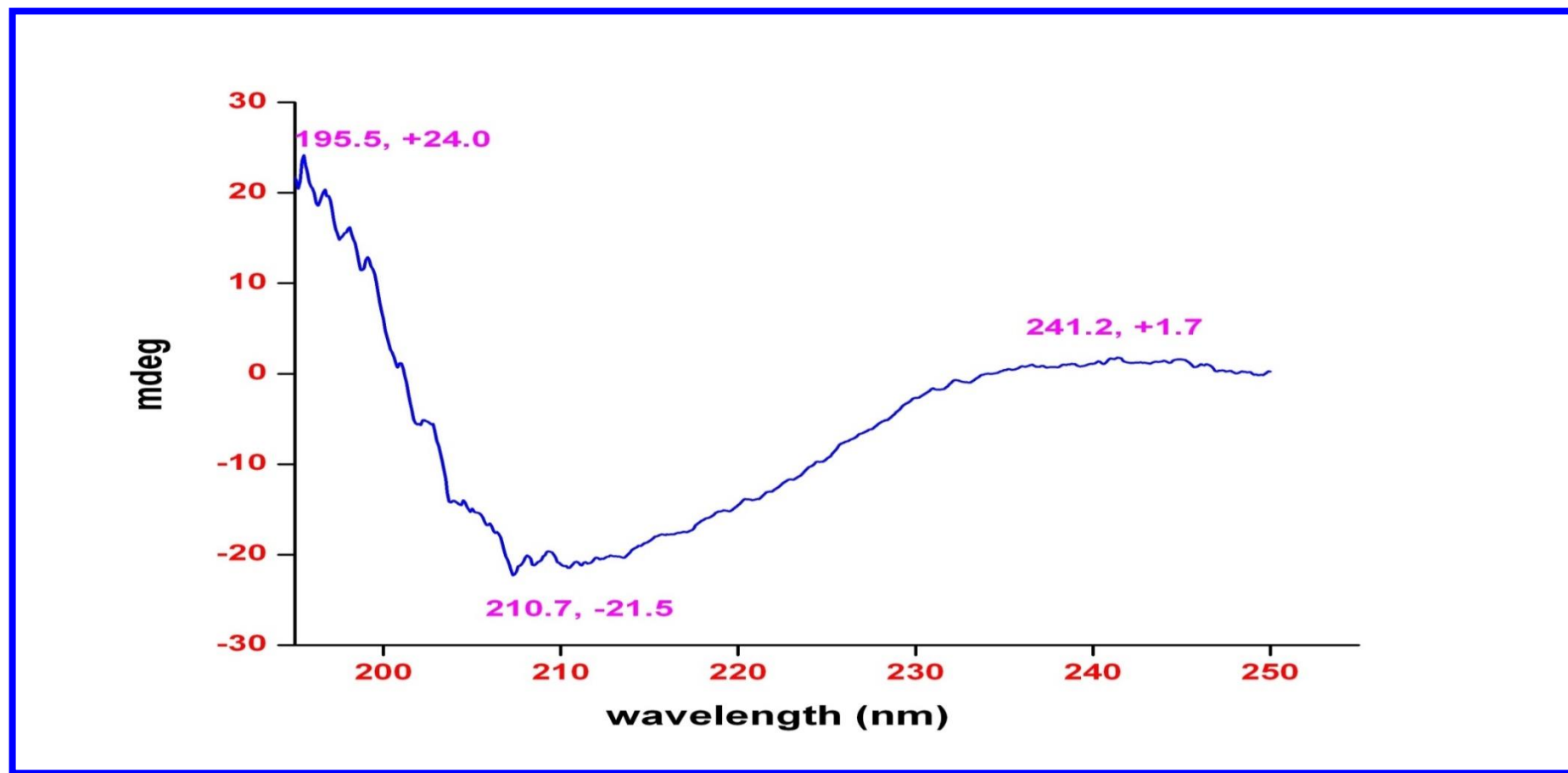


Figure S10. Circular Dichroism Spectrum of R3 in methanol CD: [MeOH, [nm], (mdeg)] $\lambda_{\max}(\Delta\epsilon)$ 195 (+24.0), 210 (-21.5), 241 (+1.7)

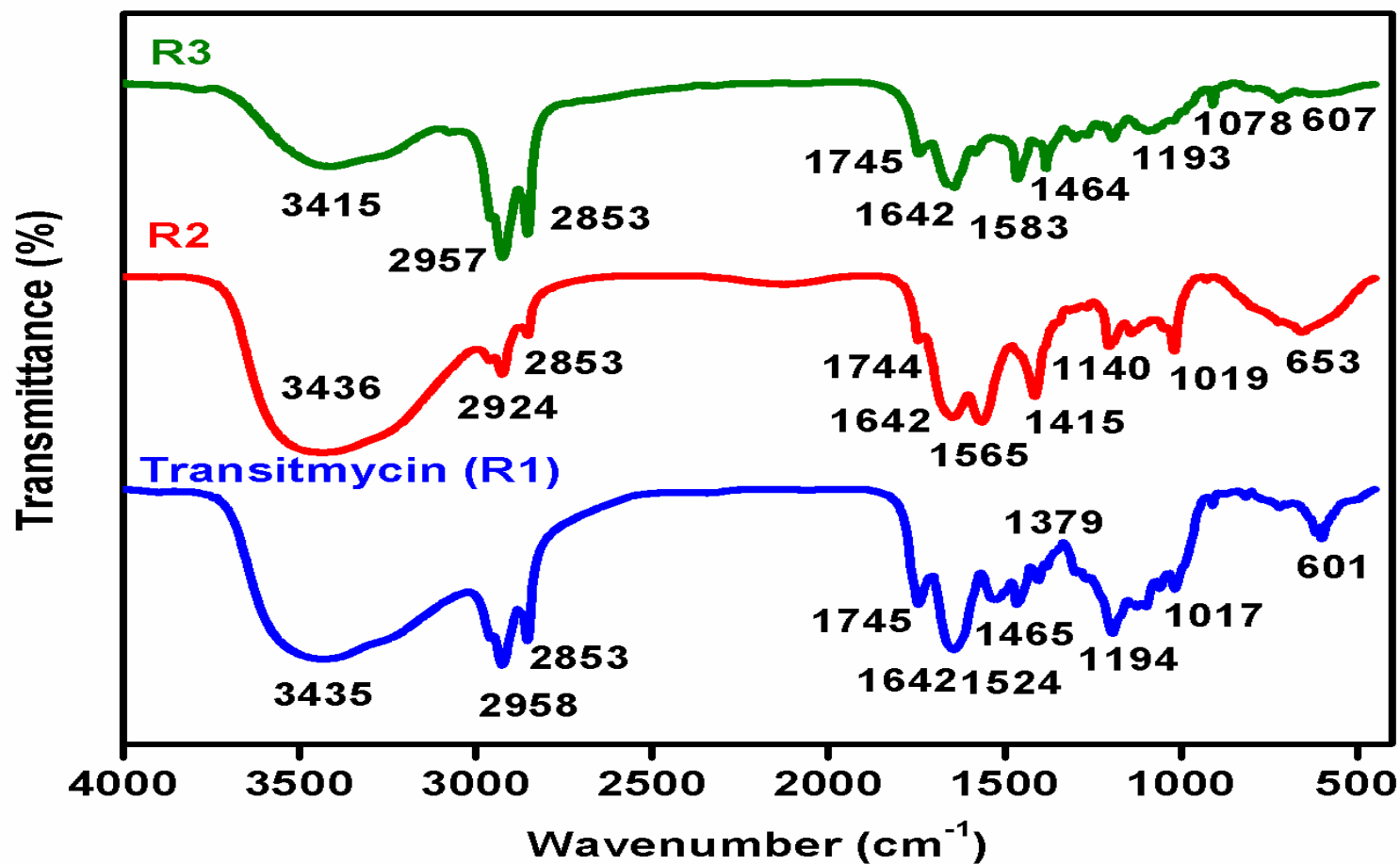


Figure S11. FT-IR Spectrum of Transitmycin (R1), R2, R3

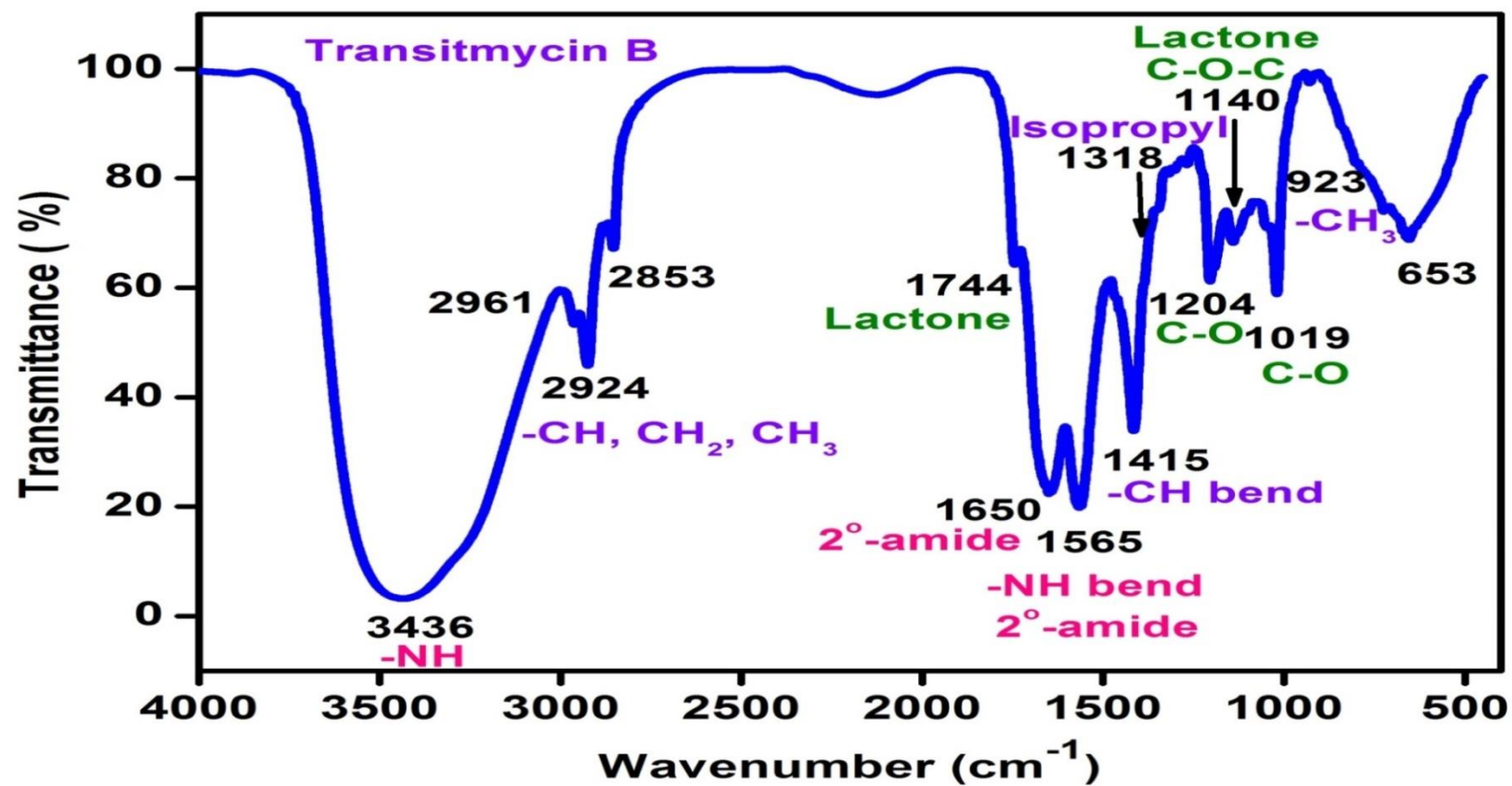


Figure S12. FT-IR Spectrum of R2

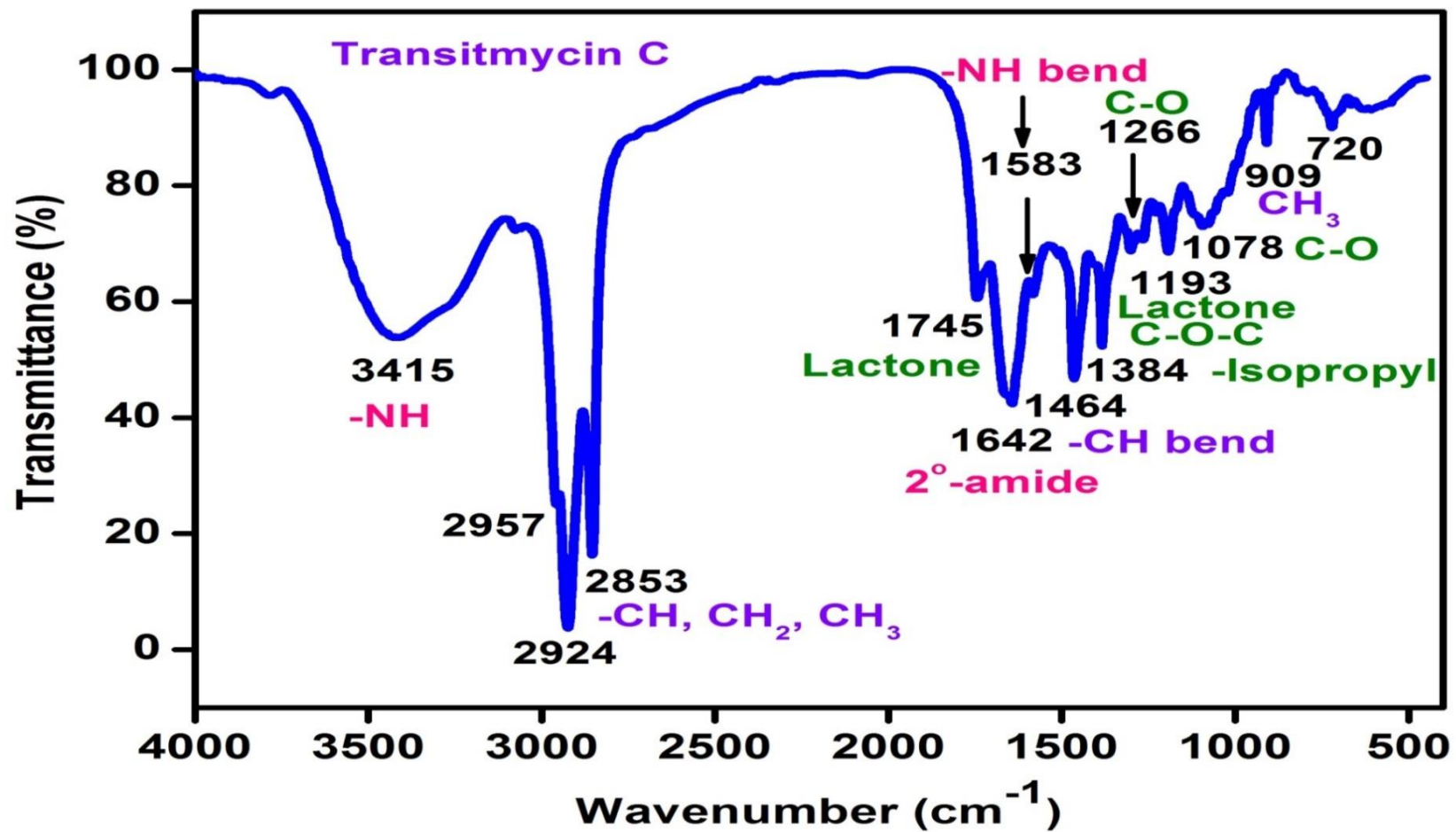


Figure S13. FT-IR Spectrum of R3

R1	IR (KBr cm^{-1}), 3435 cm^{-1} for NH, 2958, 2924 cm^{-1} (m, -CH str, asym, CH_3 and CH_2), 2872 cm^{-1} , 2853 cm^{-1} (m, -CH str, sym, CH_3 and CH_2), 1746 cm^{-1} (s, C=O str, lactone ring), 1642 cm^{-1} (s, -C=O str, 2^0 amide), 1524, 1503 (m, -NH bend, 2^0 amide), 1466 (m, CH bend (scissoring), CH_2), 1379 cm^{-1} (s, -CH bend, isopropyl group), 1268 (s, C-O str, ester), 1194 (C-O-C of lactone), 1099, 1059, 1017 (s, C-O or C-N), 720, 712, 694, 689 (s, -CH bend, oop, aromatic ring), 909 (w, CH_3 rocking).
R2	IR (KBr cm^{-1}), 3436 cm^{-1} for NH, 2961, 2924 cm^{-1} (m, -CH str, asym, CH_3 and CH_2), 2872 cm^{-1} , 2853 cm^{-1} (m, -CH str, sym, CH_3 and CH_2), 1744 cm^{-1} (s, C=O str, lactone ring), 1650 cm^{-1} (s, -C=O str, 2^0 amide), 1565, 1503 (m, -NH bend, 2^0 amide), 1415 (m, CH bend (scissoring), CH_2), 1318 cm^{-1} (s, -CH bend, isopropyl group), 1268, 1204 (s, C-O str, ester), 1140 (C-O-C of lactone), 1045, 1019 (s, C-O or C-N), 720, 712, 653 (s, -CH bend, oop, aromatic ring), 929 (w, CH_3 rocking).
R3	IR (KBr cm^{-1}), 3415 cm^{-1} for NH, 2957, 2924 cm^{-1} (m, -CH str, asym, CH_3 and CH_2), 2872 cm^{-1} , 2853 cm^{-1} (m, -CH str, sym, CH_3 and CH_2), 1745 cm^{-1} (s, C=O str, lactone ring), 1642 cm^{-1} (s, -C=O str, 2^0 amide), 1583, 1507 (m, -NH bend, 2^0 amide), 1464 (m, CH bend (scissoring), CH_2), 1384, 1301 cm^{-1} (s, -CH bend, isopropyl group), 1266, 1228 (s, C-O str, ester), 1193 (C-O-C of lactone), 1093, 1078, 1017 (s, C-O or C-N), 909 (w, CH_3 rocking) 720, 712, 694, 689 (s, -CH bend, oop, aromatic ring).

Table S4. IR Absorption Frequencies of Functional Groups Present in Transitmycin (R1), R2, R3

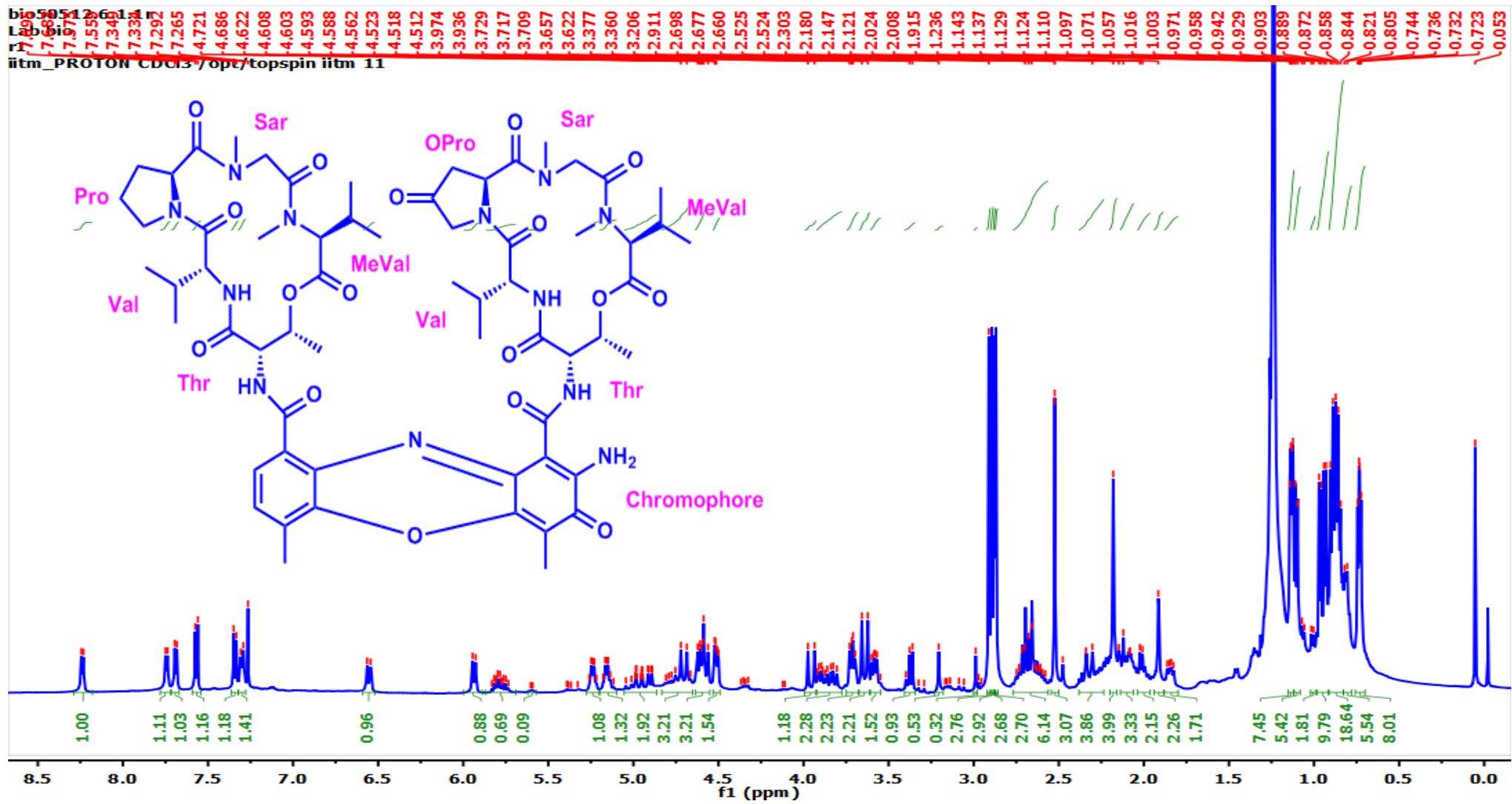


Figure S14. ¹H-NMR (500 MHz, CDCl₃) Spectrum of Transitmycin (R1)

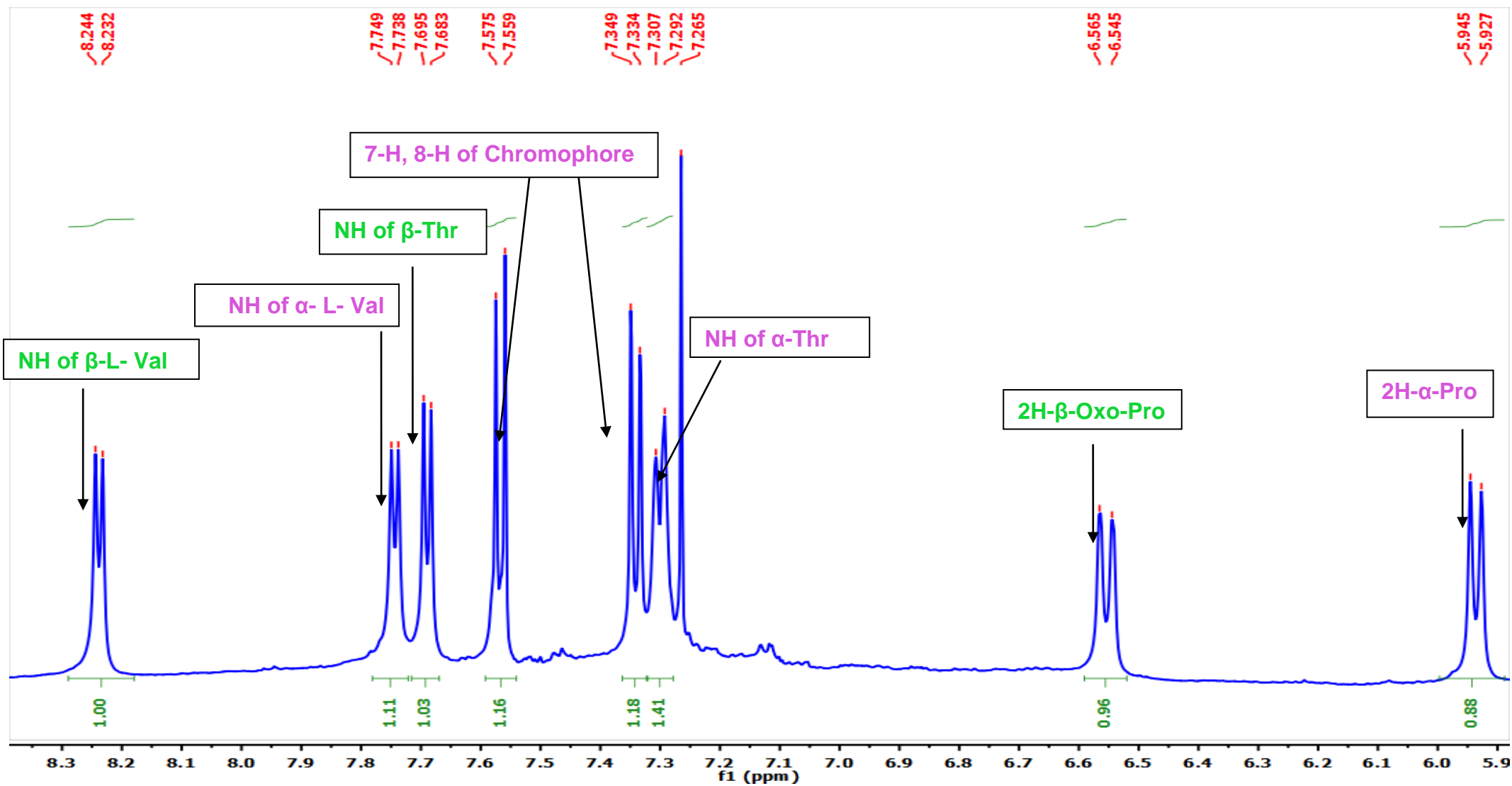


Figure S15. Expansion of $^1\text{H-NMR}$ (500 MHz, CDCl_3) Spectrum of Transitymycin (R1)

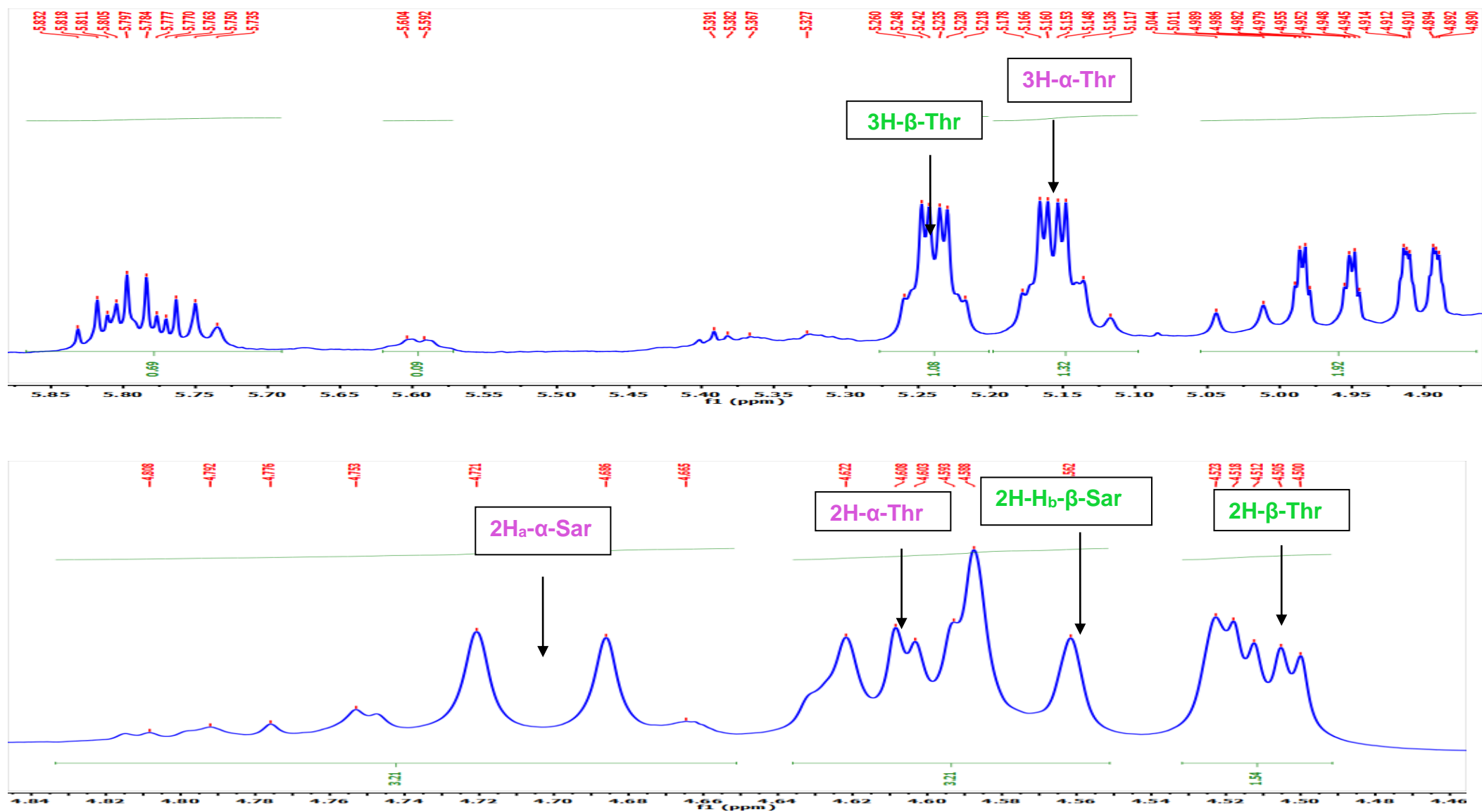


Figure S16. Expansion of ¹H-NMR (500 MHz, CDCl₃) Spectrum of Transitymycin (R1)

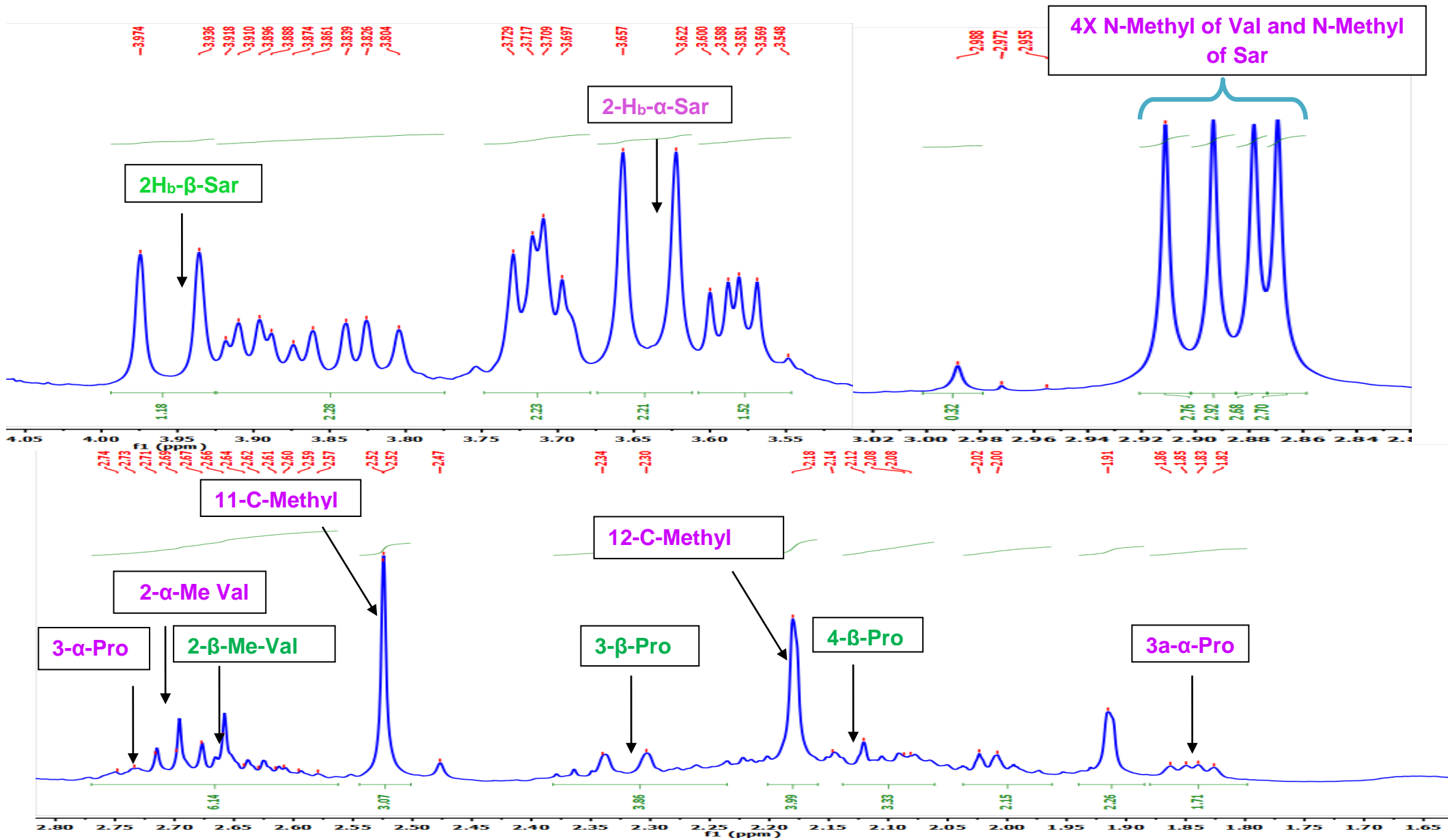


Figure S17. Expansion of ¹H-NMR (500 MHz, CDCl₃) Spectrum of Transitmecin (R1)

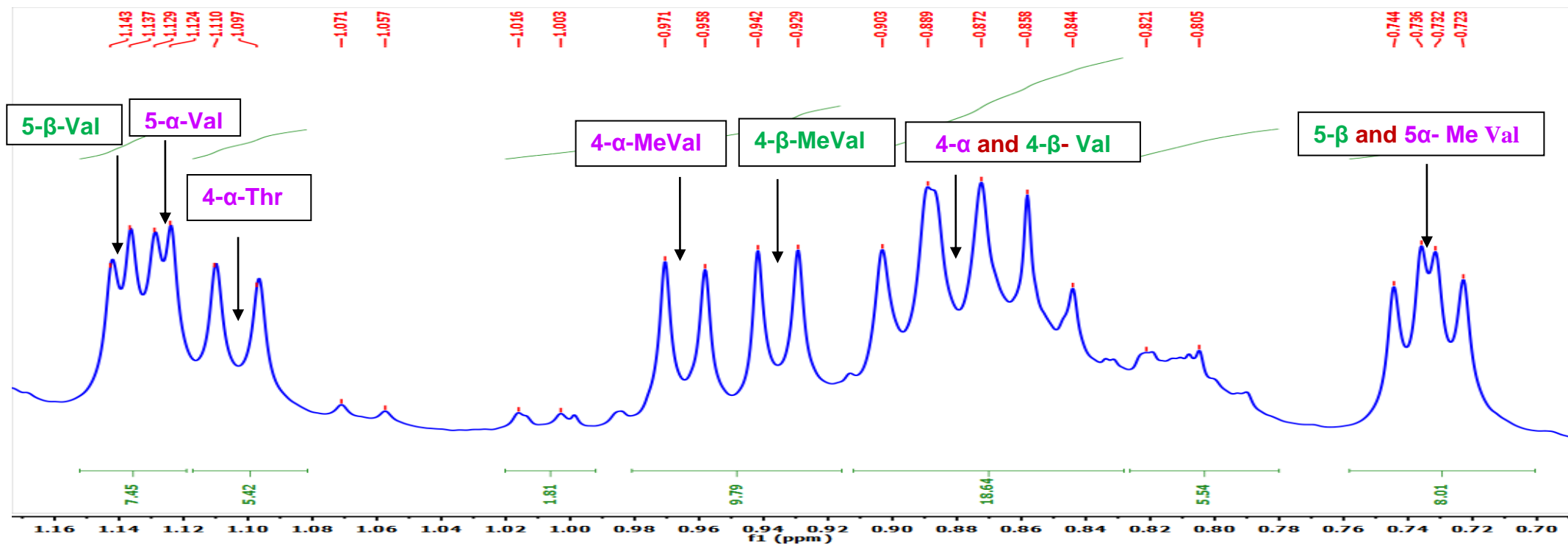


Figure S18. Expansion of ¹H-NMR (500 MHz, CDCl₃) Spectrum of Transitmycin (R1)

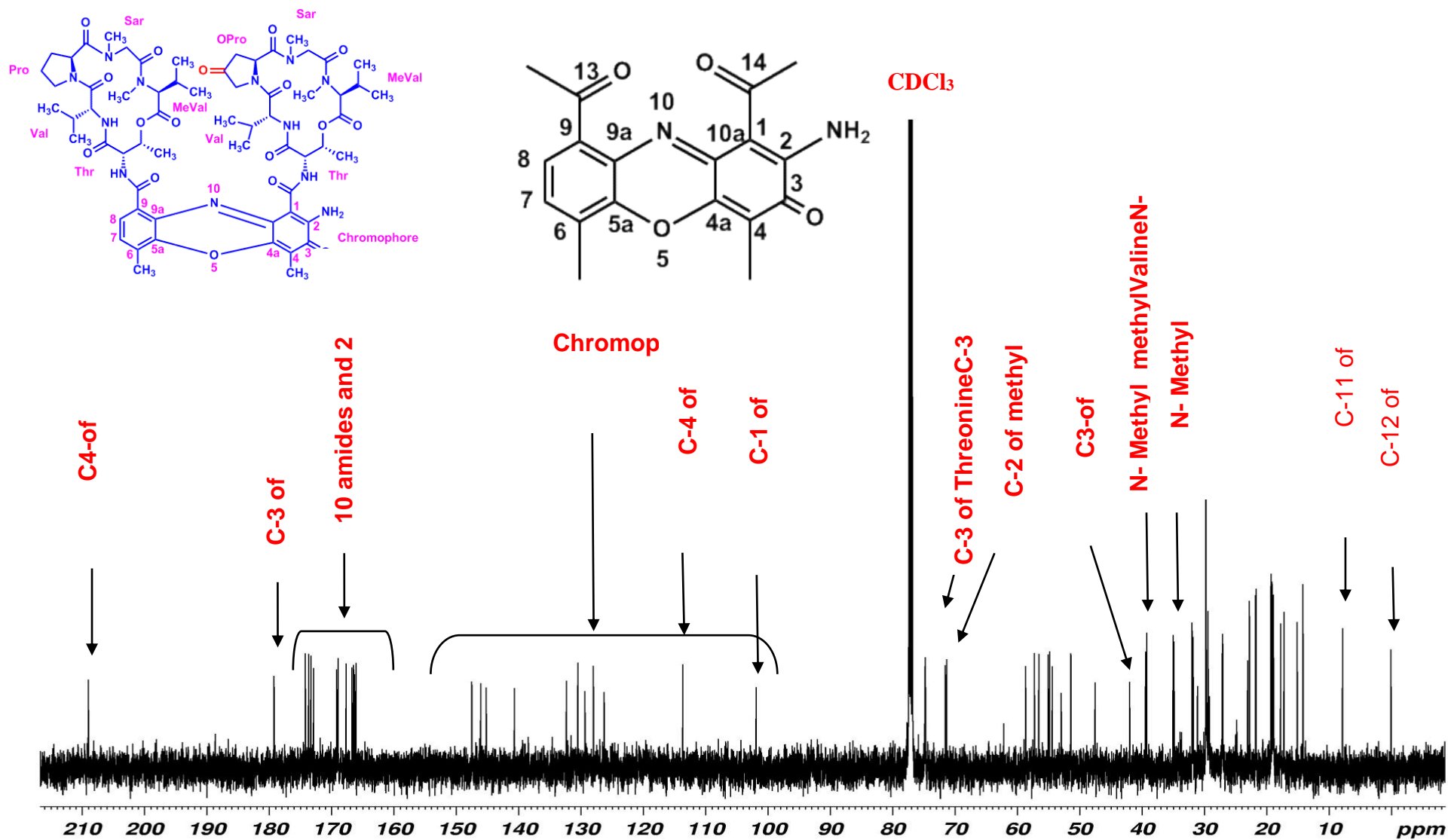


Figure S19. ¹³C-NMR (125 MHz, CDCl₃) Spectrum of Transitmycin (R1)

110312_senthilkumar.2.fid

R1

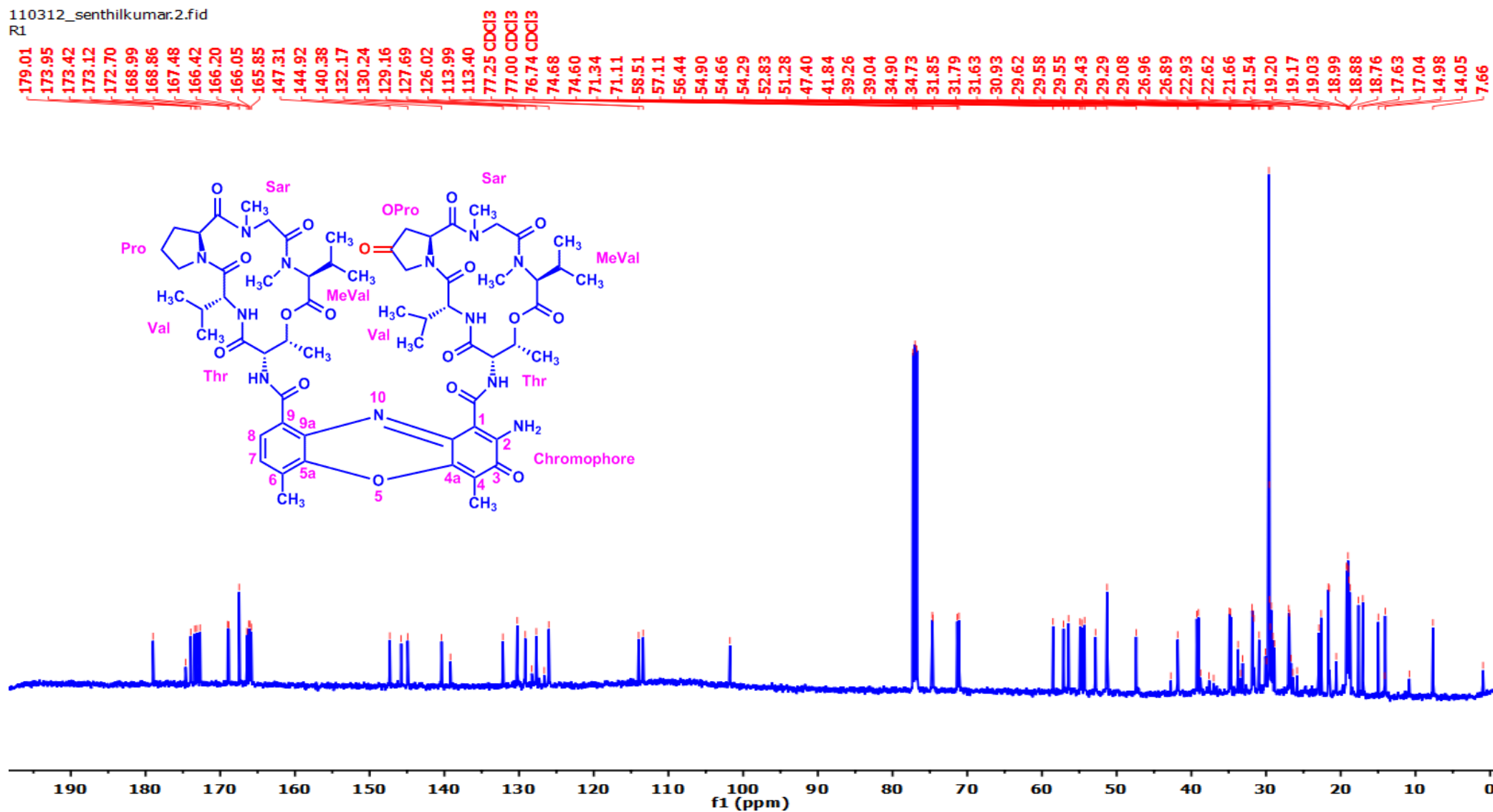


Figure S20. ¹³C-NMR (125 MHz, CDCl₃) Spectrum of Transitmycin (R1)

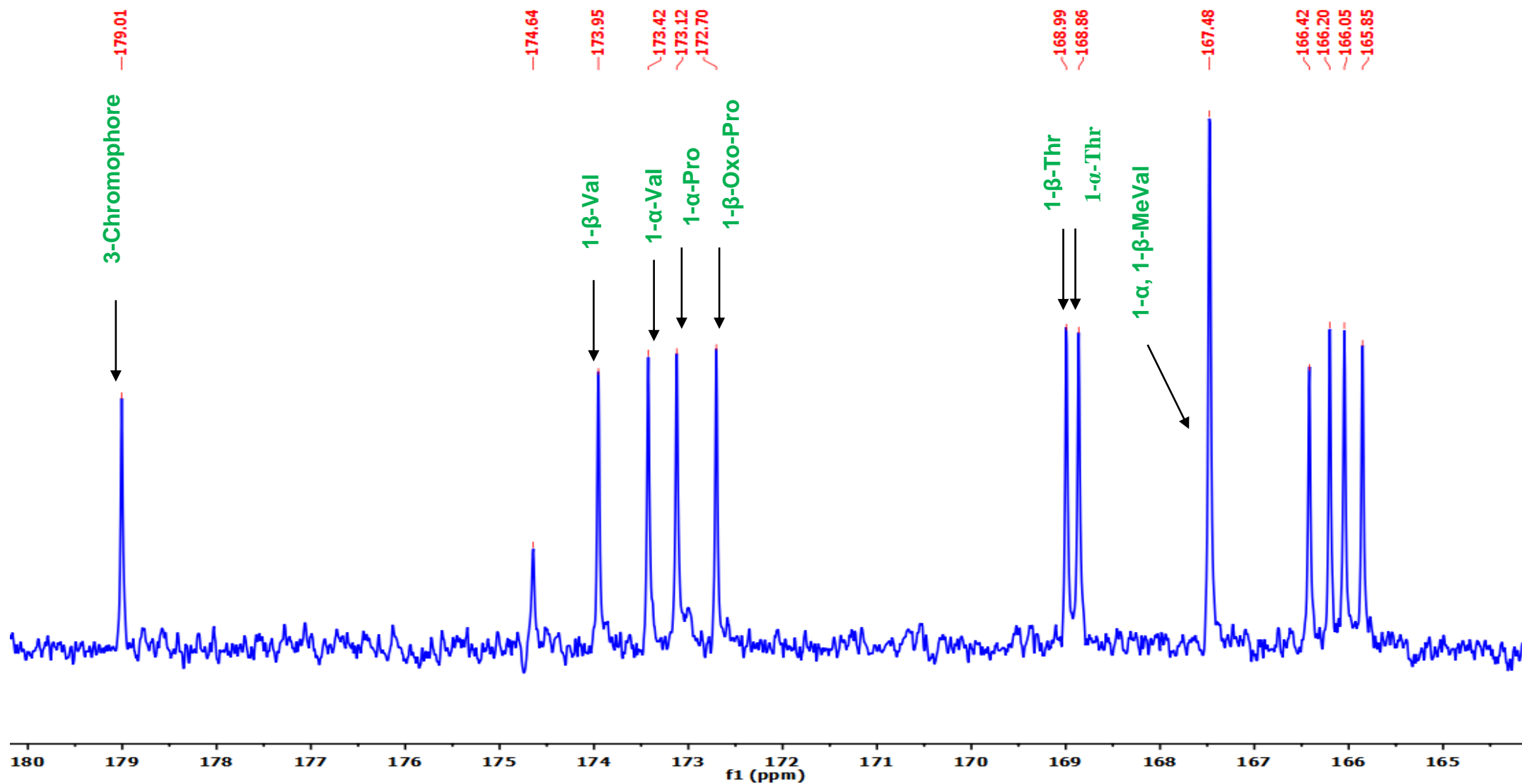


Figure S21. ^{13}C -NMR (125 MHz, CDCl_3) Spectrum of Transitmycin (R1)

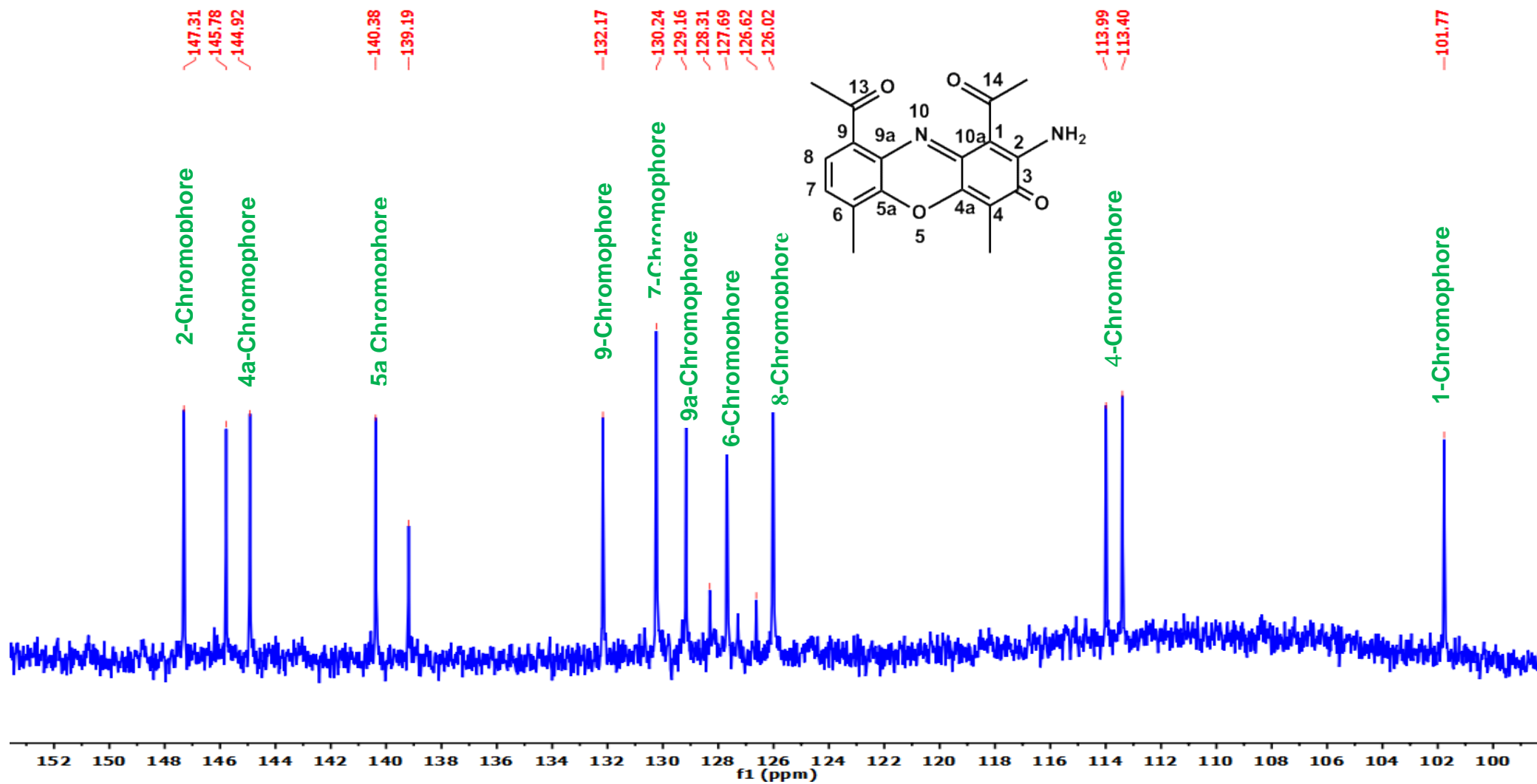


Figure S22. ¹³C-NMR (125 MHz, CDCl₃) Spectrum of Transitmycin (R1)

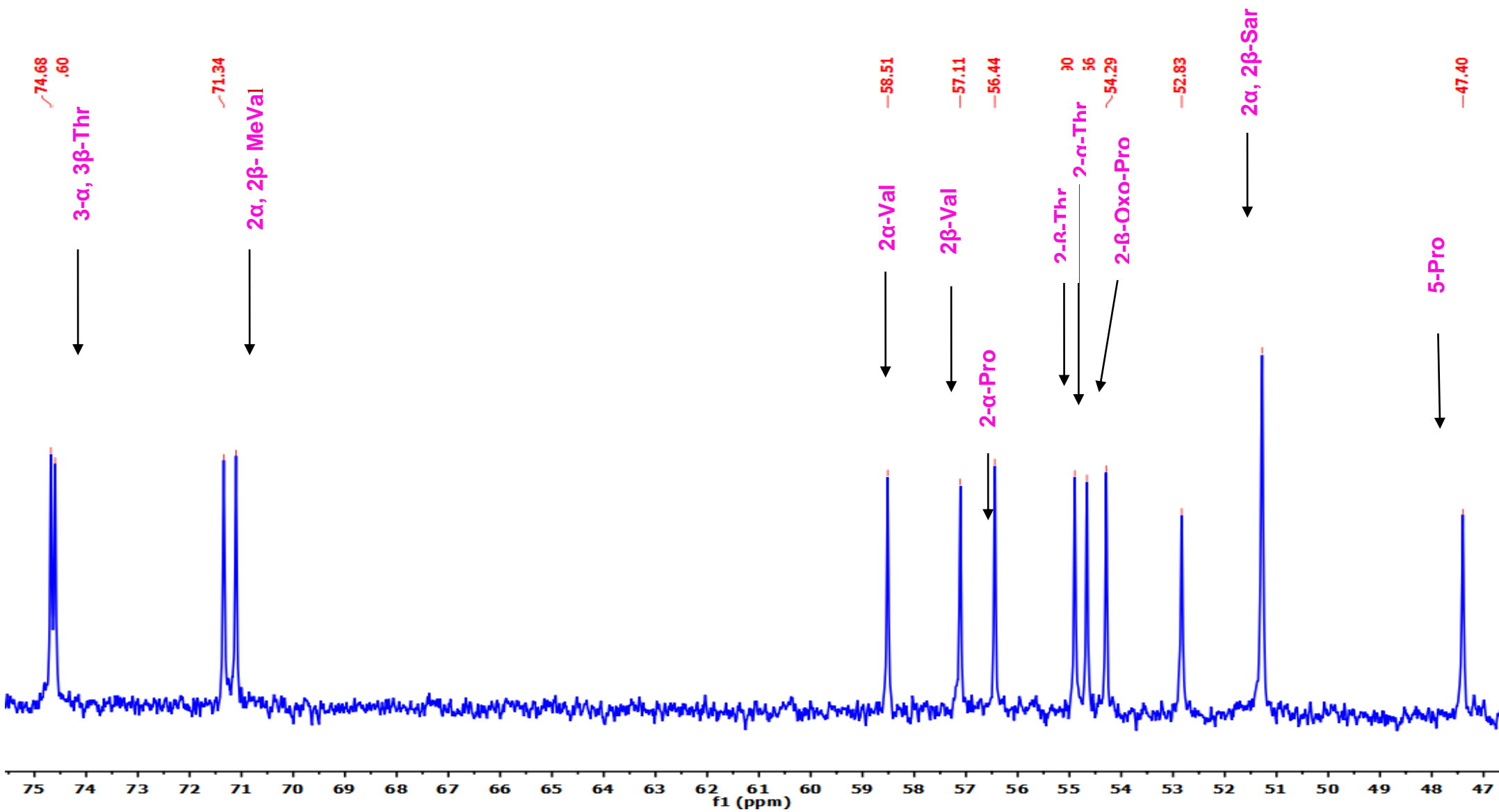


Figure S23. ¹³C-NMR (125 MHz, CDCl₃) Spectrum of Transitycin (R1)

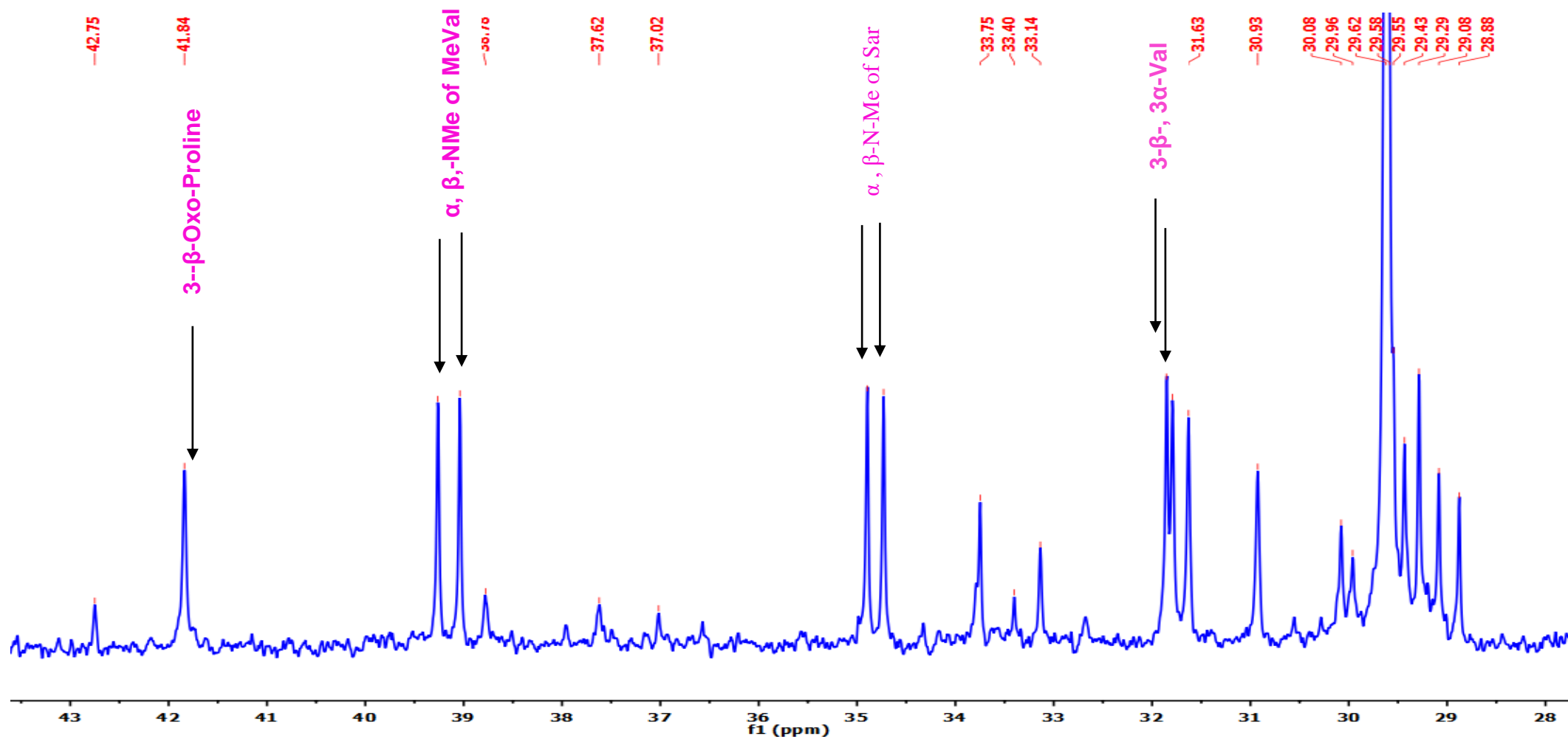


Figure S24. ¹³C-NMR (125 MHz, CDCl₃) Spectrum of Transimycin (R1)

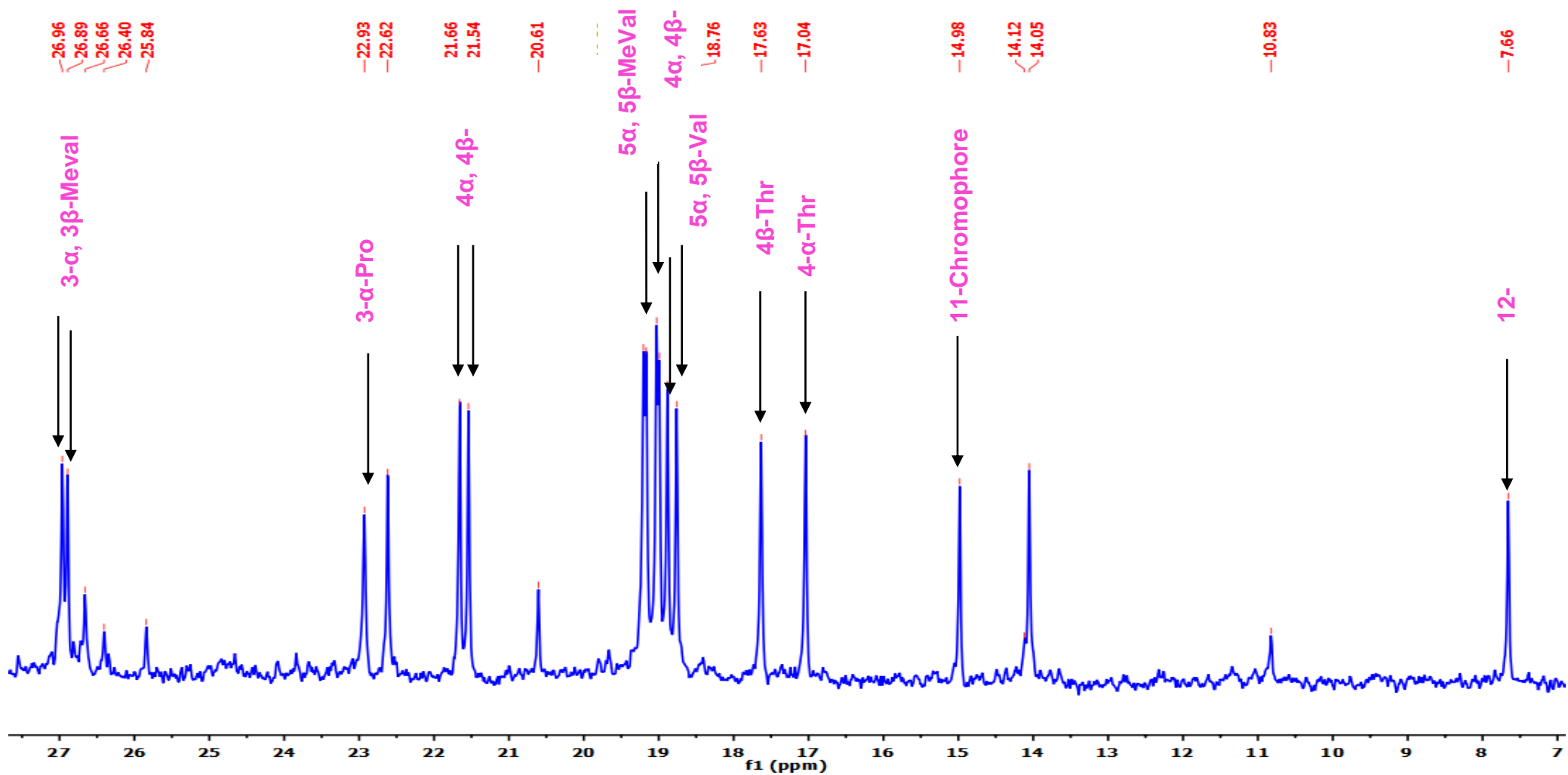


Figure S25. ^{13}C -NMR (125 MHz, CDCl_3) Spectrum of Transitmecin (R1)

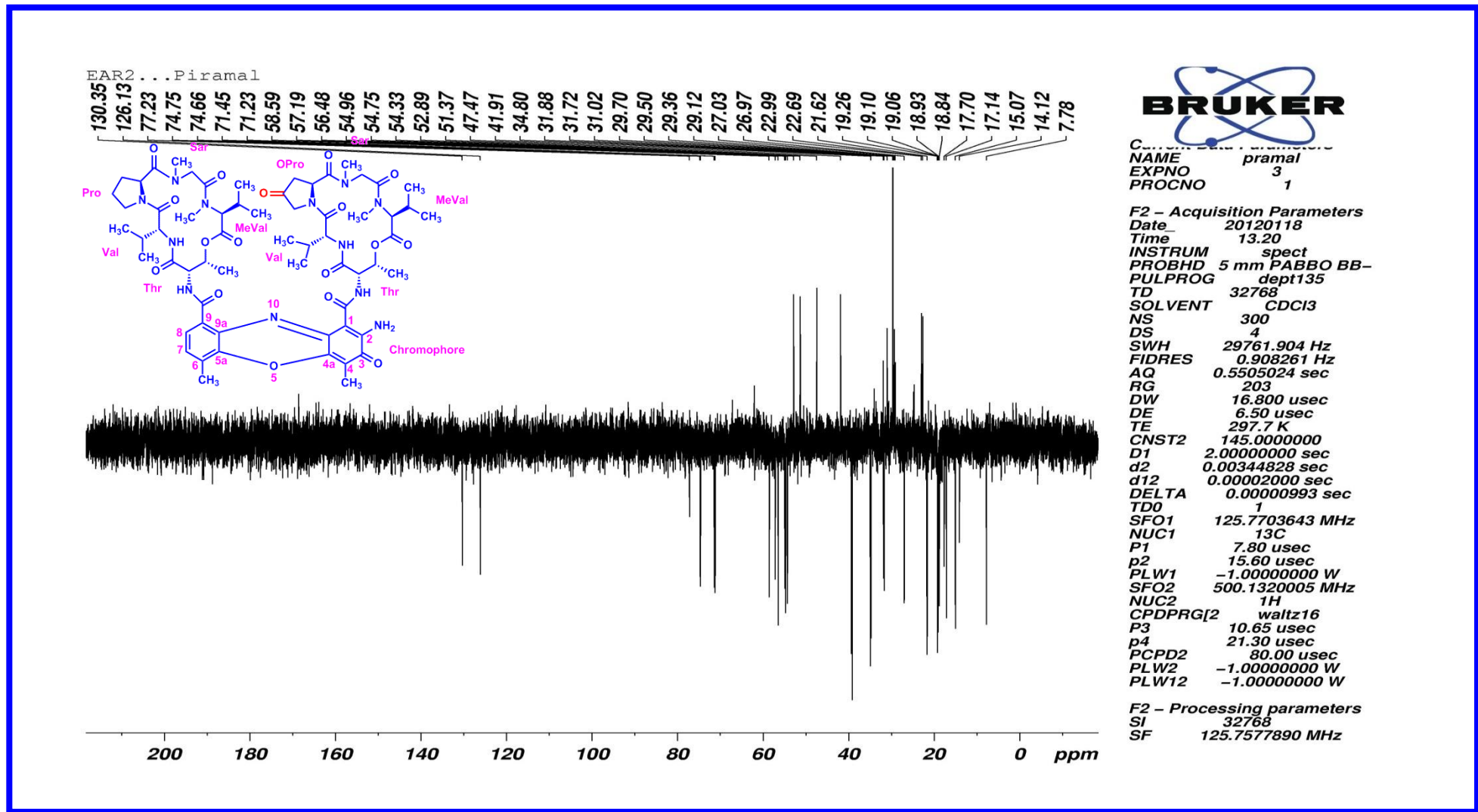


Figure S26. DEPT135 (125 MHz, CDCl₃) Spectrum of Transimycin (R1)

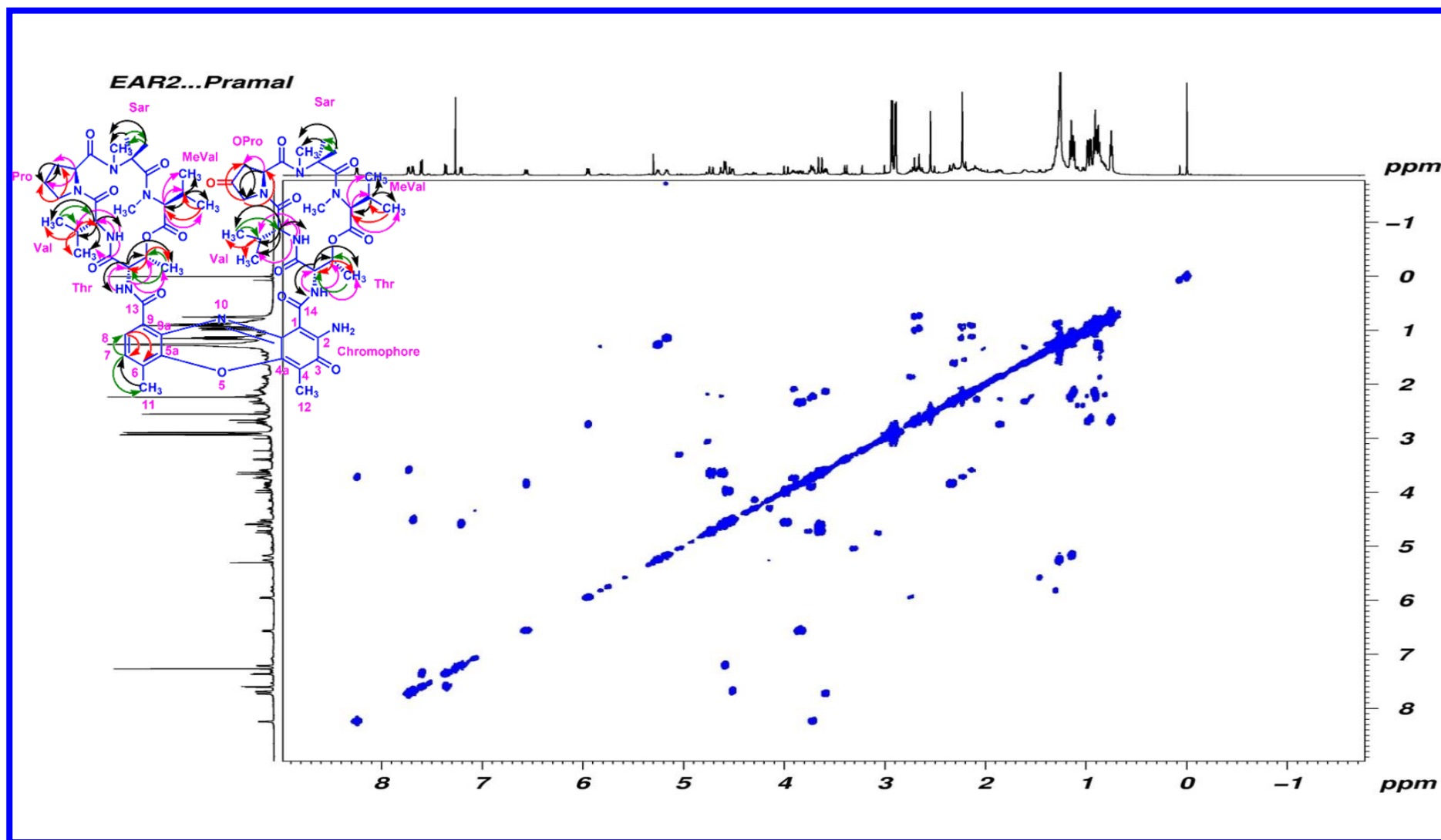


Figure S27. COSY (500 MHz, CDCl₃) Spectrum of Transitmycin (R1)

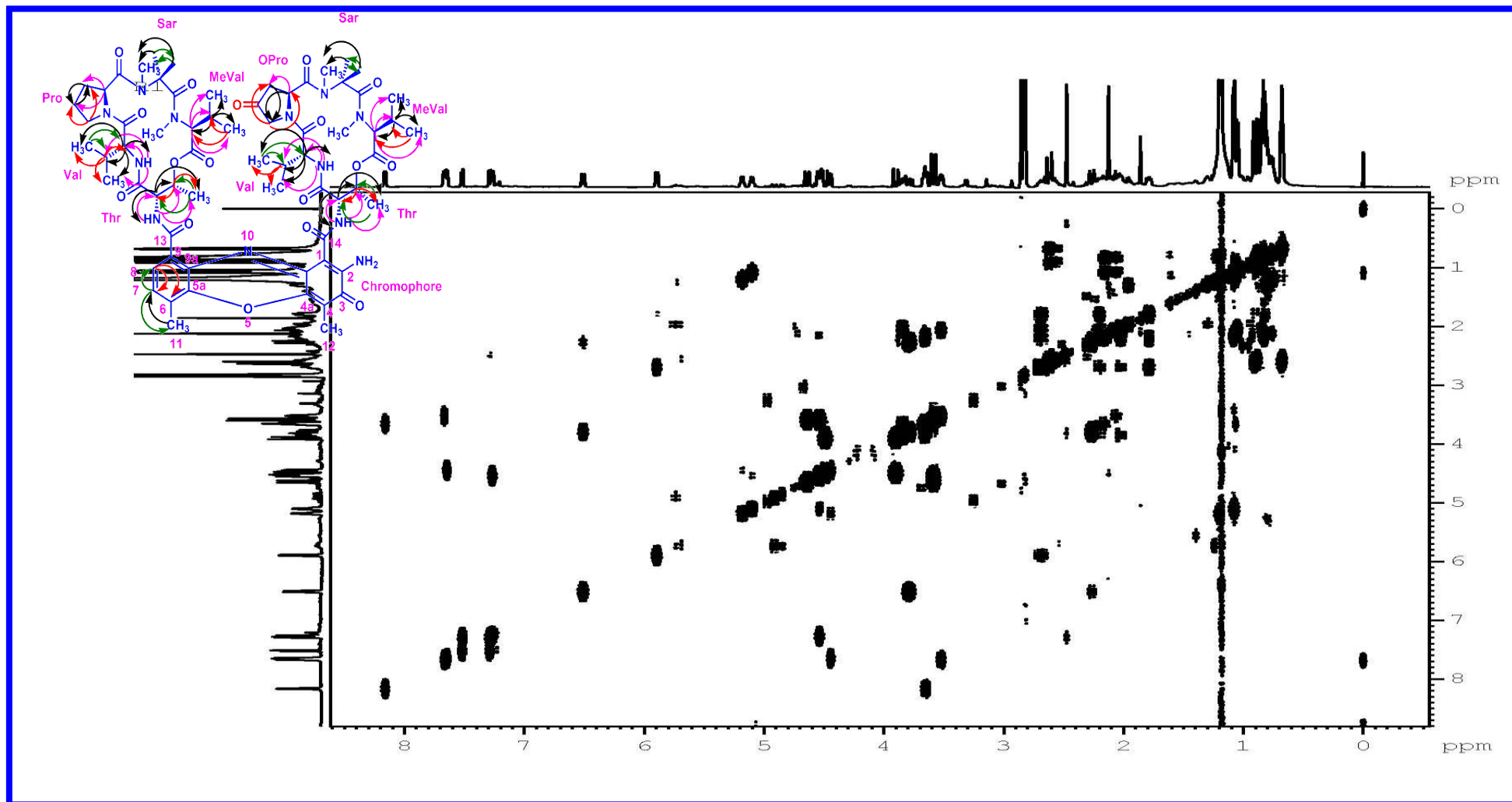


Figure S28. DQF-COSY (500 MHz, CDCl₃) Spectrum of Transimycin (R1)

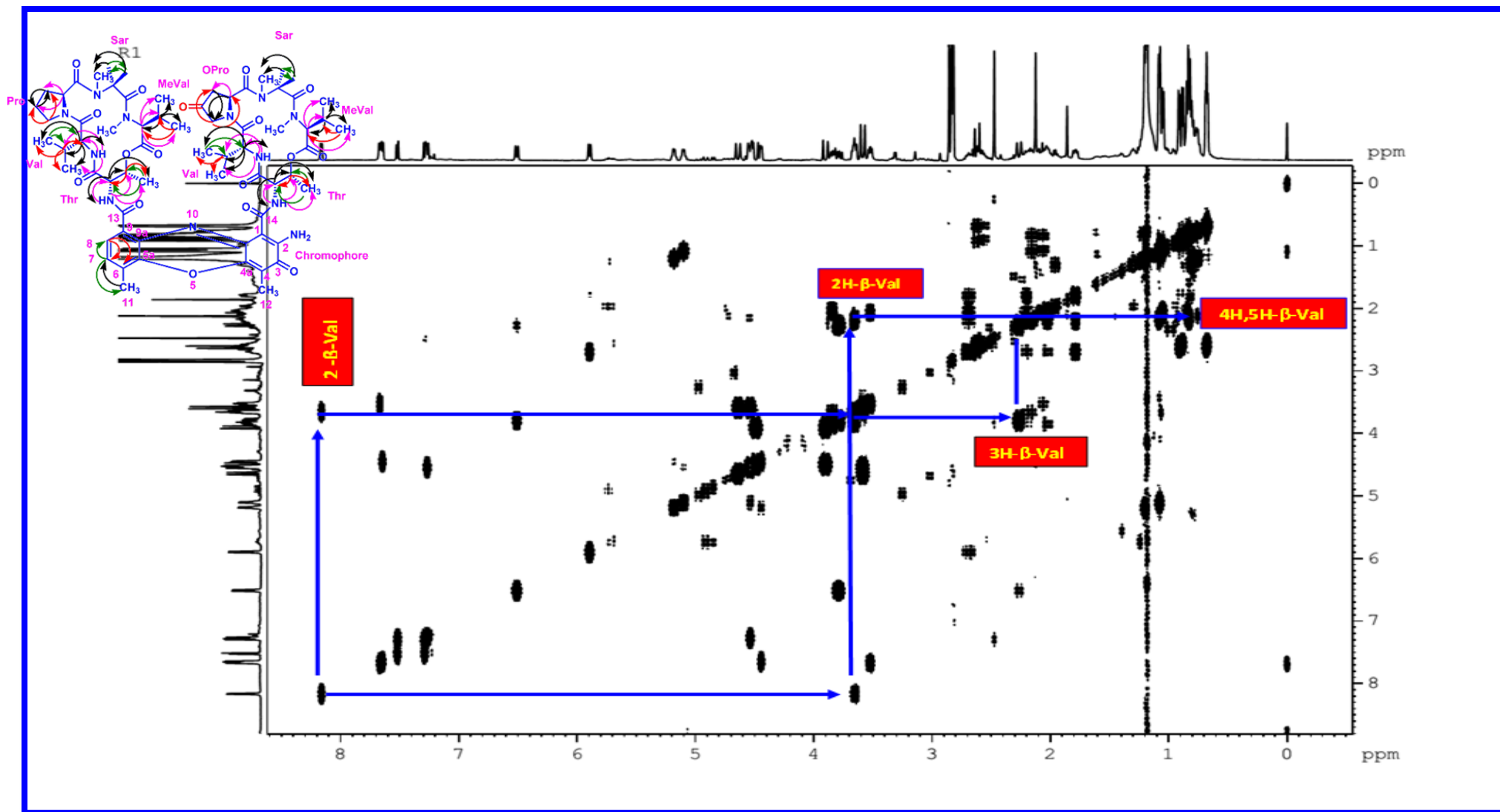


Figure S29. Expansion of DQF-COSY (500 MHz) Spectrum of Transitycin (R1)

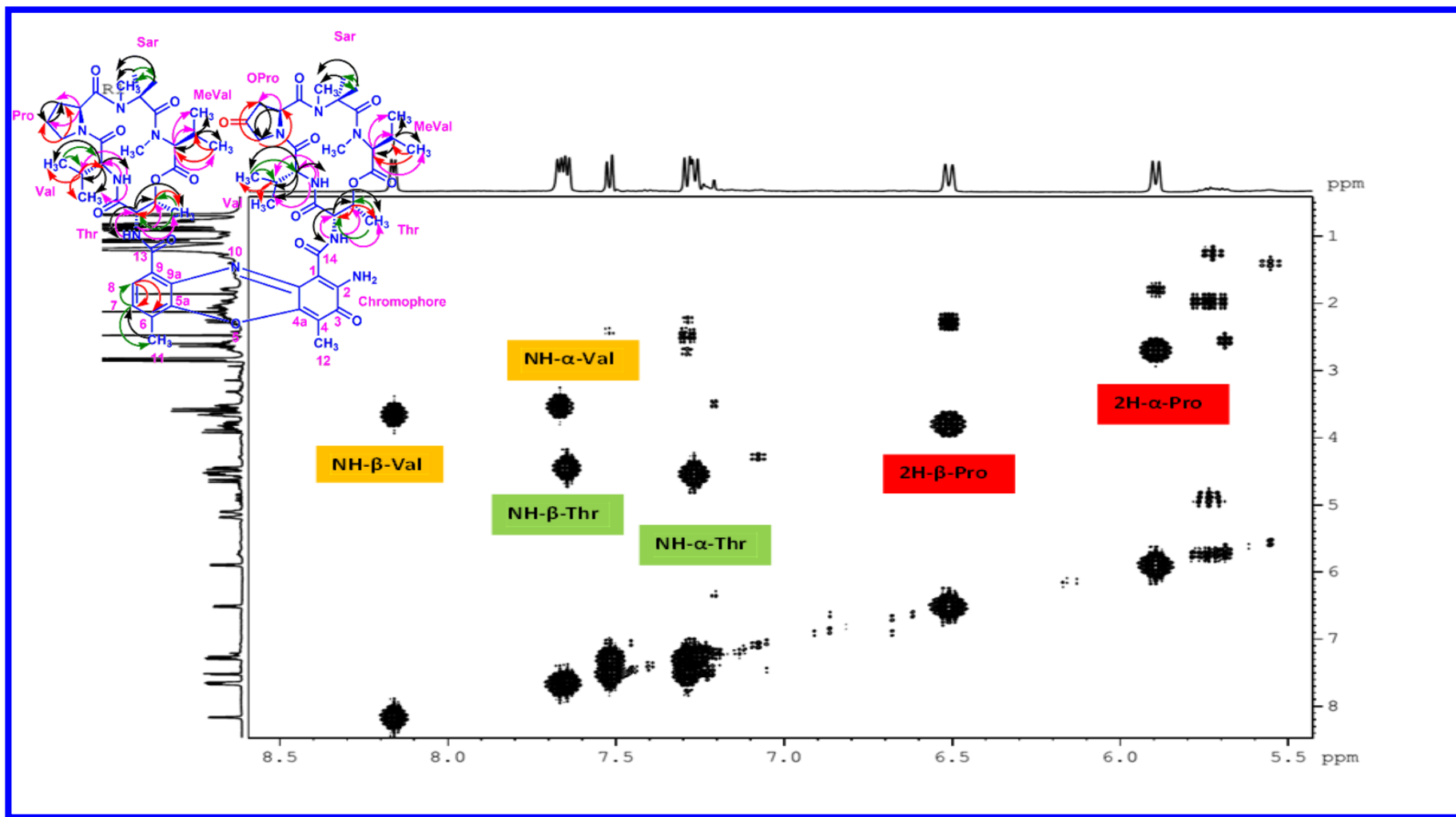


Figure S30. Expansion of DQF-COSY (500 MHz) Spectrum of Transitmycin (R1)

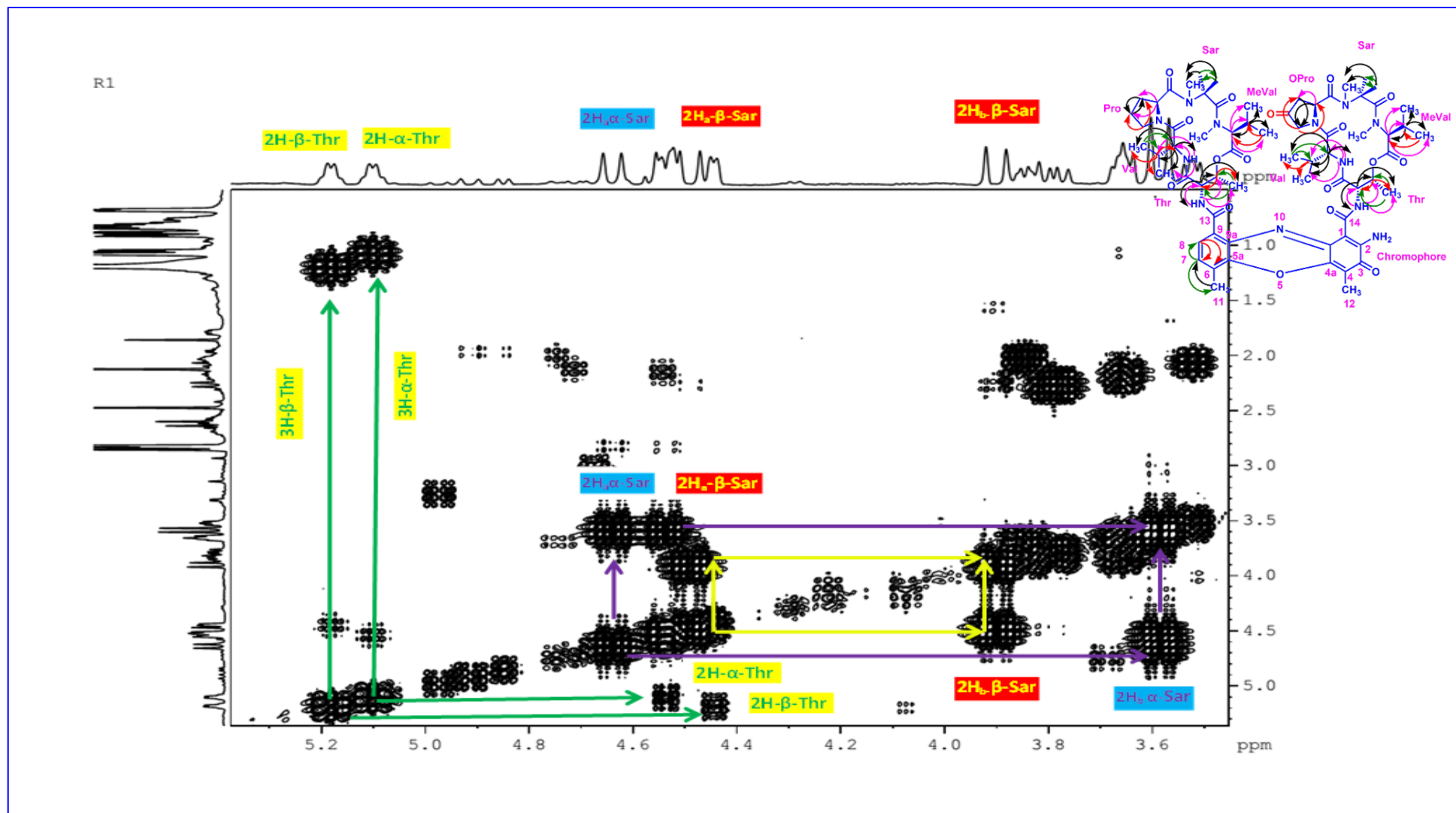


Figure S31. Expansion of DQF-COSY (500 MHz) Spectrum of Transimycin (R1)

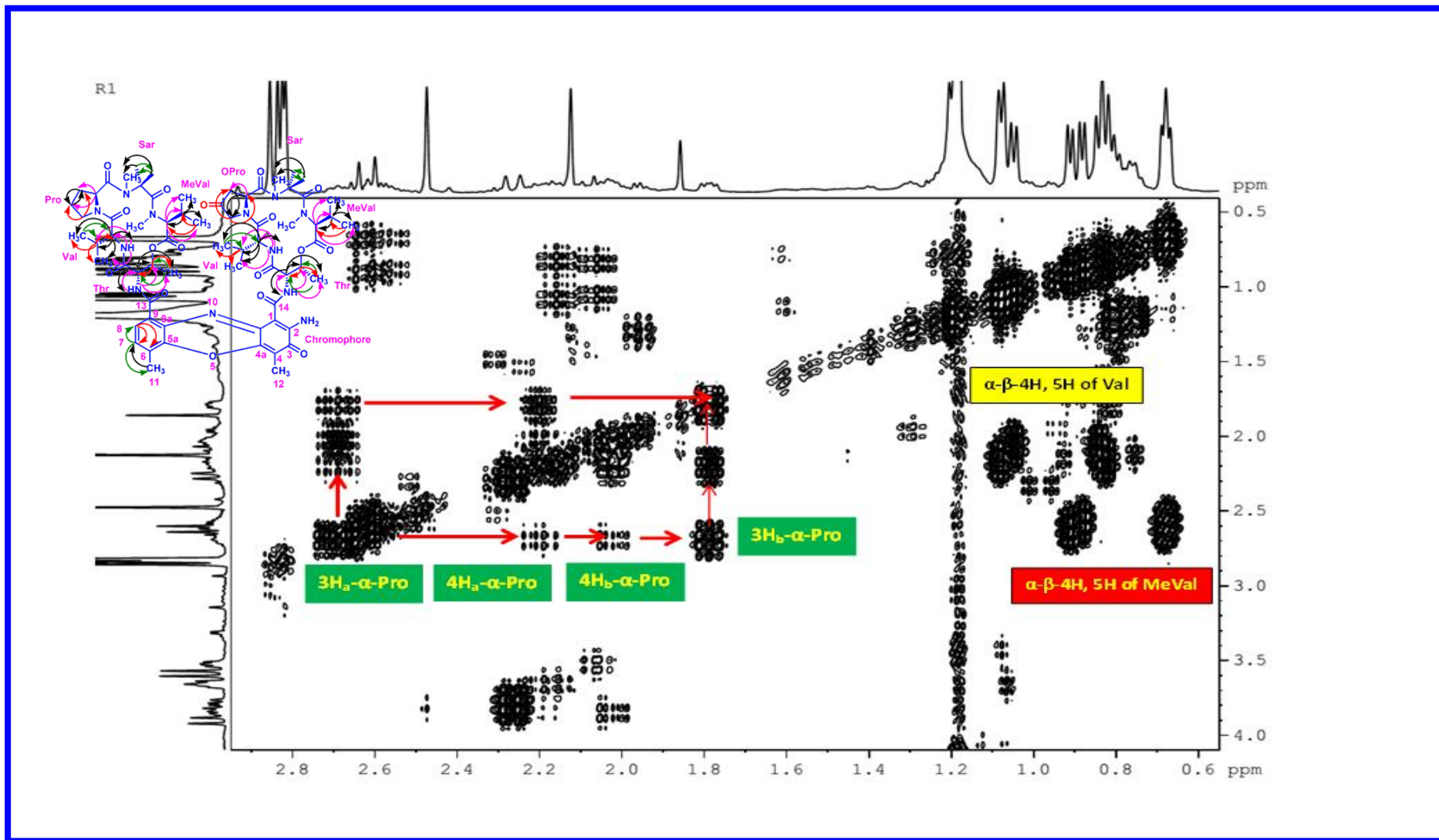


Figure S32. Expansion of DQF-COSY (500 MHz) Spectrum of Transitmycin (R1)

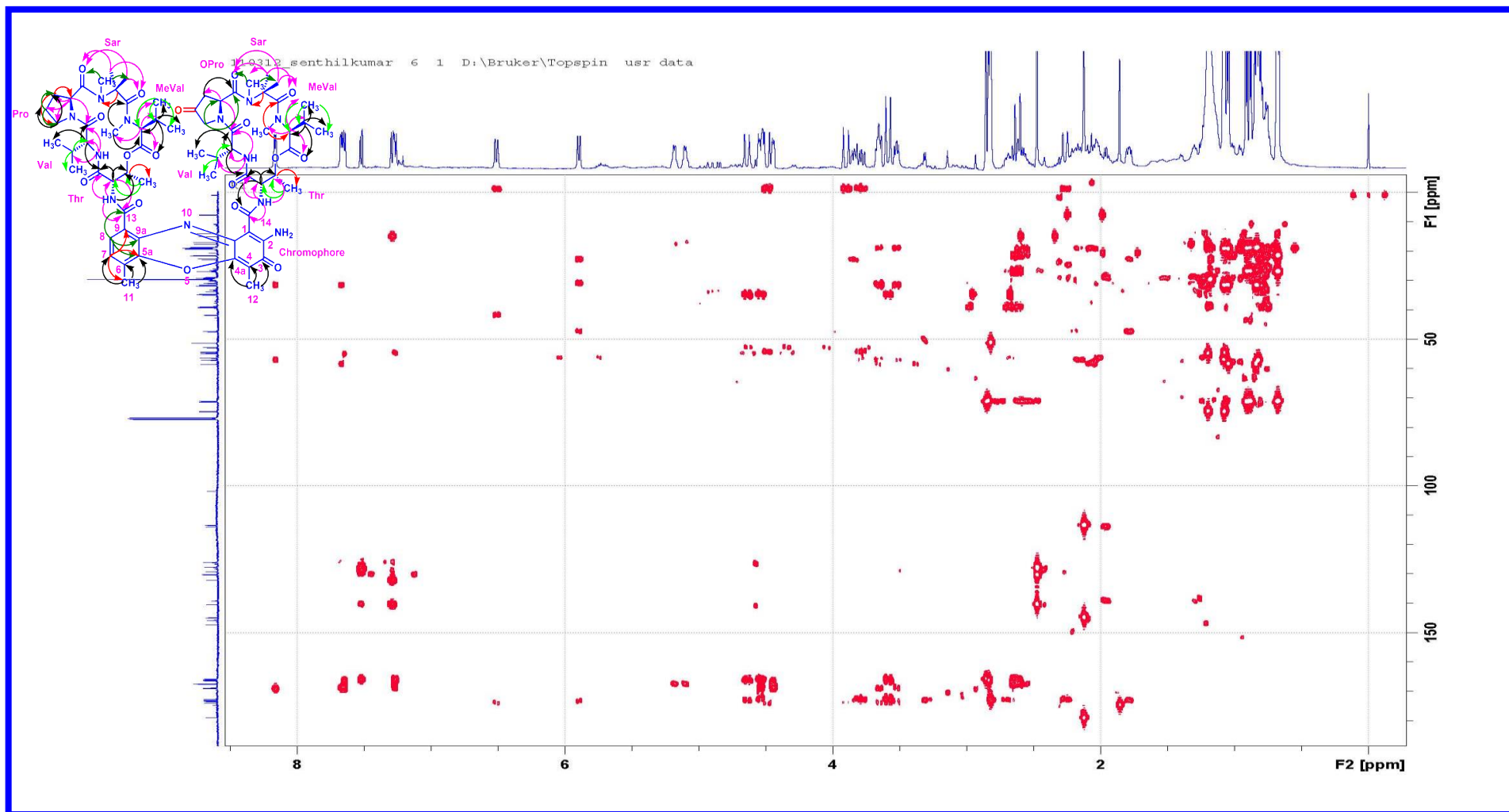


Figure 33. HMBC (500 MHz) Spectrum of Transitmycin (R1)

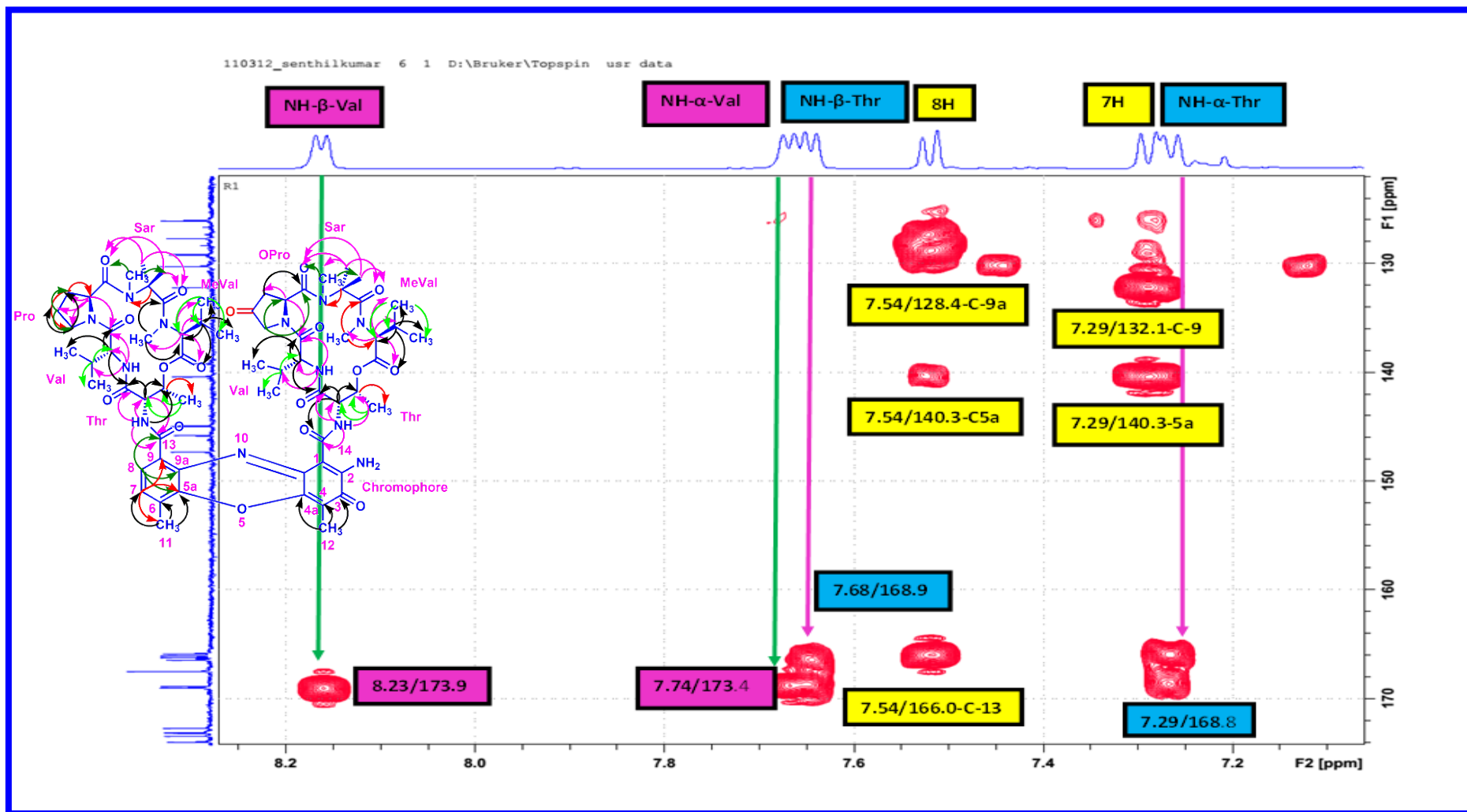


Figure S34. Expansion of HMBC (500 MHz, CDCl₃) Spectrum of Transitycin (R1)

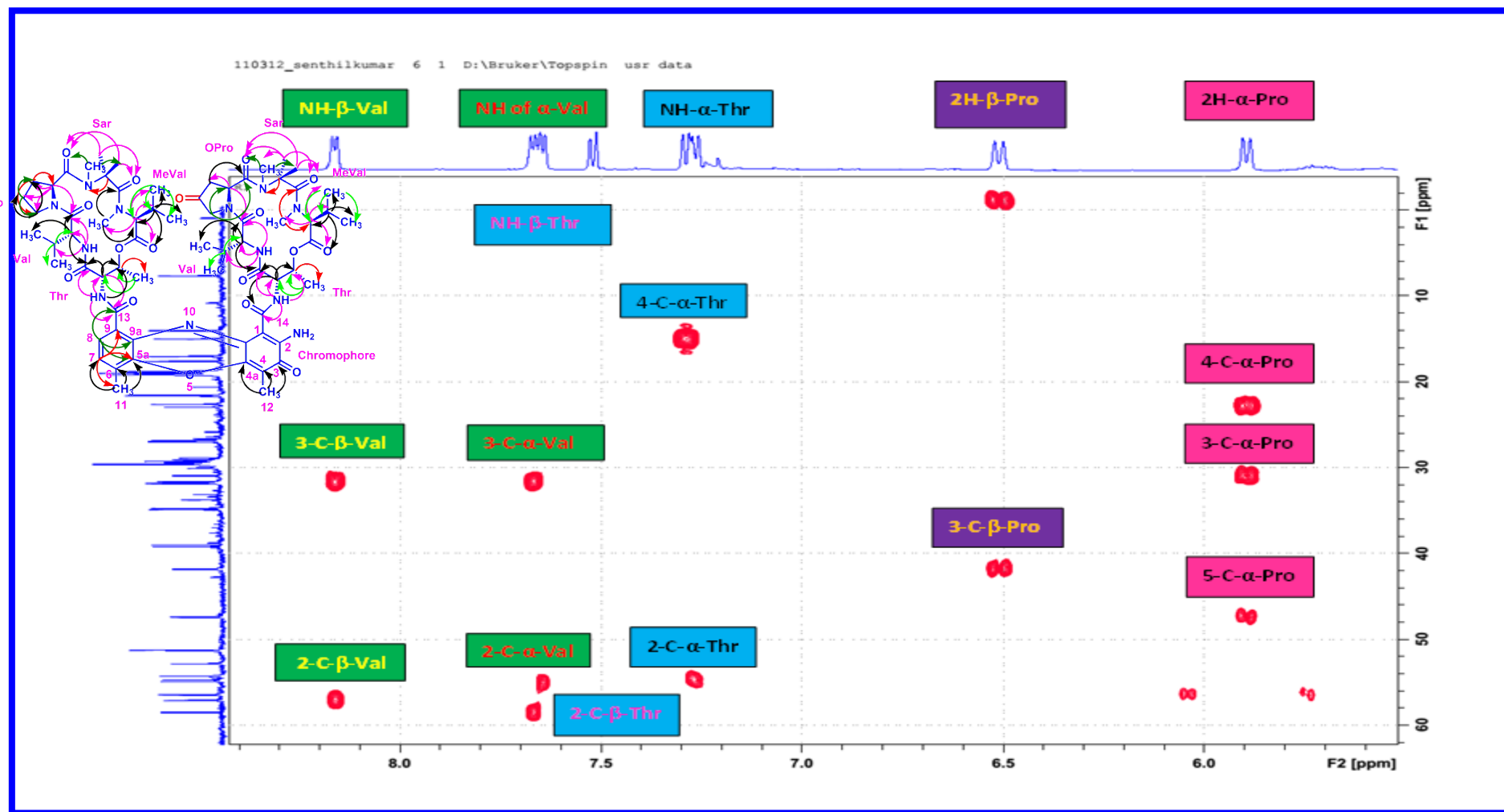


Figure S35. Expansion of HMBC (500 MHz, CDCl_3) Spectrum of Transitmycin (R1)

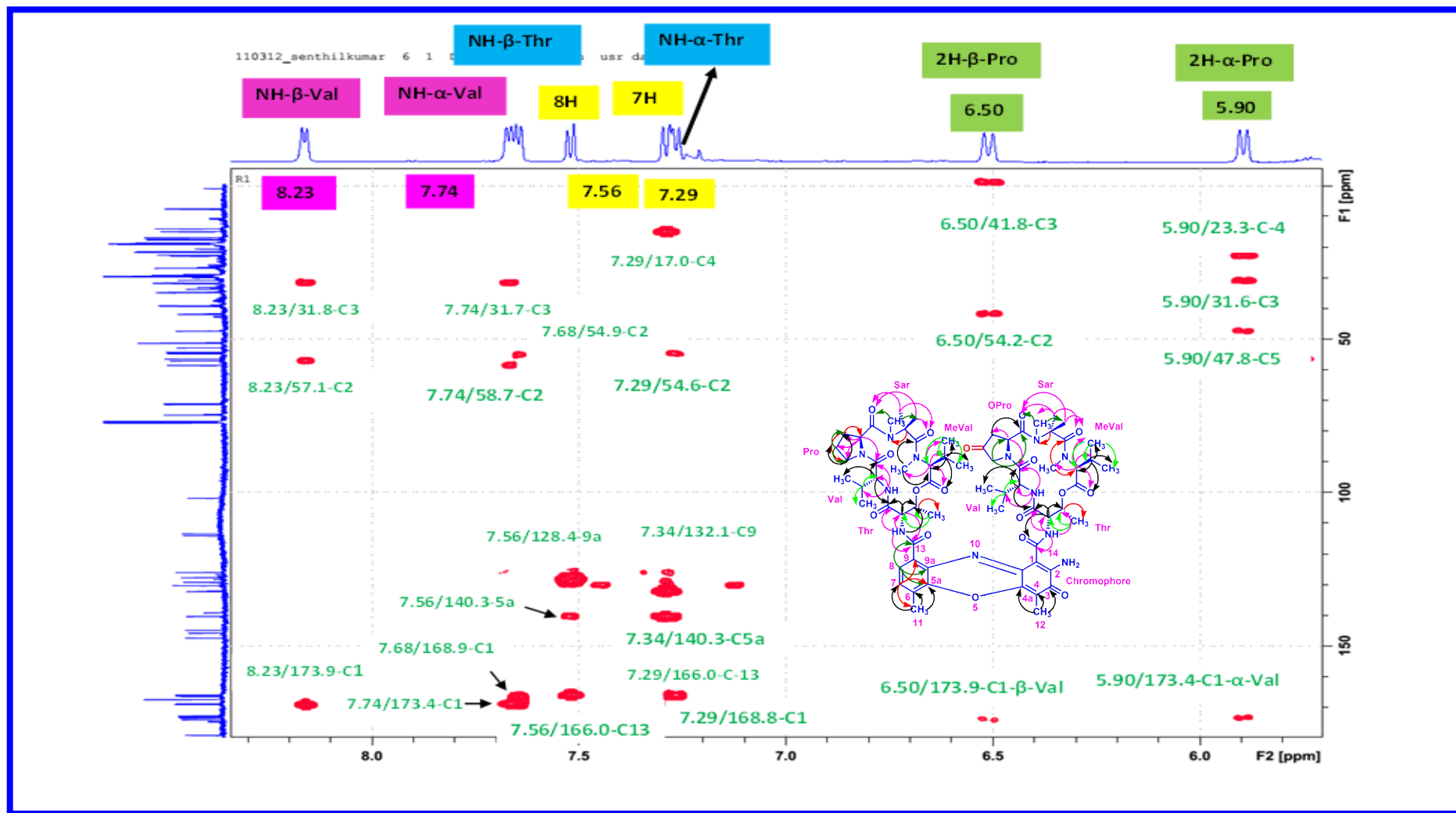


Figure S36. Expansion of HMBC (500 MHz, CDCl₃) Spectrum of Transitmycin (R1)

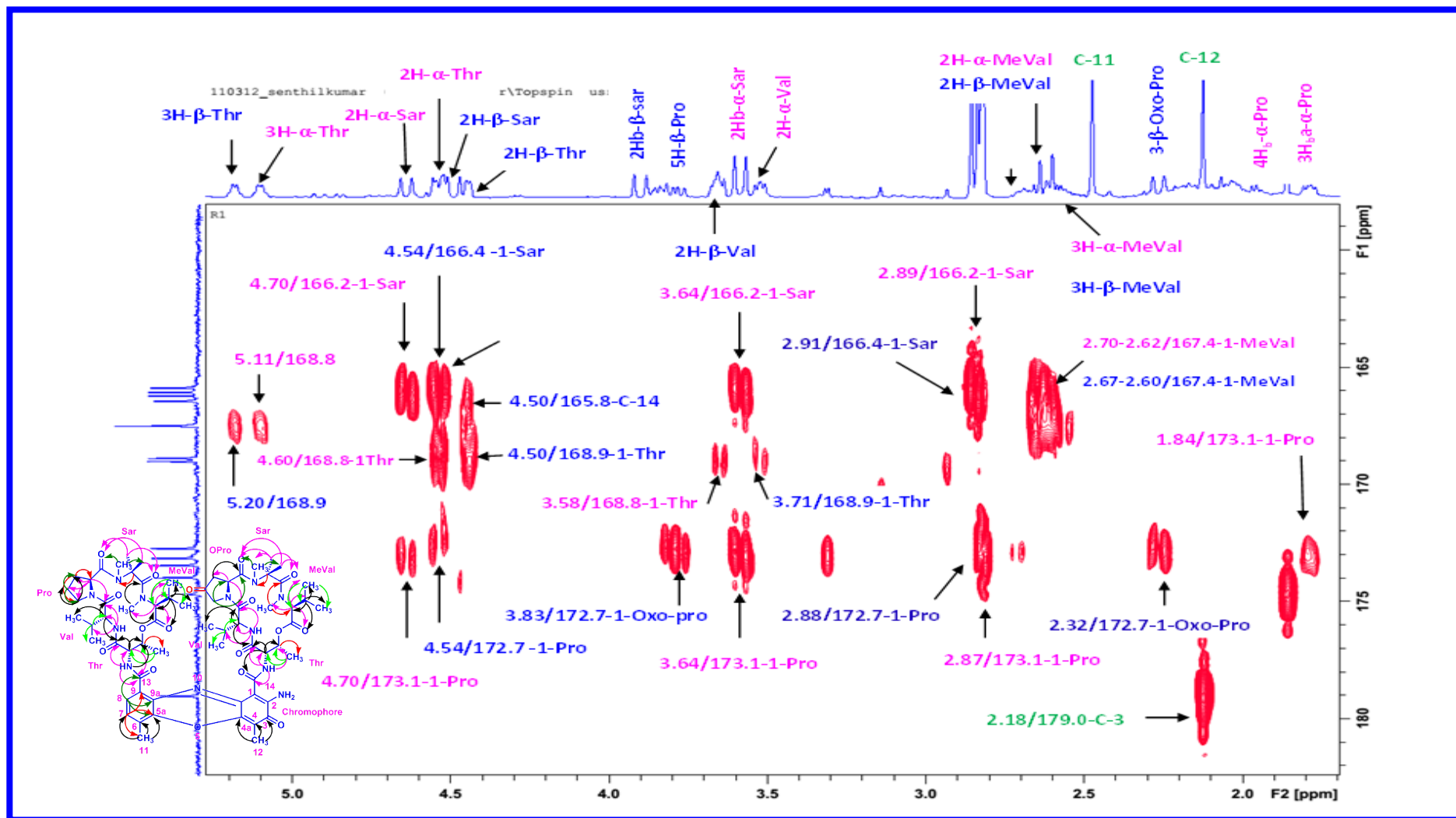


Figure S37. Expansion of HMBC (500 MHz, CDCl₃) Spectrum of Transitmycin (R1)

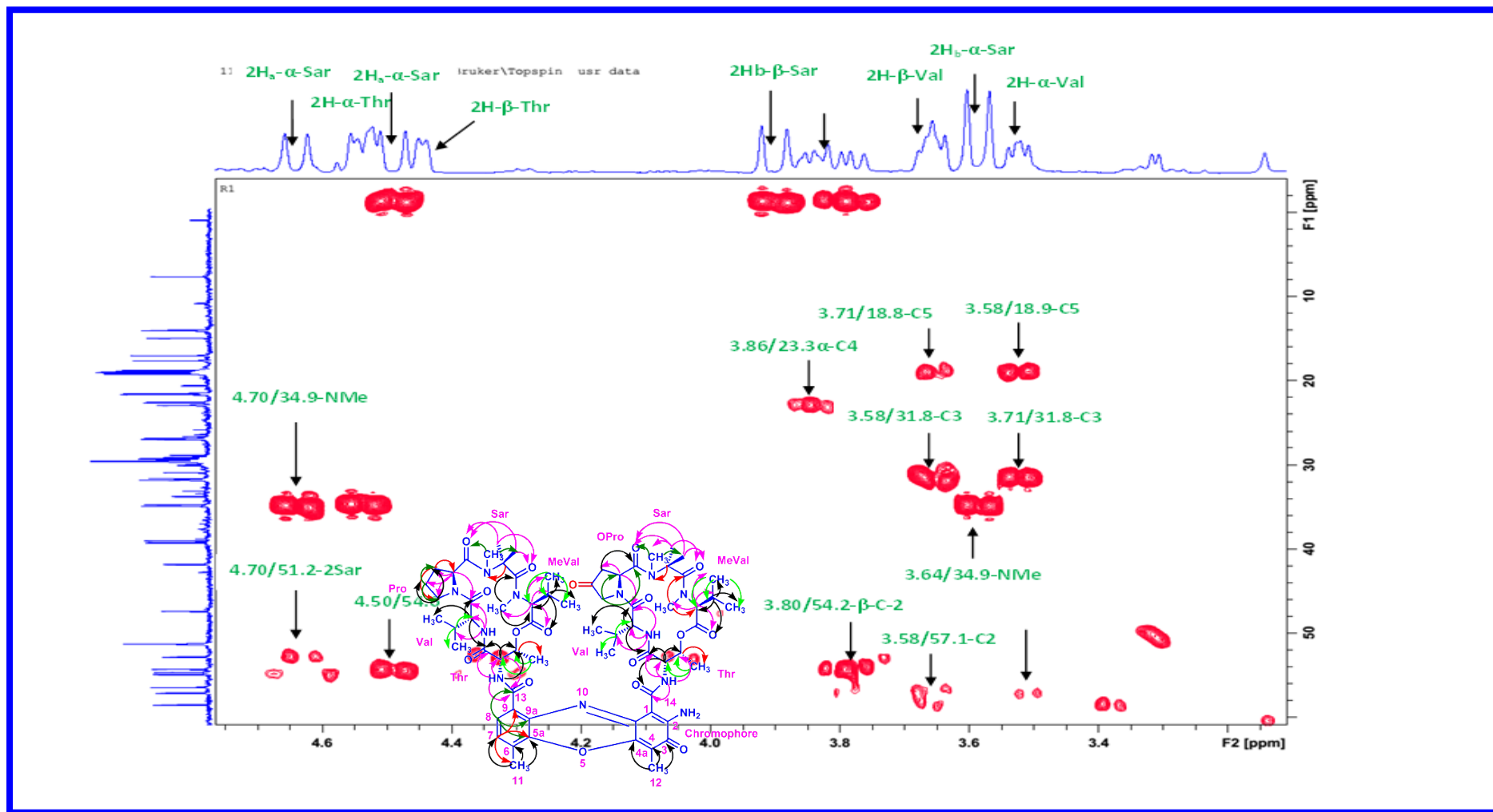


Figure S38. Expansion of HMBC (500 MHz, CDCl₃) Spectrum of Transimycin (R1)

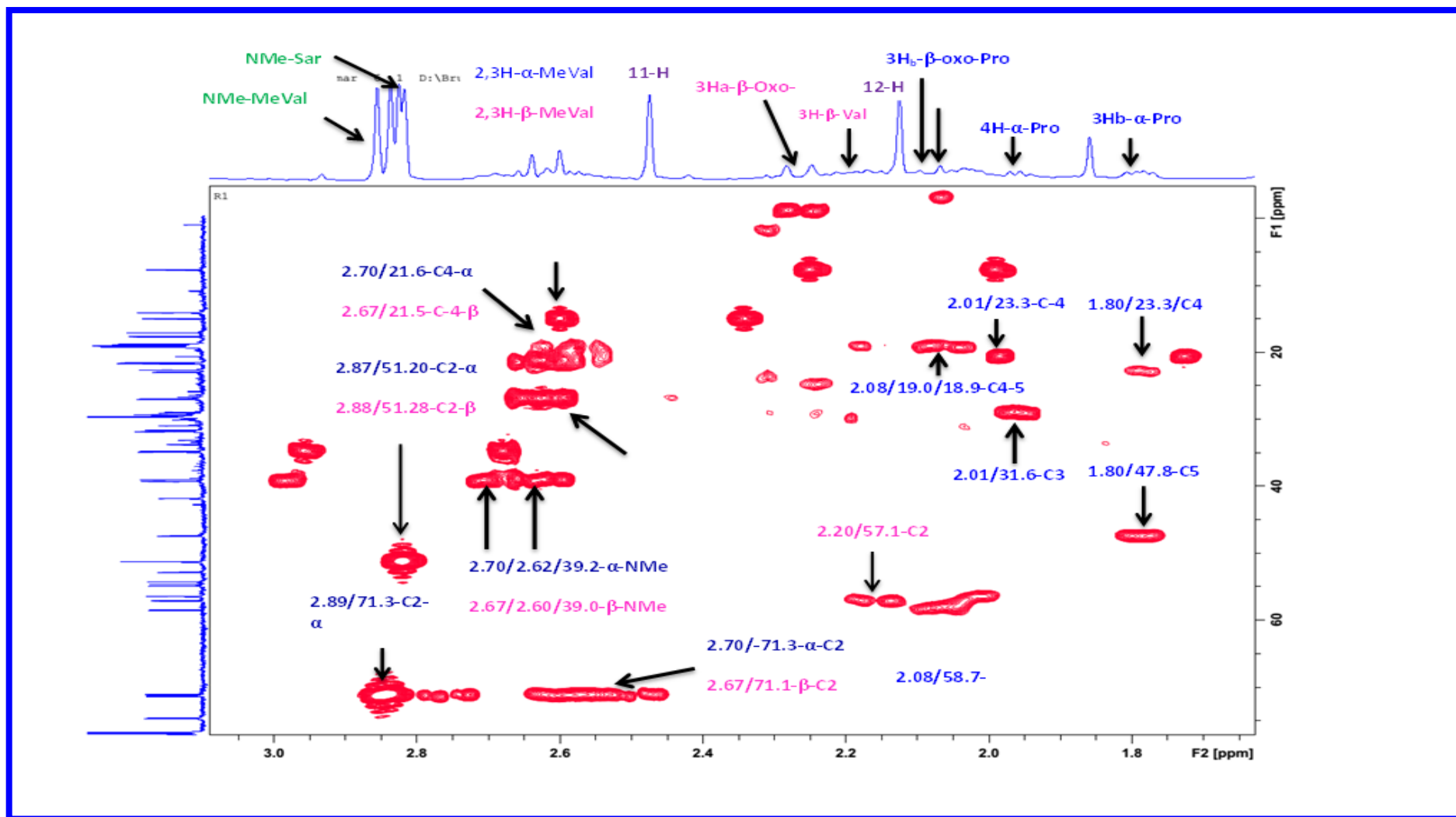


Figure S39. Expansion of HMBC (500 MHz, CDCl₃) Spectrum of Transitmycin (R1)

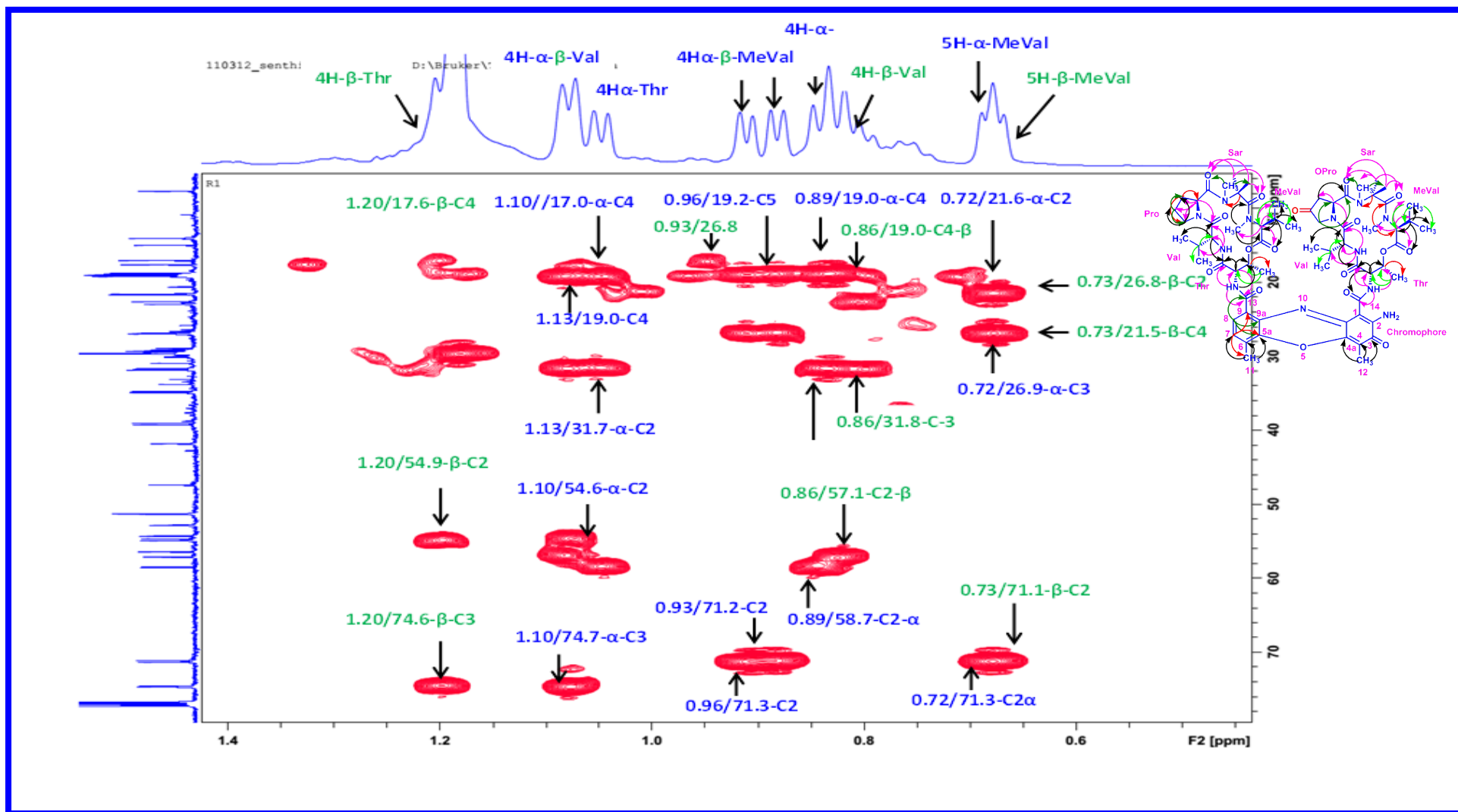


Figure S40. Expansion of HMBC (500 MHz, CDCl₃) Spectrum of Transitmycin (R1)

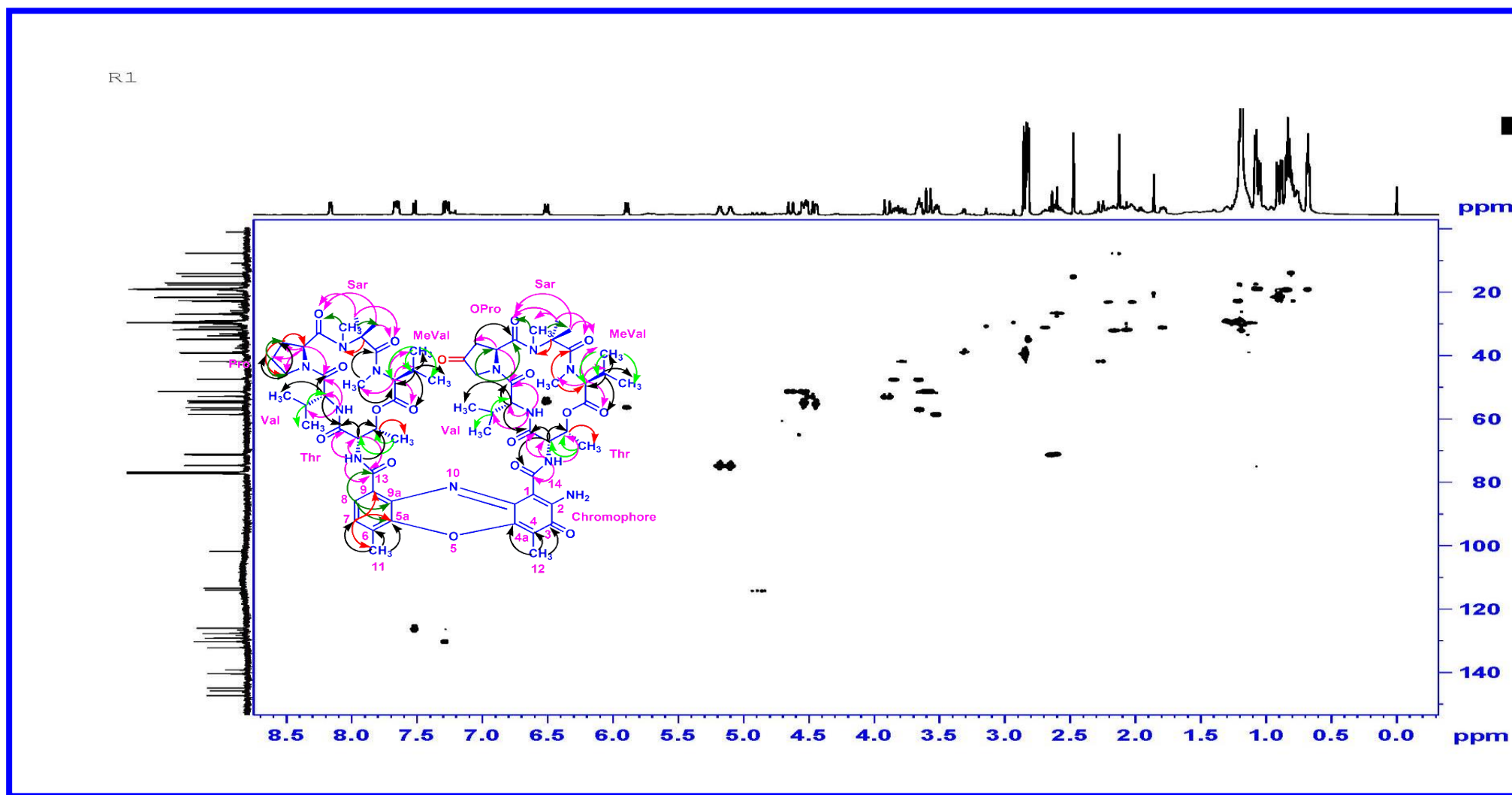


Figure S41. HSQC (500 MHz, CDCl₃) Spectrum of Transitmycin (R1)

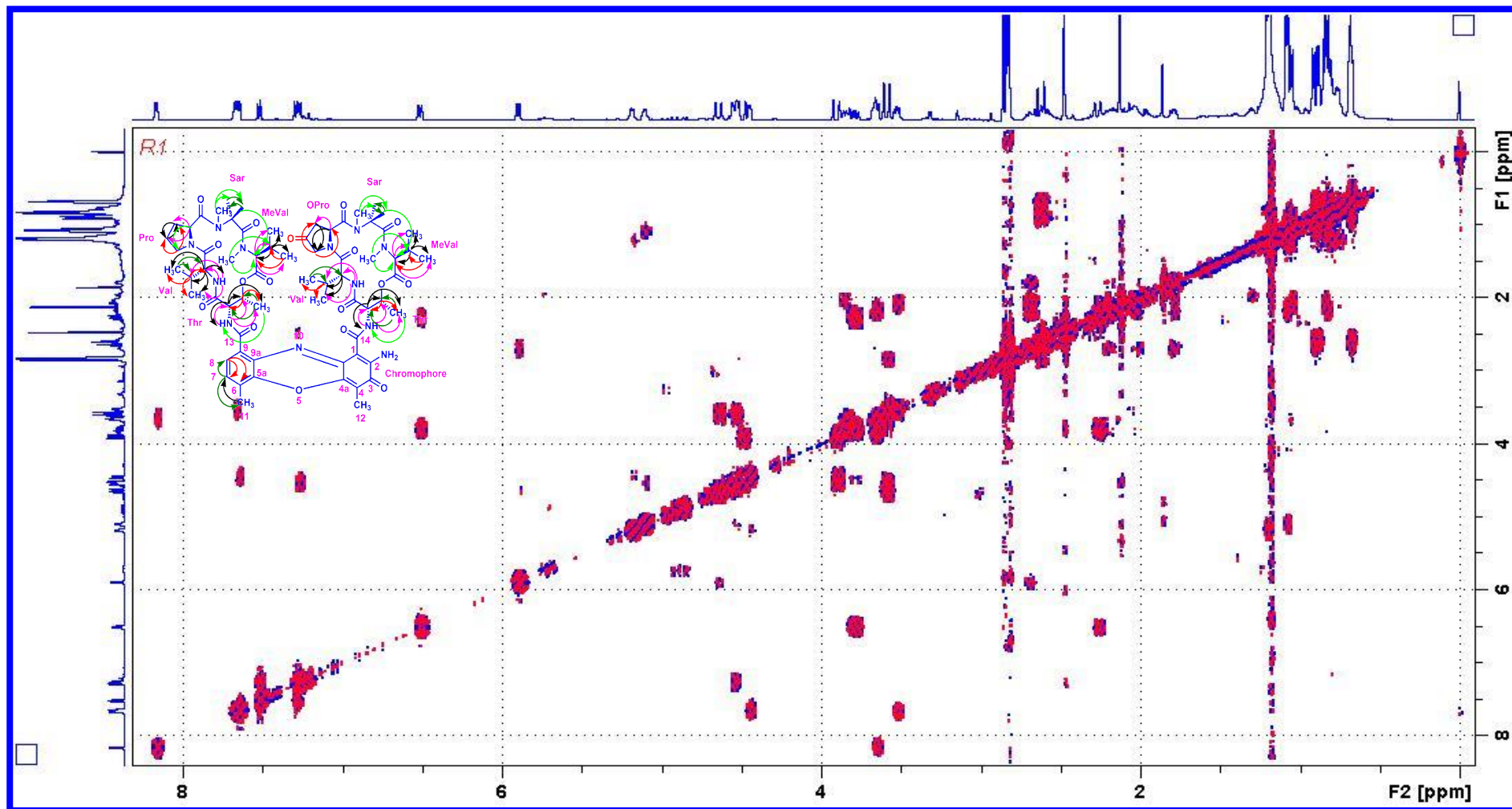


Figure S42. TOCSY (500 MHz, CDCl₃) Spectrum of Transimycin (R1)

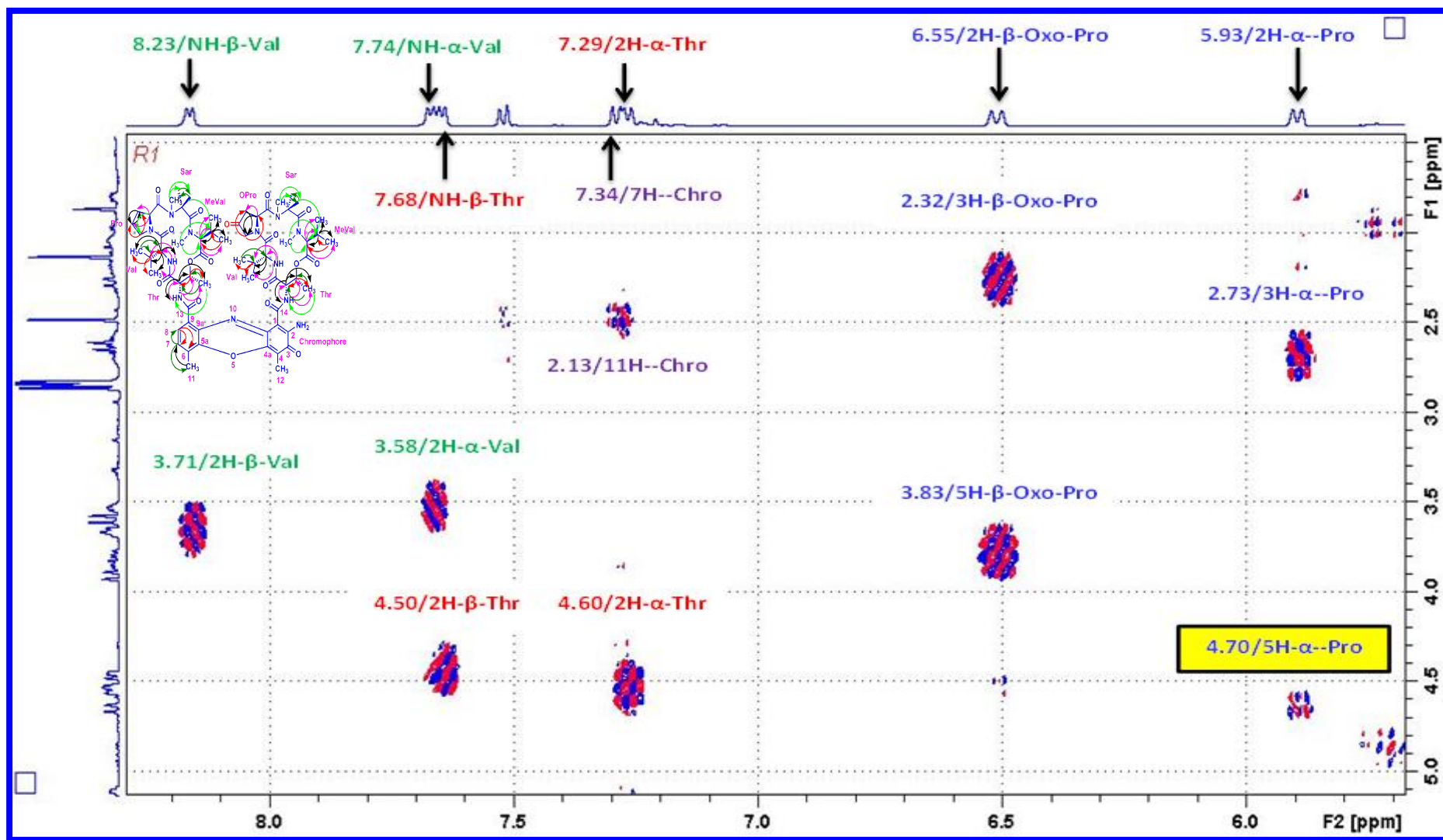


Figure S43. Expansion of TOCSY (500 MHz, CDCl₃) Spectrum of Transitymycin (R1)

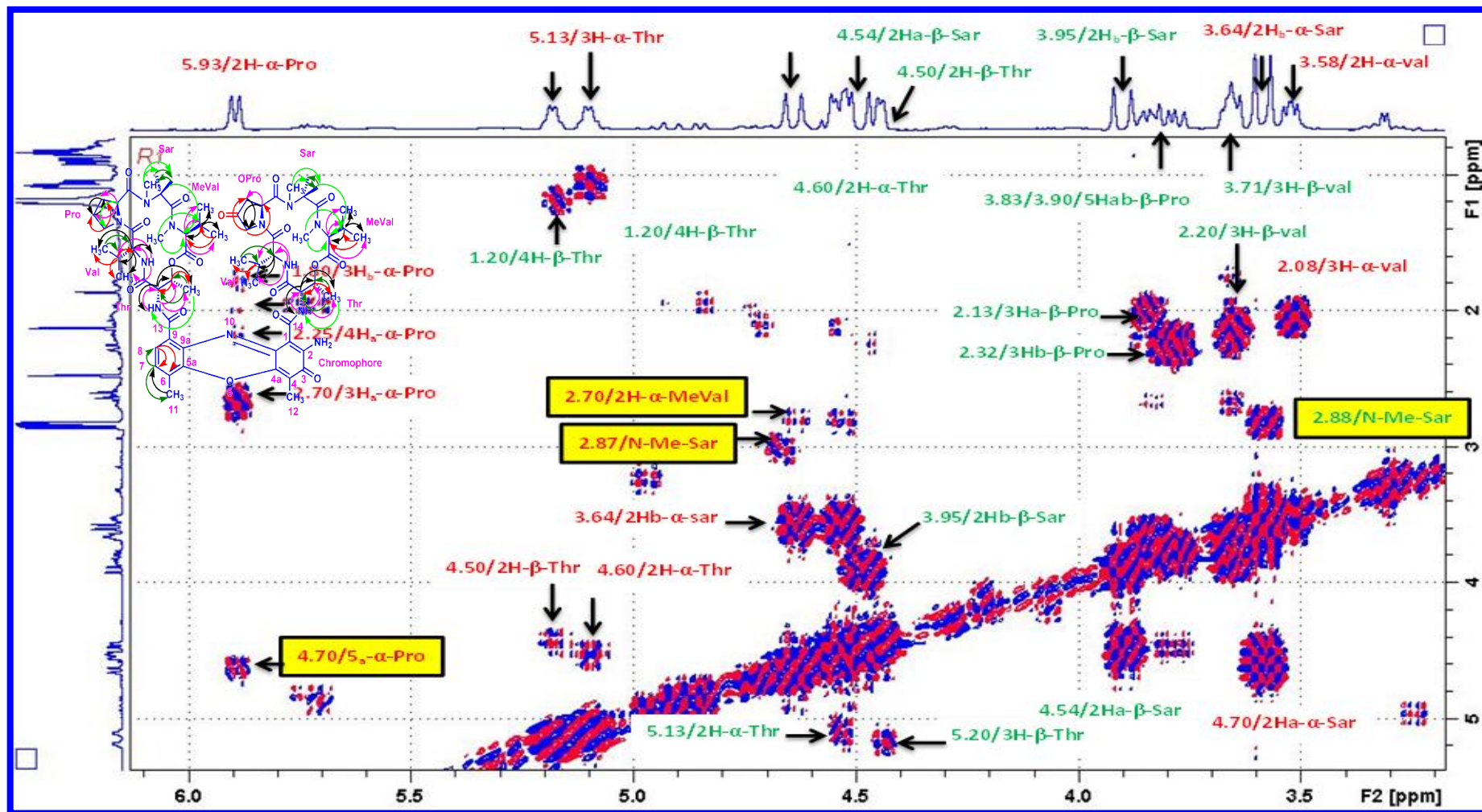


Figure S44. Expansion of TOCSY (500 MHz, CDCl_3) Spectrum of Transitmycin (R1)

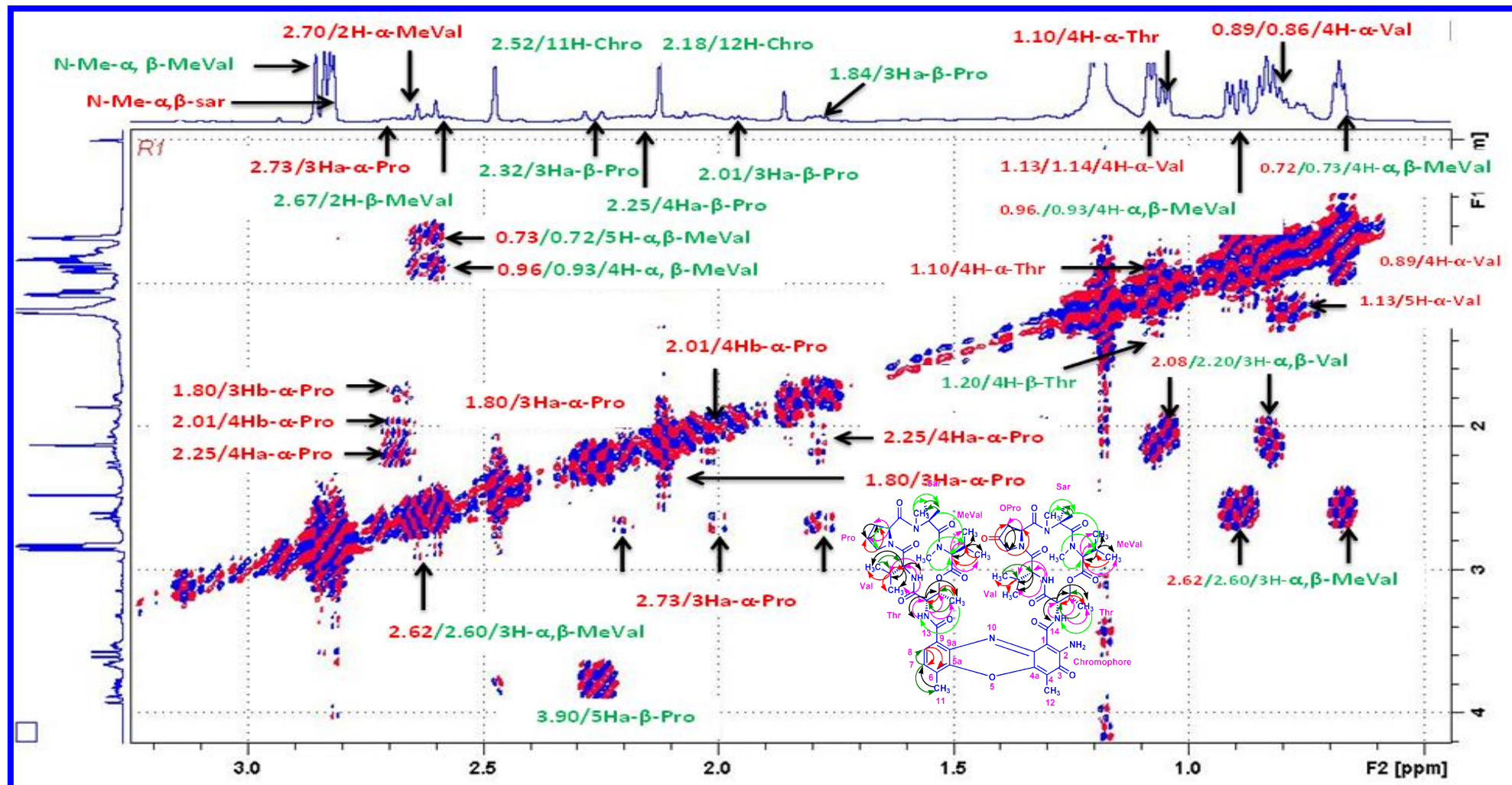


Figure S45. Expansion of TOCSY (500 MHz, CDCl₃) Spectrum of Transitmycin (R1)

R1...Pramal Biswa

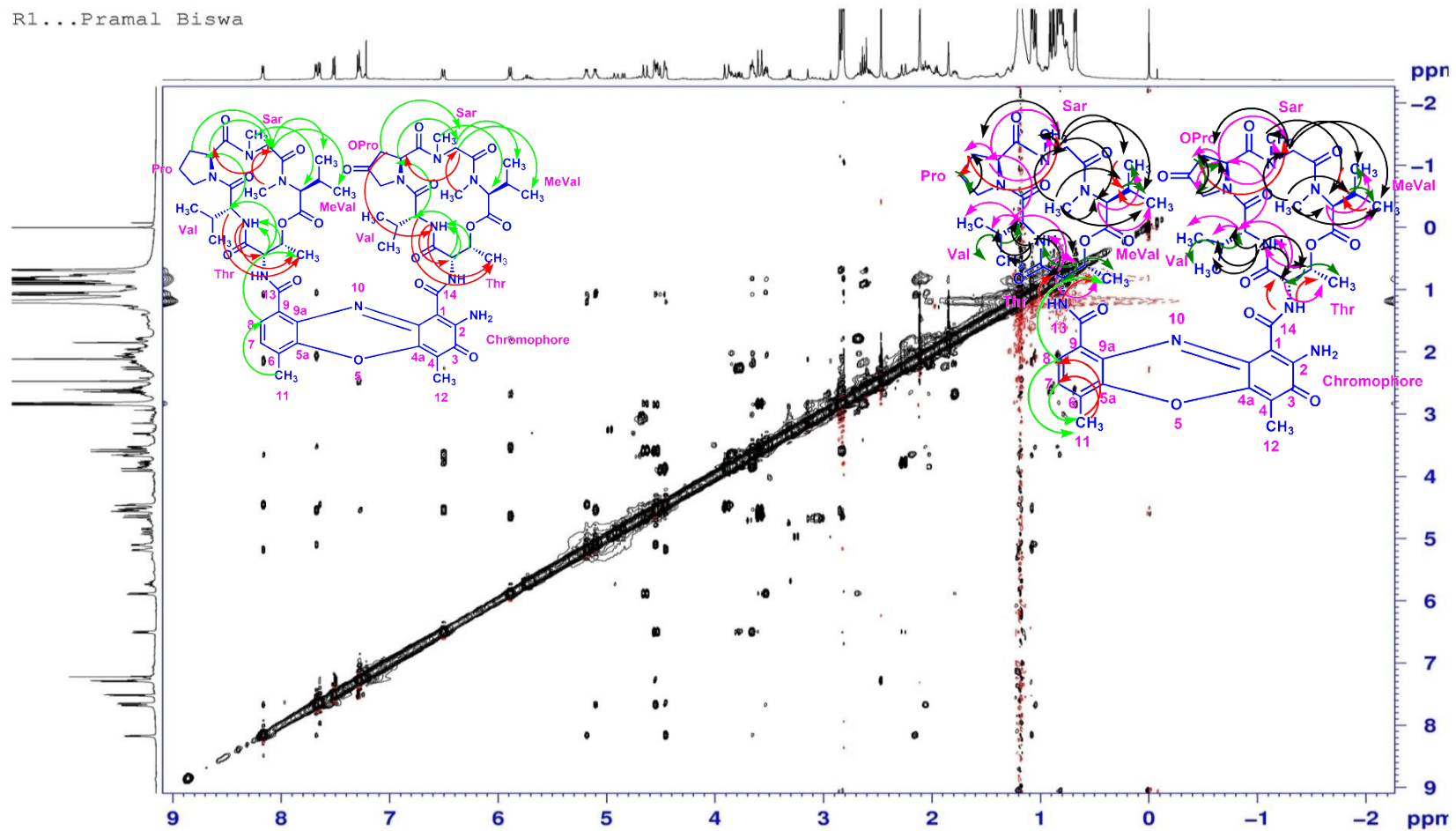


Figure S46. NOESY (500 MHz, CDCl₃) Spectrum of Transitmycin (R1)

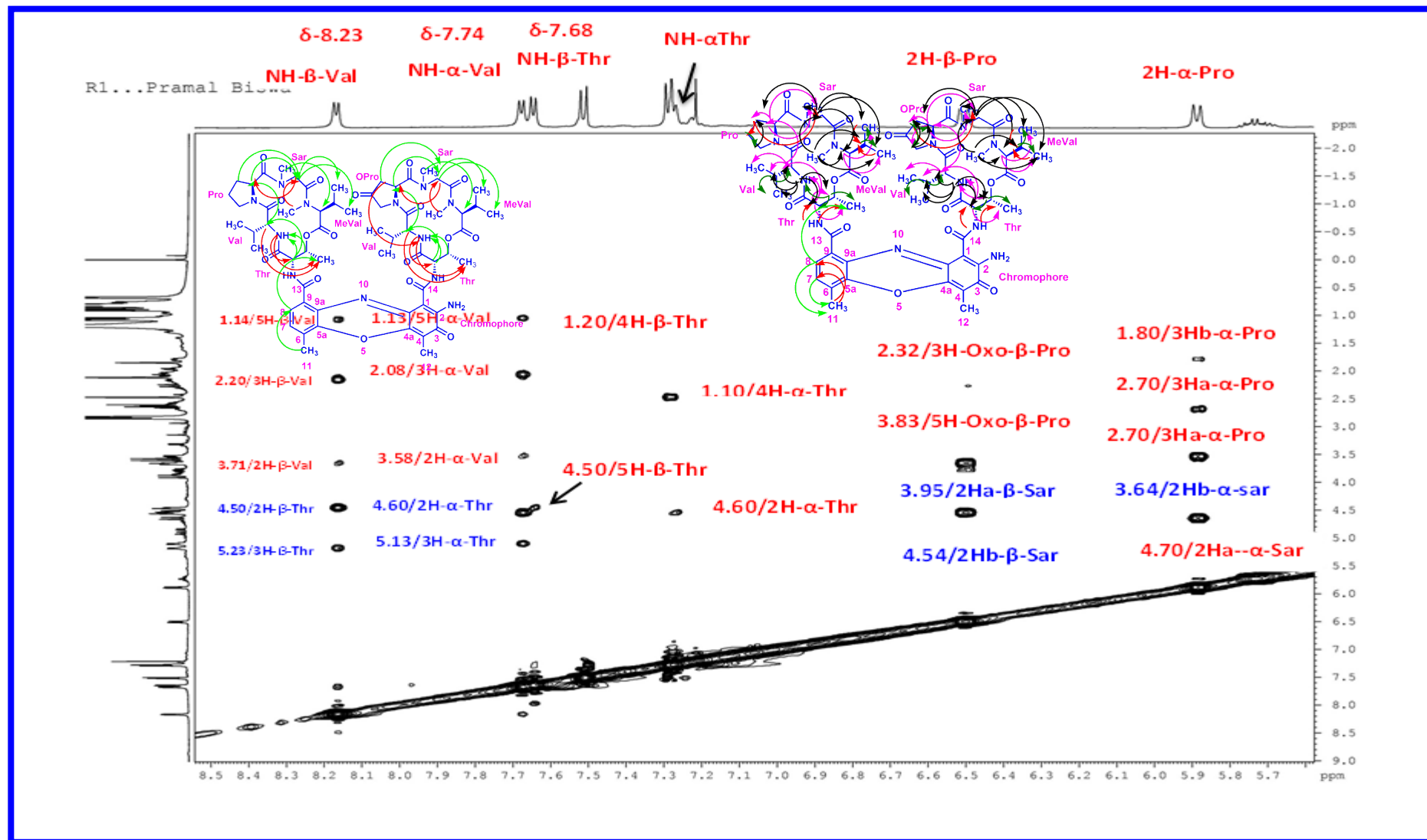


Figure S47. Expansion of NOESY (500 MHz, CDCl₃) Spectrum of Transitmycin (R1)

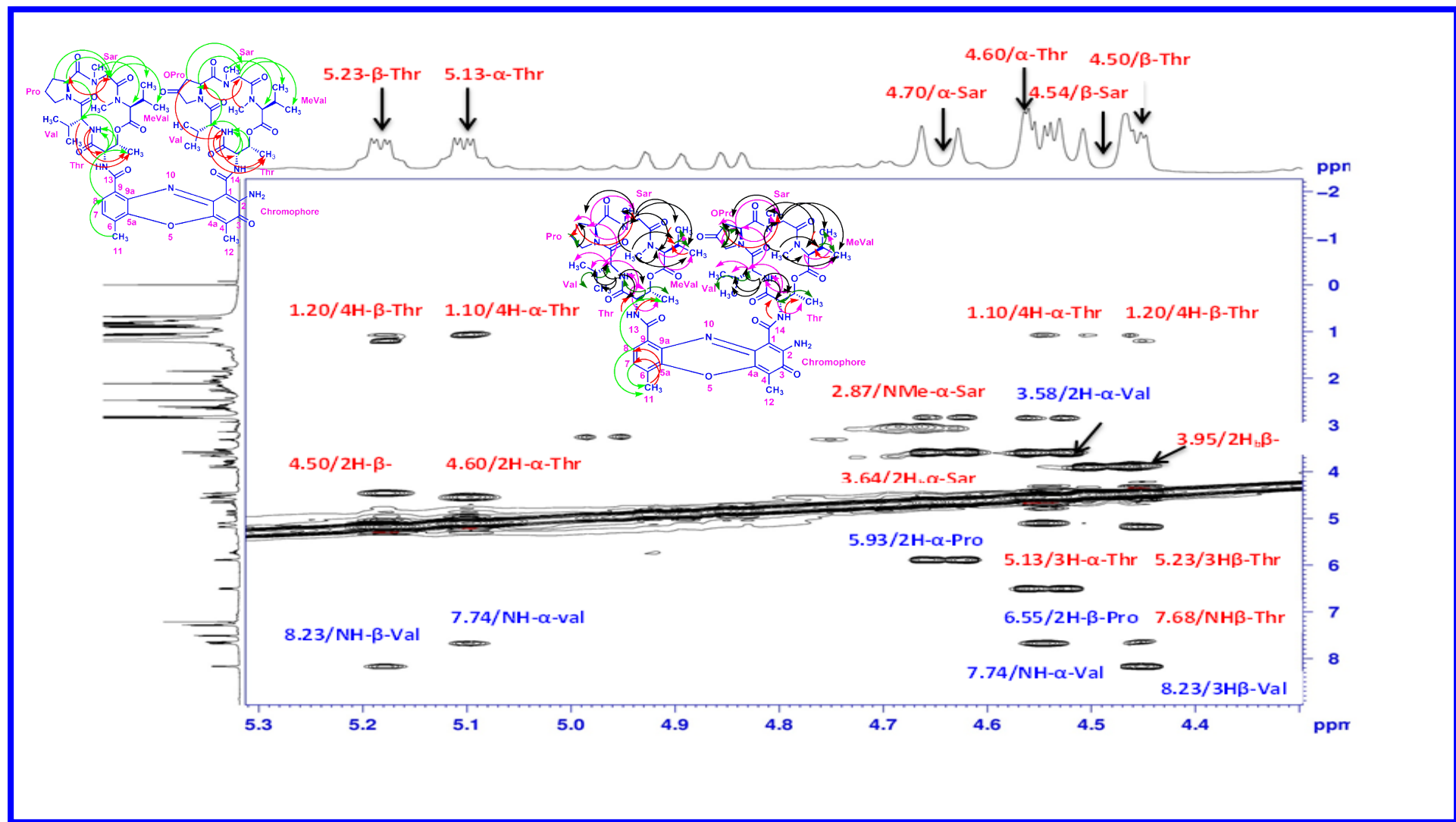


Figure S48. Expansion of NOESY (500 MHz, CDCl₃) Spectrum of Transitmycin (R1)

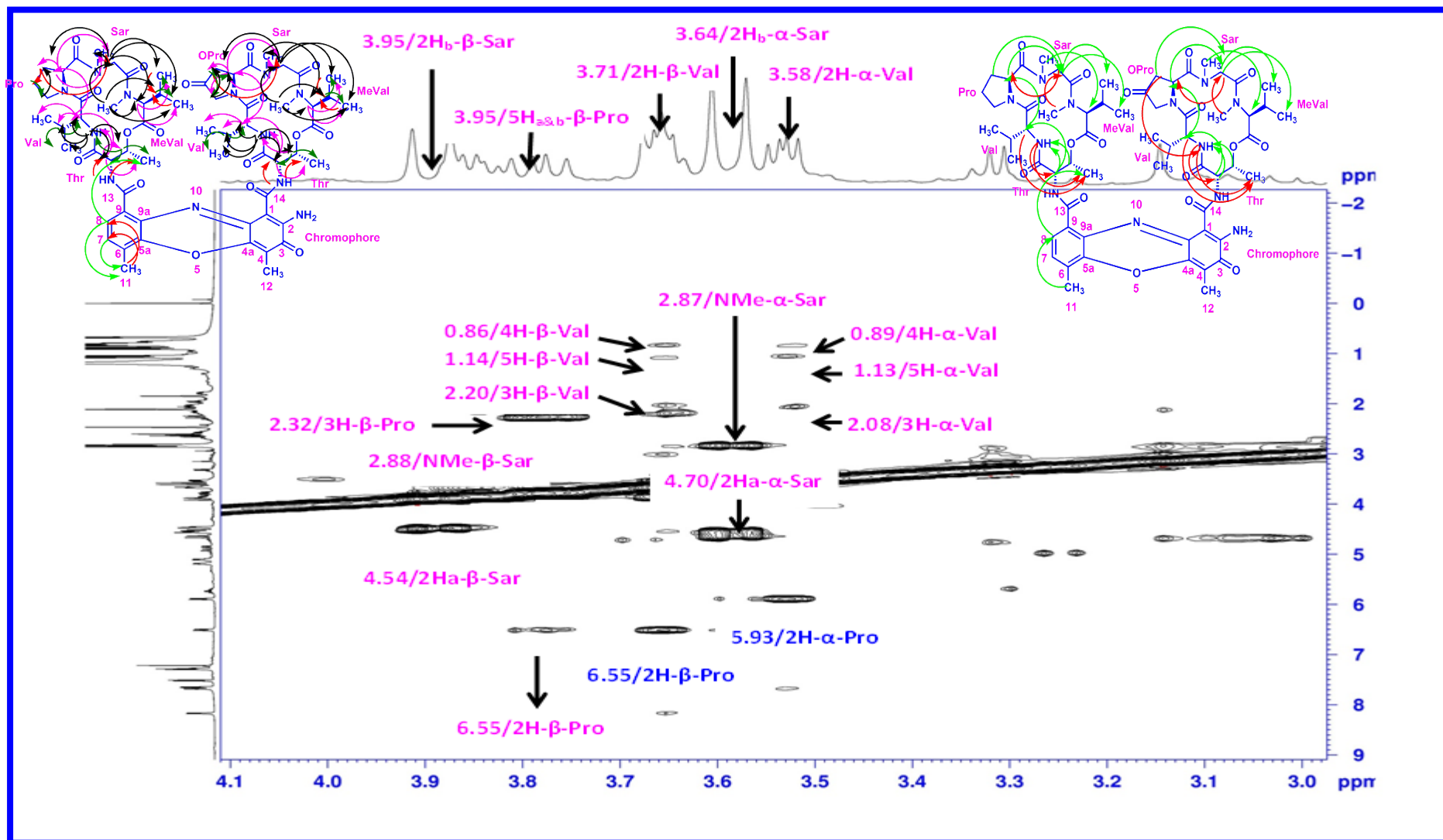


Figure S49. Expansion of NOESY (500 MHz, CDCl_3) Spectrum of Transimycin (R1)

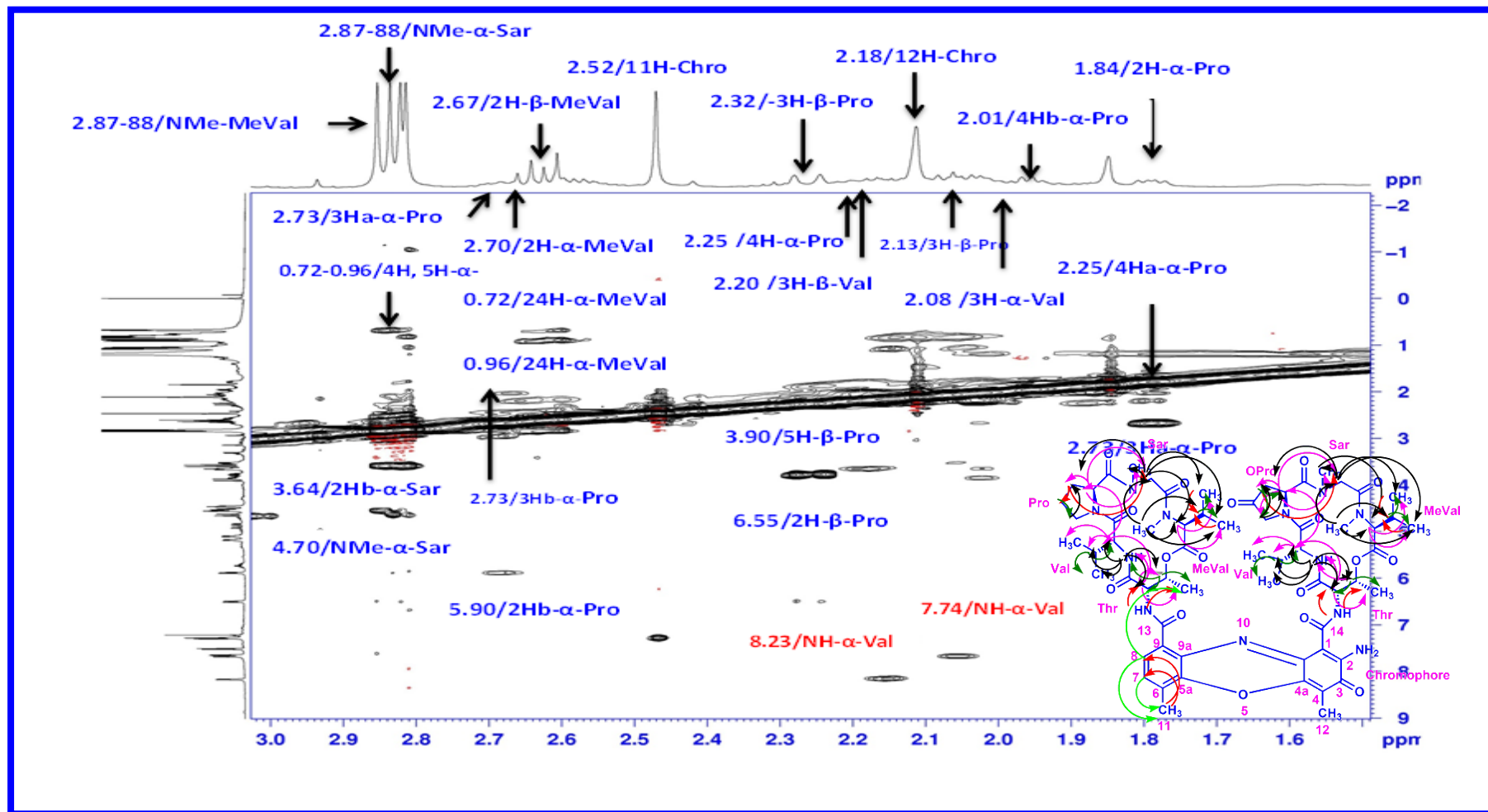


Figure S50. Expansion of NOESY (500 MHz, CDCl₃) Spectrum of Transitmycin (R1)

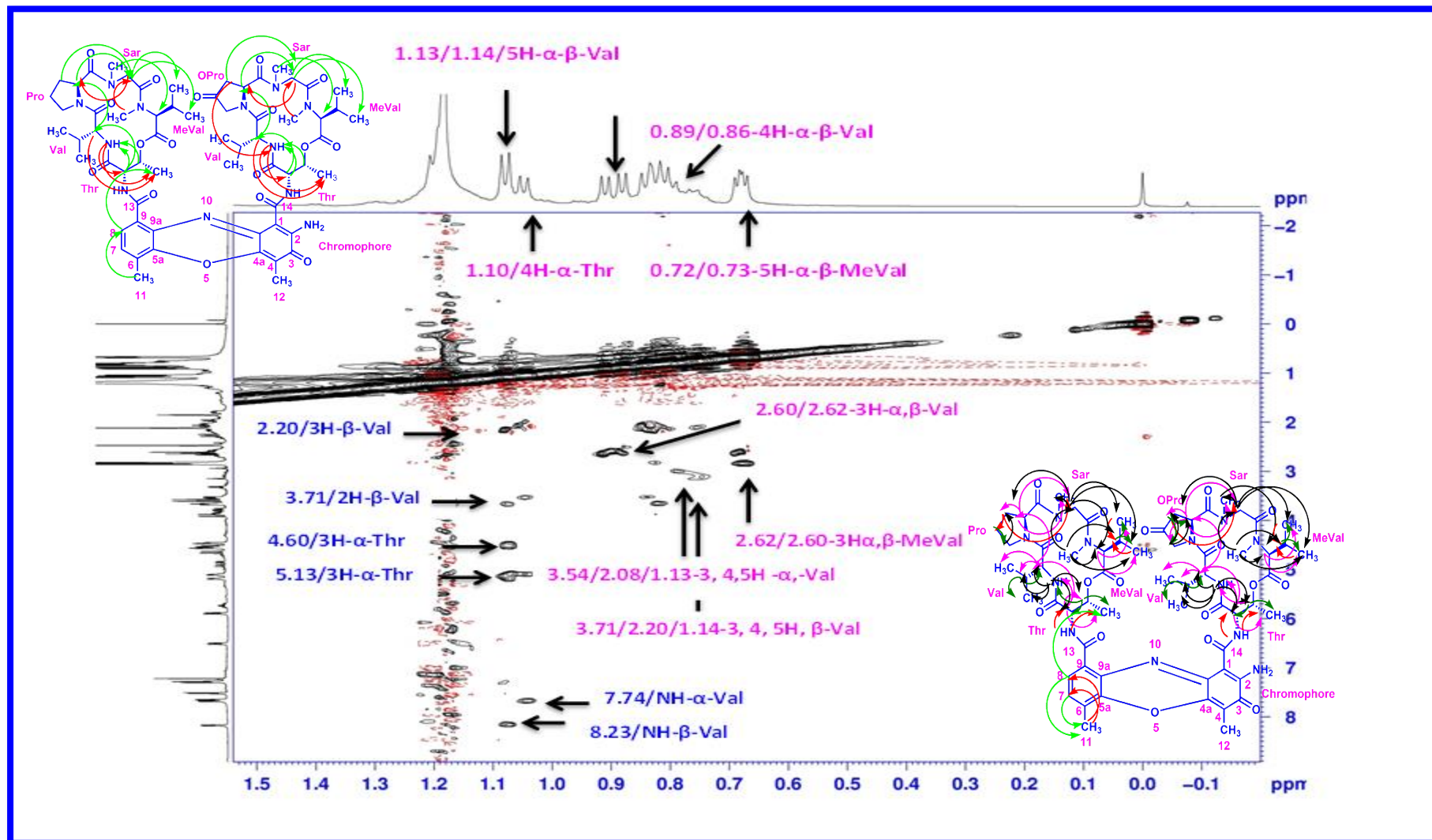


Figure S51. Expansion of NOESY (500 MHz, CDCl₃) Spectrum of Transitmycin (R1)

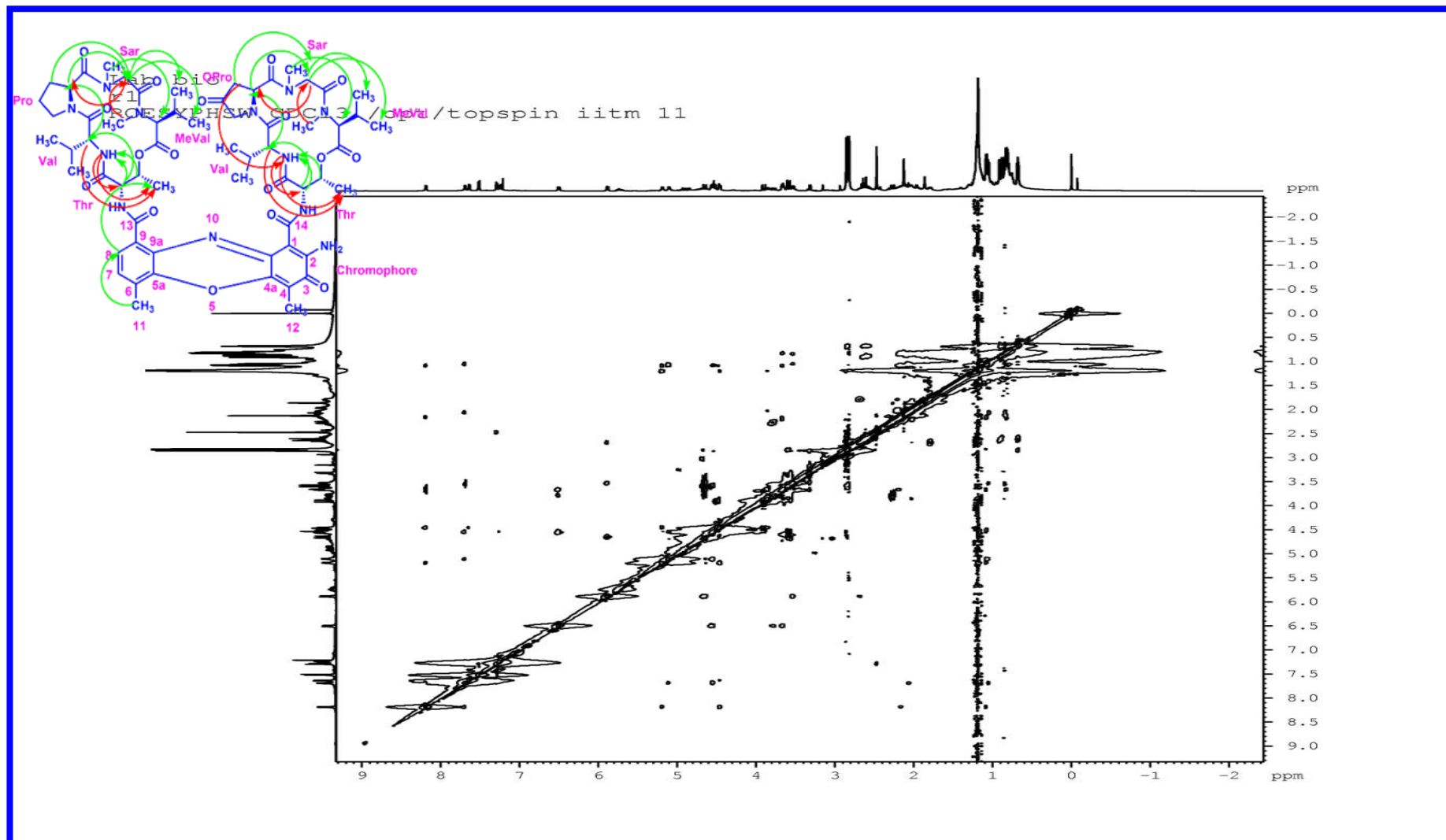


Figure S52. ROESY (500 MHz) Spectrum of Transitmycin (R1)

Table S5: NMR data of Trasitmycin (R1) in CDCl₃ (¹H: 500 MHz ¹³C: 125 MHz)

α- ring	position	δC	δH	J (Hz)	COSY	TOCSY	HMBC	ROSEY
Thr	1	168.8	-					
	2	54.6	4.60	d , 10.0	3, 4, -NH	3, 4	1, 3, 13	3, 4, 2-Val, Val-NH
	3	74.7	5.13	m	2, 4,- NH	2, 4,	4	2, 4, Val-NH
	4	17.0	1.10	d, 6.5	2, 3	2, 3, -NH	2, 3	2, 3, Val-NH
	NH	-	7.29	d, 7.0	2, 3, 4	2, 3, 4	1, 3, 13	2, 4
L-Val	1	173.4						
	2	58.7	3.58	dd, 10.5,6.5	3, 4, 5, - NH	3, 4, 5, - NH	1, 5, 1-Thr	3, 4, 5, 2-Pro
	3	31.7	2.08	m	2, 4, 5	2, 4, 5	2,5	4, 5, 4-Thr
	4	19.0	0.89	d, 7.0	2, 3	2, 3, -NH	2,3,5	2, 3, 5
	5	18.9	1.13	d, 6.5	2, 3	2, 3, -NH	2,3,4	2, 3, 2-Val, Val-NH
	NH	-	7.74	d, 5.5	2, 3, 4, 5	2, 3, 4, 5	2, 3, 1-Thr	2, 3, 4, 5 2- Thr, 3-Thr
Pro	1	173.1	-					
	2	56.4	5.93	d, 9.5	3a,3b,4a,4b	3a,3b 4a,	3, 4, 5,	3a, 3b,

						4b	1-Val	2a-Sar,2b-Sar, Sar-NMe
	3	31.6	2.73 1.84	dd, 17.5,7.0 dd, 19.5, 6.5	3b, 4a, 4b 3a, 4a,	3b, 4a, 4b 3a, 4a,	1, 2, 4 1, 4, 5	3b, 2a-Sar, 2b-Sar 3a, 4a, 4b
	4	23.3	2.26 2.01	d, 16.5 d, 8.0	3a, 3b, 4b 3b, 4a	3a, 3b, 4b 3b, 4a	3, 5 3, 5	4b, 5a, 5b 4a, 5a
	5a 5b	47.8	3.86 3.67	d, 18.5 d, 18.5	3a, 4a, 4b 3a, 4a, 4b	3a, 4a, 4b 3a, 4a, 4b	4, 1-Val	5b
Sar	1	166.2	-					
	2	51.2	2a, 4.70 2b, 3.64	d, 17.5 d, 17.5	2b 2a	2b, NMe 2a, NMe	1, NMe,1- pro 1, NMe,1- Pro	2b, NMe, 2-Pro 4-MeVal, 5-MeVal, NMe
	N-Me	34.9	2.87	s		2a, 2b	2, 1-Pro	2b, 3-MeVal
MeVal	1	167.4	-					
	2	71.3	2.70	d, 9.0	3, 4, 5	3, 4, 5	1, 3,4,NMe	4, 5
	3	26.9	2.62	d, 7.0	2, 4, 5	2, 4, 5	1, 3, 4, 5, NMe	4, 5

	4	21.6	0.96	d, 6.0	2, 3	2, 3, 5	2, 3, 5	3
	5	19.2	0.72	d, 6.5	2, 3	2, 3, 4	2, 3, 4	3
	N-Me	39.2	2.89	s	-	2, 3	2, 1-Sar	2, 3, 5, 2a-Sar, 2b-Sar

β- ring	position	δC	δH	J (Hz)	COSY	TOCSY	HMBC	NOESY
Thr	1	168.9	-					
	2	54.9	4.50	d, 9.0	3,4, -NH	3, 4	1, 3, 14	3, 4, 2-Val, Val-NH
	3	74.6	5.23	m	2,4,- NH	2, 4	4	2,4, Val-NH
	4	17.6	1.20	d, 6.0	2, 3	2, 3, - NH	2, 3	2,3, Val-NH
	NH	-	7.68	d, 6.0	2, 3, 4	2, 3, 4	1, 3, 14	2, 4
L-Val	1	173.9	-					
	2	57.1	3.71	dd, 10.5, 6.5	3, 4, 5, -NH	3, 4, 5, -NH	1, 3, 5, 1-Thr,	3, 4, 5, 2-Oxo pro
	3	31.8	2.20	m	2, 4, 5	2, 4, 5	2, 5	4, 5, 4-Thr
	4	19.0	0.86	d, 7.0	2, 3	2, 3, -NH	2, 3, 5	2, 3, 5
	5	18.8	1.14	d, 7.0	2, 3	2, 3, -NH	2, 3, 4	2, 3, 2-Val, Val-NH
	NH		8.23	d, 6.0	2, 3, 4, 5	2, 3, 4, 5	2, 3, 1-Thr	2, 3, 4, 5 2-Thr, 3-Thr
Oxo-Pro	1	172.7	-					

	2	54.2	6.55	dd, 10.0, 2.0	3, 5	3, 5	3, 1-Val	3, 5 2a-Sar, 2b-sar NMe
	3	41.8	2.32 2.13	d, 18.5 d, 13.0	2, 5 2, 5	2, 5 2, 5	1 1	2, 5 2, 5
	4	208.0	-	-			-	
	5	53.7	3.83 3.90	d, 18.5 dd, 18.5 12.0	2, 3 2, 3	2, 3 2, 3	1, 2 1, 2	2, 3 2, 3
Sar	1	166.4						
	2	51.28	2a, 4.54 2b, 3.95	d, 19.5 d, 19.0	2b 2a	2b, NMe 2a, NMe	1, NMe, 1-Pro 1, NMe, 1-Pro	2b, NMe, 2-oxopro 4-MeVal, 5-MeVal, NMe
	N-Me	34.7	2.88	s		2a, 2b	2, 1-Pro	2b, 2MeVal
MeVal	1	167.4	-	-				
	2	71.1	2.67	d, 8.5	3, 4, 5	3, 4, 5	1, 3, 4, 5, NMe	4, 5

	3	26.8	2.60	d, 8.0	2, 4, 5	2, 4, 5	1, 3, 4, 5, NMe	4, 5
	4	21.5	0.93	d, 6.0	2, 3	2, 3, 5	2, 3, 5	3
	5	19.1	0.73	d, 6.0	2, 3	2, 3, 4	2, 3, 4	3
	N-Me	39.0	2.91	s	-	2, 3	2, 1- Sar	2, 5, 2a-Sar, 2b-Sar

Chromophore

Position	δC	δH	J (Hz)	COSY	TOCSY	HMBC	NOESY
1	101.8	-					
2	147.3	-					
3	179.0	-					
4	113.4	-					
4a	144.9						
5	-						
5a	140.3						
6	127.6	-					
7	130.2	7.34	d, 8.0	8, 11	8, 11	5a, 9, 11-Me	11
8	126.0	7.56	d, 7.5	7, 11	7, 11	9a, 5a, 13	11

9	132.1	-					
9a	128.4	-					
10	-	-					
11	14.9	2.52	s	7, 8	7, 8	5a, 6, 7	7, 8
12	7.6	2.18	s	-	-	3, 4, 4a	-
13	166.0	-					
14	165.8	-					

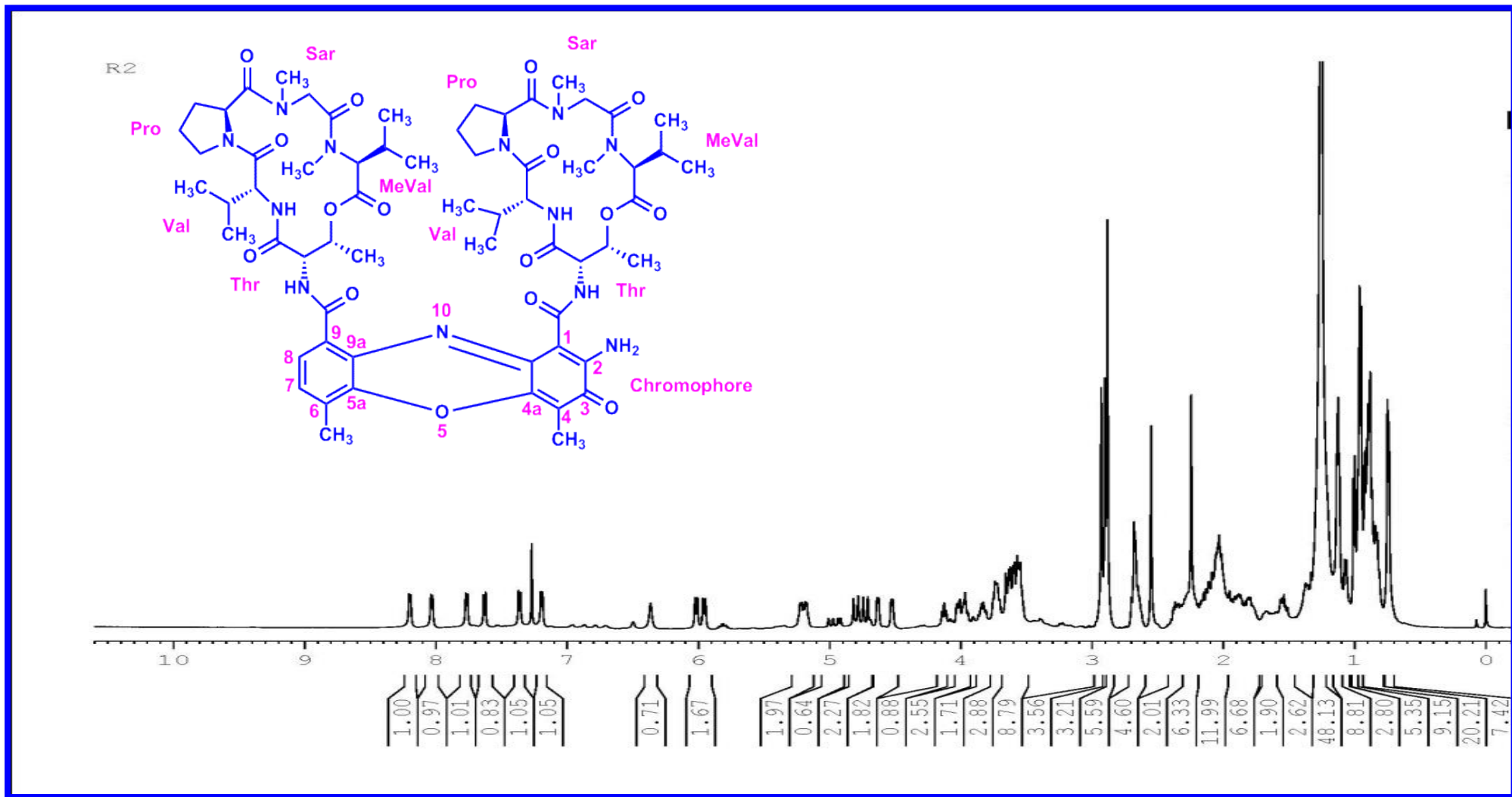


Figure S53. ¹H-NMR (500 MHz, CDCl₃) Spectrum Of Compound R2

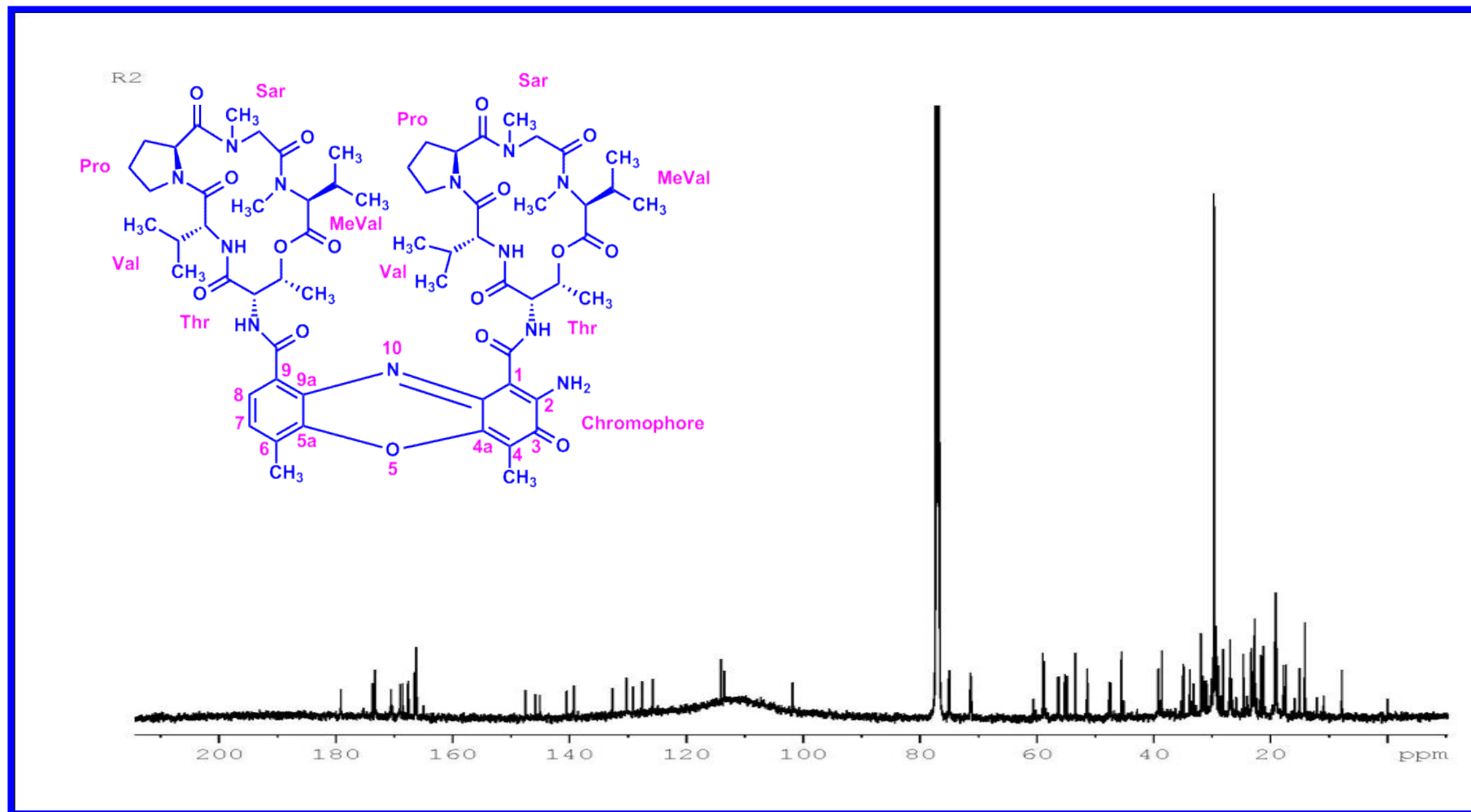


Figure S54. ¹³C NMR (125 MHz, CDCl₃) Spectrum Of Compound R2

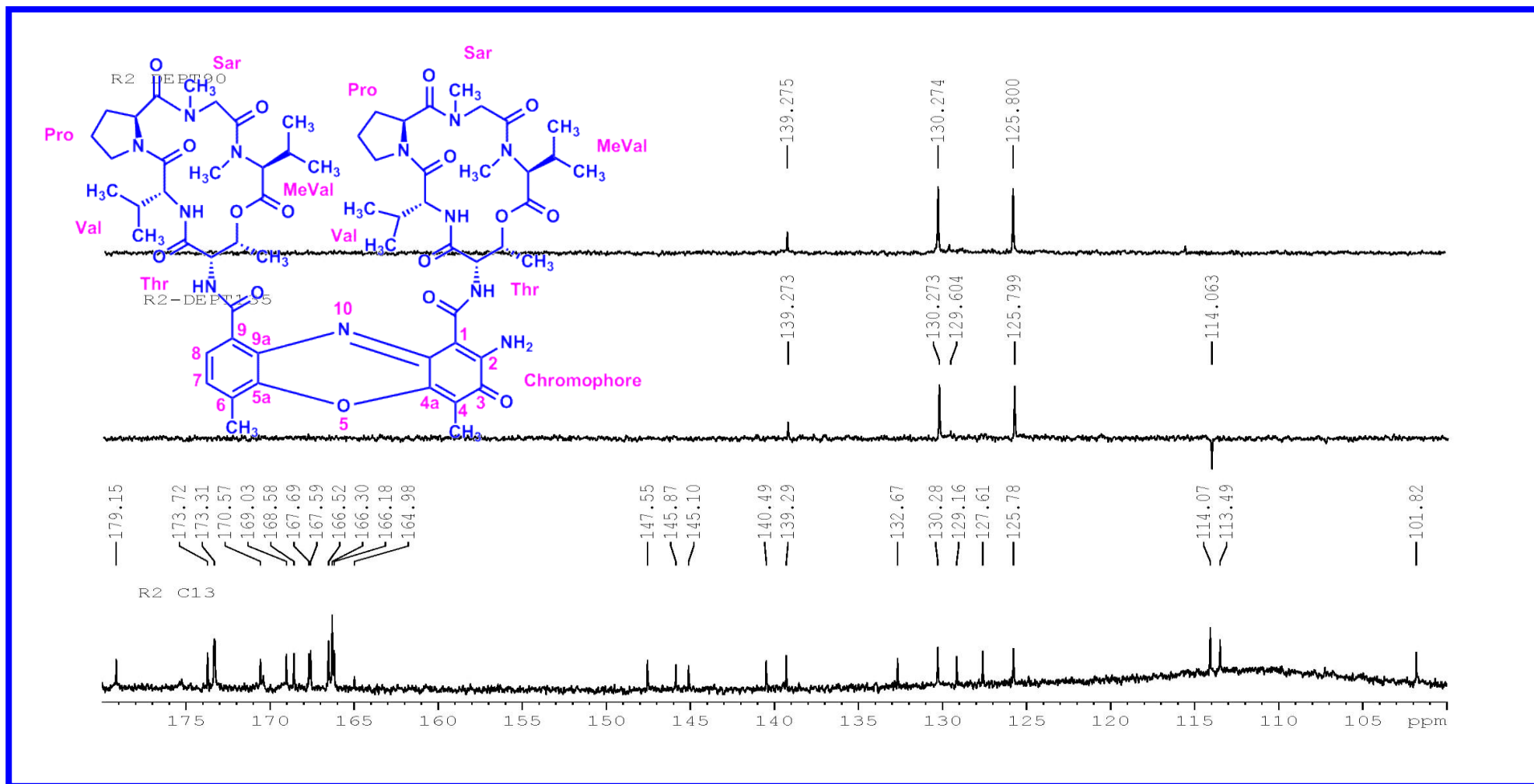


Figure S55. DEPT135&90 (125 MHz, CDCl₃) Spectrum of Compound R2

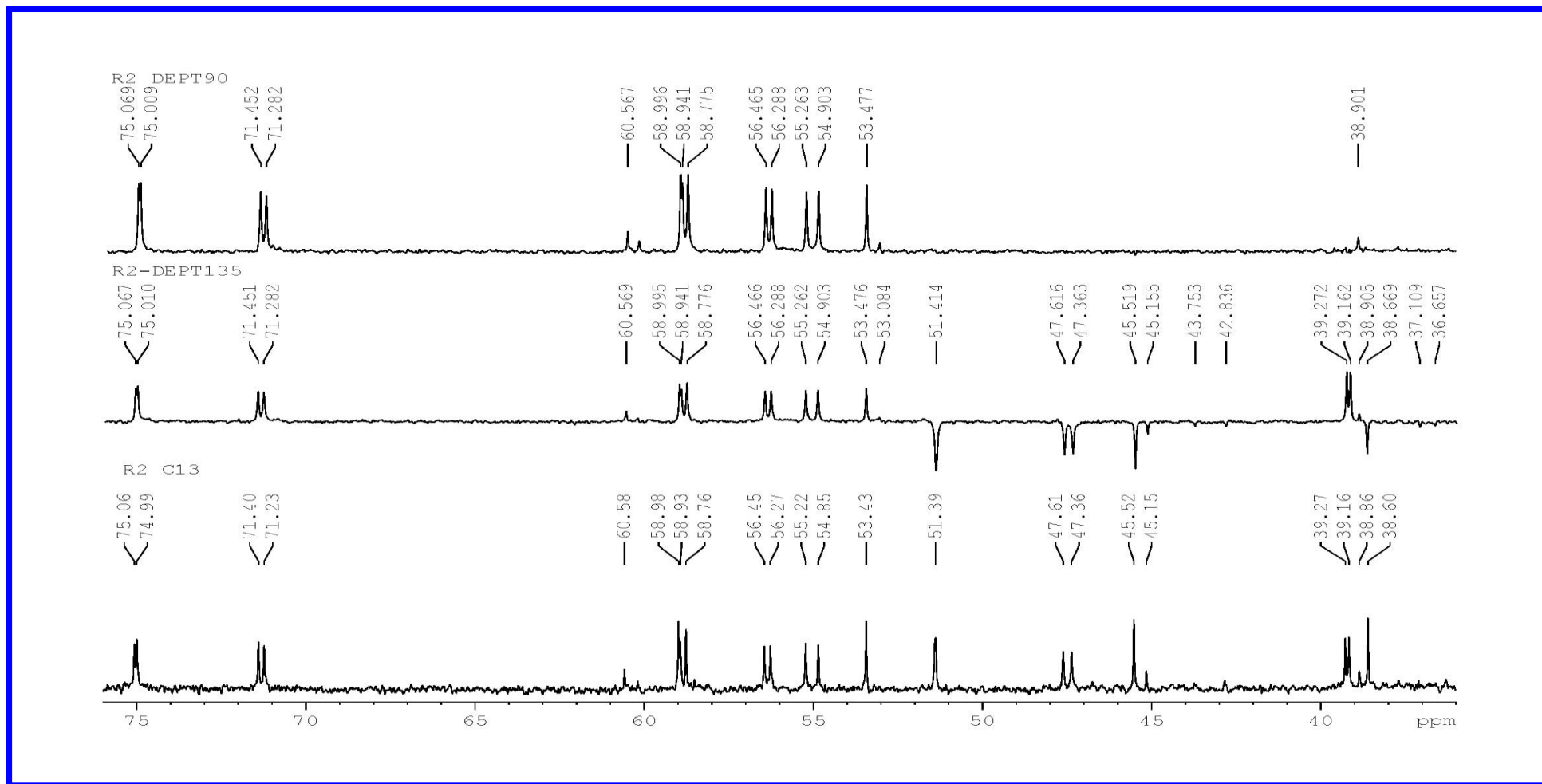


Figure S56. Expansion of DEPT135 &90 (125 MHz, CDCl₃) Spectrum of Compound R2

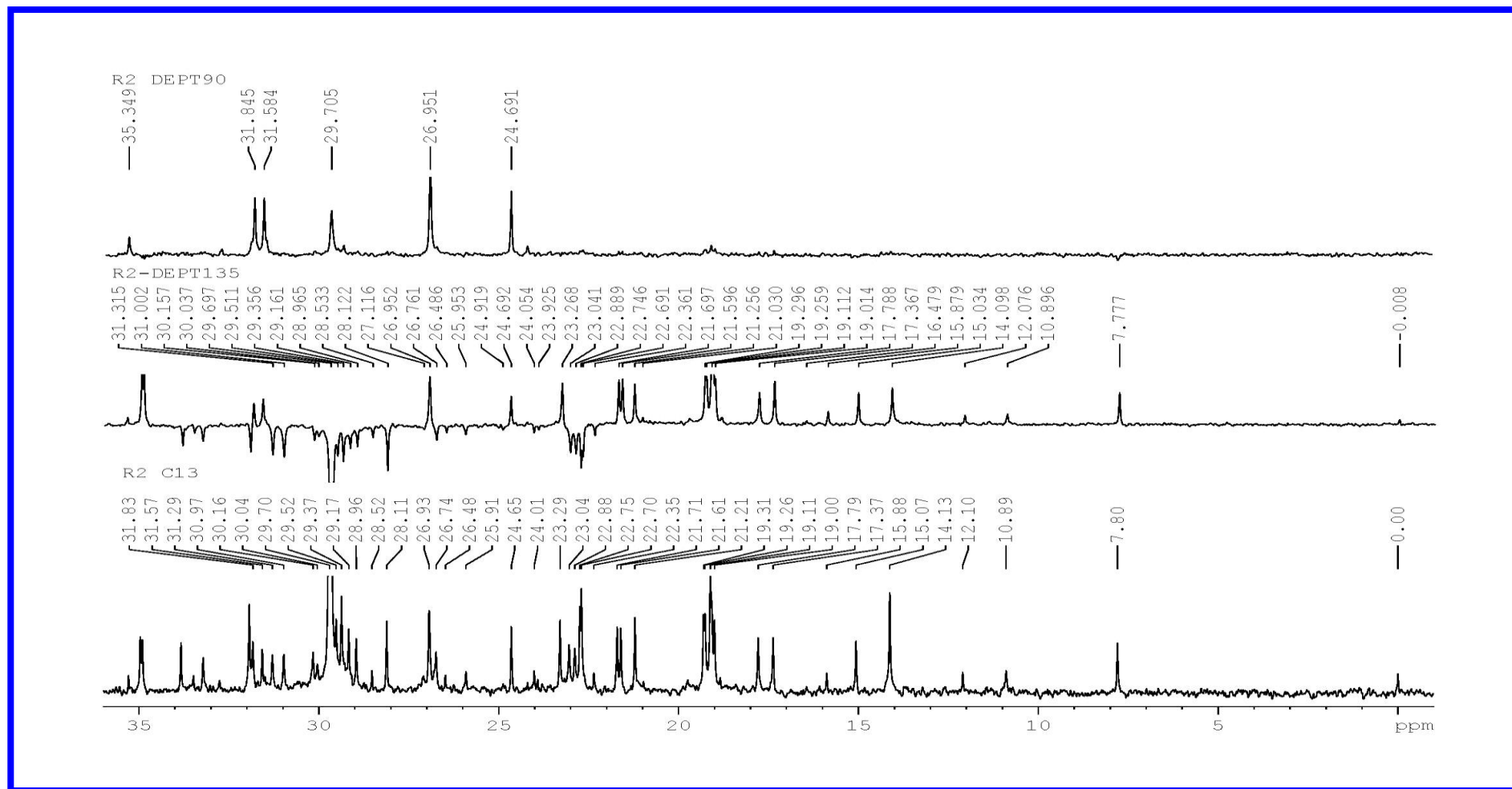


Figure S57. Expansion of DEPT135 & 90 (125 MHz, CDCl₃) Spectrum of Compound R2

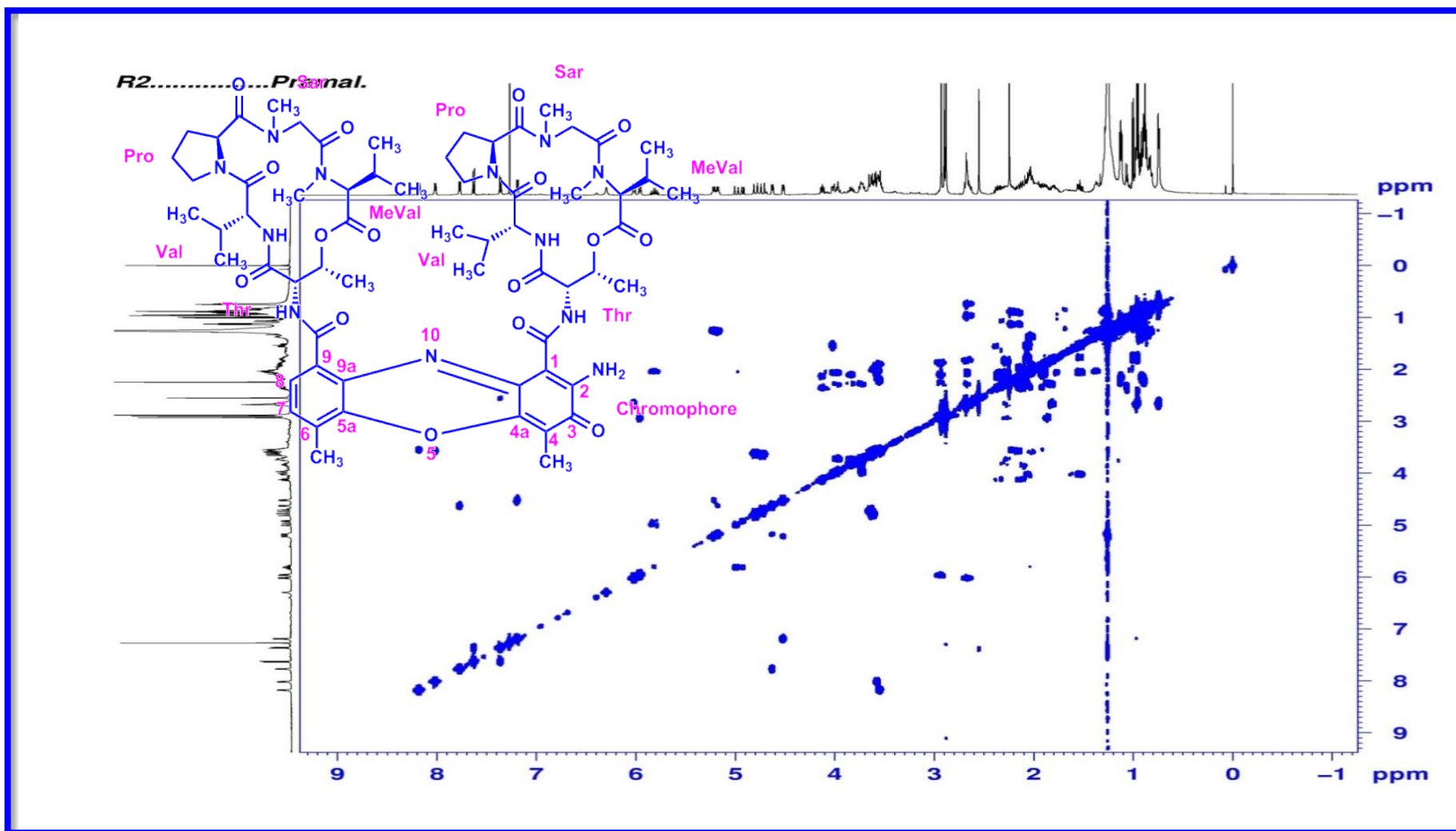


Figure S58. COSY (500 MHz) Spectrum of Compound R2

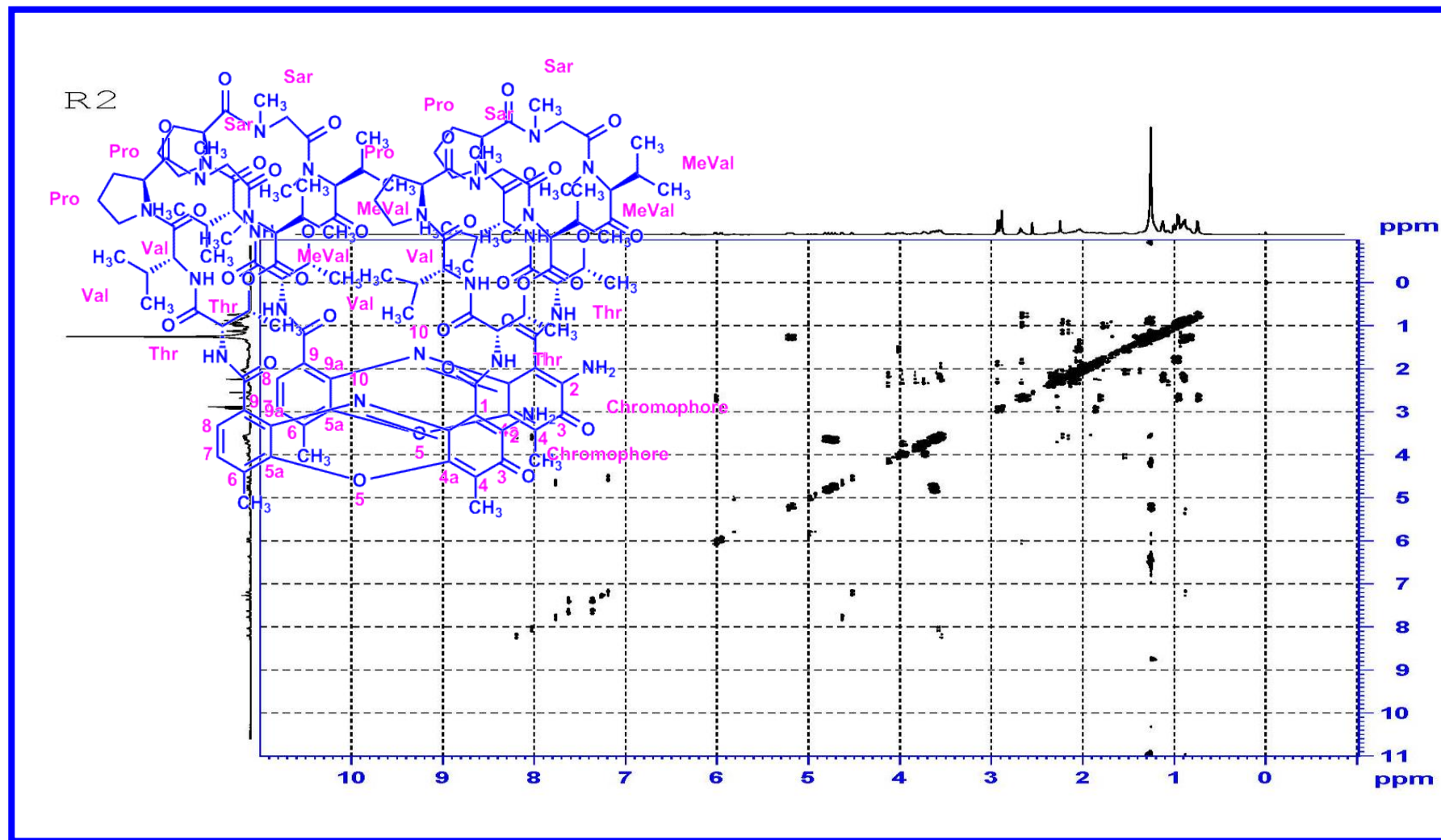


Figure S59. DQF-COSY (500 MHz) Spectrum of Compound R2

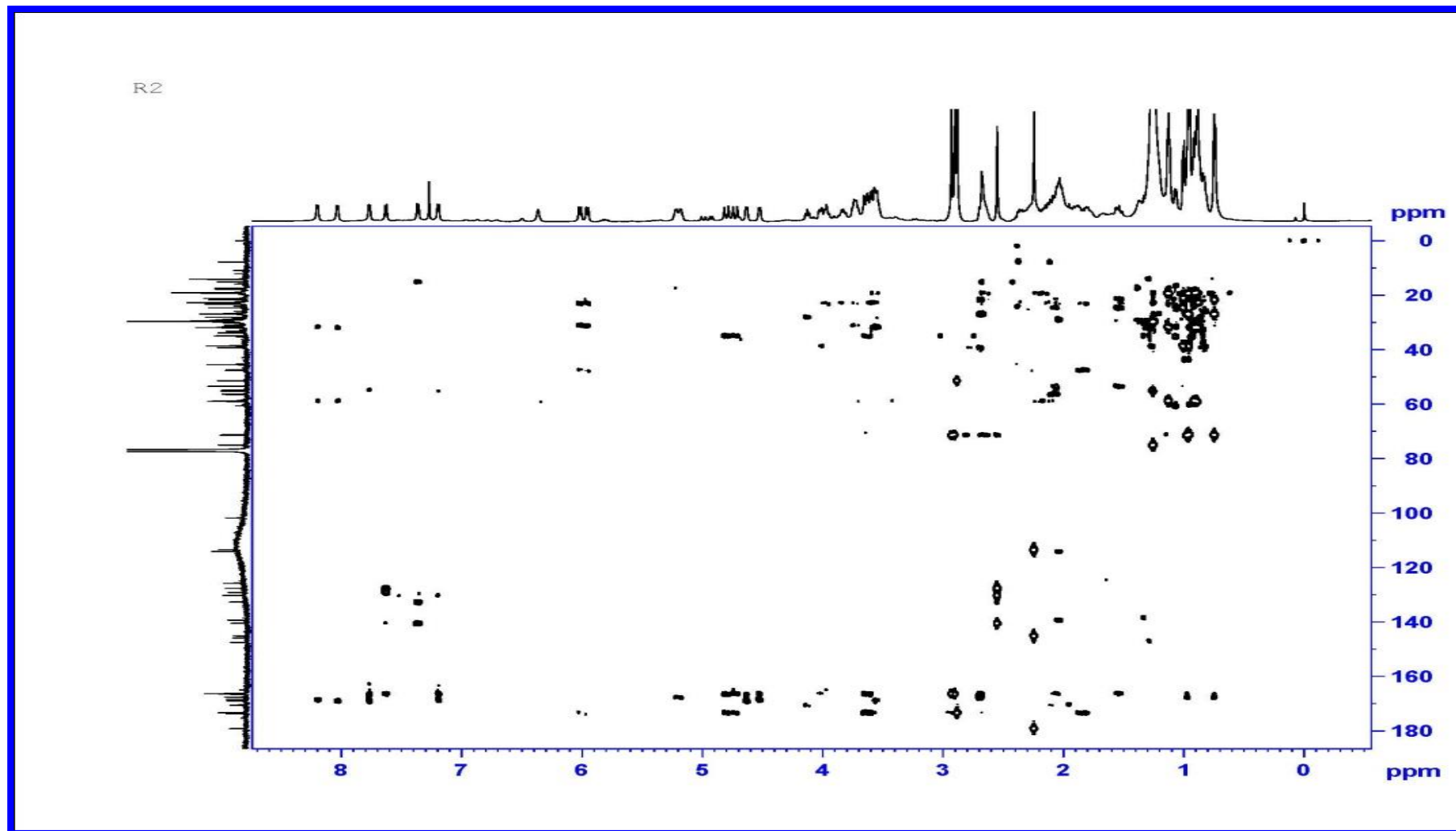


Figure S60. HMBC (500 MHz) Spectrum Compound of R2

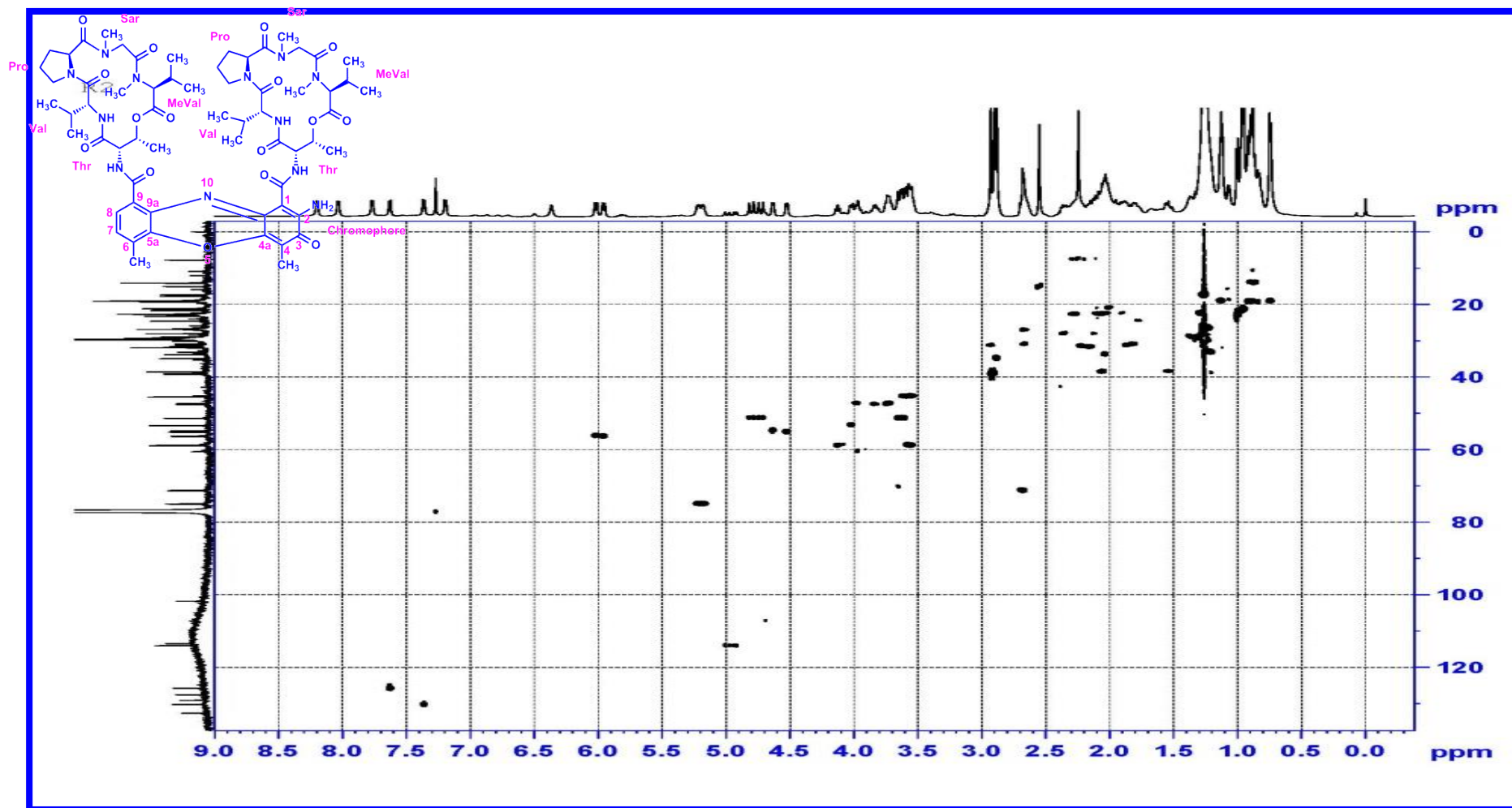


Figure S61. HSQC (500 MHz) Spectrum of Compound R2

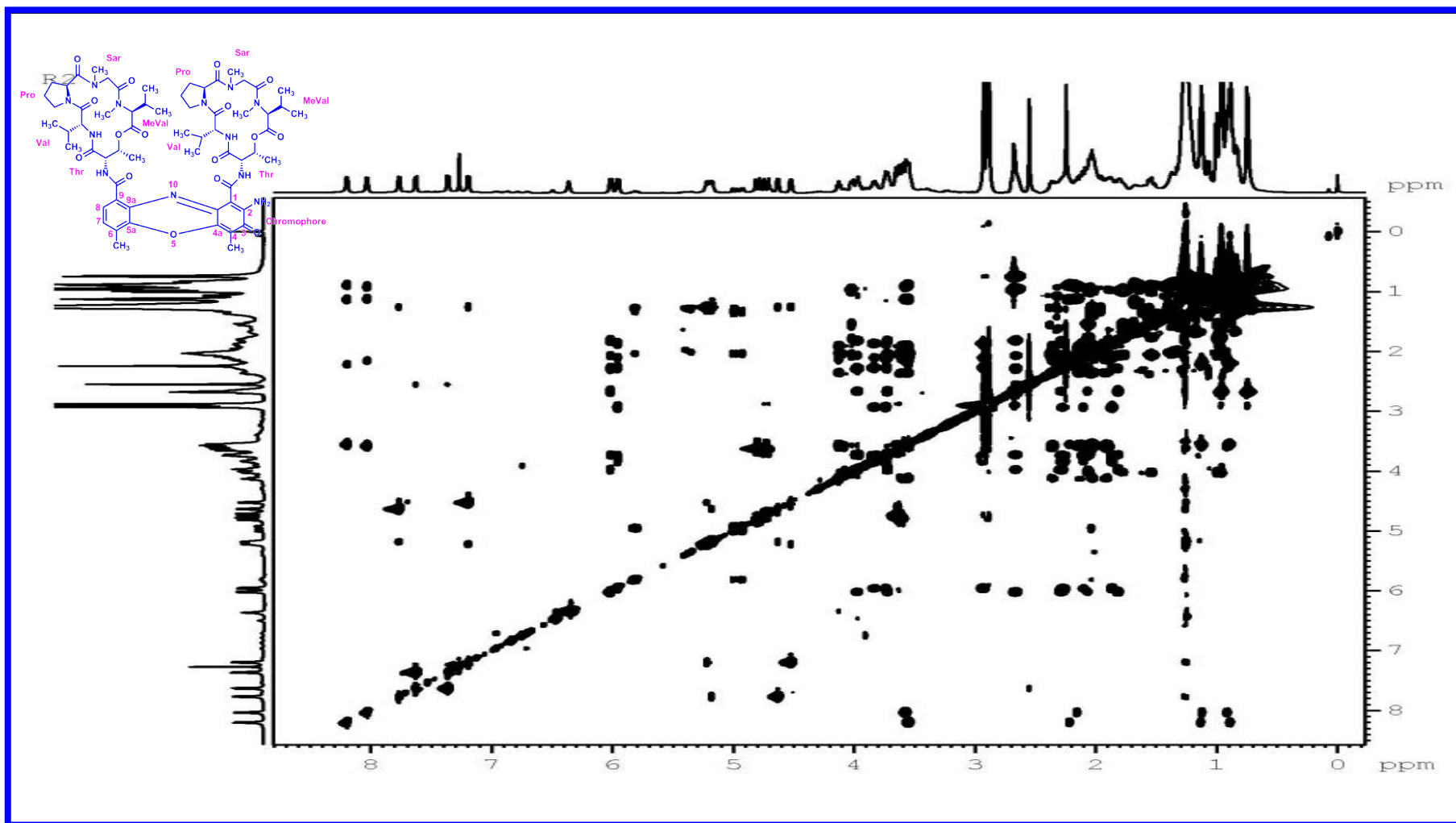


Figure S62. TOCSY (500 MHz) Spectrum of Compound R2

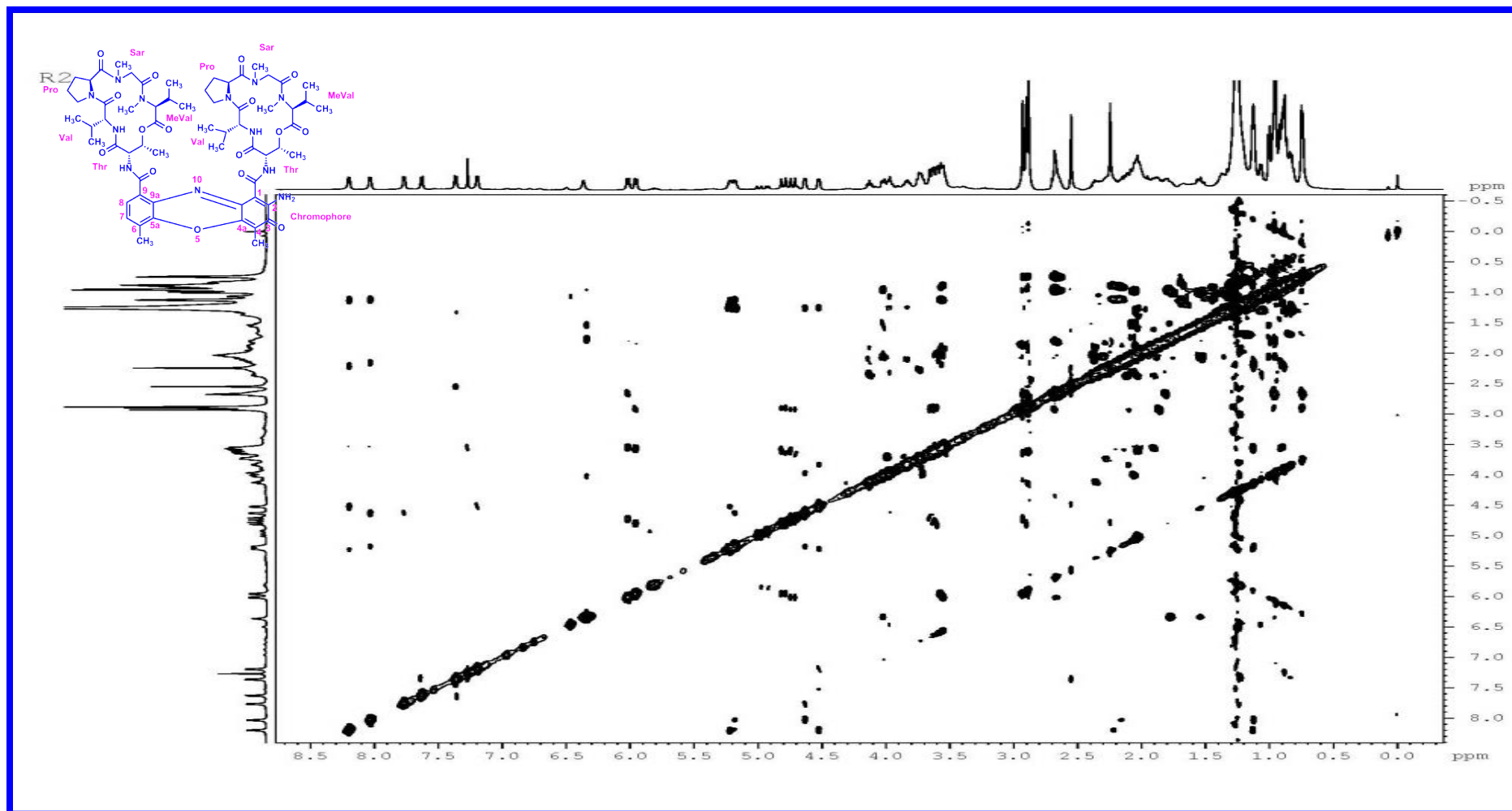


Figure S63. NOESY (500 MHz) Spectrum of Compound R2

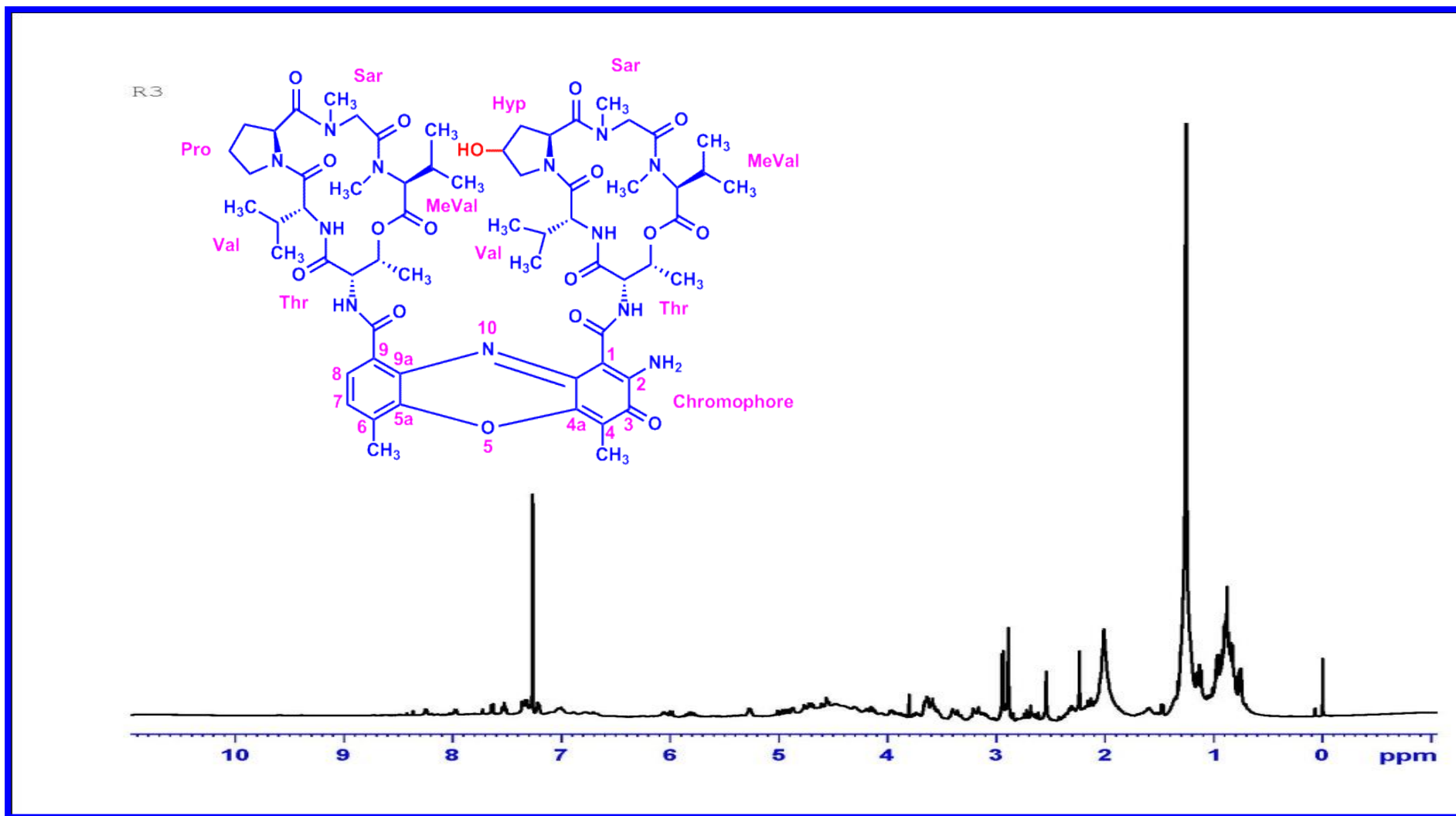


Figure S64. $^1\text{H-NMR}$ (500 MHz, CDCl_3) Spectrum of Compound R3

R3

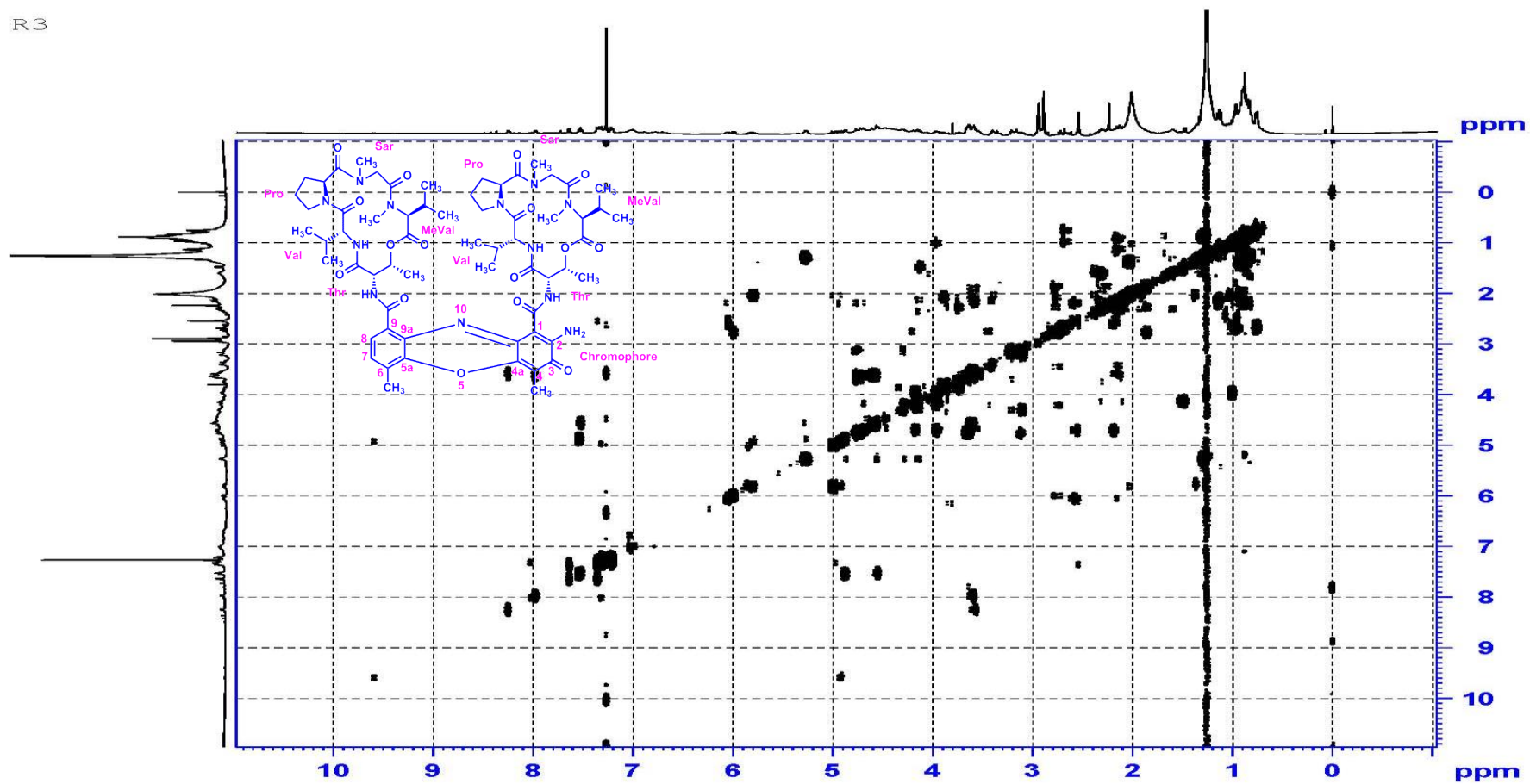


Figure S65. DQF-COSY (500 MHz, CDCl₃) Spectrum of Compound R3

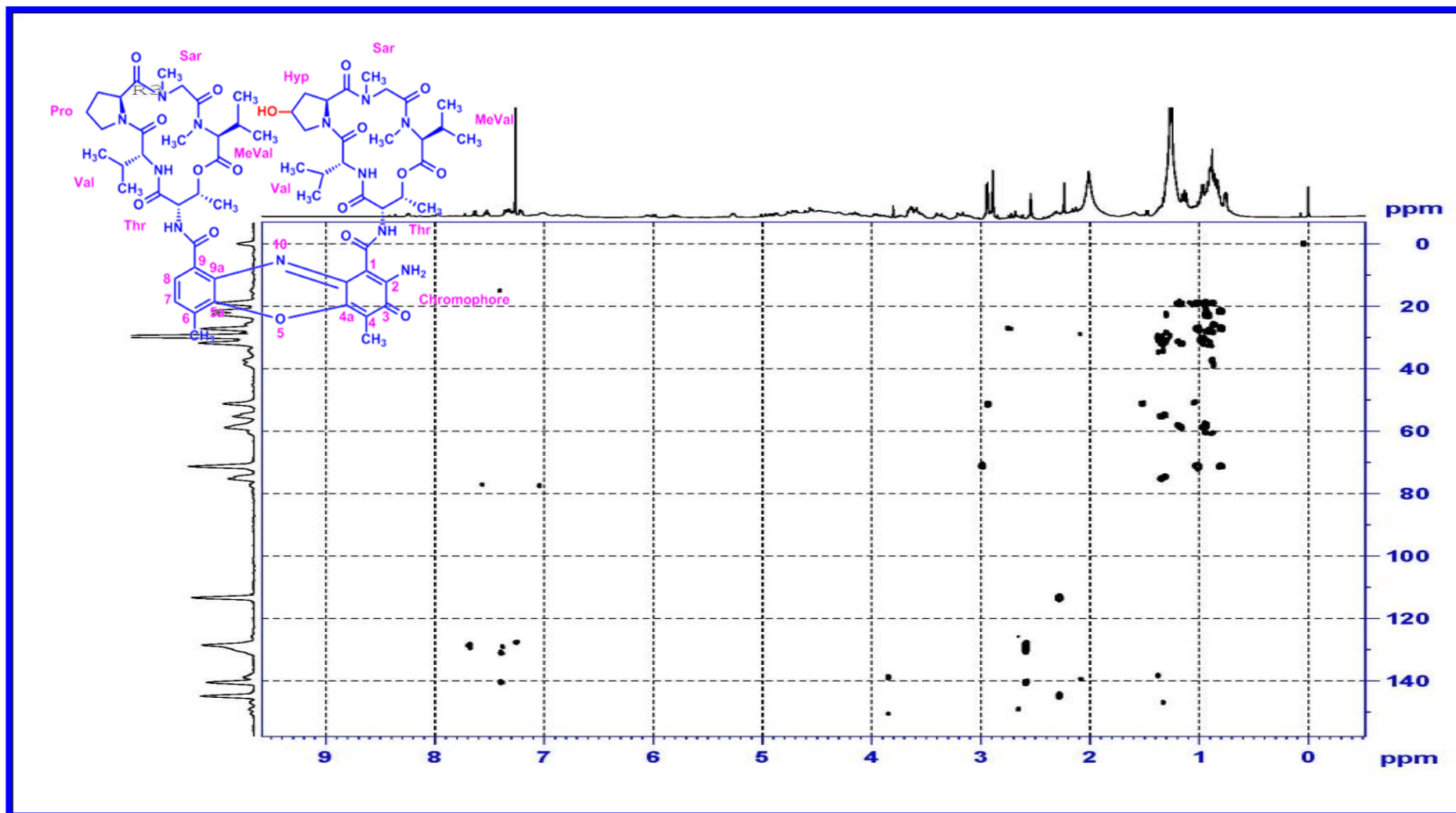


Figure S66. HMBC (500 MHz) Spectrum of Compound R3

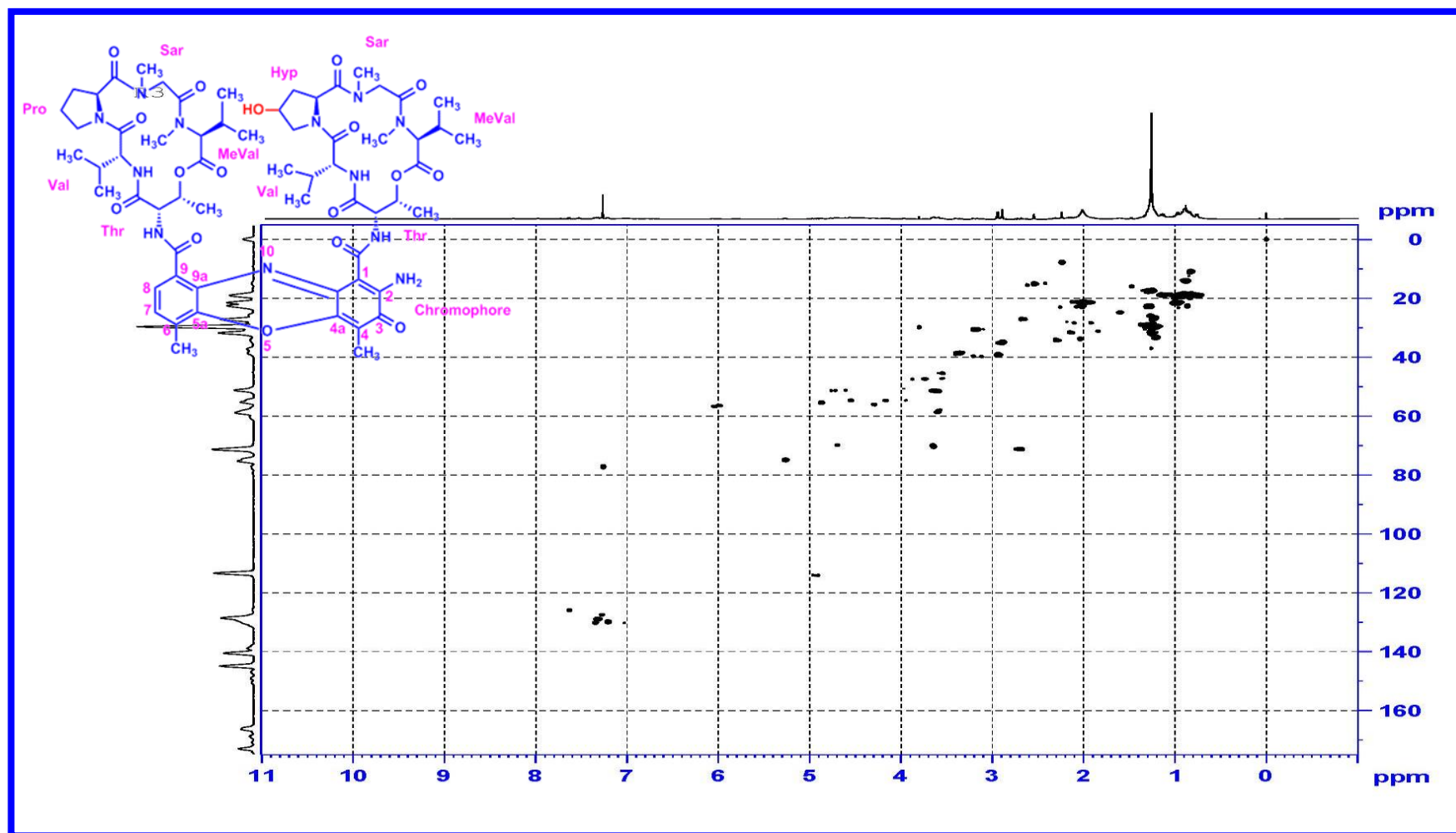


Figure S67. HSQC (500 MHz) Spectrum of Compound R3

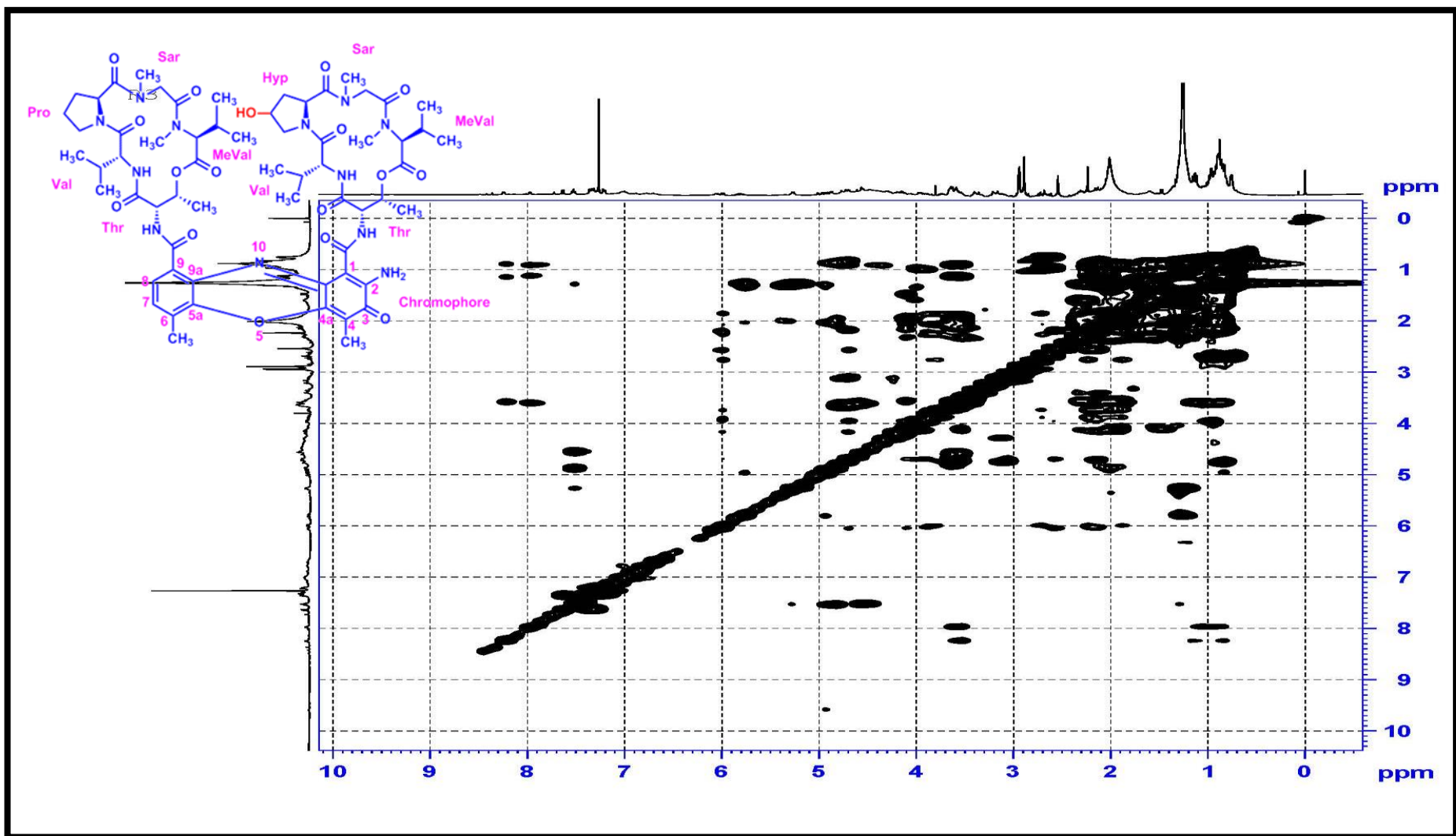


Figure S68. TOCSY (500 MHz, CDCl₃) Spectrum of Compound R3

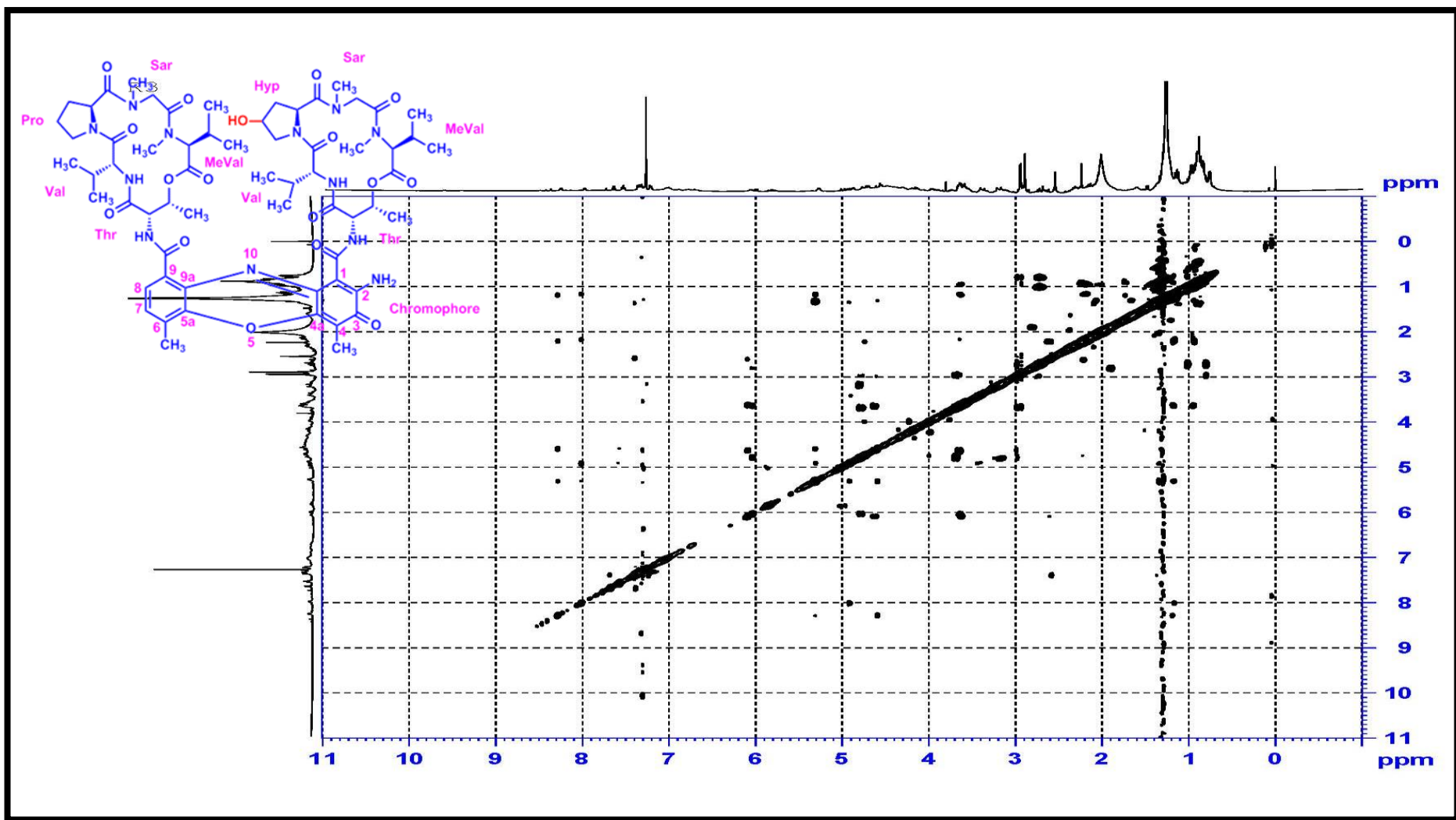


Figure S69. NOESY (500 MHz) Spectrum of Compound R3

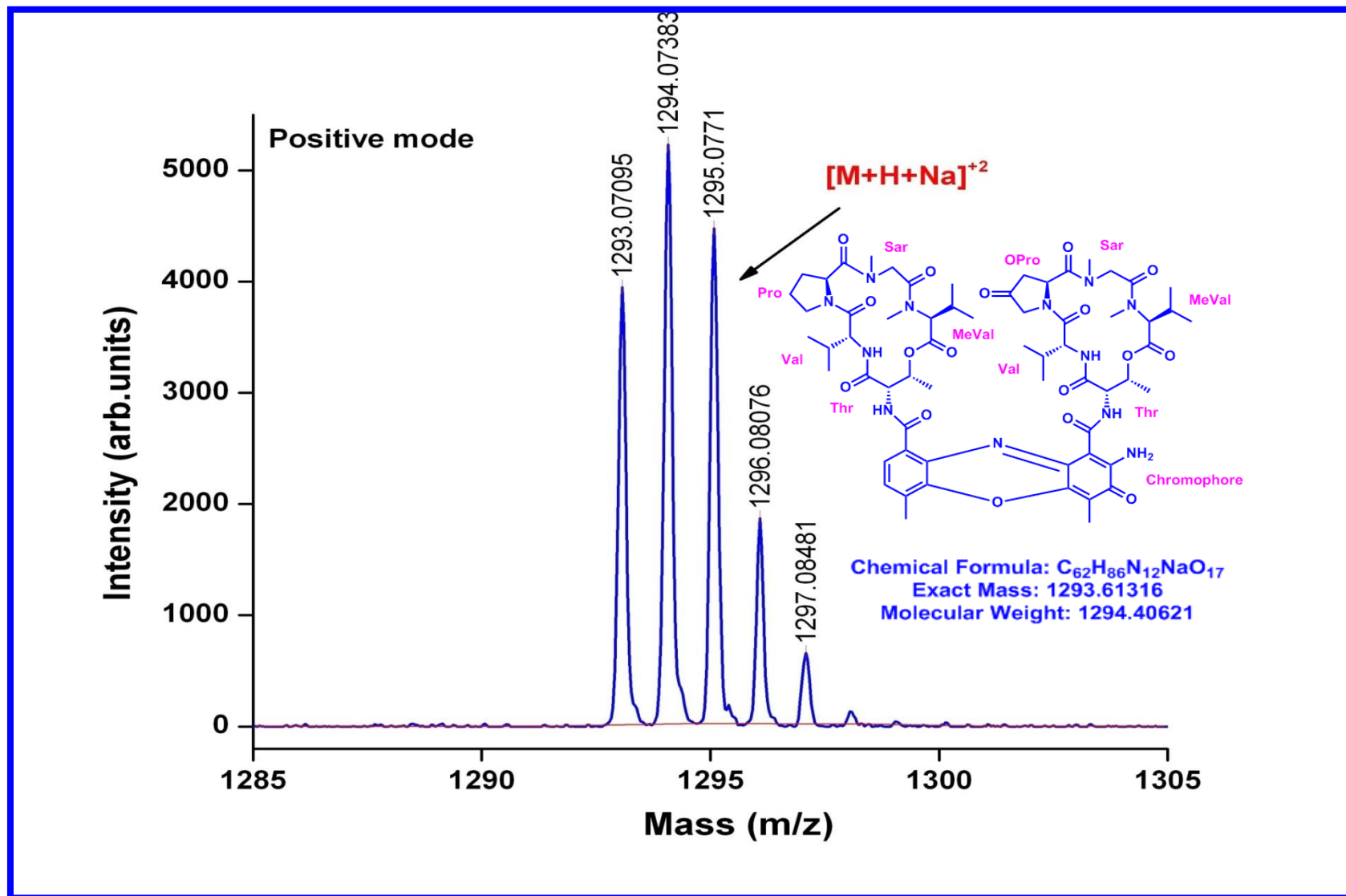


Figure S70. MALDI-TOF MS Spectrum of Transitmycin (R1) (Molecular ion peak) (positive mode)

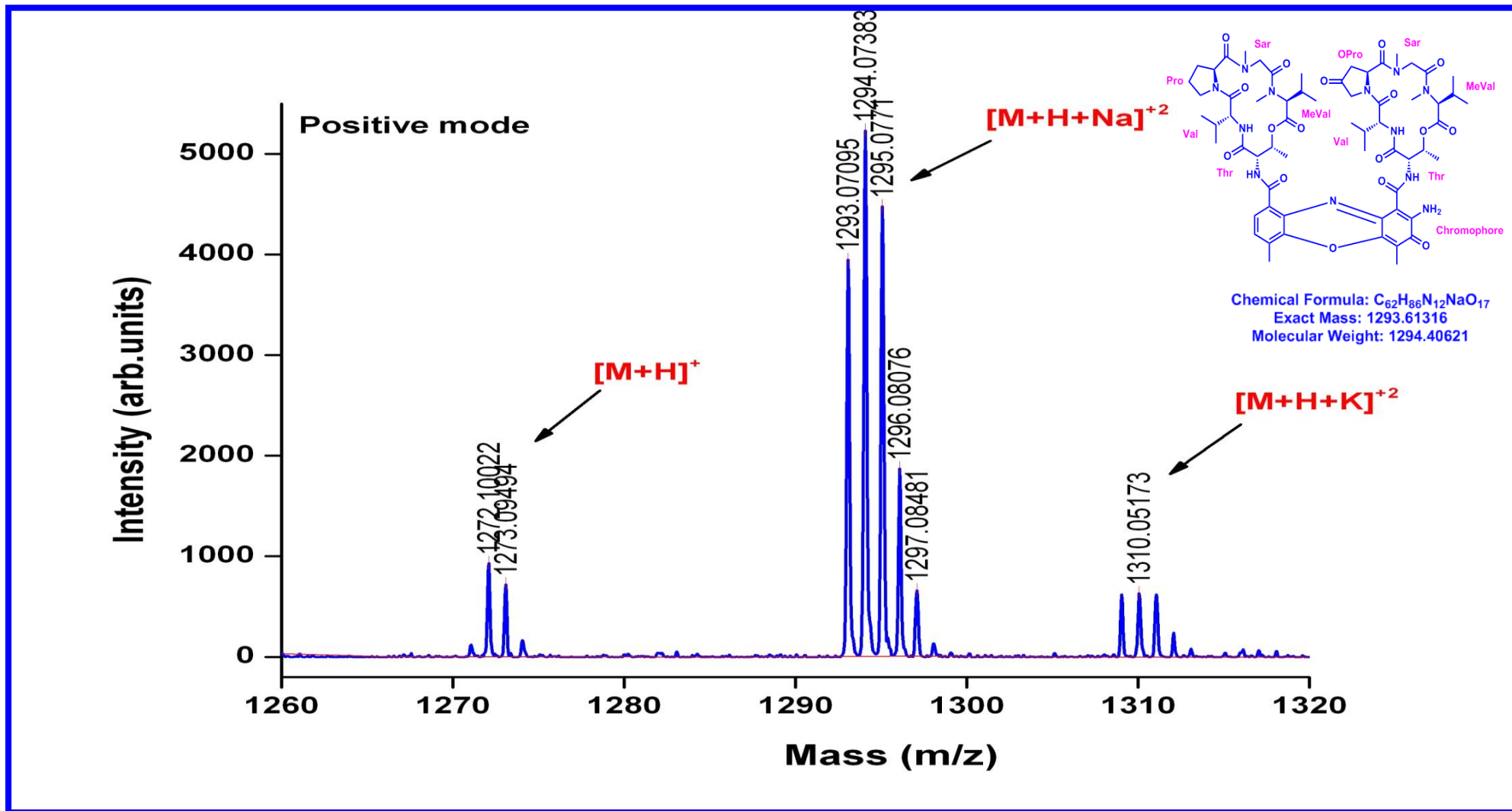


Figure S71. Expansion of MALDI-TOF MS Spectrum of Transimycin (R1) (Molecular ion peak) (positive mode)

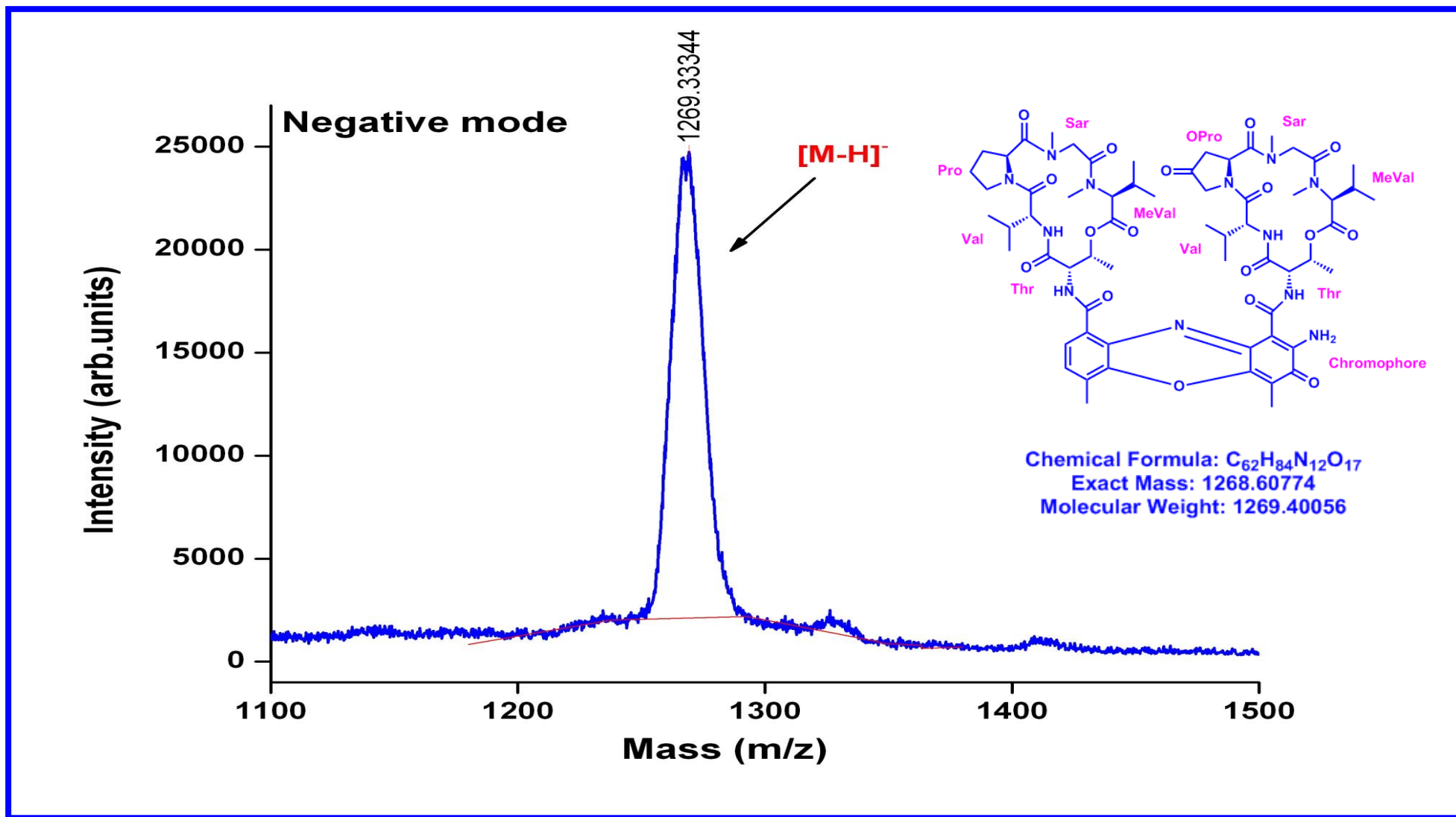


Figure S72. Expansion of MALDI-TOF MS Spectrum of Transitymycin (R1) (Molecular ion peak) (Negative mode)

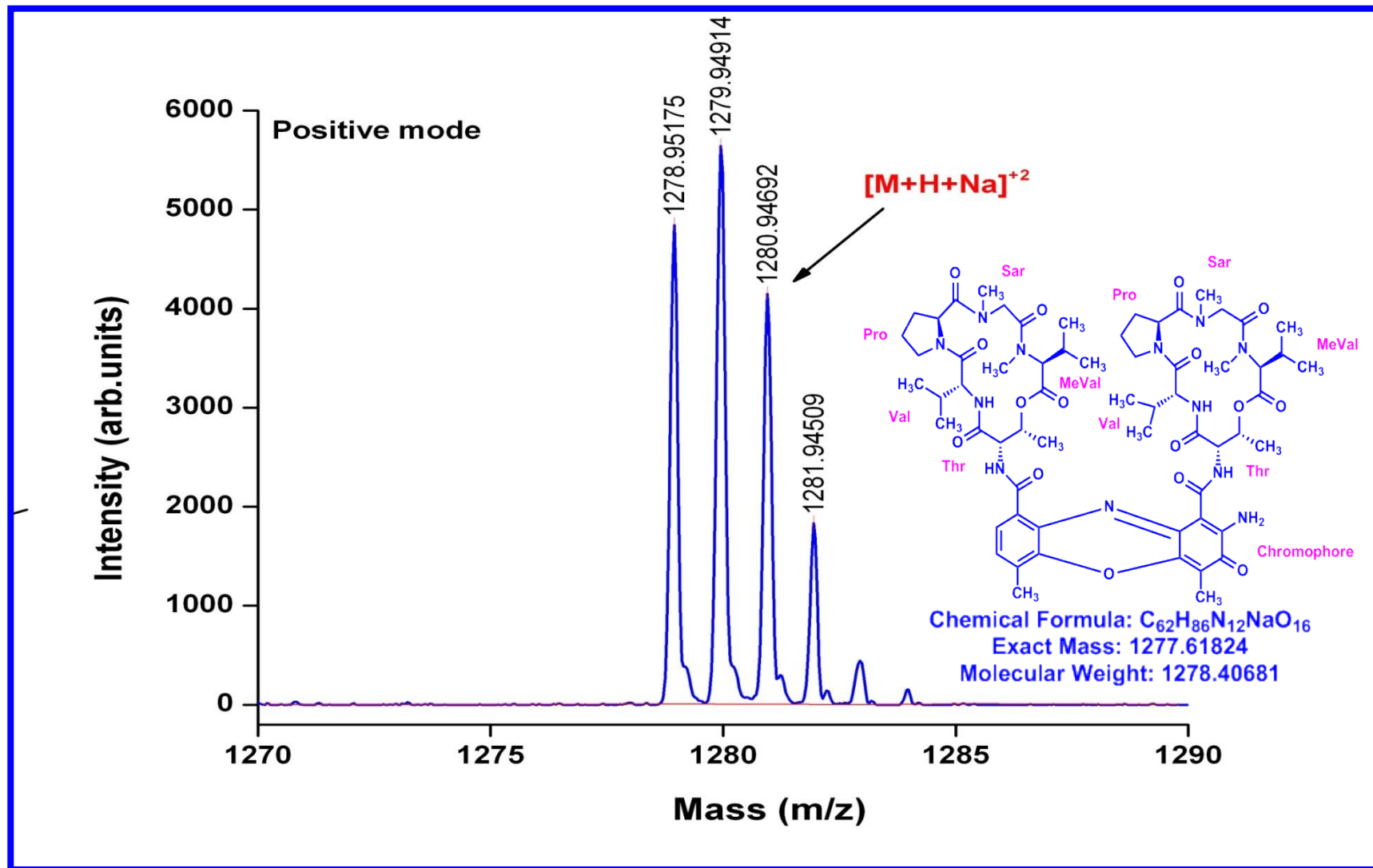


Figure S73. MALDI-TOF MS Spectrum of R2 (Molecular ion peak) (positive mode)

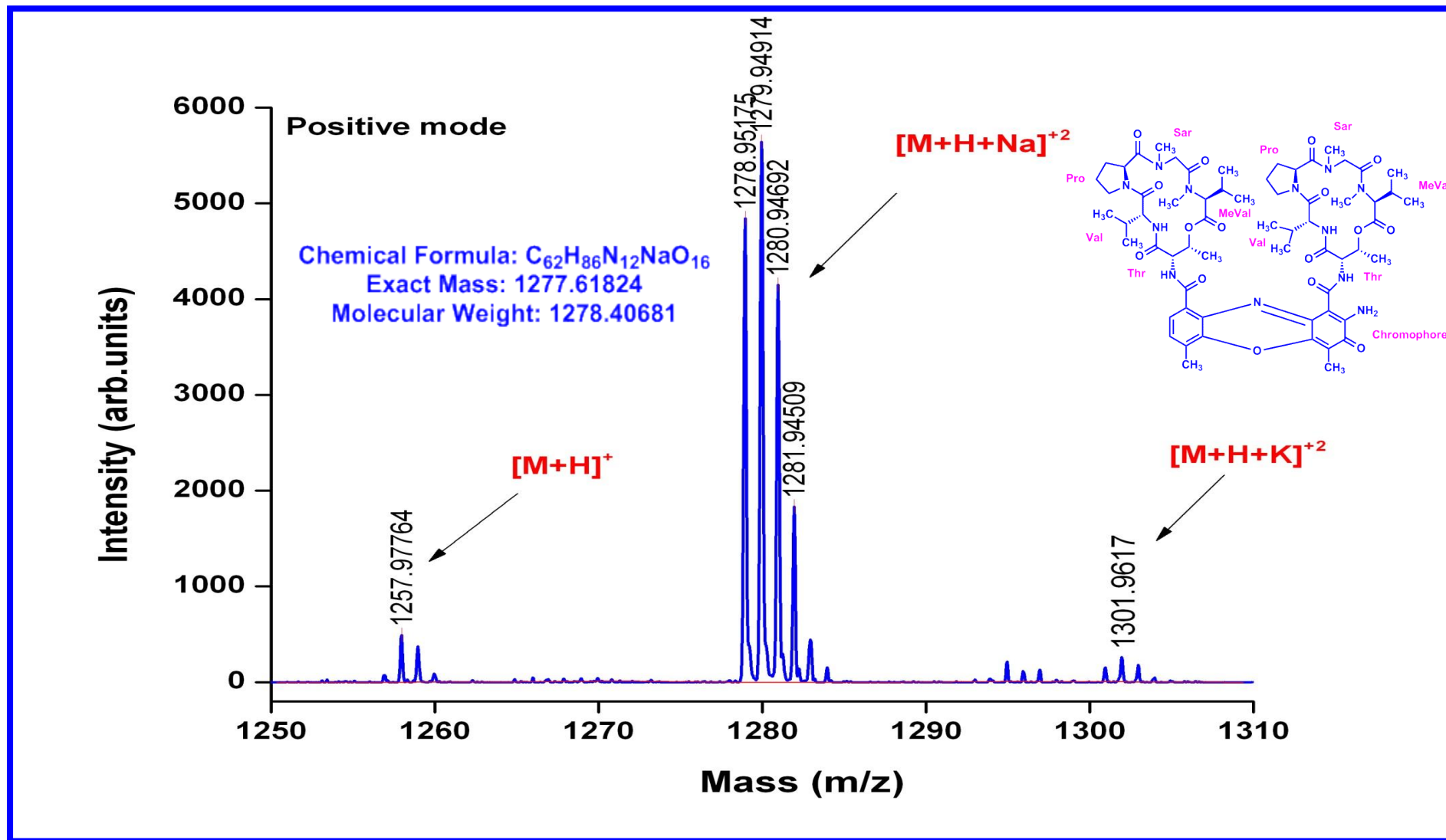


Figure S74. Expansion of MALDI-TOF MS Spectrum of R2 (Molecular ion peak) (positive mode)

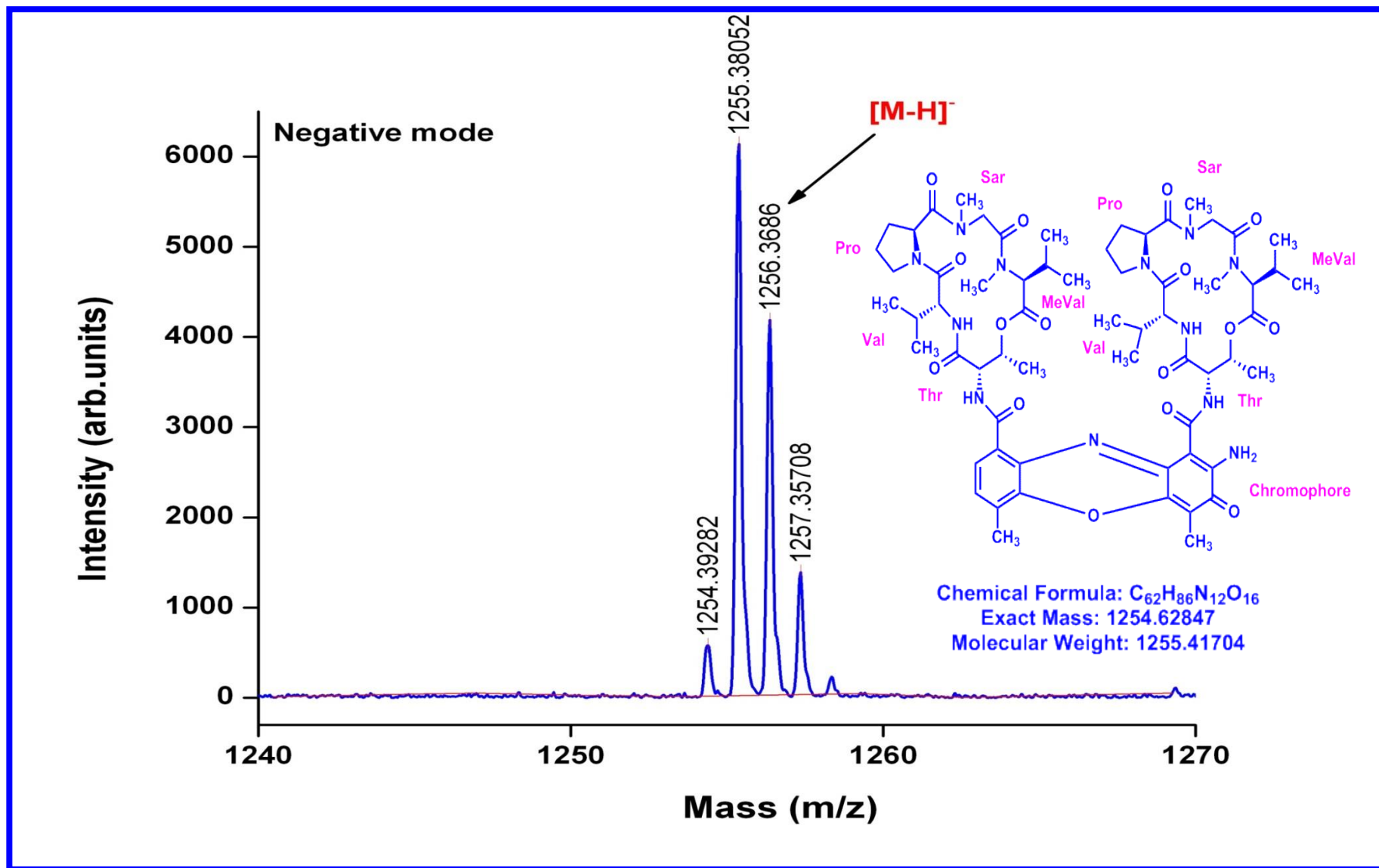


Figure S75. Expansion of MALDI-TOF MS Spectrum of R2 (Molecular ion peak) (Negative mode)

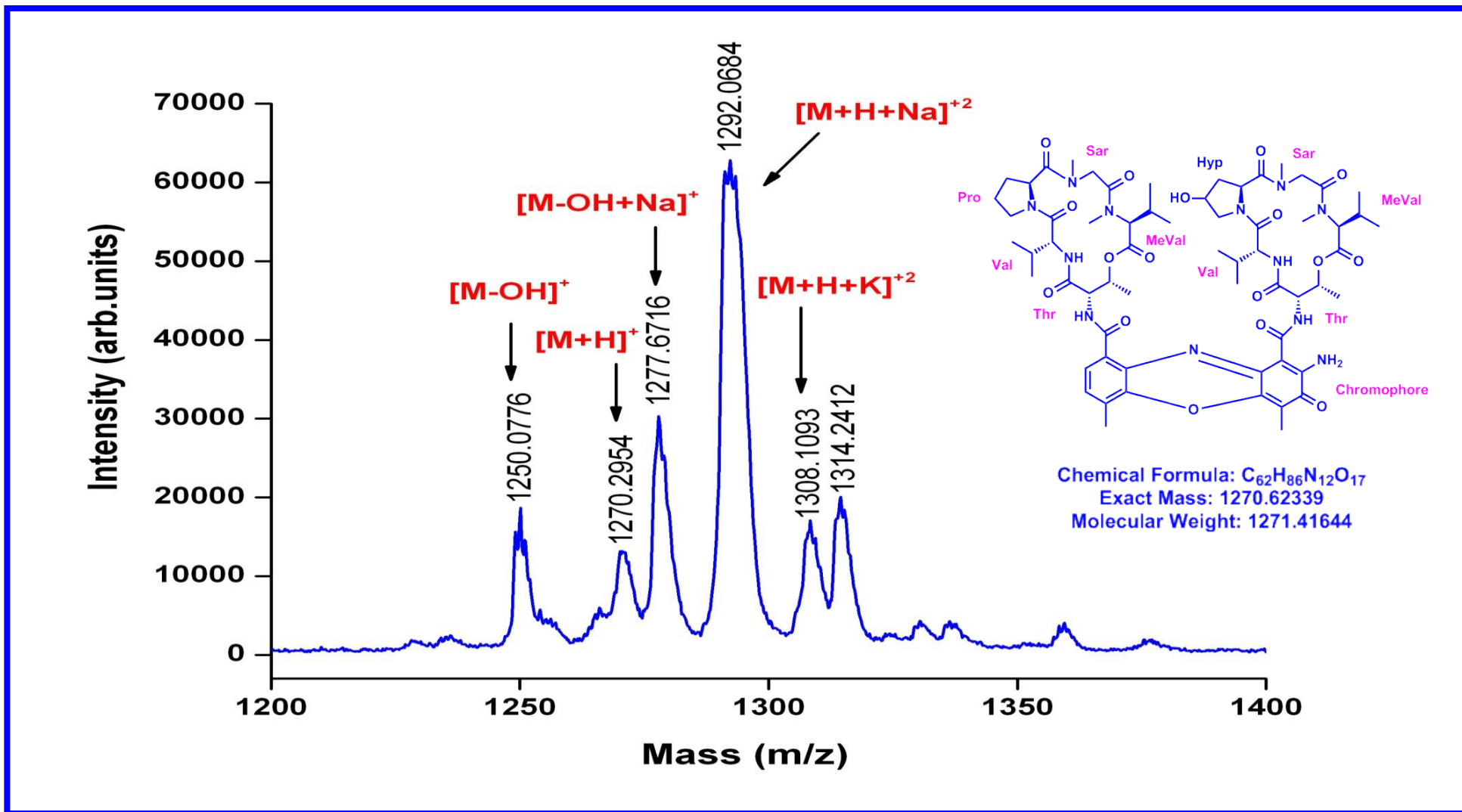


Figure S76. MALDI-TOF MS Spectrum of R3 (Molecular ion peak) (positive mode)

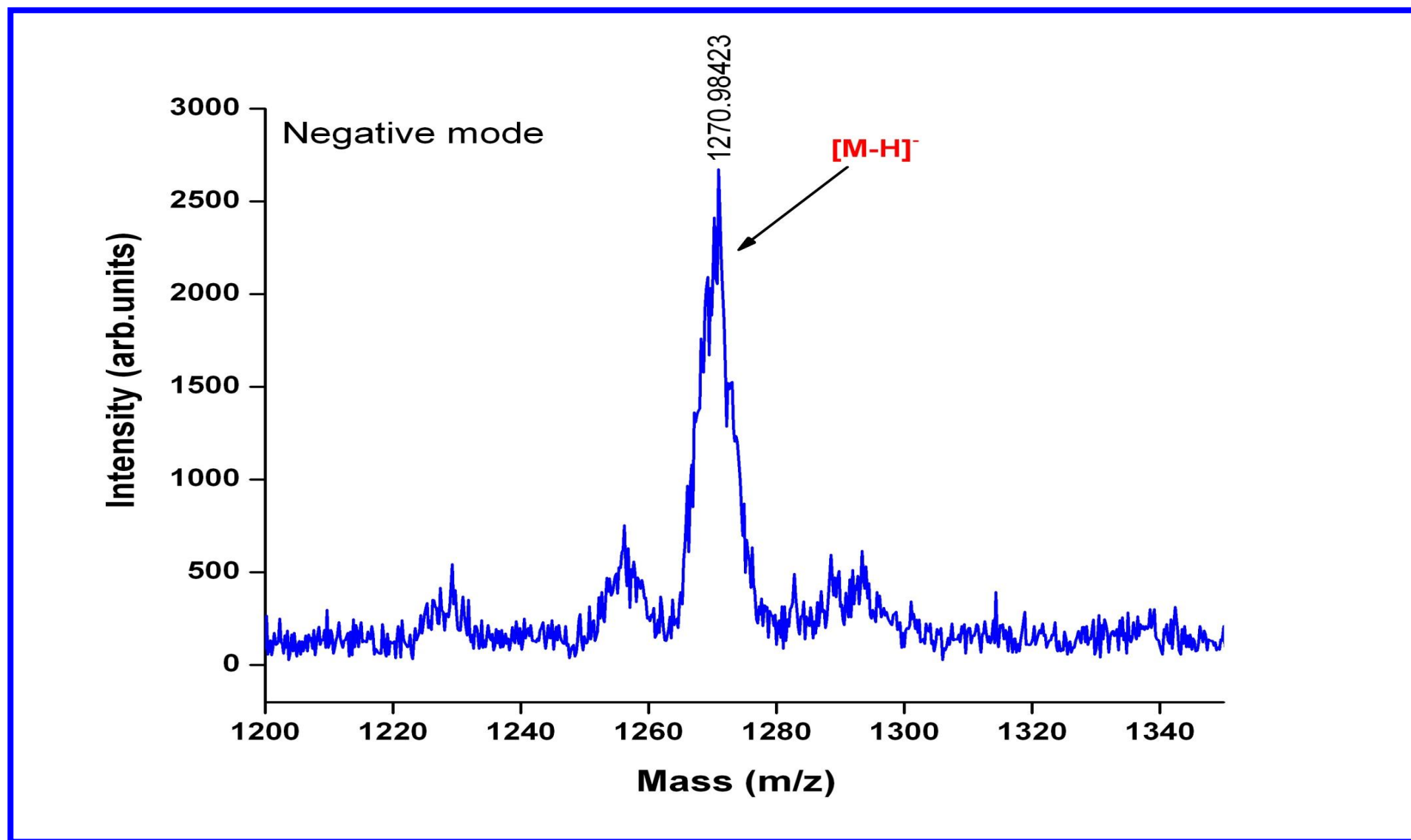


Figure S77. MALDI-TOF MS Spectrum of R3 (Molecular ion peak) (Negative mode)

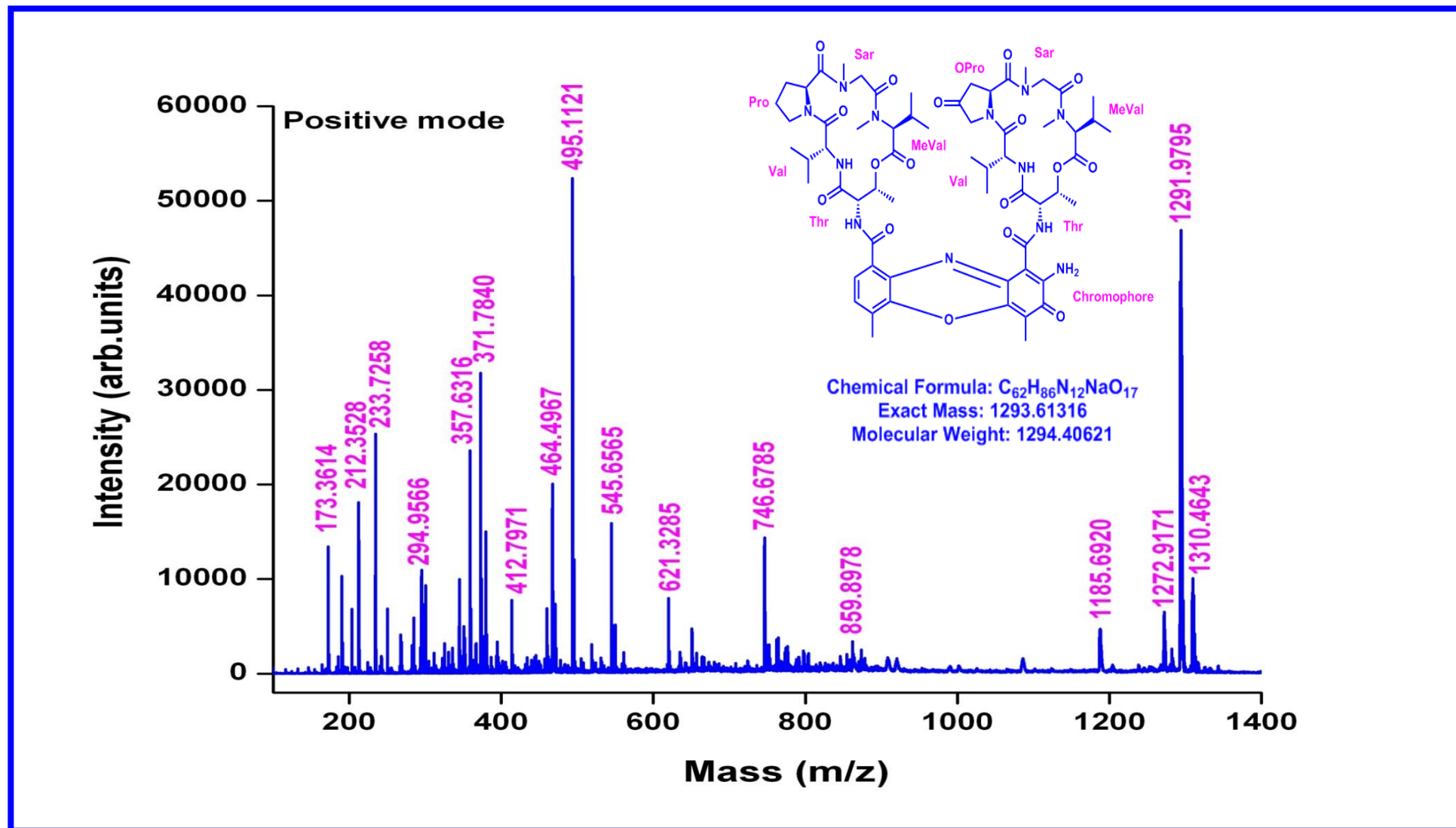


Figure S78. MALDI-TOF MS Spectrum of Transitmycin (R1) (Positive mode)

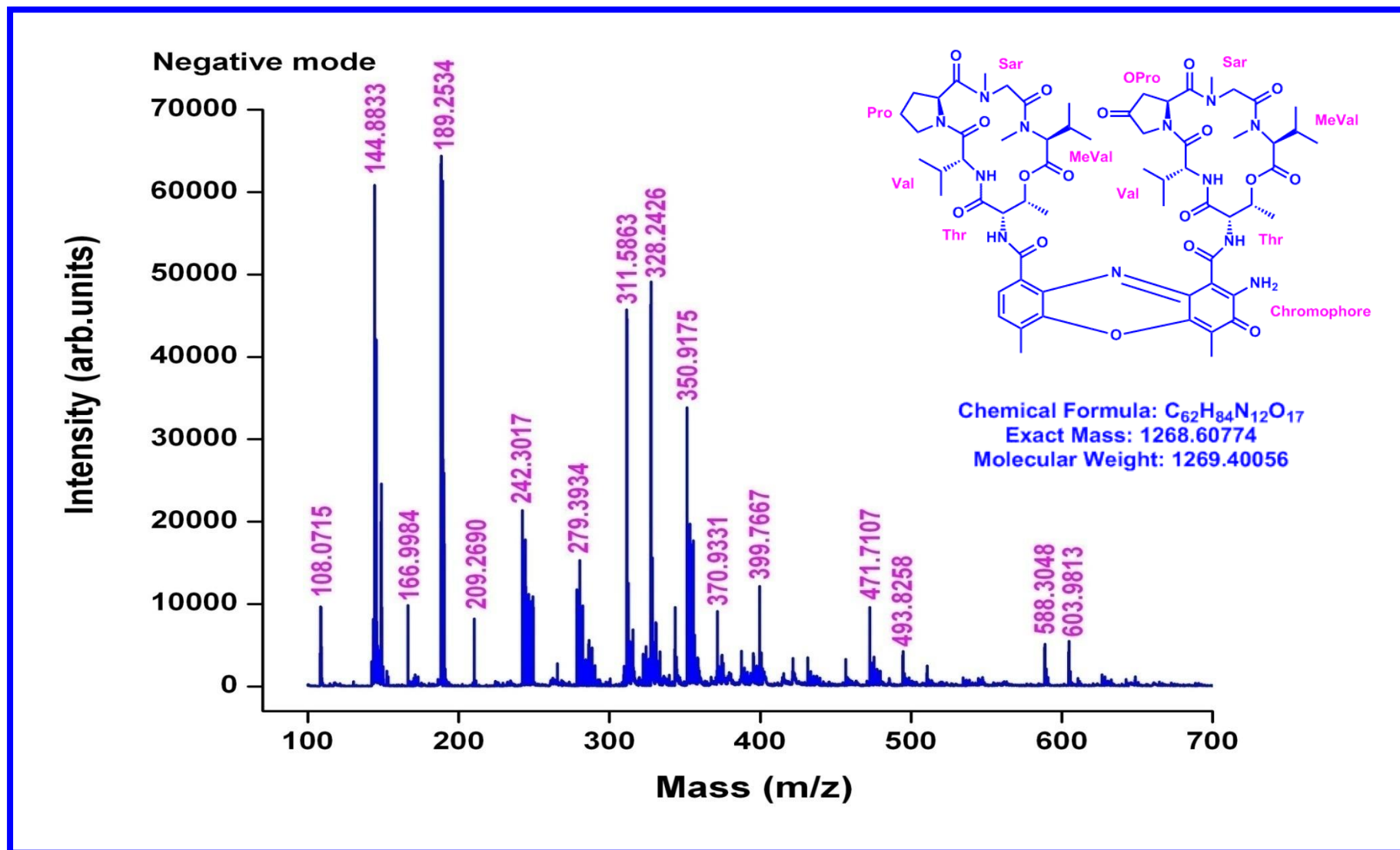
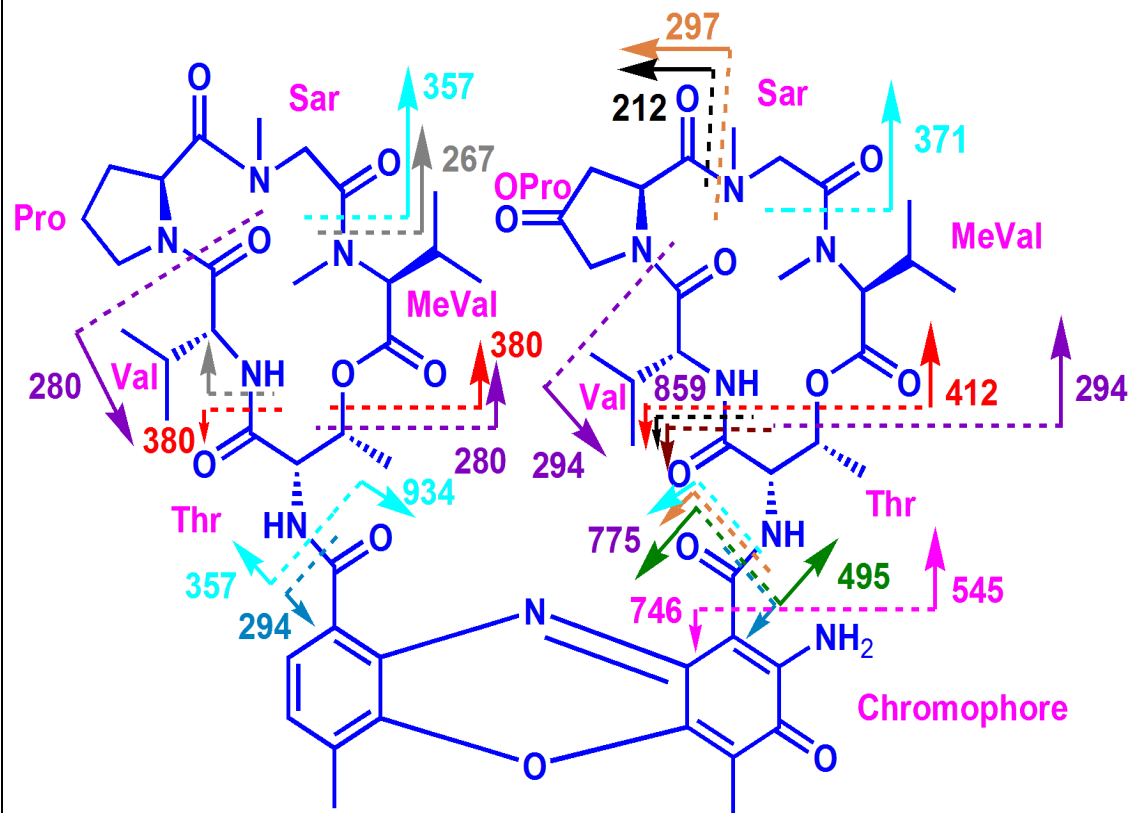


Figure S79. MALDI-TOF MS Spectrum of Transitmycin (R1) (Negative mode)

Table S6. MALDI-TOF MS Spectral Fragmentation of Transitmycin (R1) (Positive mode)

211- β -Ring-Val-Oxo-Pro
233- α -Ring-Val-Pro
294- β -Ring-Oxo-Pro-Sar-NMeVal
295-Chromophore
297- β -Ring-Thr-Val-Oxo-Pro
357- α -Ring-Val-Pro-Sar-MeVal
371- β -Ring-Val-Oxo-Pro-Sar-MeVal
412- β -Ring-Val-Oxo-Pro-Sar-NMeVal
412- α -Ring-Val-Pro-Sar-NMeVal+859 (Y ion)
495- β -Ring-Thr-Val-Oxo-Pro-Sar-NMeVal
496- α -Ring-Thr-Val-Pro-Sar-NMeVal
464 α -Ring-Thr-Val-Oxo-Pro-Sar-NMeVal
746-Y-113 (MeVal)
747- α -Ring-Val-Pro-Sar-NMeVal+Y-MeVal+545.6
1291-495
1291=746-545
1291=651+621
1291=495+775
1291=859+432
1291=920+371
1291=796+495
495= β -Ring-Thr-Val-Oxo-Pro-Sar-NMeVal
495-371=124-23=101 MeVal (β -Ring-Thr-Val-Oxo-Pro-Sar)
371(β -Ring-Thr-Val-Oxo-Pro-Sar)
294 (β -Ring-Thr-Val-Oxo-Pro)



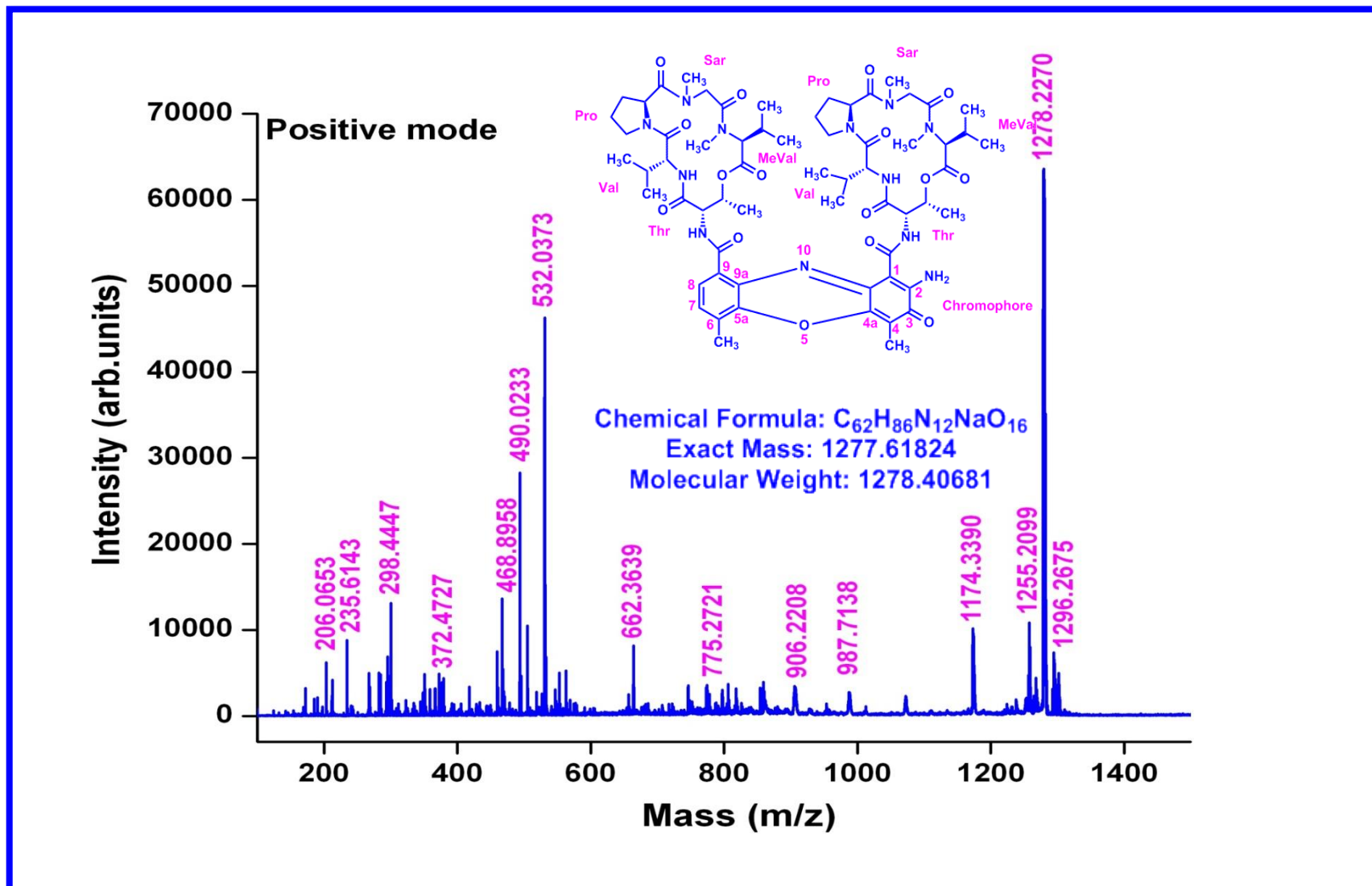


Figure S80. MALDI-TOF MS Spectrum of R2 (Positive mode)

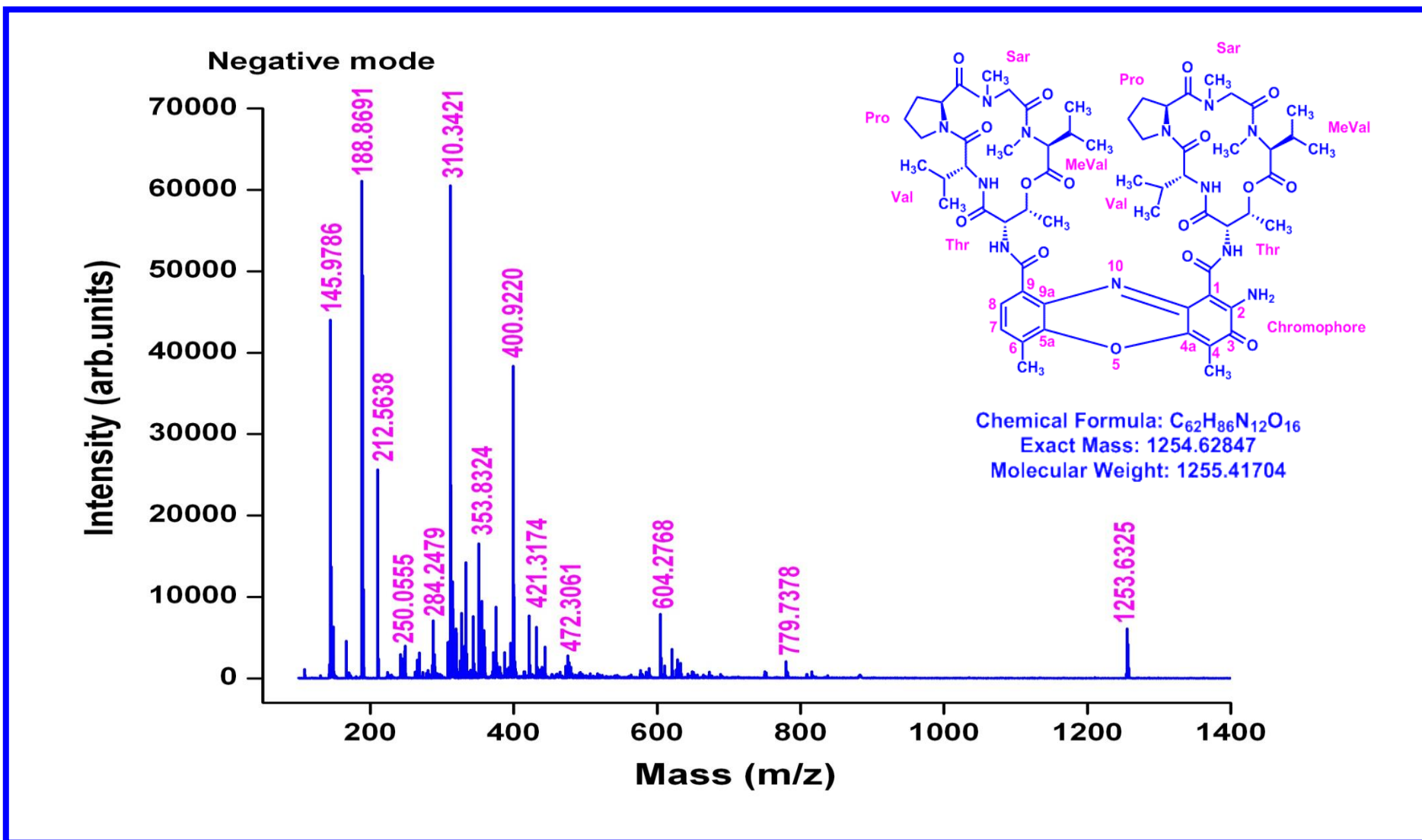


Figure S81. MALDI-TOF MS Spectrum of R2 (Negative mode)

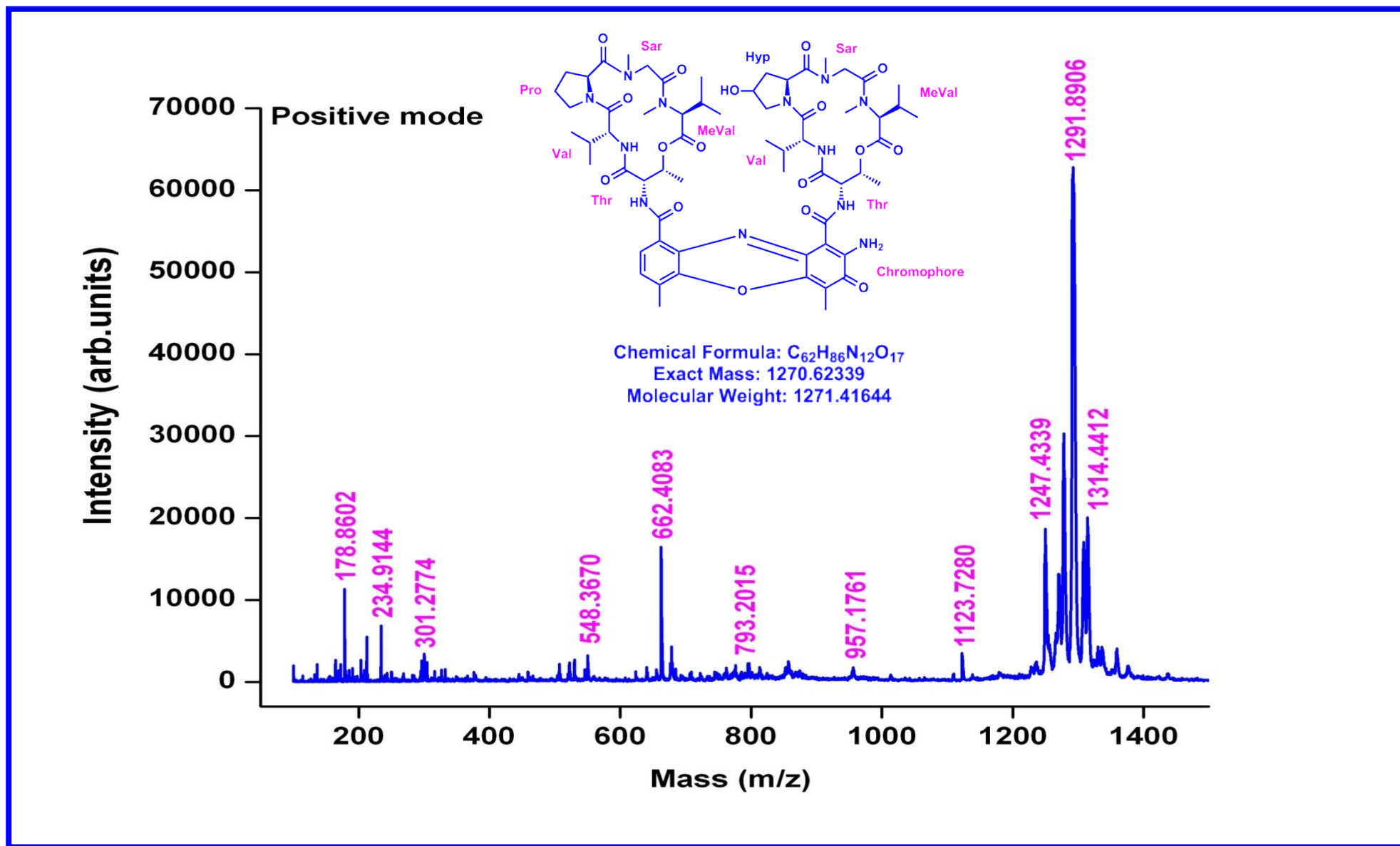


Figure S82. MALDI-TOF MS Spectrum of R3 (Positive mode)

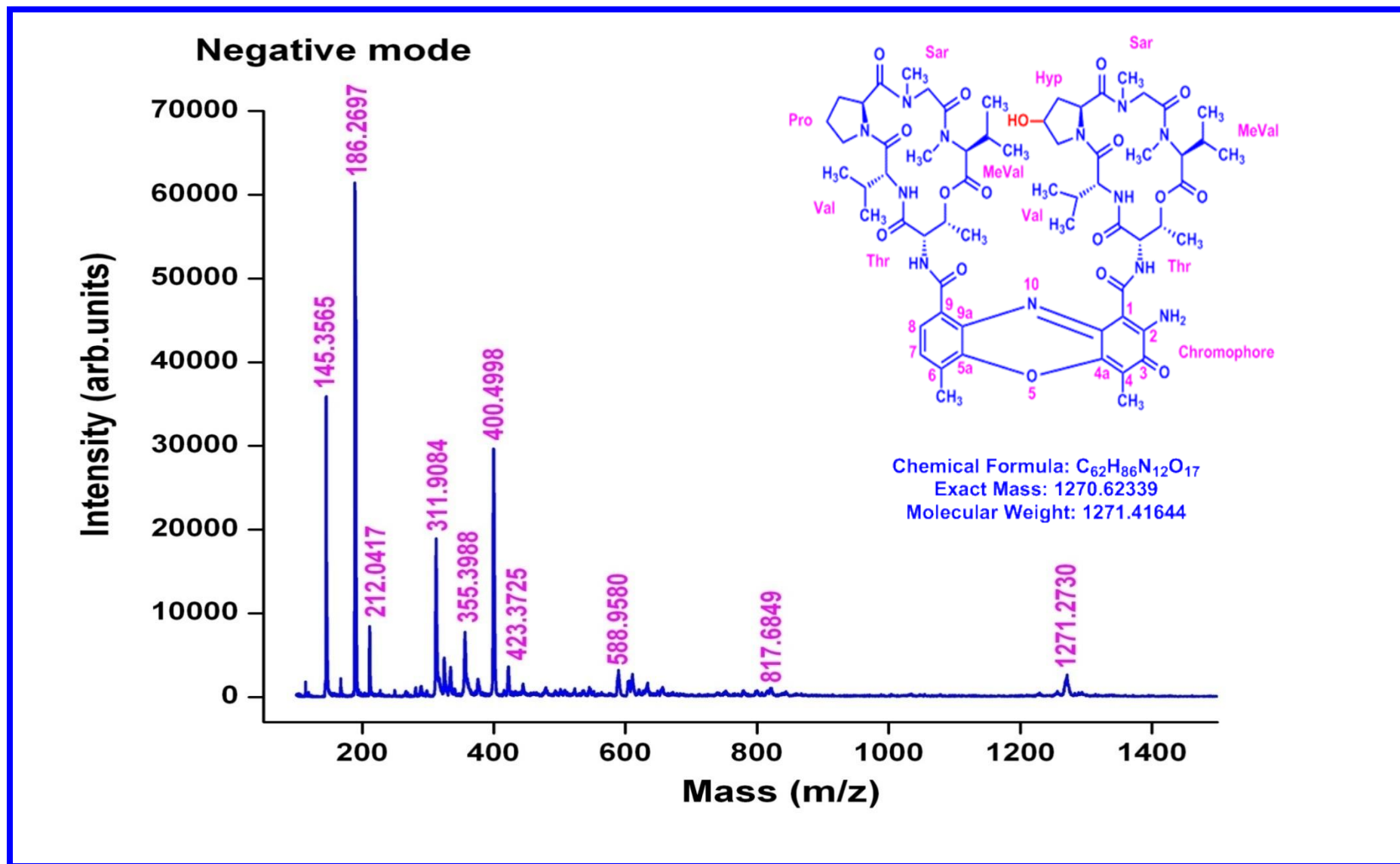


Figure S83. MALDI-TOF MS Spectrum of R3 (Negative mode)

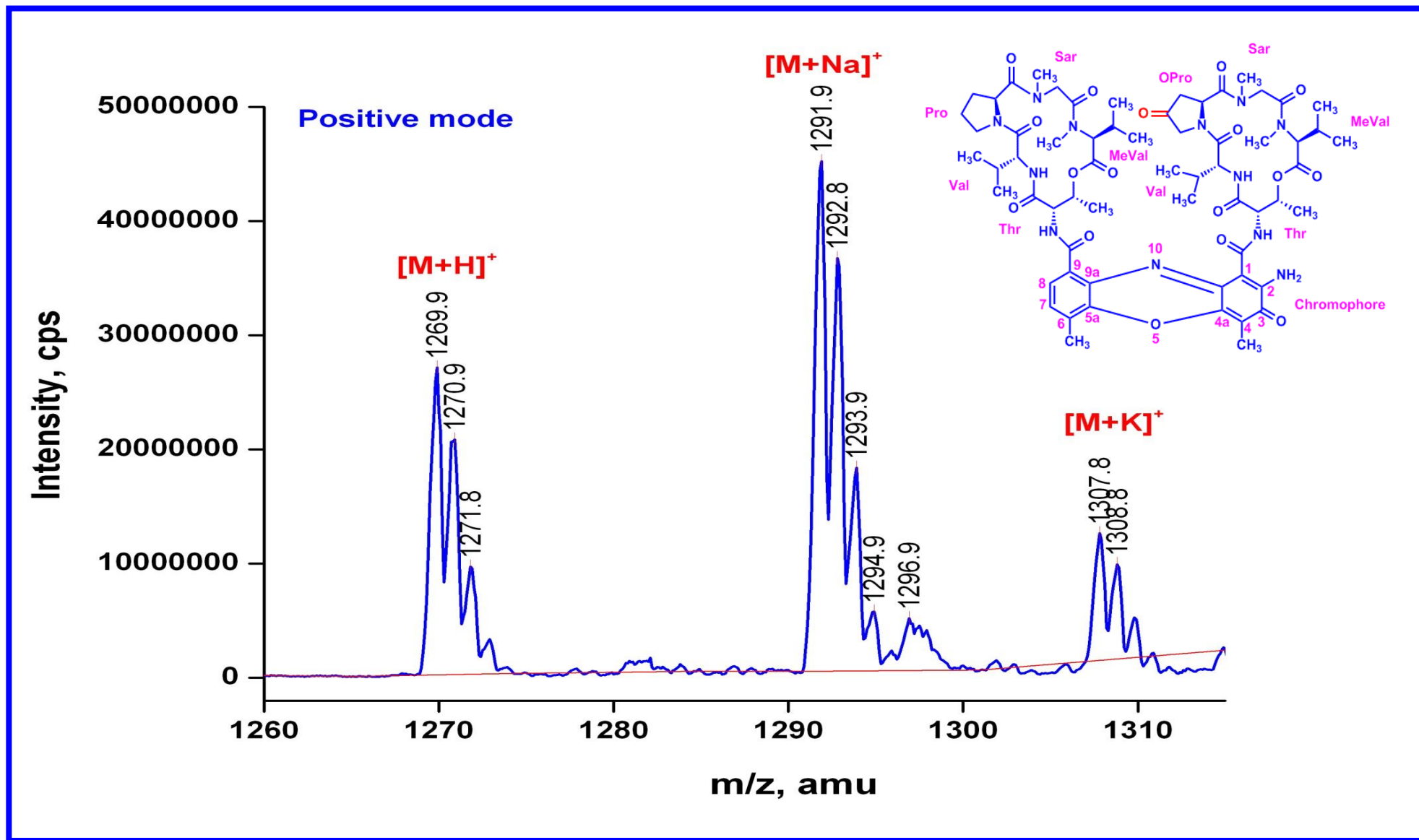


Figure S84. QTRAP MS/MS Transitmycin (R1) (Molecular ion peak) (Positive mode)

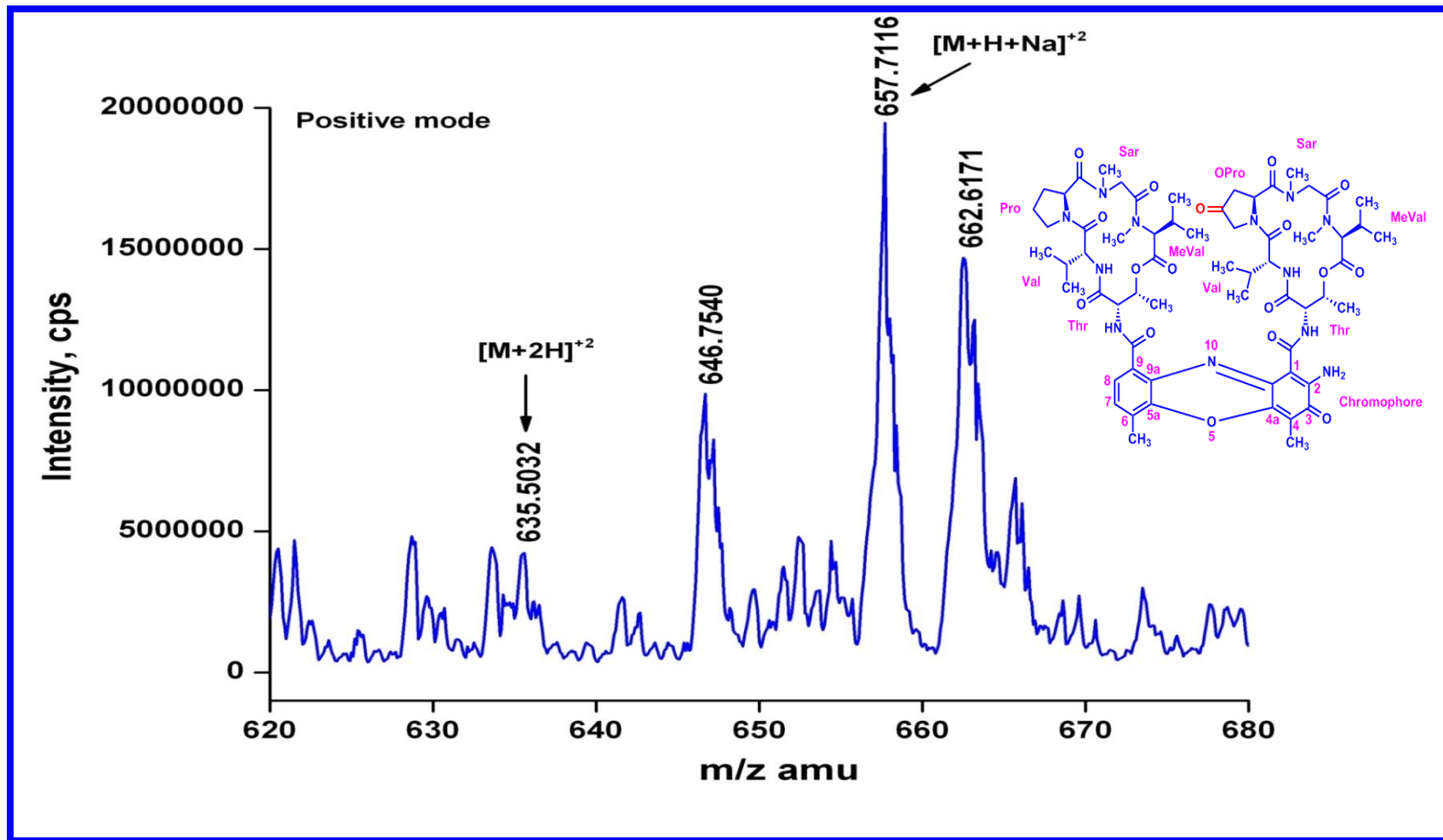


Figure S85 QTRAP MS/MS Transitymycin (R1) (Molecular ion peak $[M+H]^{2+}$ (Positive mode))

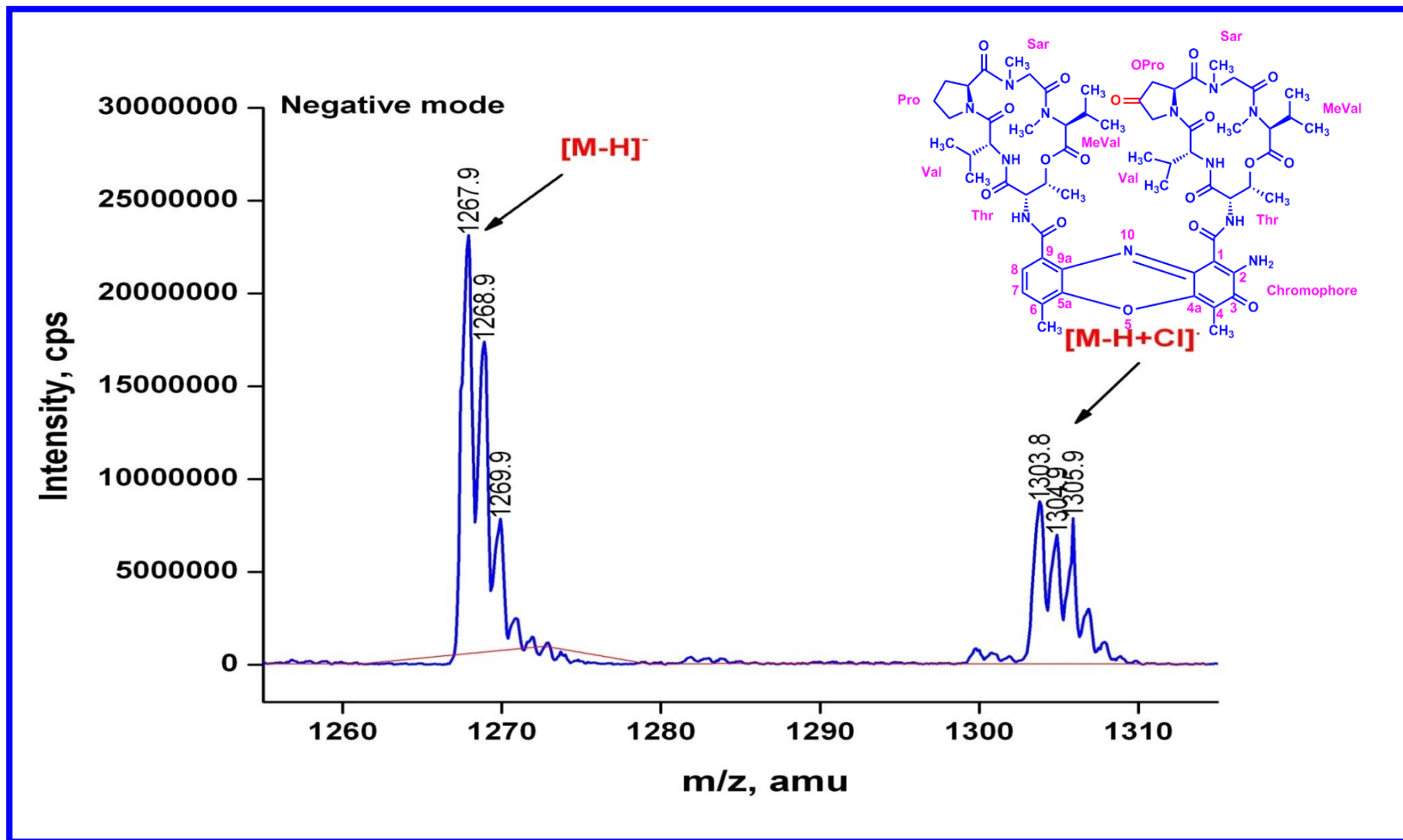


Figure S86. QTRAP MS/MS of Transitmycin (R1) (Molecular ion peak) (Negative mode)

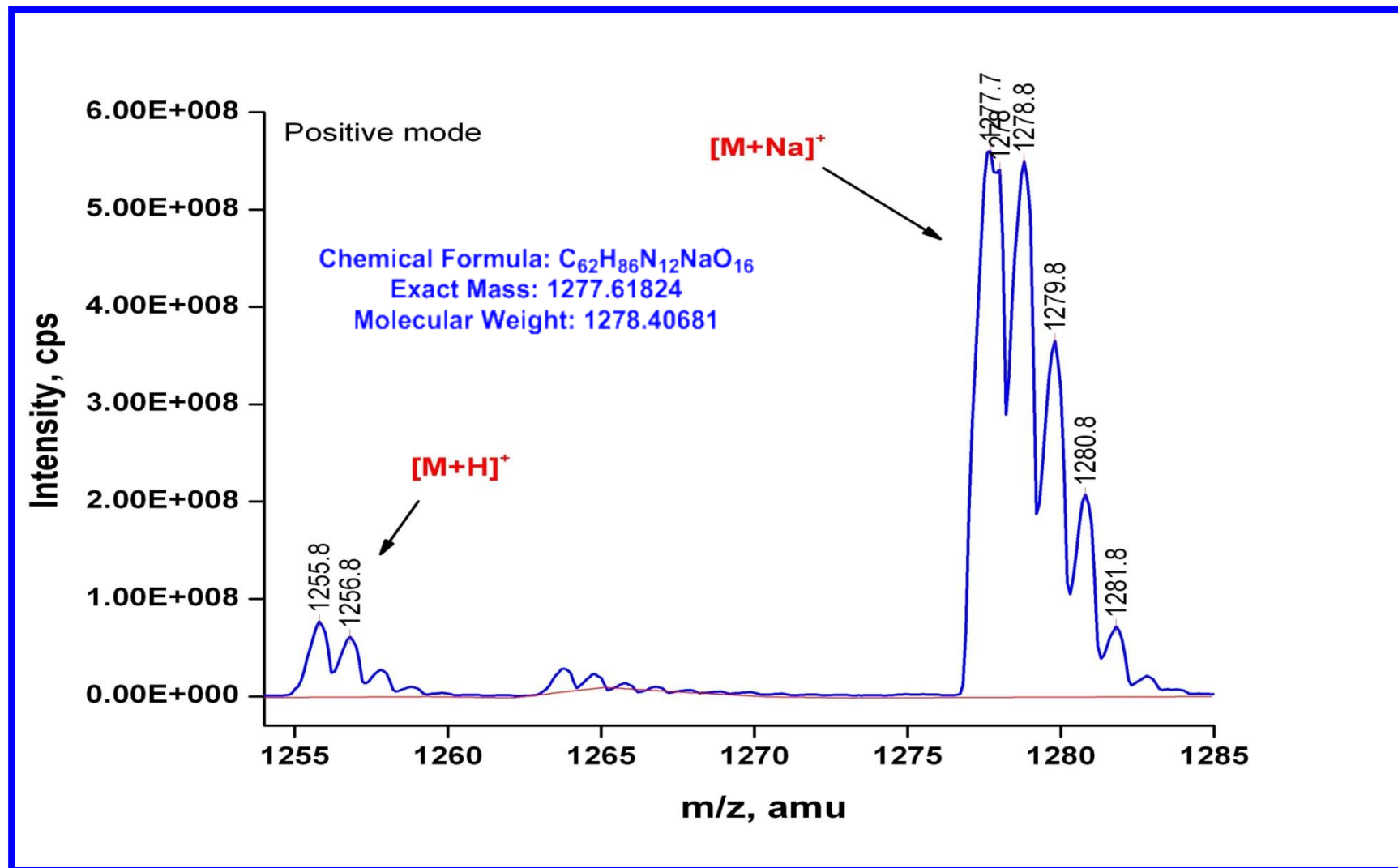


Figure S87. QTRAP MS/MS of R2 (Molecular ion peak) ((Positive mode)

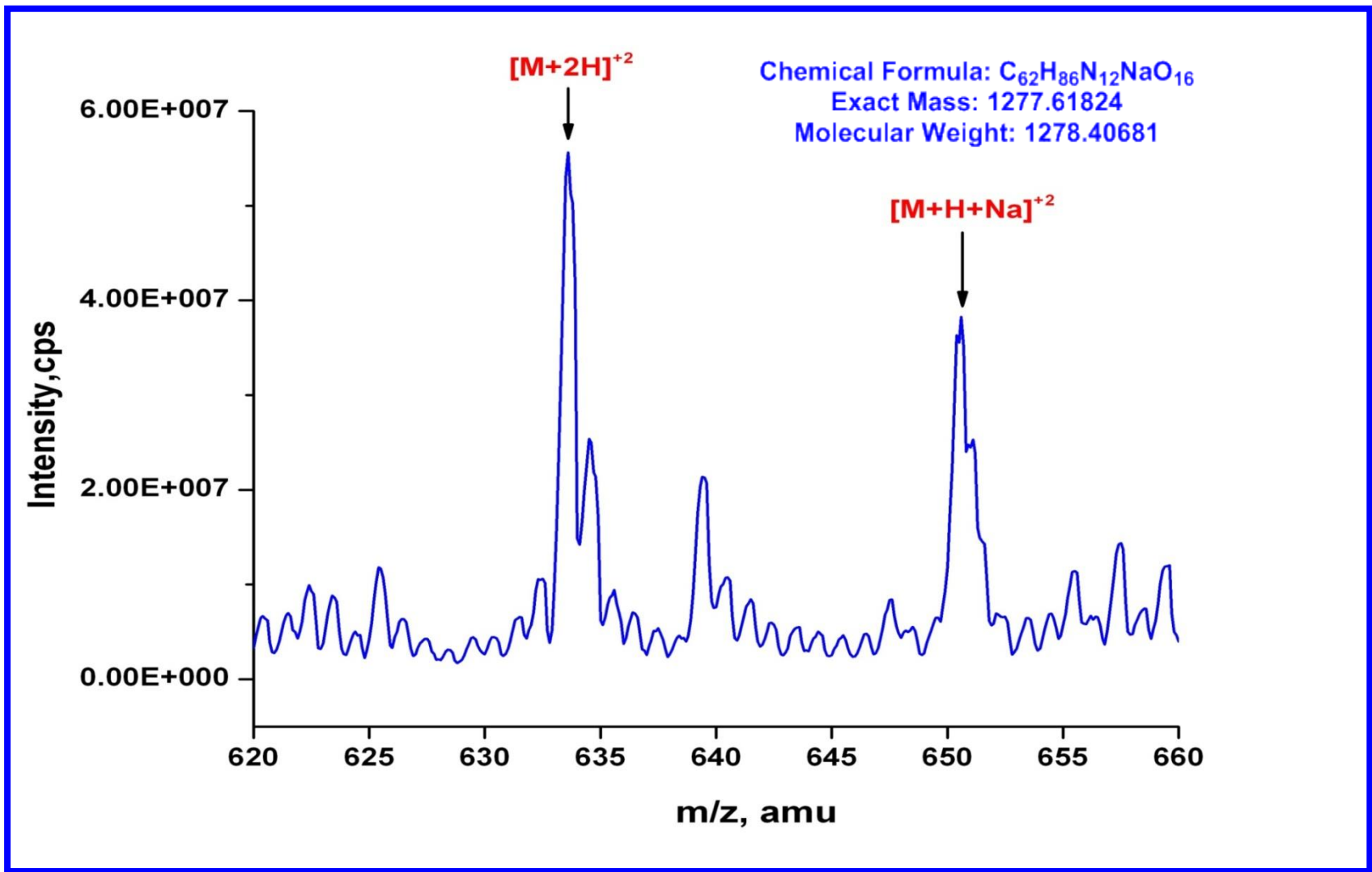


Figure S88. QTRAP MS/MS of R2 $[M+H]^{2+}$ ion peak (Positive mode)

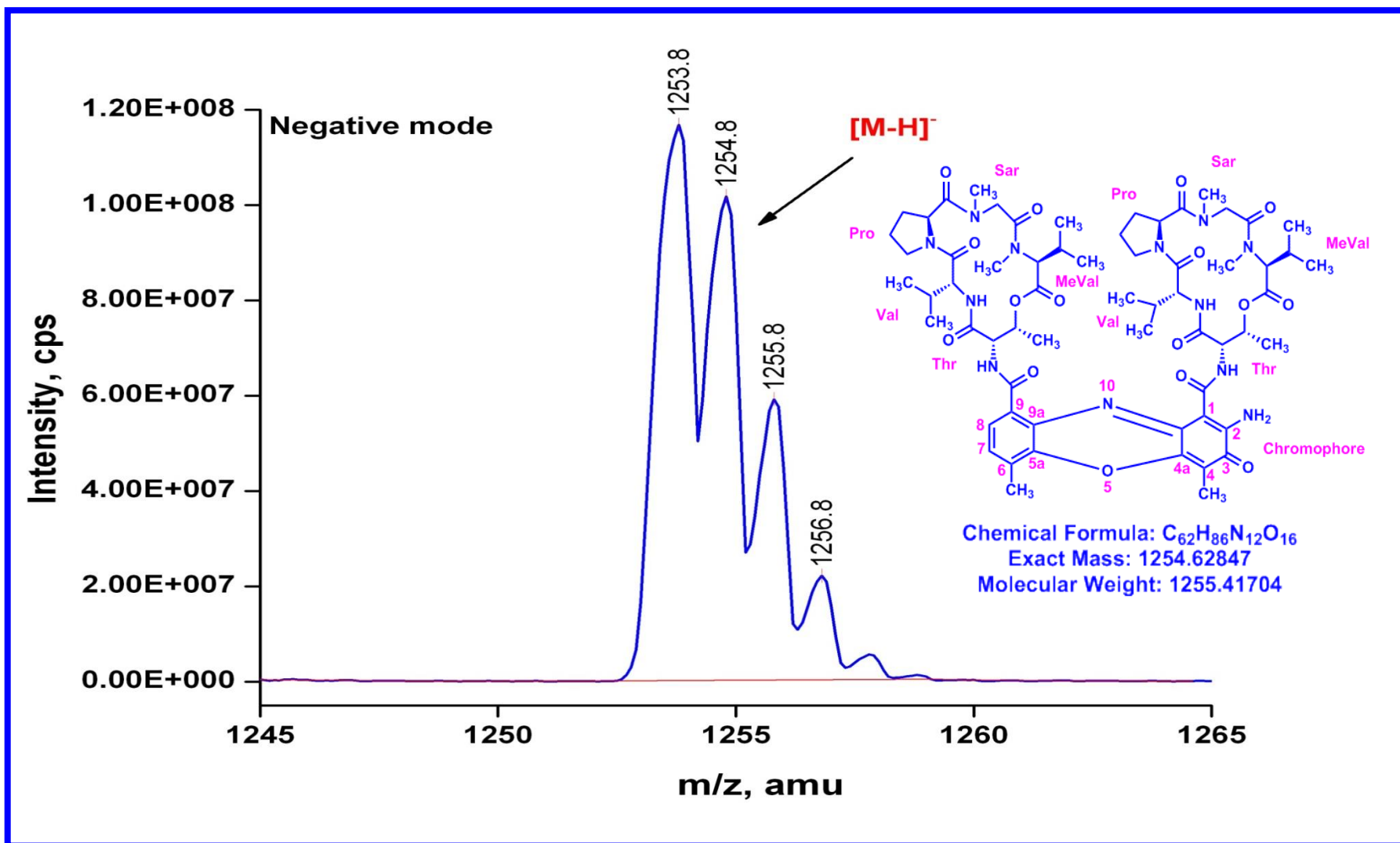


Figure S 89. QTRAP MS/MS of R2 (Molecular ion peak (Positive mode))

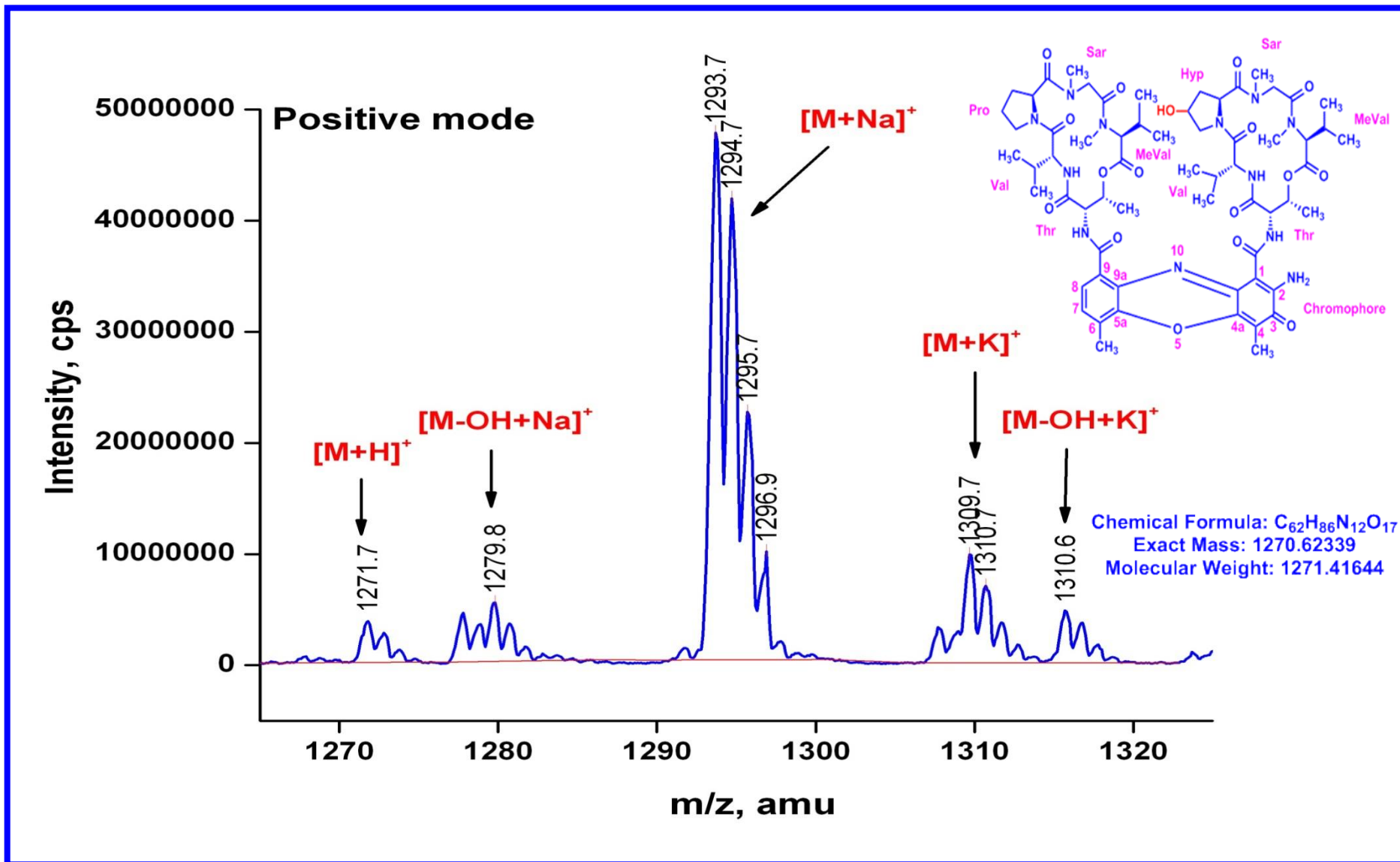


Figure S90. QTRAP MS/MS of R3 Molecular ion peak (Positive mode)

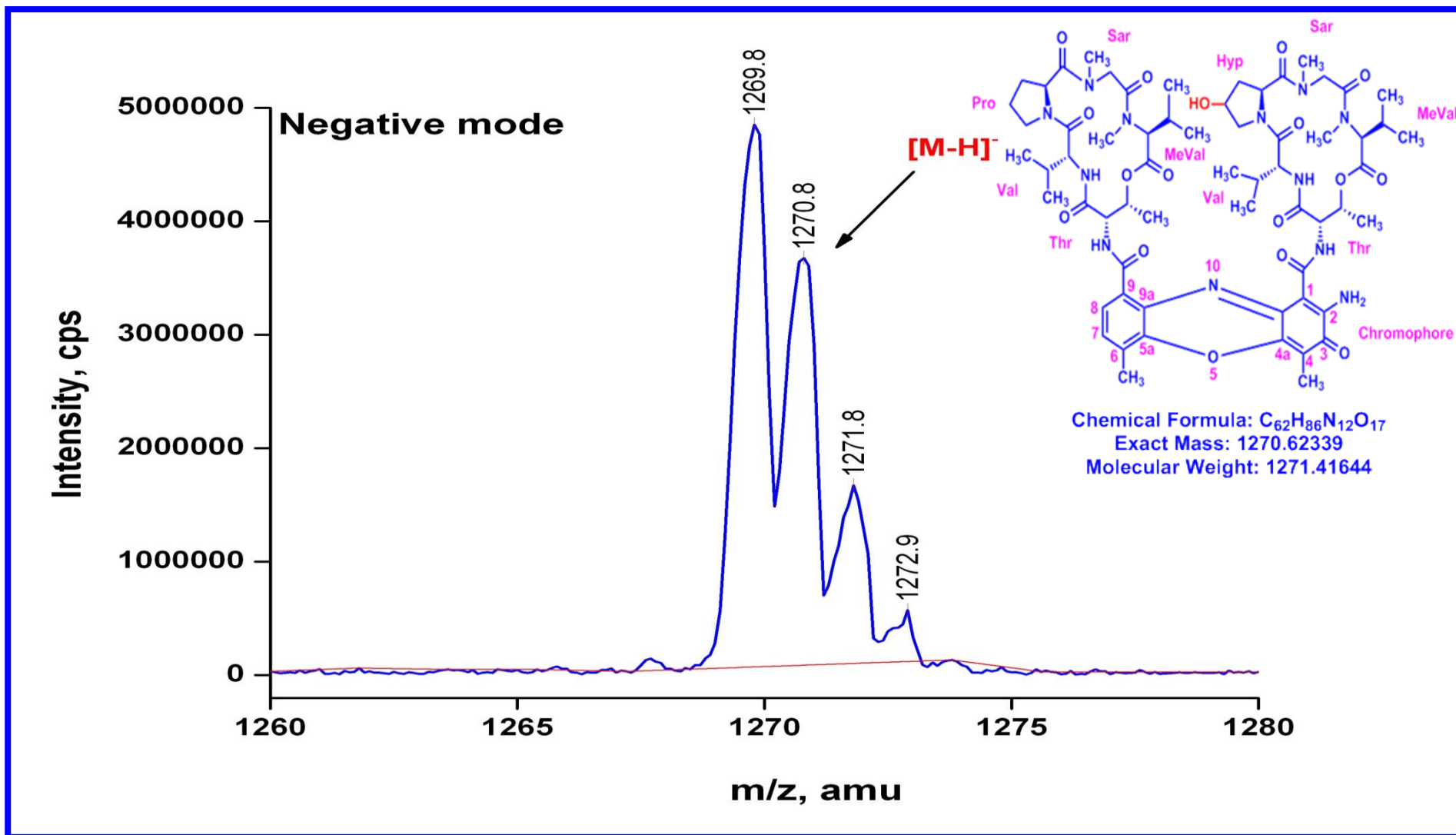


Figure S91. QTRAP MS/MS of R3 (Molecular ion peak (Negative mode))

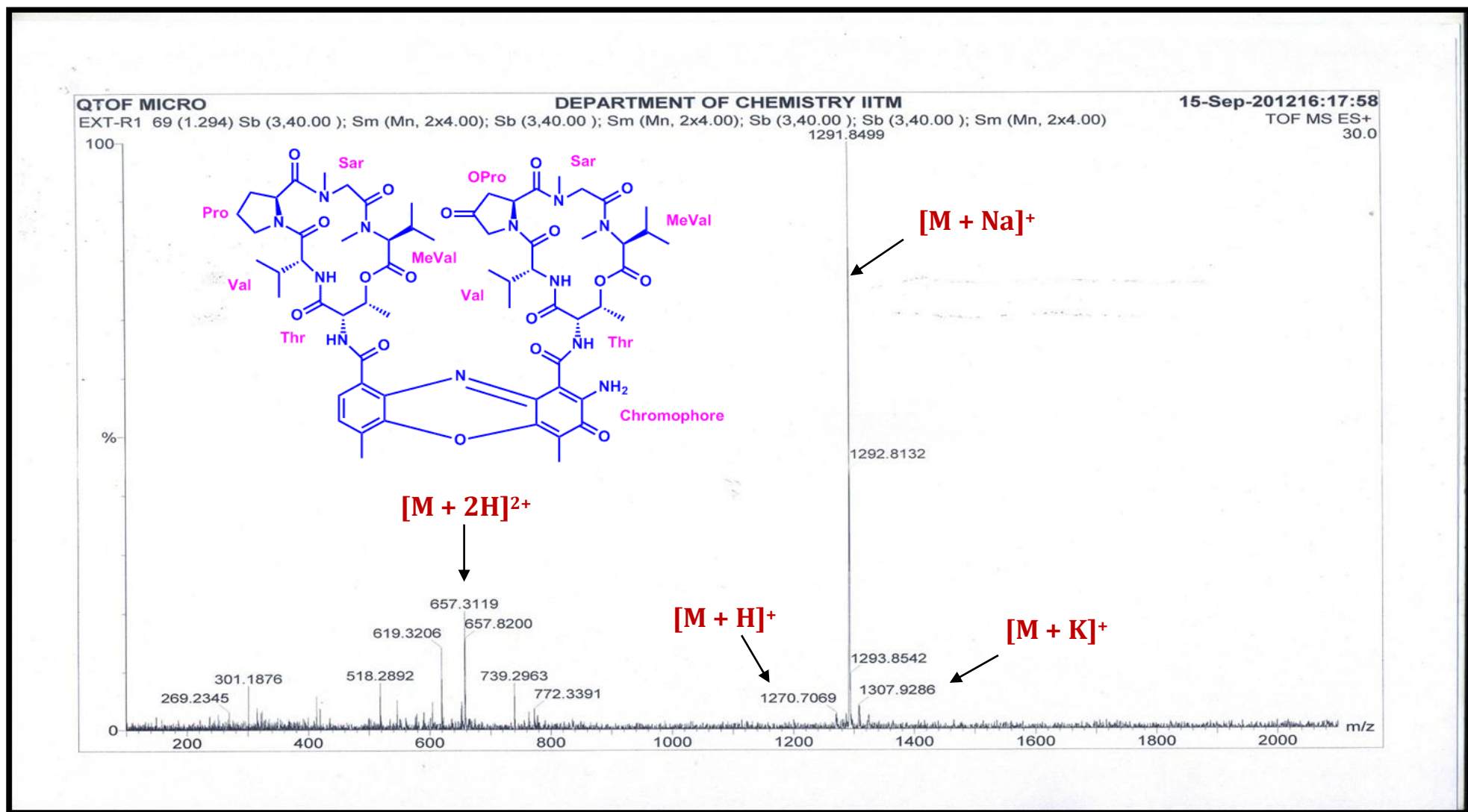


Figure S92. HR-ESI-MS Spectrum of Transitmycin (R1) (Positive mode)

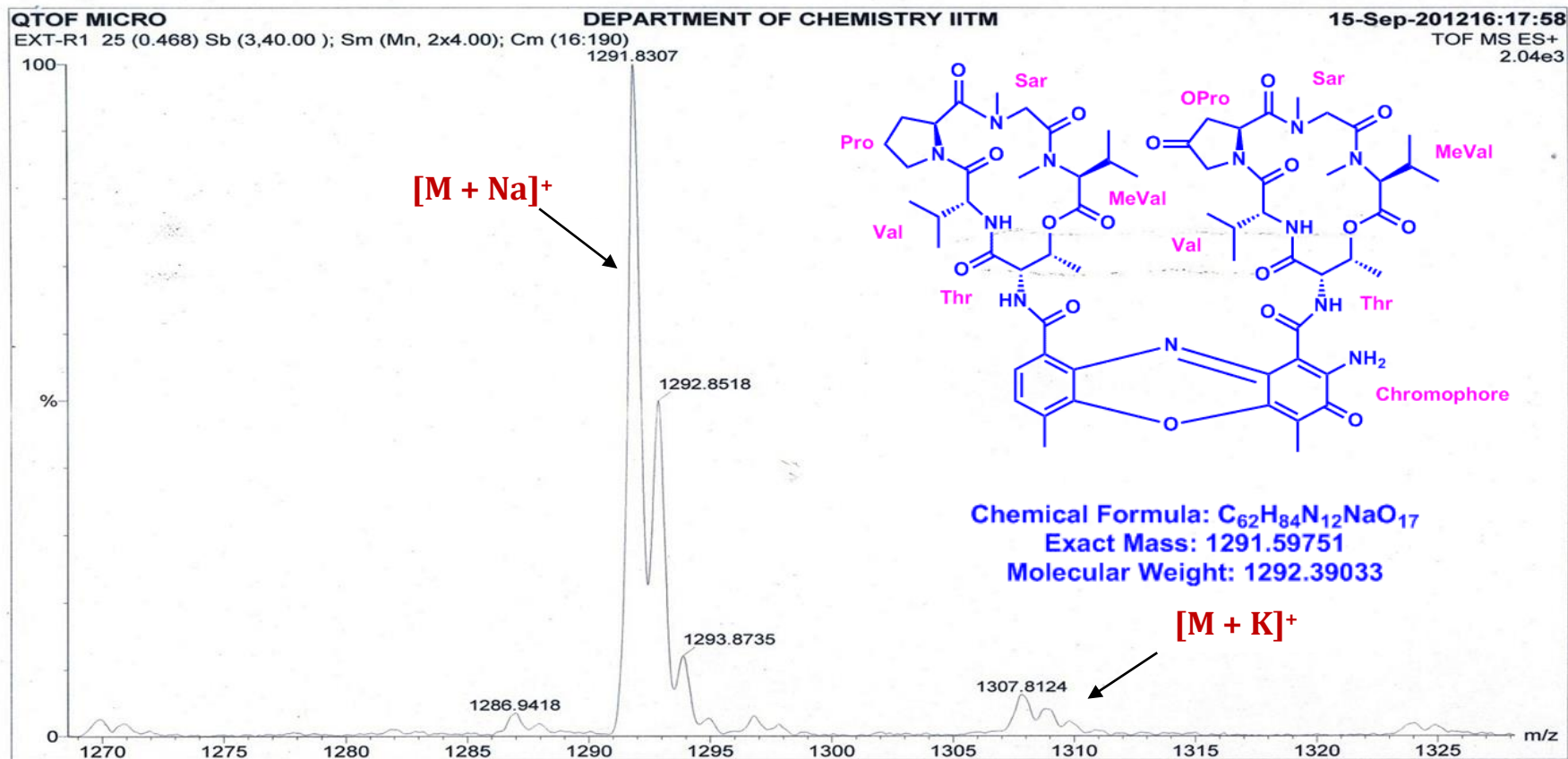


Figure S93. HR-ESI-MS Spectrum of Transitymycin (R1) (Molecular ion Peak) (Positive mode)

QTOF MICRO

EXT-R2 5 (0.093) Sb (3,40.00); Sm (Mn, 2x4.00); Cm (1:7)

DEPARTMENT OF CHEMISTRY II

15-Sep-2012 16:26:05

TOF MS ES+

227

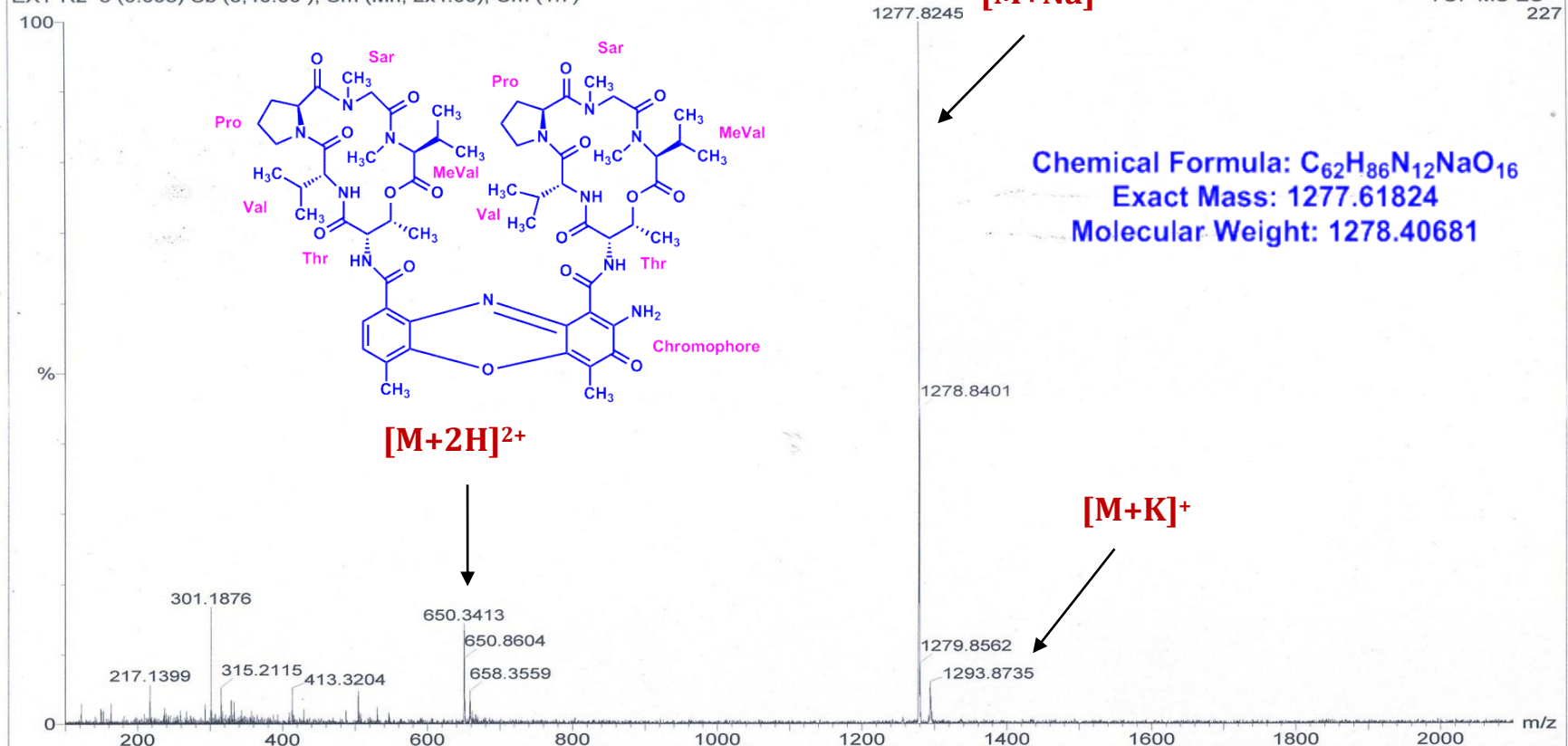


Figure S94. HR-ESI-MS Spectrum of R2 (Positive mode)

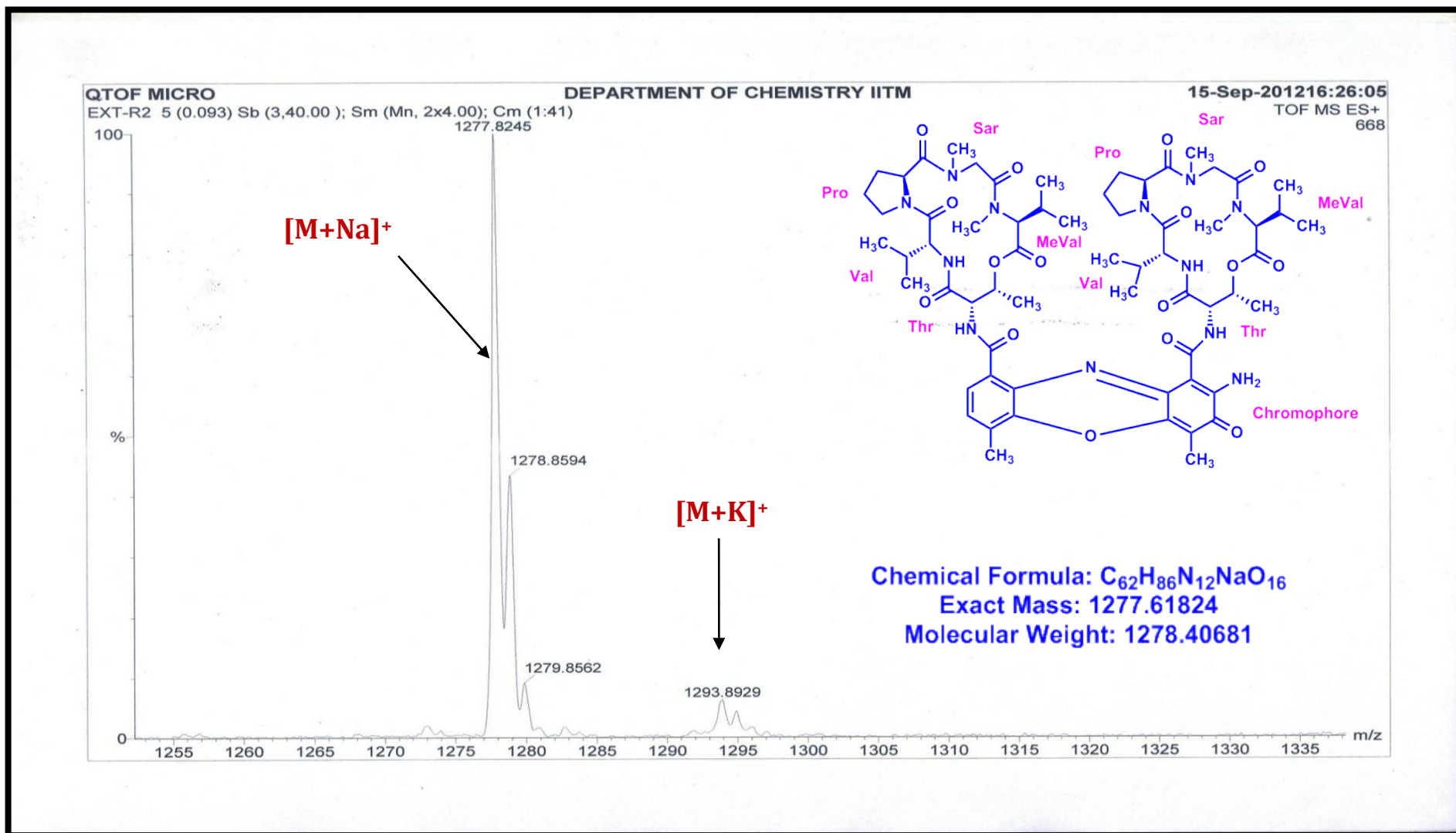


Figure S95. HR-ESI-MS Spectrum of R2 (Molecular ion Peak) (Positive mode)

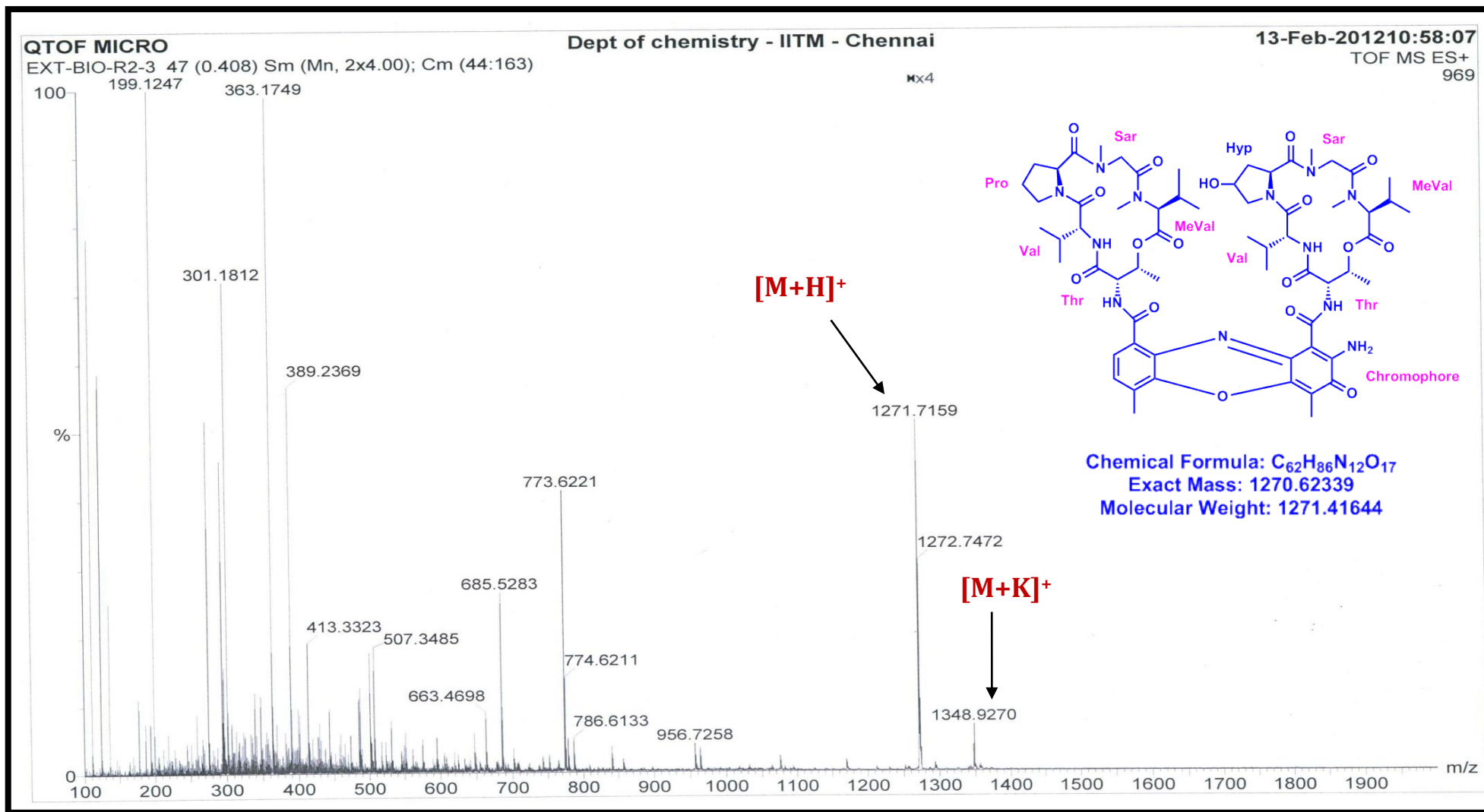


Figure S96. HR-ESI-MS Spectrum of R3 (Positive mode)

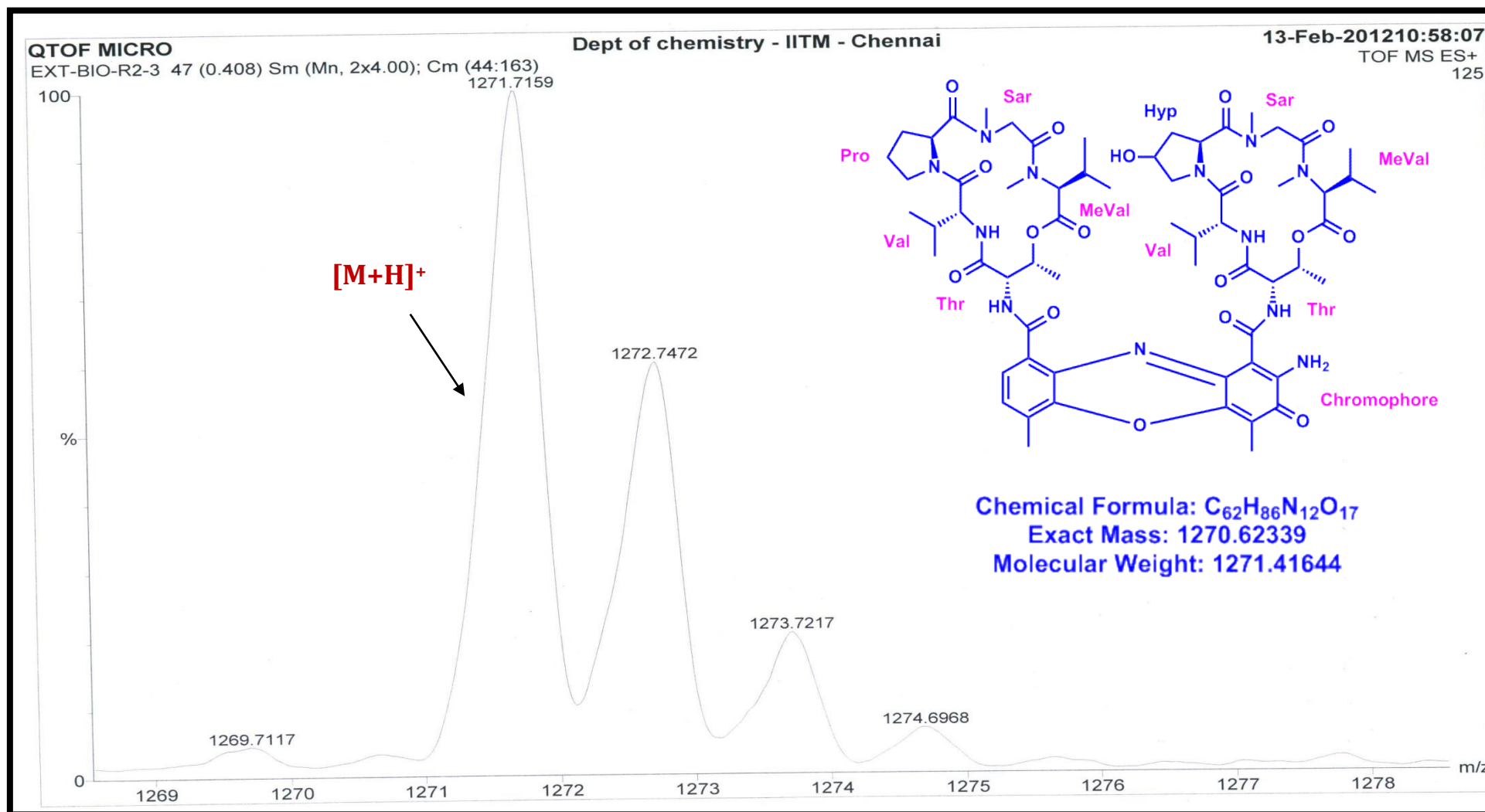


Figure S97. HR-ESI-MS Spectrum of R3 (Molecular ion Peak) (Positive mode)

Sample Name	PROF M DOBLE	Position	Vial 19	Instrument Name	Instrument 1	User Name	
Inj Vol	1	InjPosition		SampleType	Sample	IRM Calibration Status	Success
Data Filename	INTERNAL_R-1-6988-04	ACQ Method	100-1700 ISOCRATIC_	Comment		Acquired Time	6/15/2012 8:27:08 PM

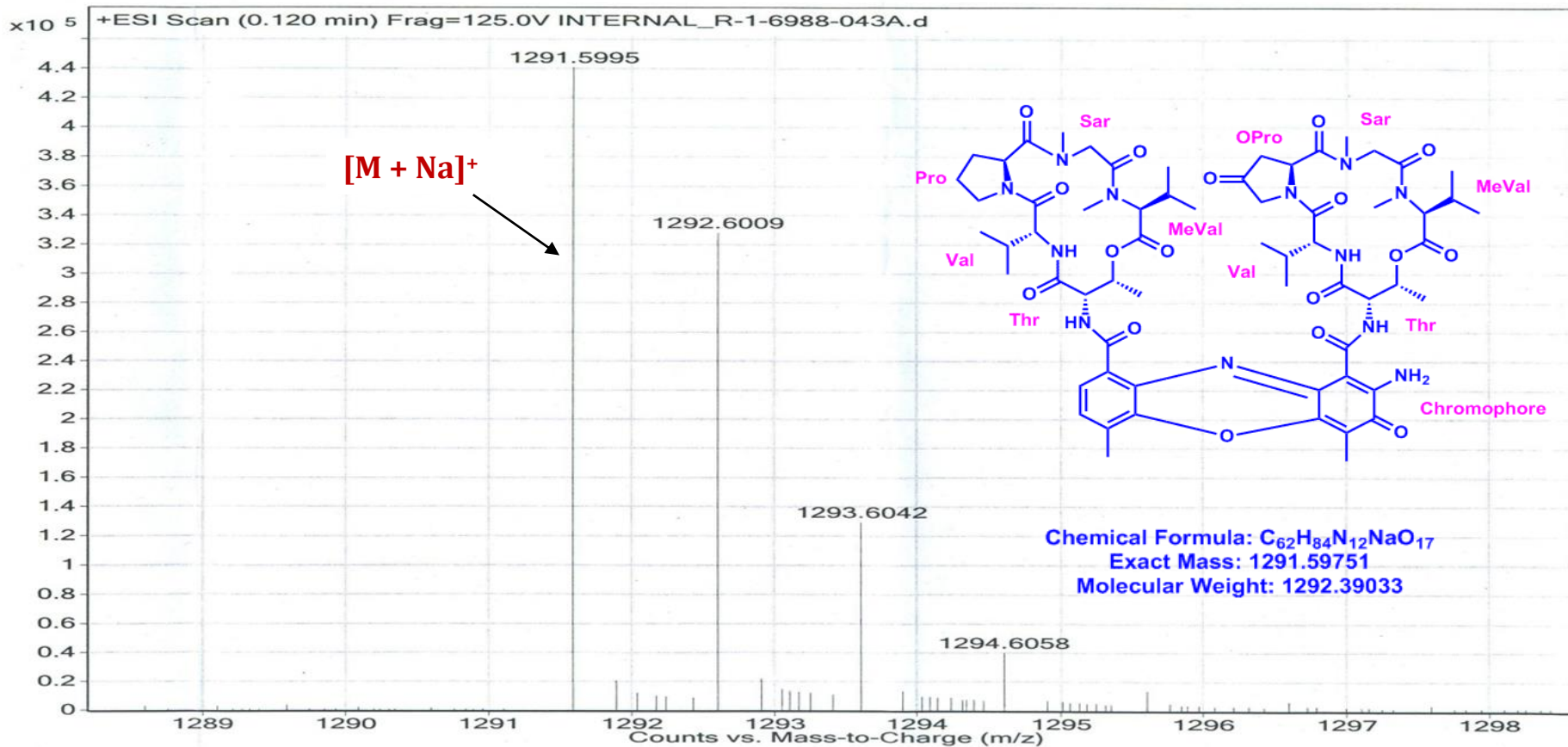


Figure S98. LC-ESI-MS Spectrum of Transitmycin (R1) (Molecular ion peak) (Positive mode)

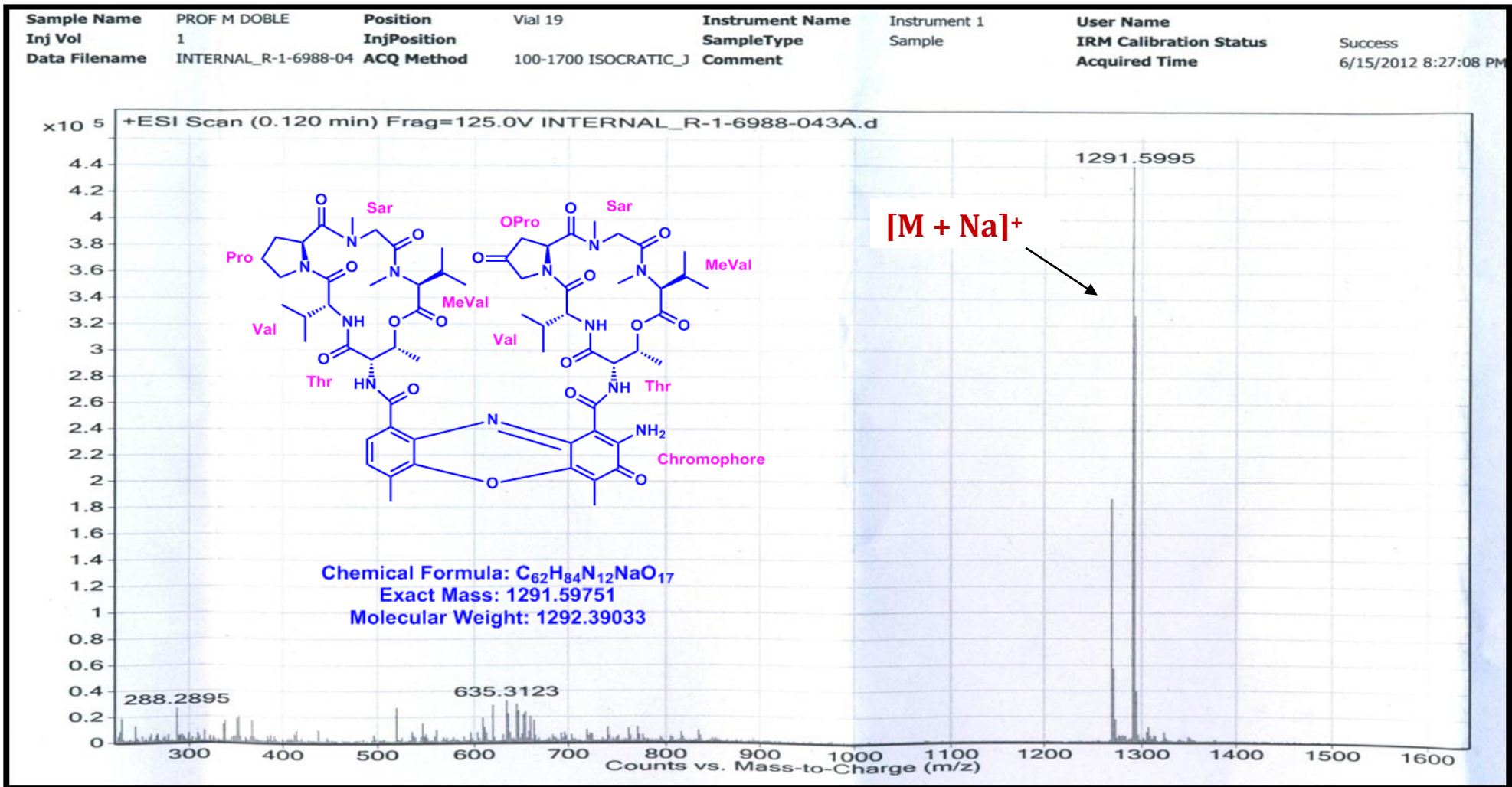


Figure S99. LC-ESI-MS Spectrum of Transitmycin (R1) (Positive mode)

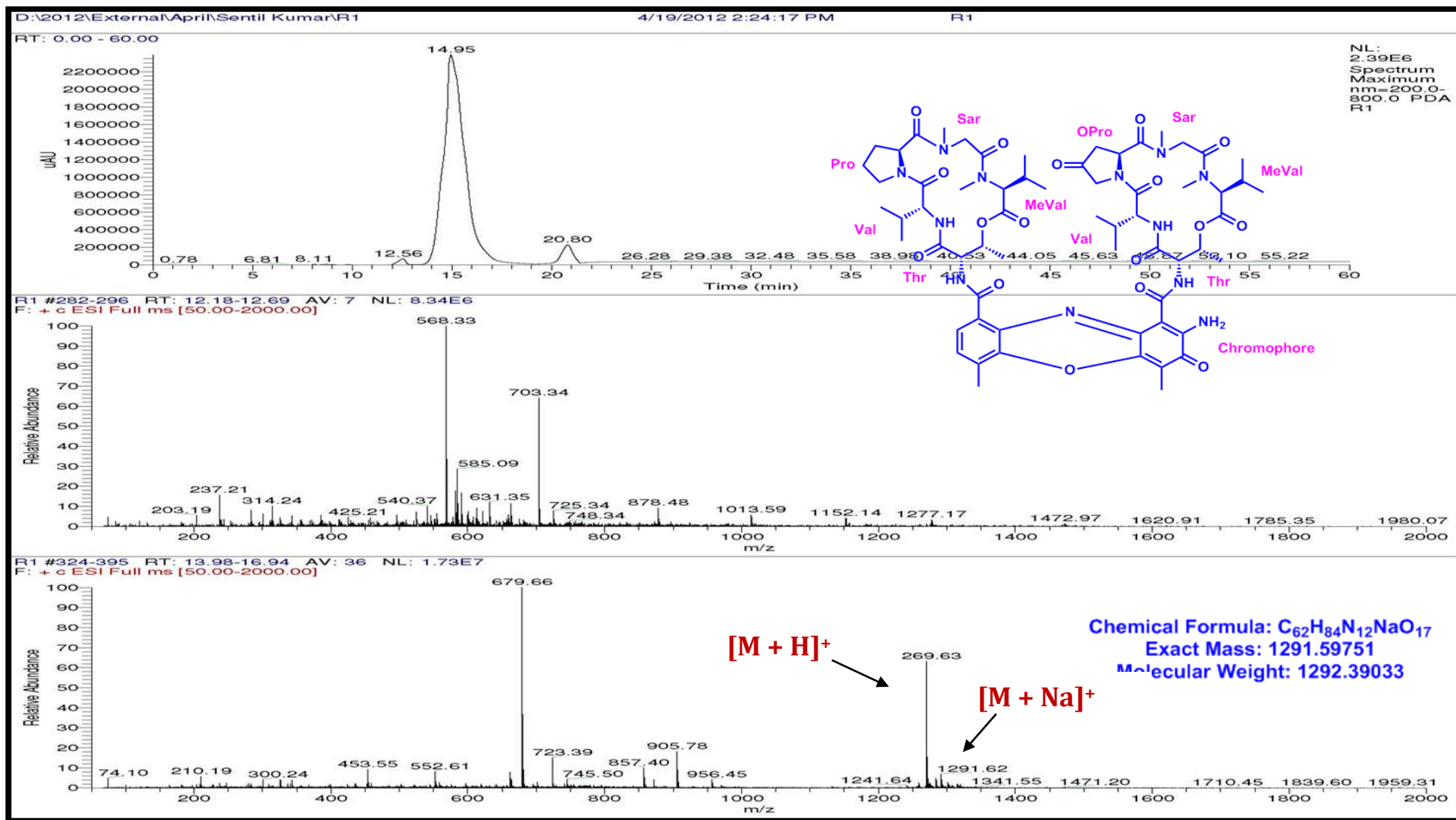


Figure S100. LC-ESI-MS Spectrum of Trasitmycin (R1) (Positive mode)

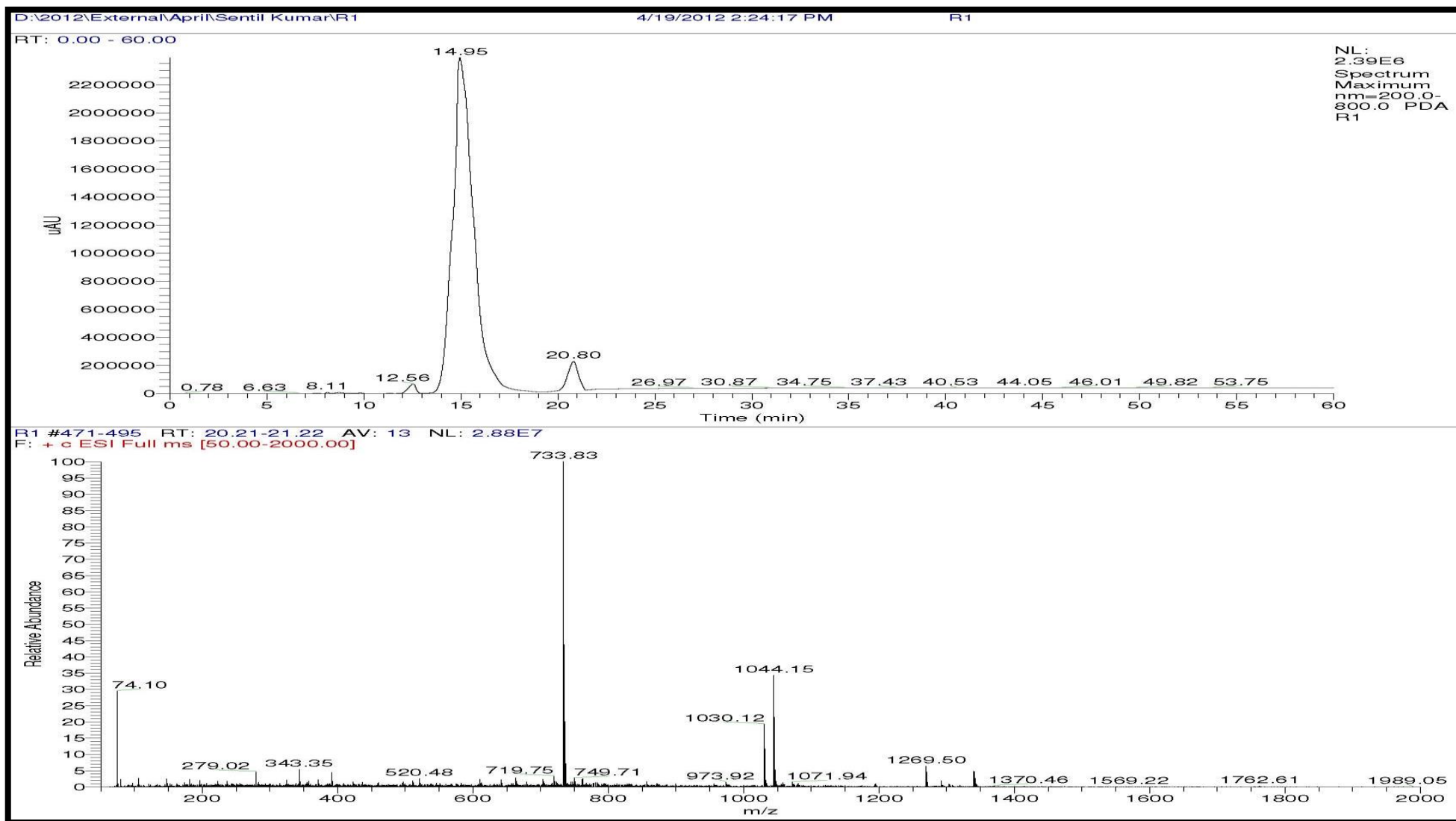


Figure S101. LC-ESI-MS Spectrum of Trasitmycin (R1) (Positive mode)

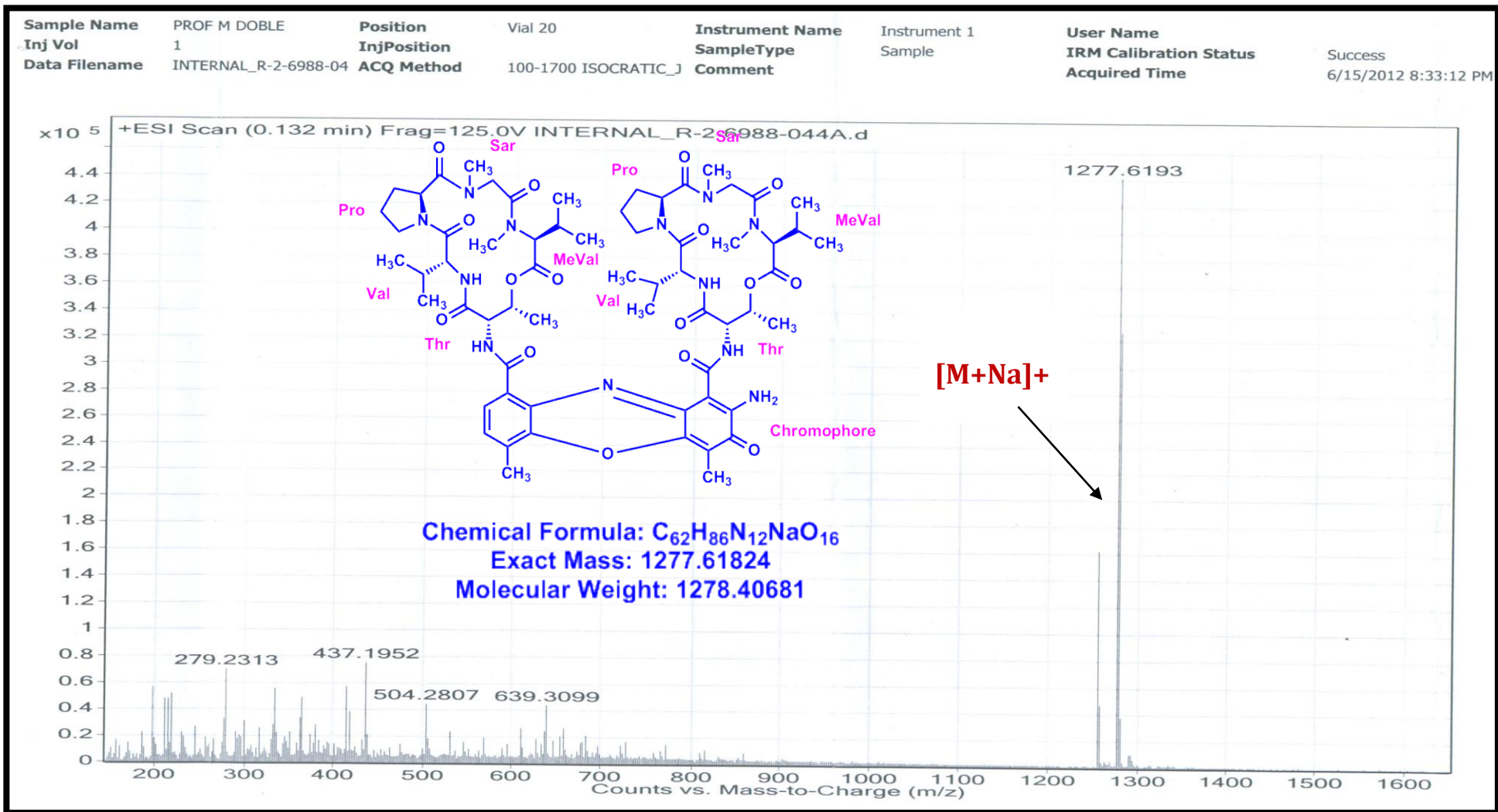


Figure S102. LC-ESI-MS Spectrum of R2 (Positive mode)

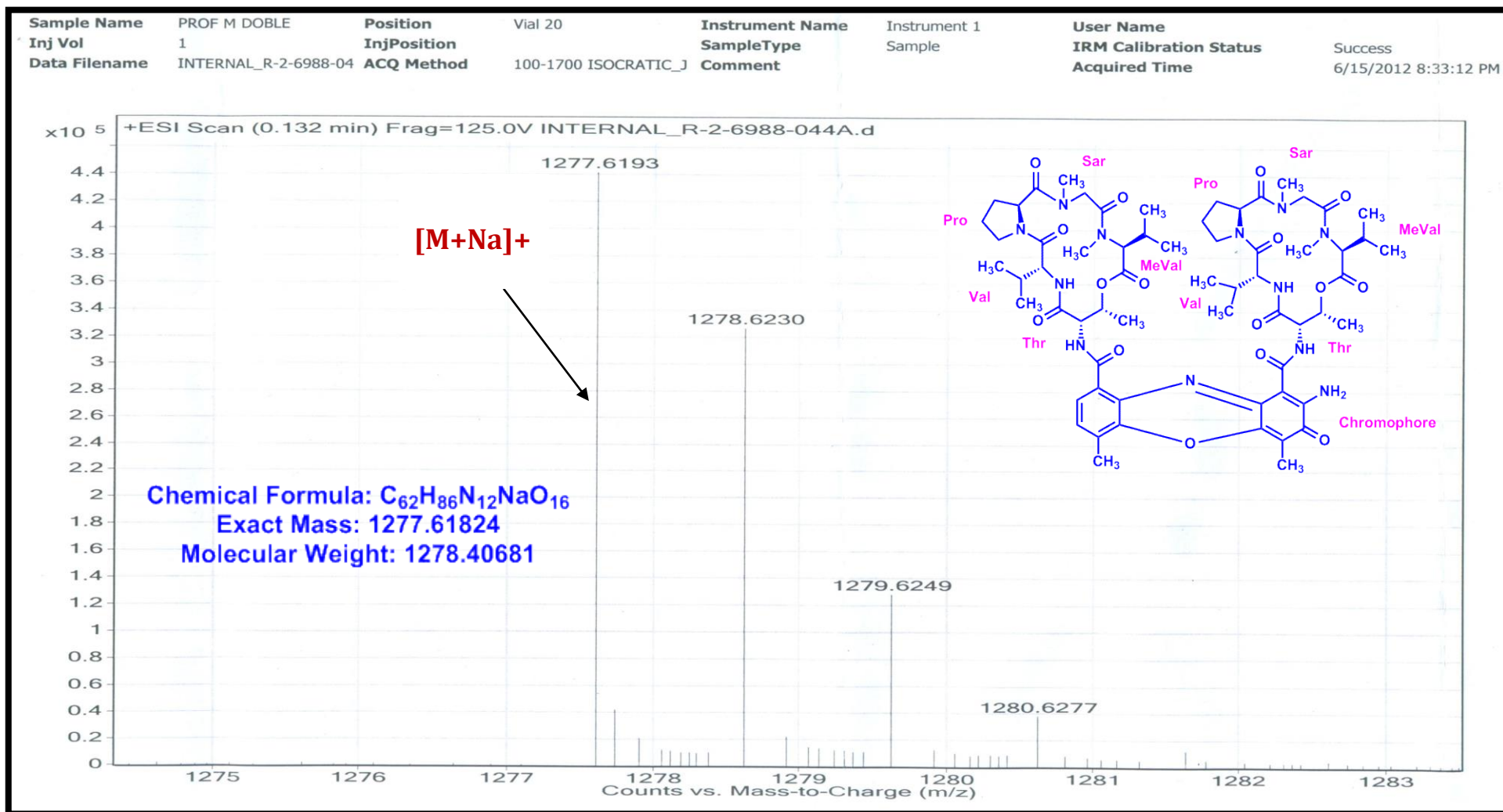


Figure S103. LC-ESI-MS Spectrum of R2 (Molecular ion) (Positive mode)

Sample Name	PROF M DOBLE	Position	Vial 41	Instrument Name	Instrument 1	User Name	
Inj Vol	1	InjPosition		SampleType	Sample	IRM Calibration Status	Success
Data Filename	INTERNAL_R-3-6998-04	ACQ Method	100-1700 ISOCRATIC_J	Comment		Acquired Time	6/15/2012 8:39:14 PM



Figure S104. LC-ESI-MS Spectrum of R3 (Positive mode)

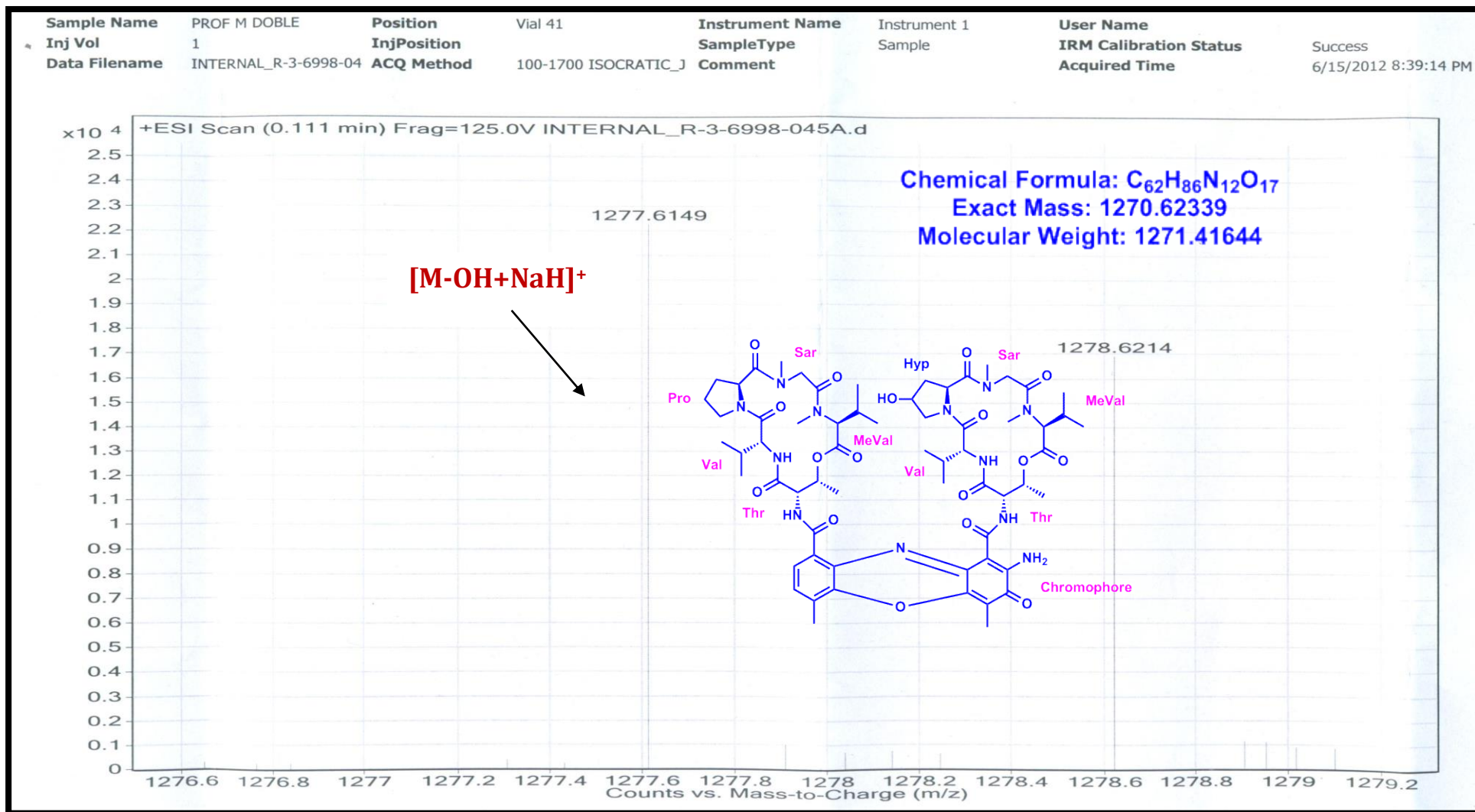


Figure S105. LC-ESI-MS Spectrum of R3 (Positive mode)

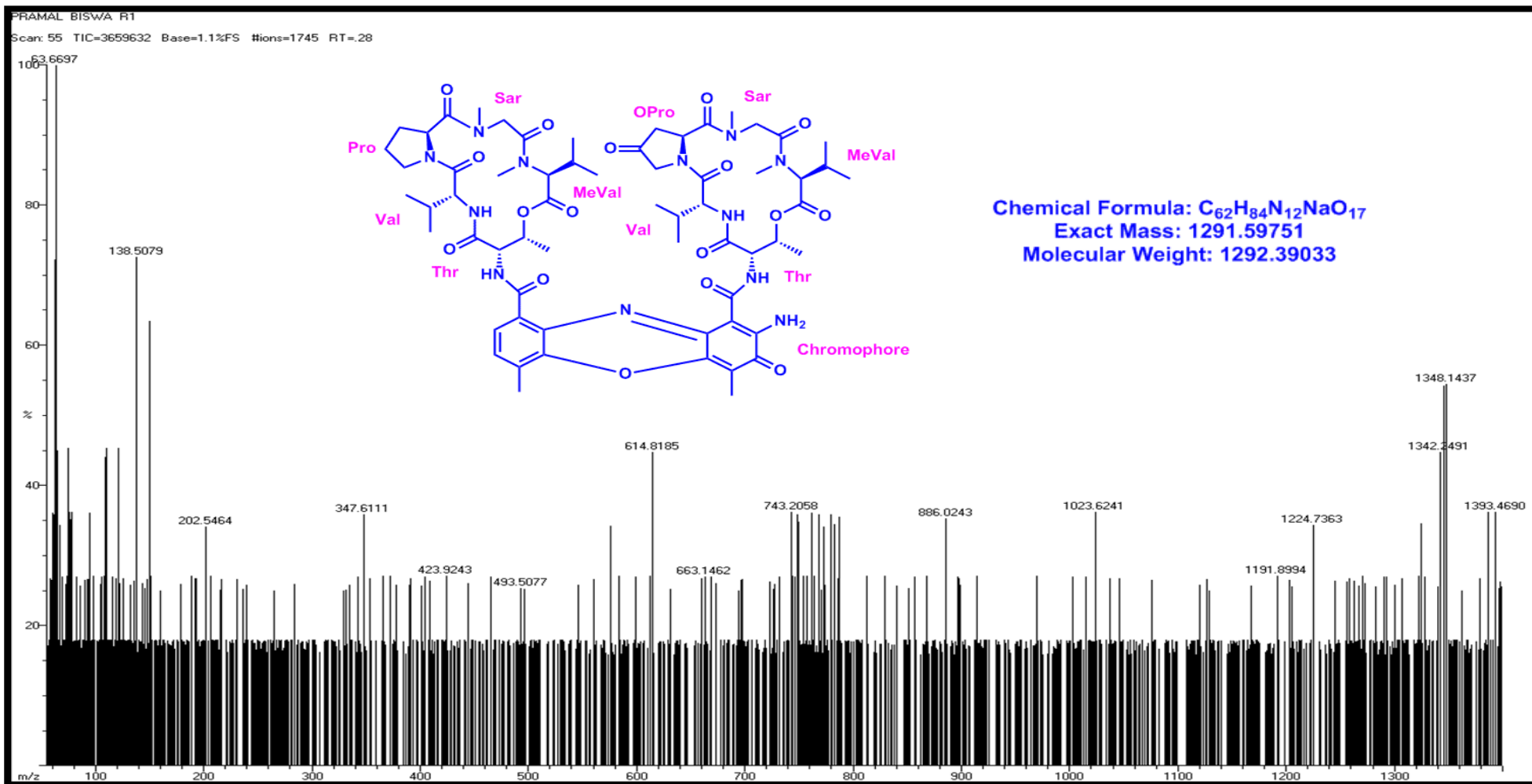


Figure S106. EI-MS Spectrum of Transitmycin (R1) (Positive mode)

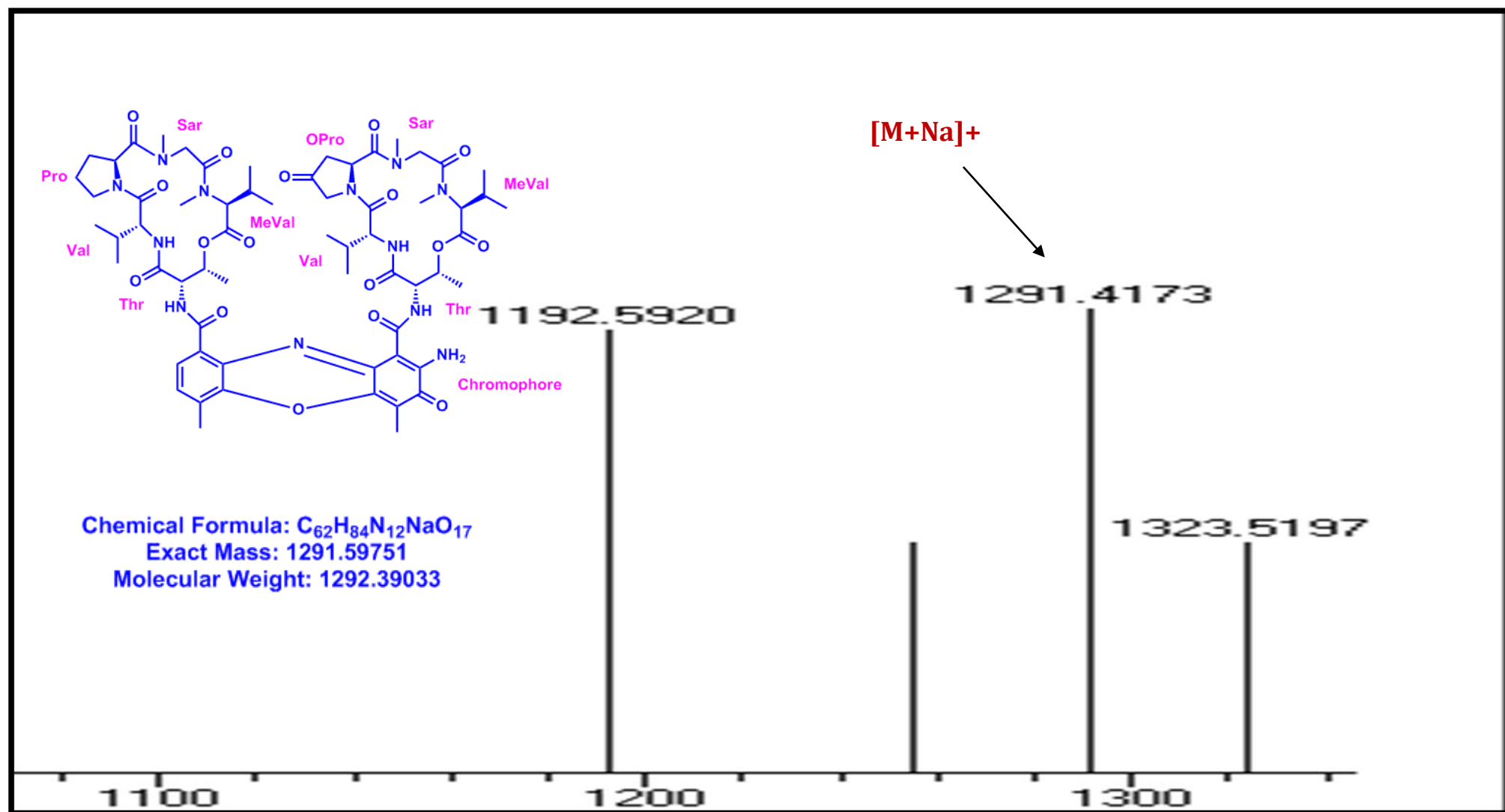


Figure S107. EI-MS Spectrum of (R1) (molecular ion peak) (Positive mode)

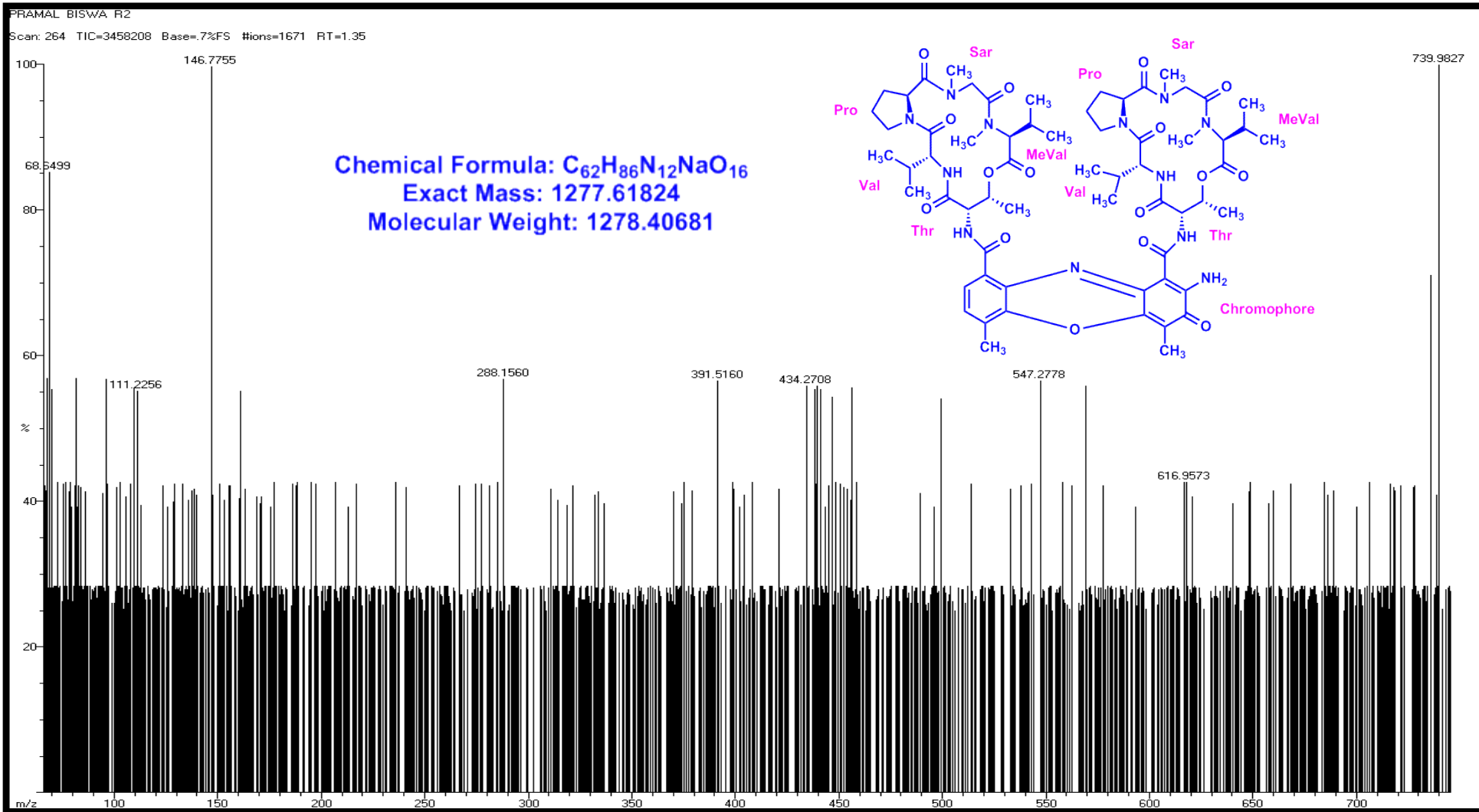


Figure S108. EI-MS Spectrum of (R2) (Positive mode)

PRAMAL BISWA R3

Scan: 67 TIC=3103904 Base=.9%FS #ions=1506 RT=.34

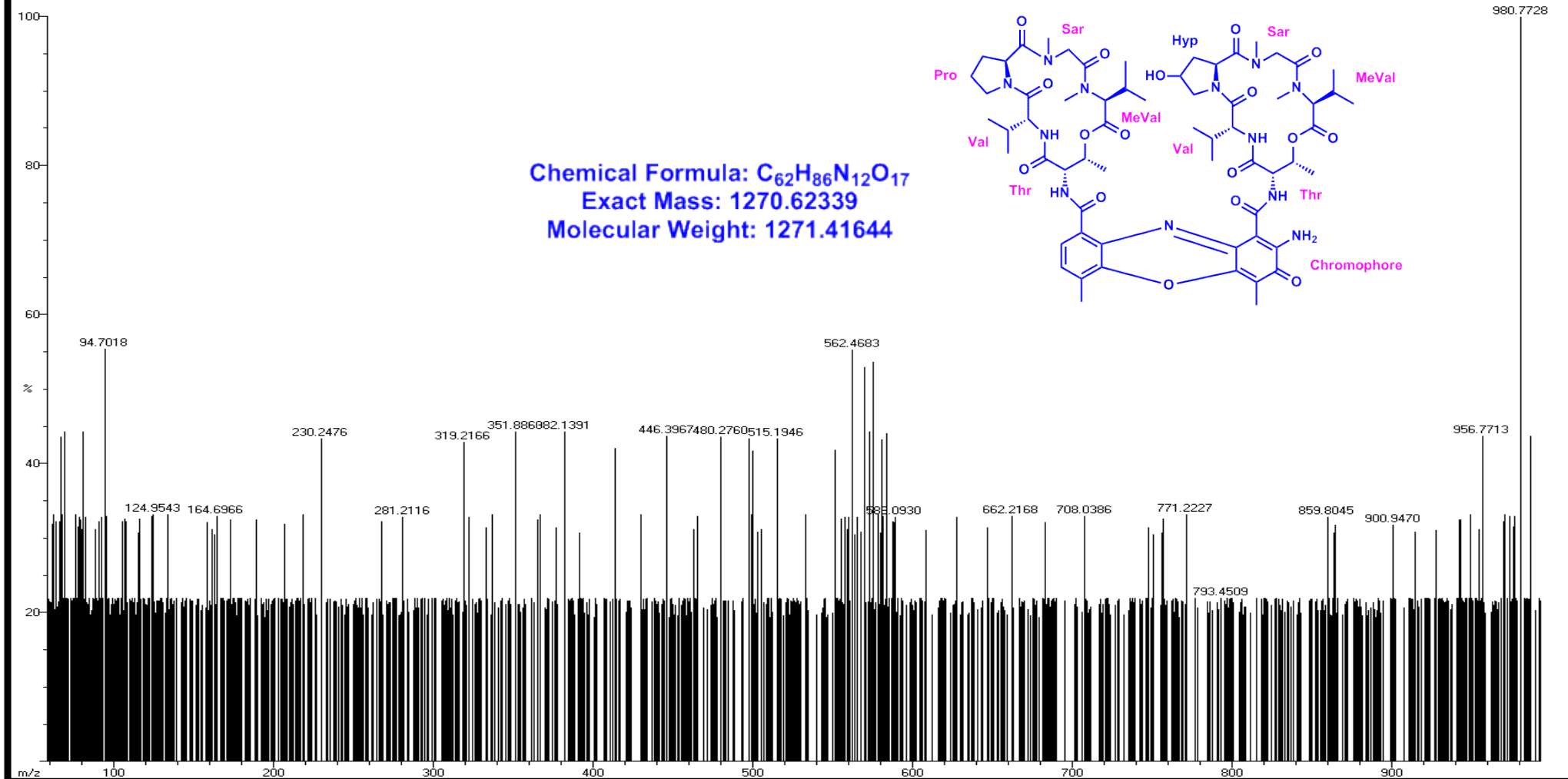


Figure S109 EI-MS Spectrum of (R3) (Positive mode)

DATE 05 09 12 TIME 18 00 52 OPERATOR ID SRIVIDYA S

RUN 53 ID 53 WEIGHT 2.717

SIGNALS

CARBON 59.72%
HYDROGEN 7.28%
NITROGEN 10.19%

ZR 10533
NR 12455
CR 37013
HR 44007

Bio tech

R₁

DATE 05 09 12 TIME 18 05 42 OPERATOR ID SRIVIDYA S

RUN 54 ID 54 WEIGHT 1.369

SIGNALS

CARBON 61.05%
HYDROGEN 7.25%
NITROGEN 11.32%

ZR 10384
NR 11657
CR 24587
HR 28421

R₂

DATE 05 09 12 TIME 18 10 32 OPERATOR ID SRIVIDYA S

RUN 55 ID 55 WEIGHT 1.700

SIGNALS

CARBON 58.75%
HYDROGEN 7.13%
NITROGEN 11.59%

ZR 10513
NR 12010
CR 27049
HR 31888

R₃

Figure S110. CHN analysis data of Transitmycin (R1), R2, R3

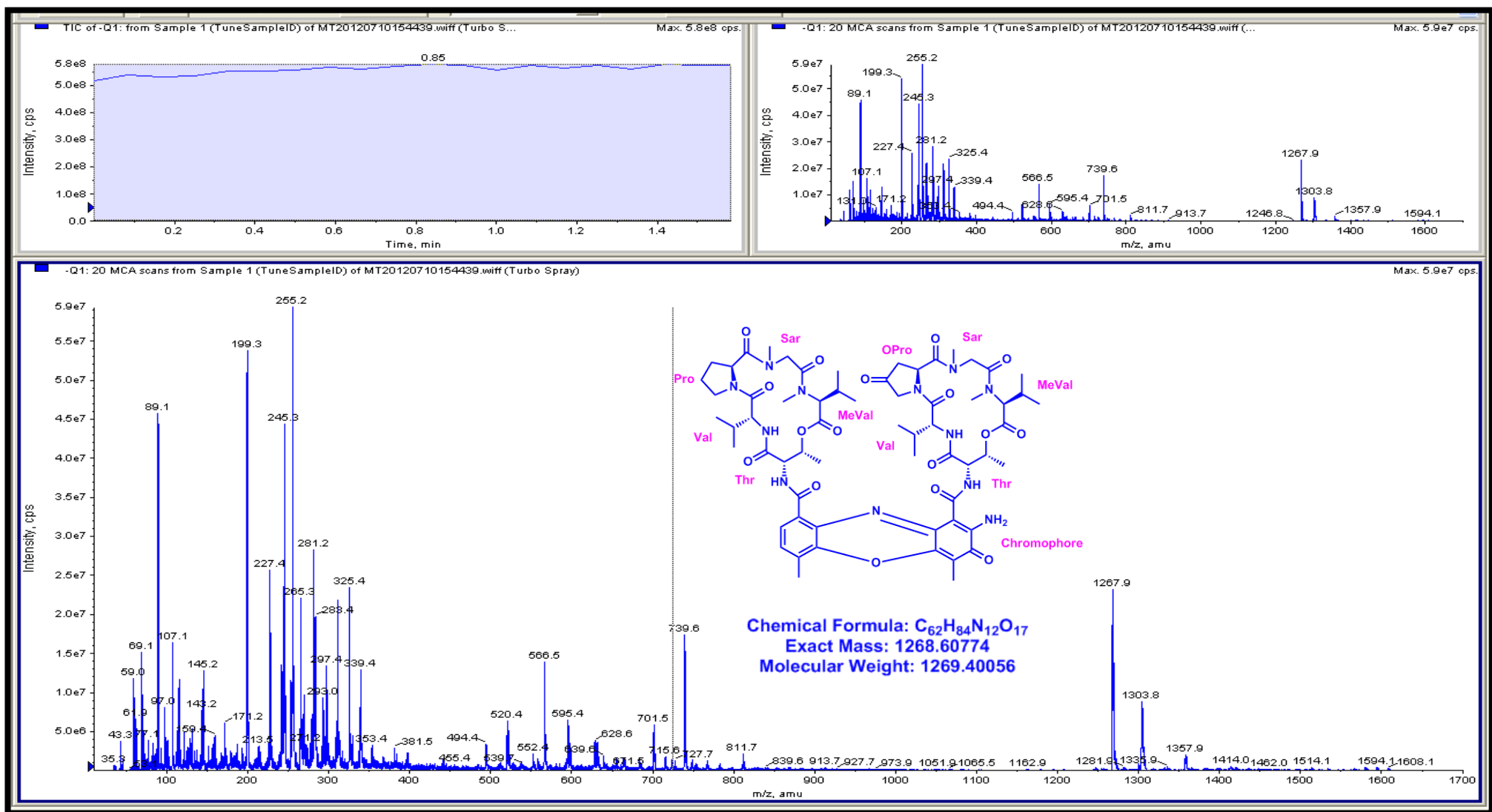


Figure S111. 3200 QTRAP LC/MS/MS Spectrum of Transitmycin (R1) (Negative mode)

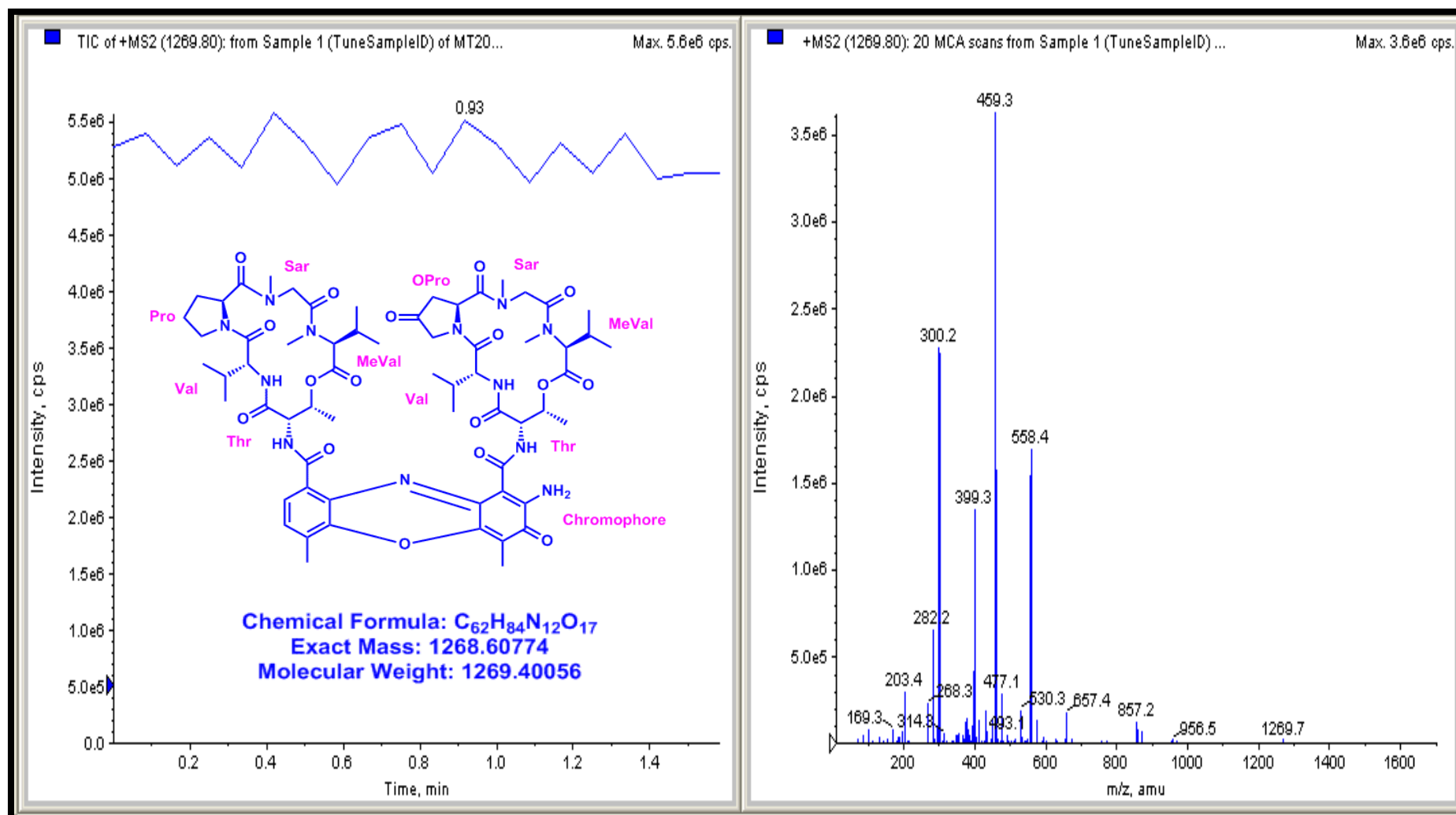


Figure S112. 3200 QTRAP LC/MS/MS Spectrum of Transitmycin (R1) (positive mode)

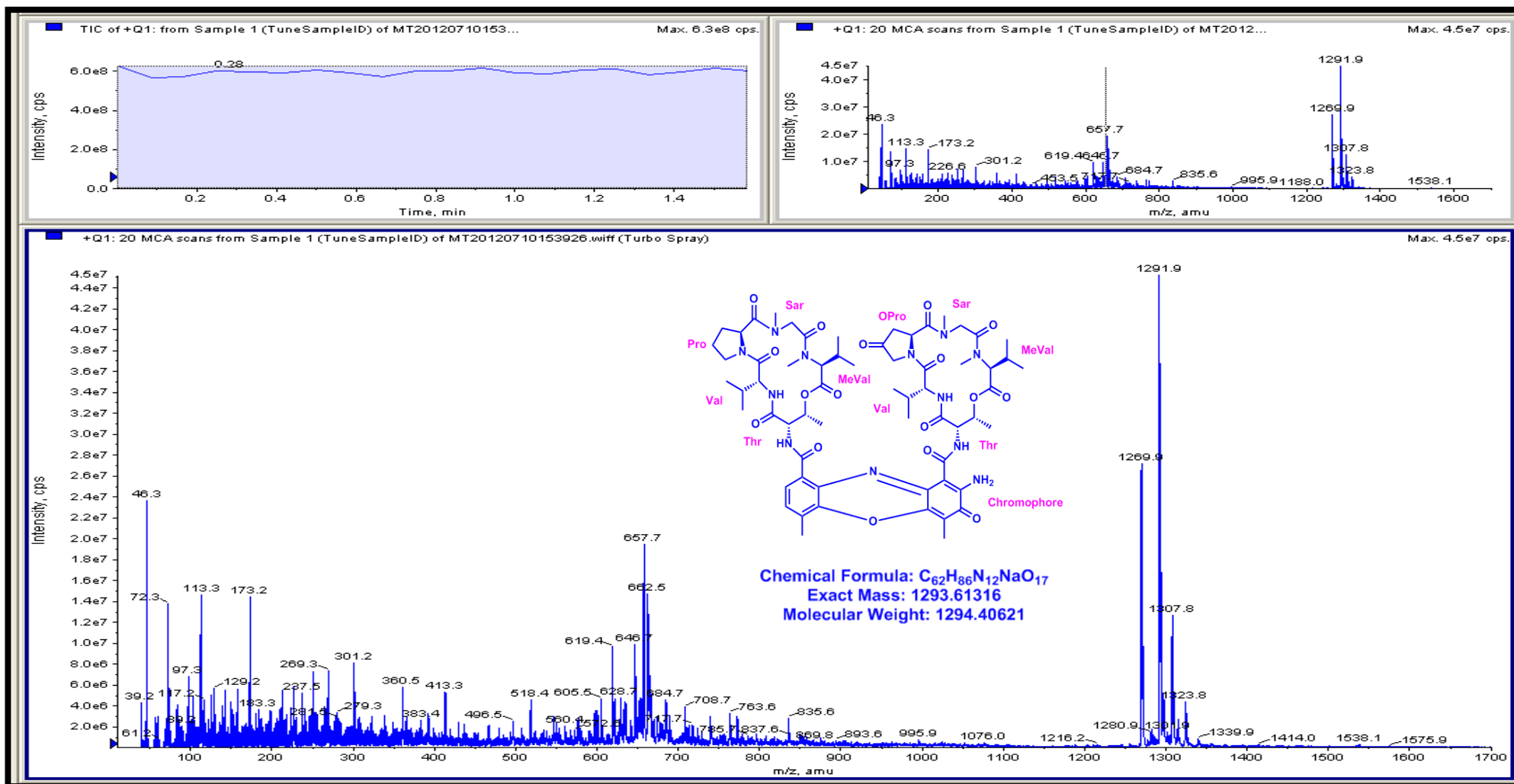


Figure S113. 3200 QTRAP LC/MS/MS Spectrum of Transitmycin (R1) (positive mode mode)

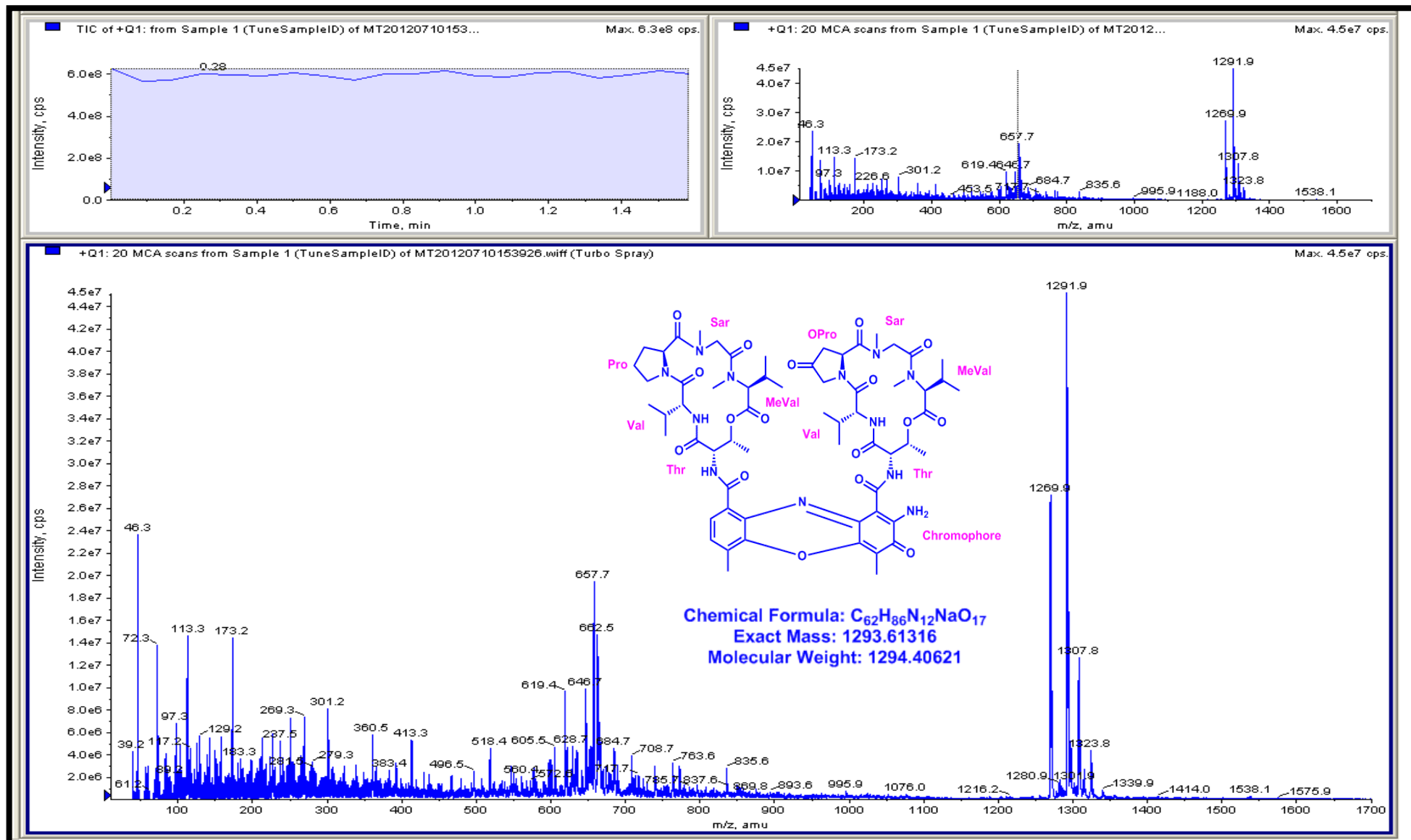


Figure S114. 3200 QTRAP LC/MS/MS Spectrum of Transitmycin (R1) (positive mode)

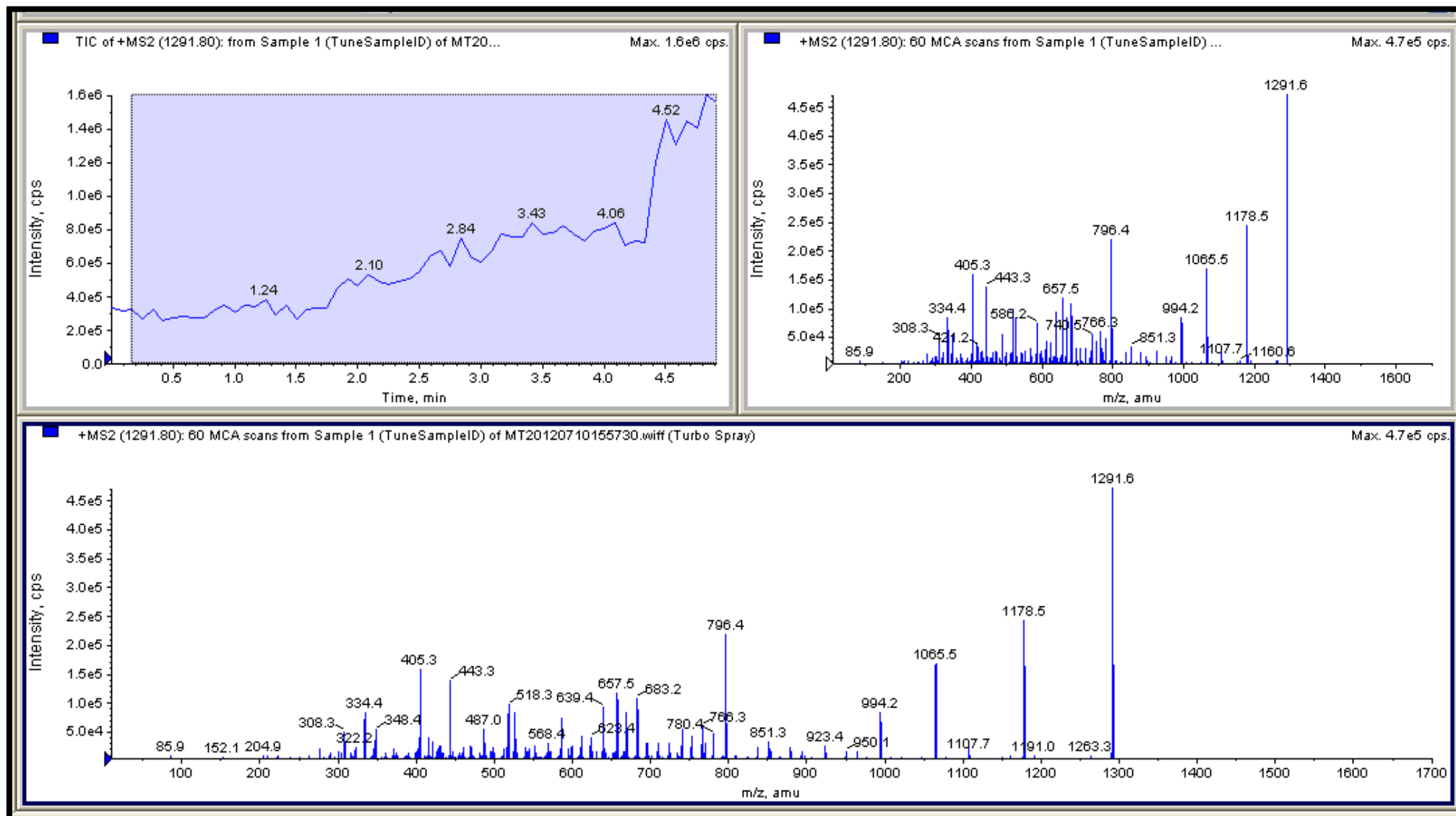
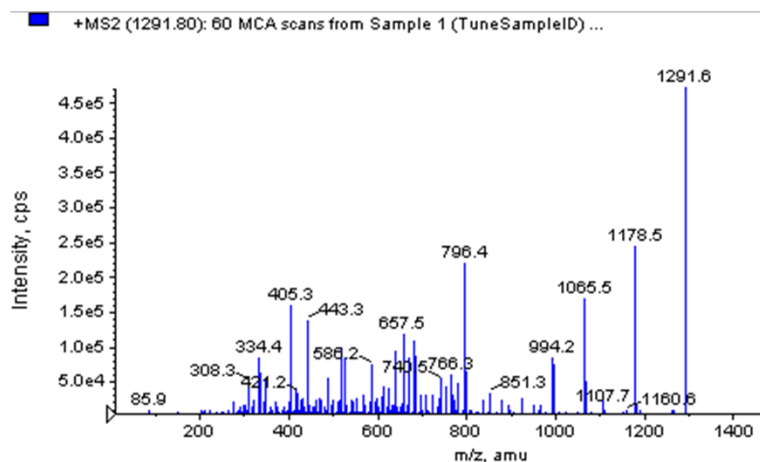


Figure S115. 3200 QTRAP LC/MS/MS Spectrum of Transitmycin (R1) (positive mode)

STRUCTURAL CHARACTERISATION OF PRODUCT IONS OF [MS2] THE [M+NA]⁺ IONS OF TRANSITMYCIN
a) TRANSITMYCIN (R1) OBTAINED BY QTRAP LCMS/MS **b) (R1) OBTAINED BY QTRAP LCMS/MS [MS2] OF 1291.6]**



1291.6 = [M+H]⁺
 1291.6-113.1 = 1178.5 Loss of H-MeVal-OH
 1291.6-226.1 = 1065.5 Loss of 2XH-MeVal-
 1291.6-297.4 = 994.2 Loss of Sar-2XH-MeVal-OH
 1291.6-368.2 = 923.4 Loss of 2XSar-2XH-MeVal-OH
 1291.6-440.3 = 851.3 Loss of 2XSar-2XH-MeVal-OH
 1291.6-495.2 = 796.4 Loss of H-Thr-Val-Oxo-Pro-Sar-MeVal-OH
 1291.6- 608.4 = 683.2 Loss of H-Thr-Val-Oxo-Pro-Sar-MeVal-OH + Loss of H-MeVal-OH
 1291.6- 634.1 = 657.5 Loss of H-Val-Pro- Sar-MeVal-OH + Loss of H-Pro- Sar-MeVal-OH
 1291.6-652.2 = 639.4 Loss of H-Val-Pro- Sar-MeVal-OH + Loss of H-Pro- Sar-MeVal-OH (18)
 1291.6-772.7 = 518.3 Loss of H⁻-Val-OXO-Pro-Sar-MeVal-OH + Loss of H-Val-Pro- Sar-MeVal-OH
 1291.6-772.7 = 518.3 Loss of H⁻-Val-OXO-Pro-Sar-MeVal-OH + Loss of H-Val-Pro- Sar-MeVal-OH
 1291.6-804.0 = 487.0 Loss of H-Val-OXO-Pro-Sar-MeVal-OH + Loss of H-Val-Pro- Sar-MeVal-OH (32)
 1291.6-848.3 = 443.3 Loss of H-Val-OXO-Pro-Sar-MeVal-OH + Loss of H-Val-Pro- Sar-MeVal-OH (32)
 1291.6-886.3 = 405.3 Loss of H-Val-OXO-Pro-Sar-MeVal-OH + Loss of H-Val-Pro- Sar-MeVal-OH
 1291.6-957.2 = 334.4 Loss of H-Th-Val-Oxo-Pro-Sar-MeVal-OH + Loss of H-Th-Val-Pro- Sar-MeVal-OH

Figure S115 a-b Structural characterisation of Transitmycin (R1) obtained by QTRAP LC-MS/MS. **b** Product ions [MS2] the [M+Na]⁺ ions Transitmycin (R1) obtained by QTRAP LCMS/MS [MS2] of 1291.6, 1291.6 [M+H]⁺, 1178.5 Loss of H-MeVal-OH, 1065.5 Loss of 2XH-MeVal, 994.2 Loss of Sar-2XH-MeVal-OH, 923.4 Loss of 2XSar-2XH-MeVal-OH, 851.3 Loss of 2XSar-2XH-MeVal-OH, 796.4 Loss of H-Thr-Val-Oxo-Pro-Sar-MeVal-OH, 683.2 Loss of H-Thr-Val-Oxo-Pro-Sar-MeVal-OH + Loss of H-MeVal-OH, 657.5 Loss of H-Val-Pro- Sar-MeVal-OH + Loss of H-Pro- Sar-MeVal-OH, 639.4 Loss of H-Val-Pro- Sar-MeVal-OH + Loss of H-Pro- Sar-MeVal-OH (18), 518.3 Loss of H⁻-Val-OXO-Pro-Sar-MeVal-OH + Loss of H-Val-Pro- Sar-MeVal-OH, 518.3 Loss of H⁻-Val-OXO-Pro-Sar-MeVal-OH + Loss of H-Val-Pro- Sar-MeVal-OH, 487.0 Loss of H-Val-OXO-Pro-Sar-MeVal-OH + Loss of H-Val-Pro- Sar-MeVal-OH (32), 443.3 Loss of H-Val-OXO-Pro-Sar-MeVal-OH + Loss of H-Val-Pro- Sar-MeVal-OH (32), 405.3 Loss of H-Val-OXO-Pro-Sar-MeVal-OH + Loss of H-Val-Pro- Sar-MeVal-OH, 334.4 Loss of H-Th-Val-Oxo-Pro-Sar-MeVal-OH + Loss of H-Th-Val-Pro- Sar-MeVal-OH.

Table S7a. Structural characterisation of Transitmycin (R1) obtained by QTRAP LCMS/MS

Product ions of [MS2] the [M+H]⁺ ions of Transitmycin (R1) obtained by QTRAP LCMS/MS

[MS2] of 1269.7

1269.7 = [M+H]⁺

1269.7-313.2 = 956.5 Loss of H-Oxo-Pro-Sar-MeVal-OH

1269.7-412.5 = 857.2 Loss of H-Val-Oxo-Pro-Sar-MeVal-OH

1269.7-612.3 = 657.4 Loss of H-Val-Oxo-Pro-Sar-MeVal-OH + Loss of Sar-MeVal-OH

1269.7-711.3 = 558.4 Loss of H-Val-Oxo-Pro-Sar-MeVal-OH + Loss of Pro- Sar-MeVal-OH

1269.7-739.3 = 530.3 Loss of H-Val-Oxo-Pro-Sar-MeVal-OH + Loss of Pro- Sar-MeVal-OH (-28)

1269.7-810.4 = 459.3 Loss of H-Val-Oxo-Pro-Sar-MeVal-OH + Loss of Val-Pro- Sar-MeVal-OH

1269.7-870.4 = 399.3 Loss of H-Val-Pro- Sar-MeVal-OH

1269.7-969.7 = 300.2 Loss of H-Pro- Sar-MeVal-OH

1269.7-1007.5 = 262.2 Loss of H-Pro- Val-Sar-OH

1269.7-1066.3 = 203.4 Loss of H-Sar-MeVal-OH

1269.7-1100.4 = 169.3 Loss of H-Pro-Sar-OH

Table S7b. Structural characterisation of Transitmycin (R1) obtained by QTRAP LCMS/MS

Product ions of [MS2] the [M+Na] ⁺ ions of Transitmycin (R1) obtained by QTRAP LCMS/MS	
[MS2] of 1291.6	
1291.6 = [M+H] ⁺	
1291.6-113.1 = 1178.5	Loss of H-MeVal-OH
1291.6-226.1 = 1065.5	Loss of 2XH-MeVal
1291.6-297.4 = 994.2	Loss of Sar-2XH-MeVal-OH
1291.6-368.2 = 923.4	Loss of 2XSar-2XH-MeVal-OH
1291.6-440.3 = 851.3	Loss of 2XSar-2XH-MeVal-OH
1291.6-495.2 = 796.4	Loss of H-Thr-Val-Oxo-Pro-Sar-MeVal-OH
1291.6- 608.4 = 683.2	Loss of H-Thr-Val-Oxo-Pro-Sar-MeVal-OH + Loss of H-MeVal-OH
1291.6- 634.1 = 657.5	Loss of H-Val-Pro- Sar-MeVal-OH + Loss of H-Pro- Sar-MeVal-OH
1291.6-652.2 = 639.4	Loss of H-Val-Pro- Sar-MeVal-OH + Loss of H-Pro- Sar-MeVal-OH (18)
1291.6-772.7 = 518.3	Loss of H ⁻ -Val-OXO-Pro-Sar-MeVal-OH + Loss of H-Val-Pro- Sar-MeVal-OH
1291.6-772.7 = 518.3	Loss of H ⁻ -Val-OXO-Pro-Sar-MeVal-OH + Loss of H-Val-Pro- Sar-MeVal-OH
1291.6-804.0 = 487.0	Loss of H-Val-OXO-Pro-Sar-MeVal-OH + Loss of H-Val-Pro- Sar-MeVal-OH (32)
1291.6-848.3 = 443.3	Loss of H-Val-OXO-Pro-Sar-MeVal-OH + Loss of H-Val-Pro- Sar-MeVal-OH (32)
1291.6-886.3 = 405.3	Loss of H-Val-OXO-Pro-Sar-MeVal-OH + Loss of H-Val-Pro- Sar-MeVal-OH
1291.6-957.2 = 334.4	Loss of H-Th-Val-Oxo-Pro-Sar-MeVal-OH + Loss of H-Th-Val-Pro- Sar-MeVal-OH

The Transitmycin A (3.0 mg) dissolved in 6N HCl (1 mL) and heated at 110 °C for 24 h. The solvent was removed under reduced pressure, and the resulting material was subjected to further derivatization. The hydrolysate mixture (3.5 mg) or the amino acid standards (0.5 mg) were dissolved in 0.1 mL of water and treated with 0.2 mL of 1% 1-fluoro-2,4-dinitrophenyl-5-Lalaninamide (FDAA) in acetone and 0.04 mL of 1.0 M sodium bicarbonate. The vials were heated at 50 °C for 90 min, and the contents after cooling at room temperature were neutralized with 1 N HCl. After degassing, an aliquot of the FDAA derivative was diluted in MeOH and purified by chromatography using a RP C-18 column (250 X 4.6 mm) and a linear gradient of acetonitrile and water containing 0.05% trifluoroacetic acid from 20:80 to 50:50 in 20 min and then isocratic. The flow rate was 1 mL/min, and the absorbance detection was at 340 nm. The chromatogram was compared with those of amino acid standards treated in the same conditions. The above same procedure for other two compounds B and C were done.

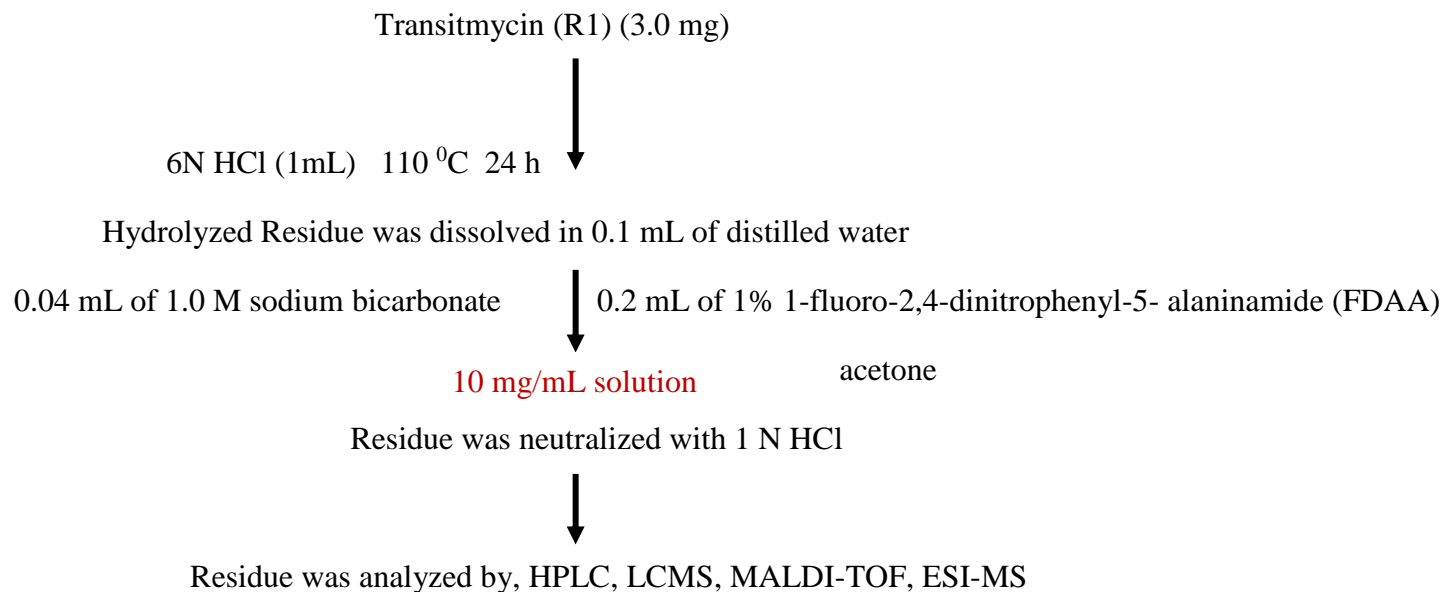


Figure S116. Hydrolysis of Amino Acid Residue of Transitmycin (R1), R2, R3

Figure S117a. HPLC analysis of standard L-FDAA-D/L-Valine

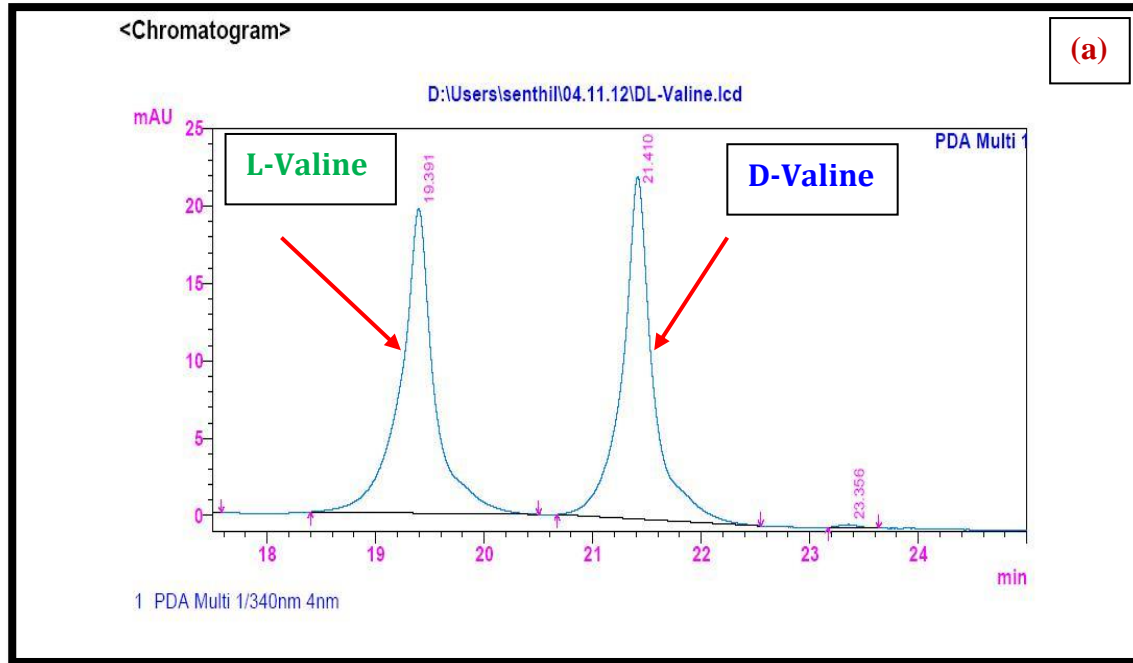


Figure S117 b. HPLC analysis of standard L-FDAA-D-Valine

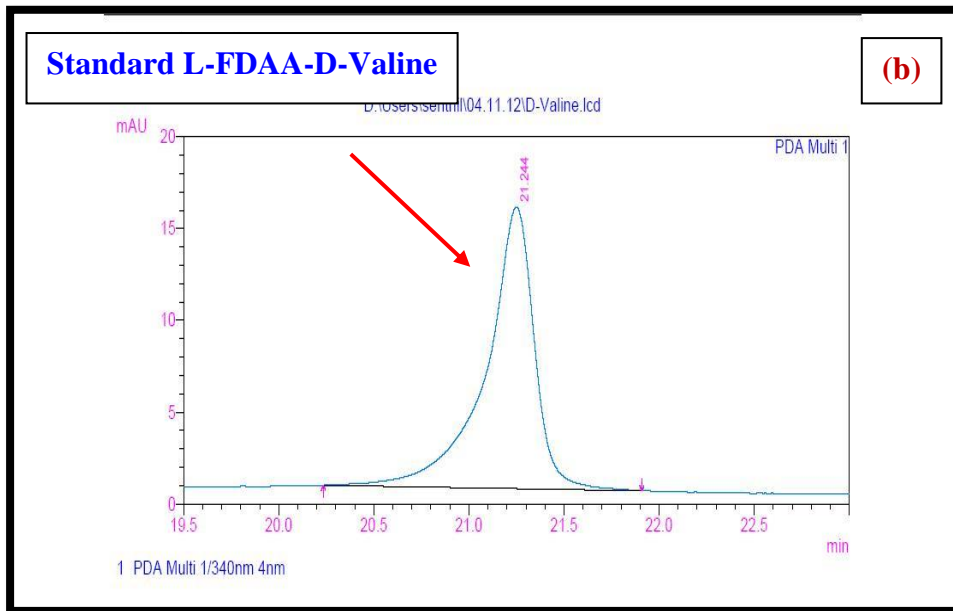


Figure S117c. HPLC analysis of standard L-FDAA-L-Valine

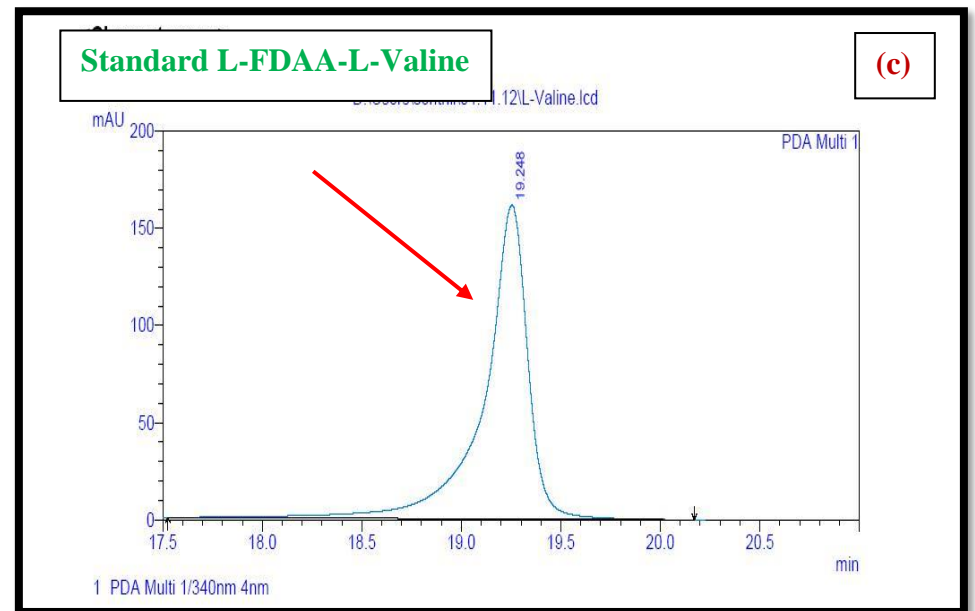


Figure S118 (a). HPLC analysis of standard L-FDAA-D/L-Proline

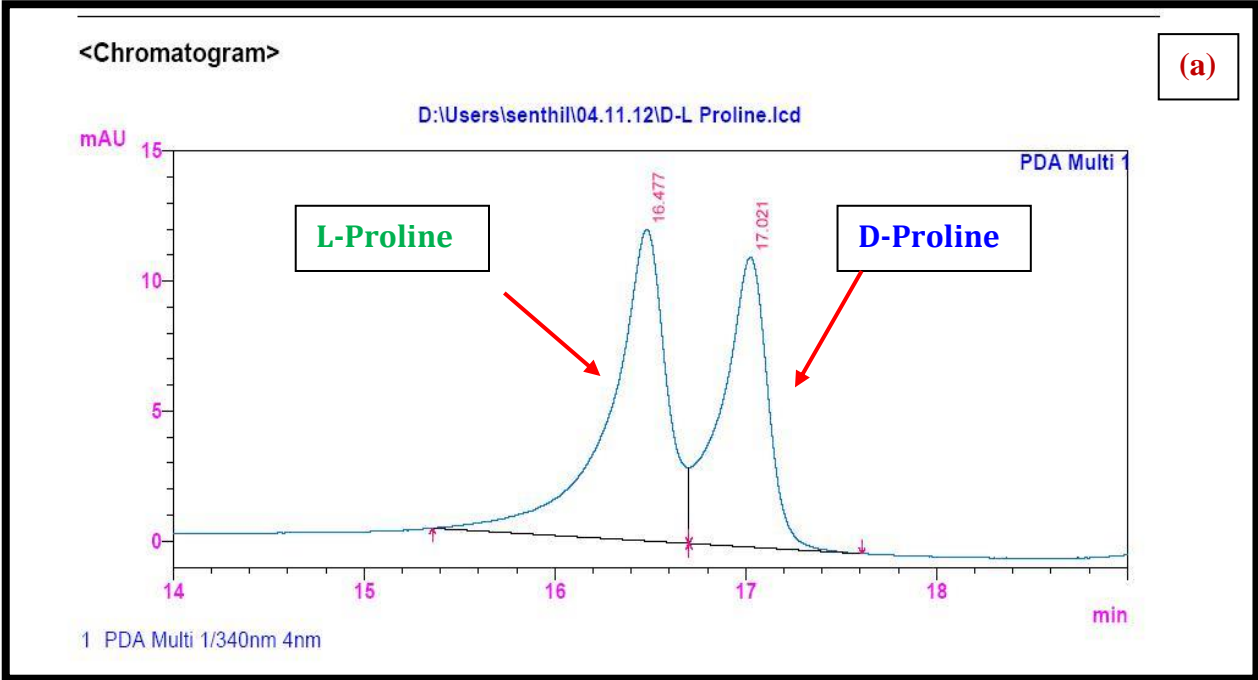


Figure S118 (b) HPLC analysis of standard L-FDAA-D-Proline

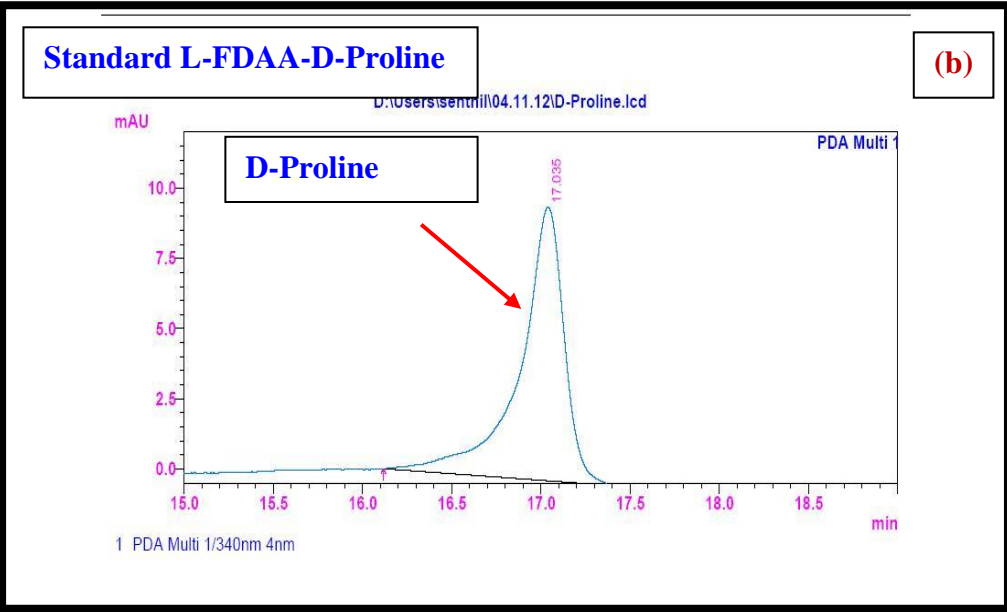


Figure S118c. HPLC analysis of standard L-FDAA-L-Proline

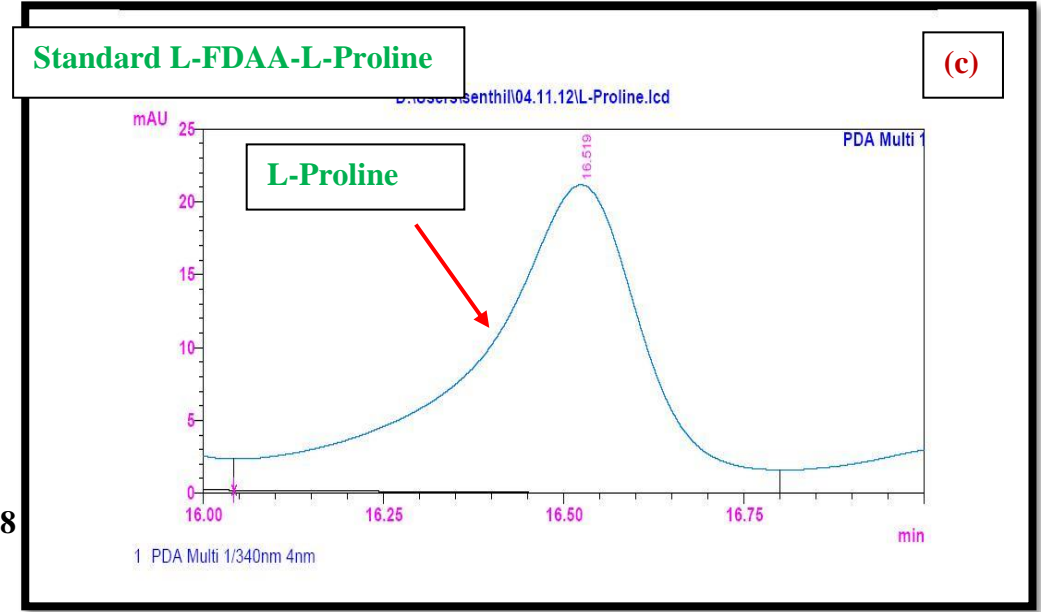


Figure S119a. HPLC analysis of standard L-FDAA-D/L-Threonine

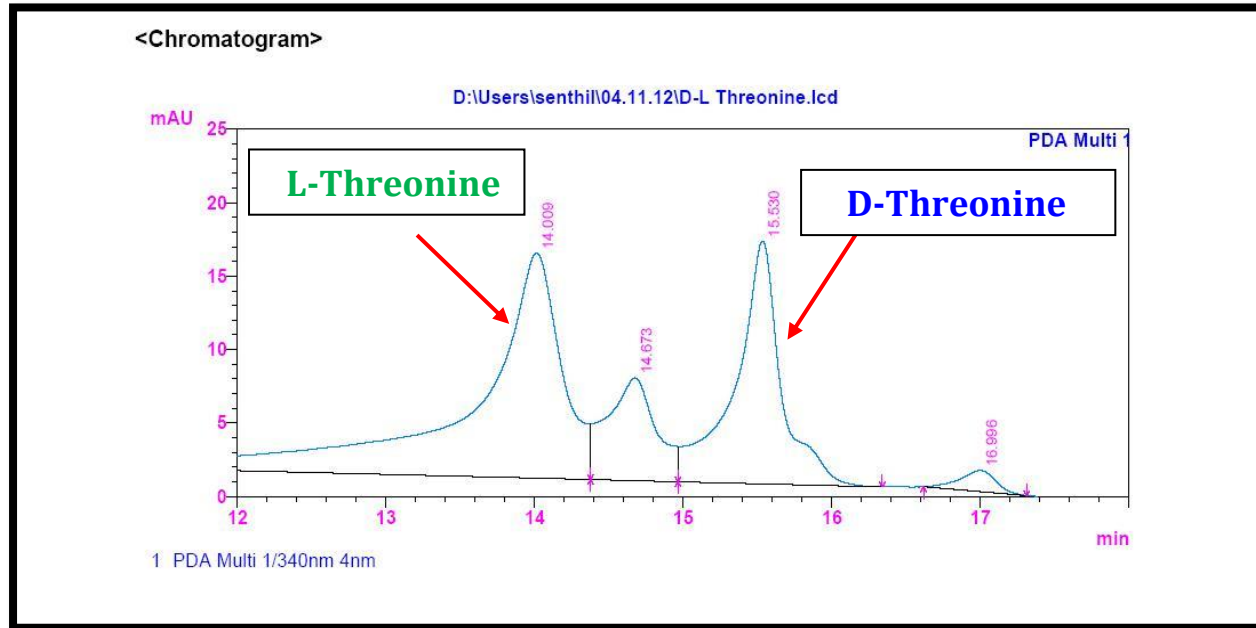


Figure S119b. HPLC analysis of standard L-FDAA-D-Threonine

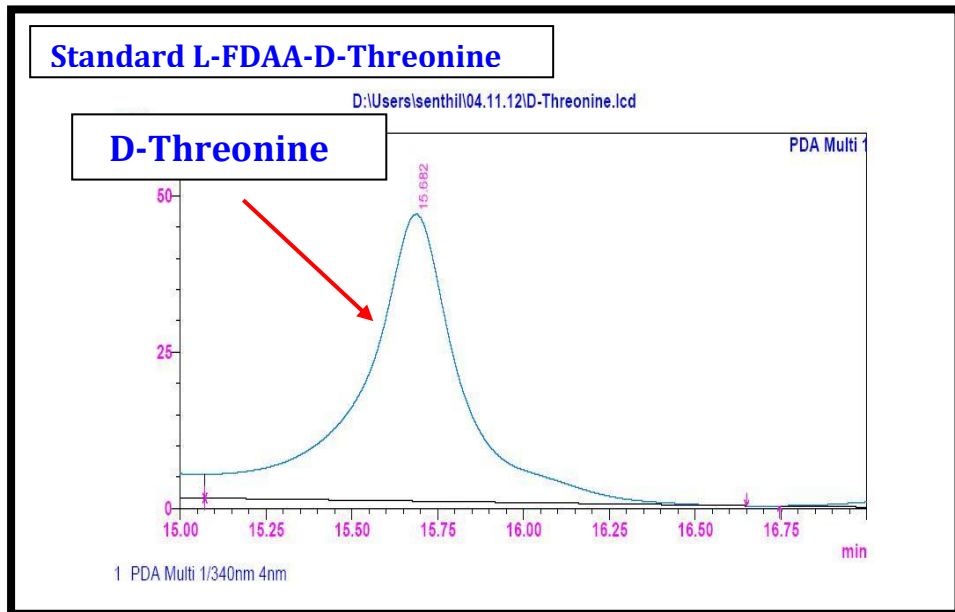


Figure S119c. HPLC analysis of standard L-FDAA-L-Threonine

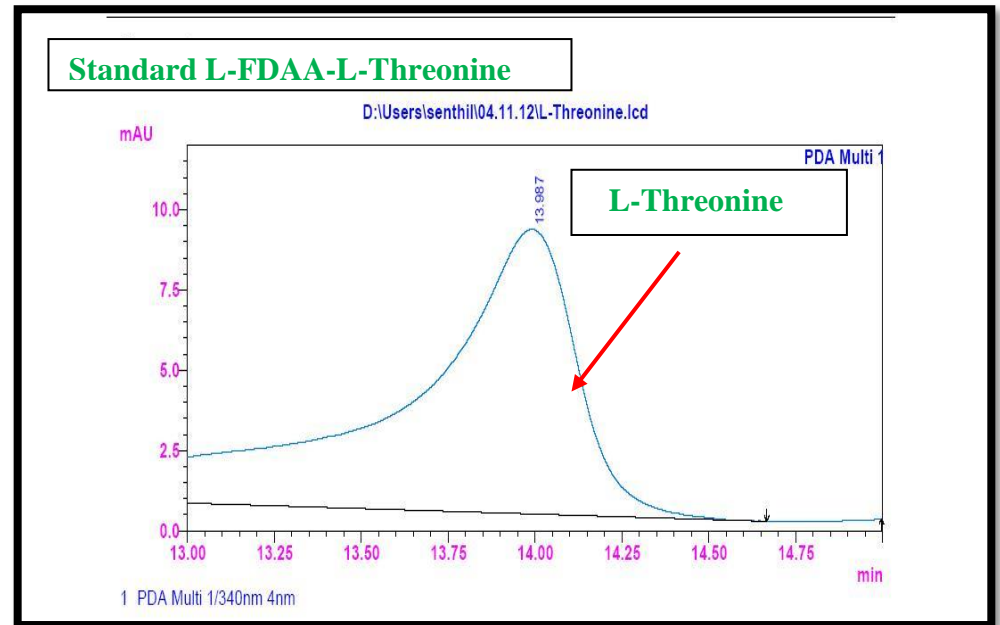


Figure S120a. HPLC analysis of standard L-FDAA-D/L-N-Methyl Valine

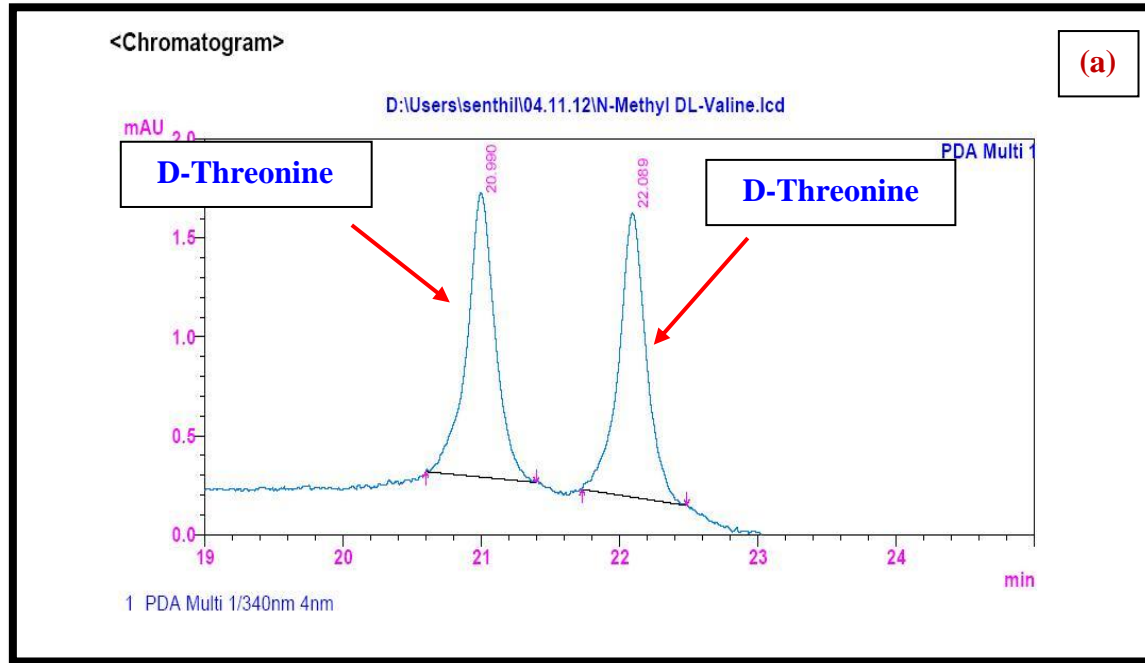


Figure S120b. HPLC analysis of standard L-FDAA-D-N-Methyl Valine

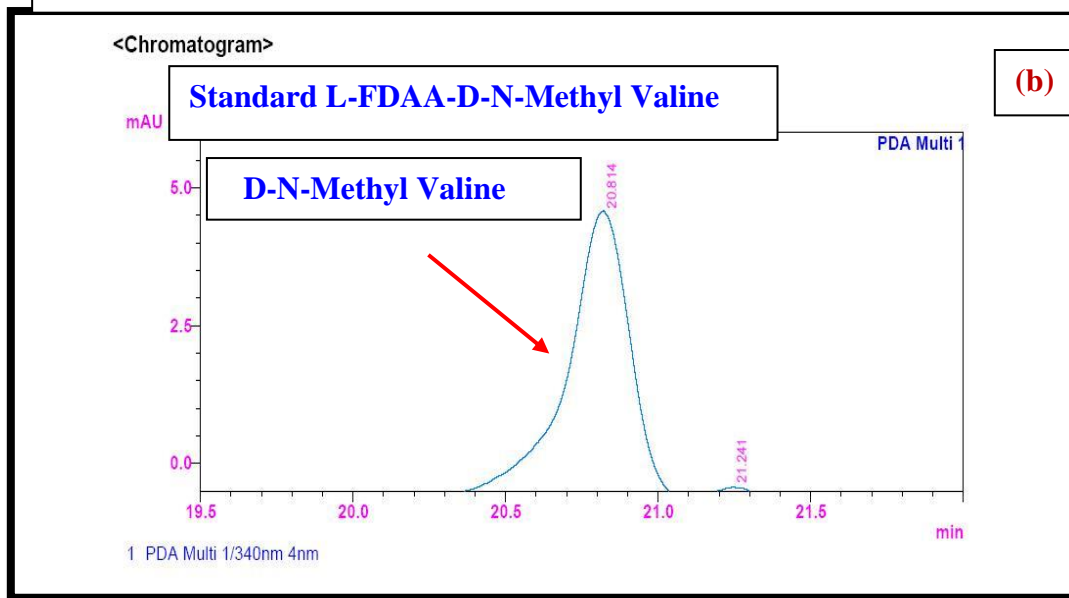


Figure S120c. HPLC analysis of standard L-FDAA-D-N-Methyl Valine

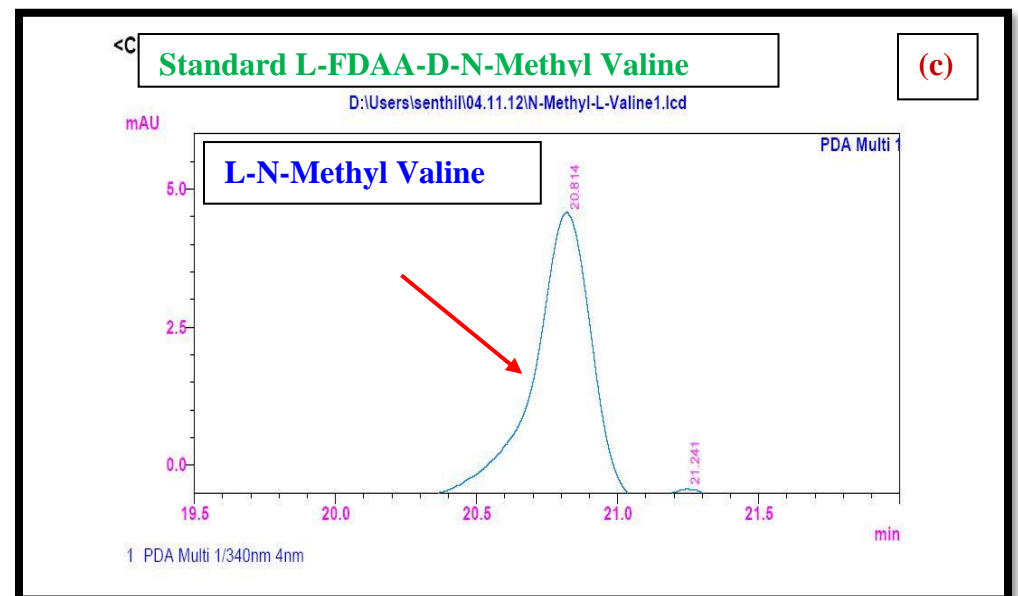


Figure S121a. HPLC analysis of standard L-FDAA-D-Valine

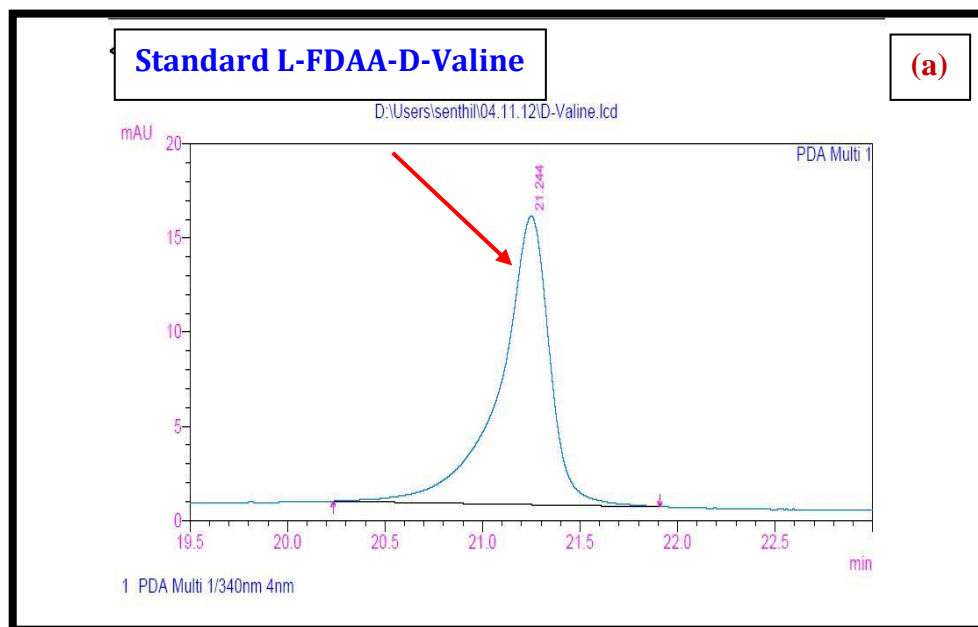


Figure S121b. HPLC analysis of standard L-FDAA-L-Valine

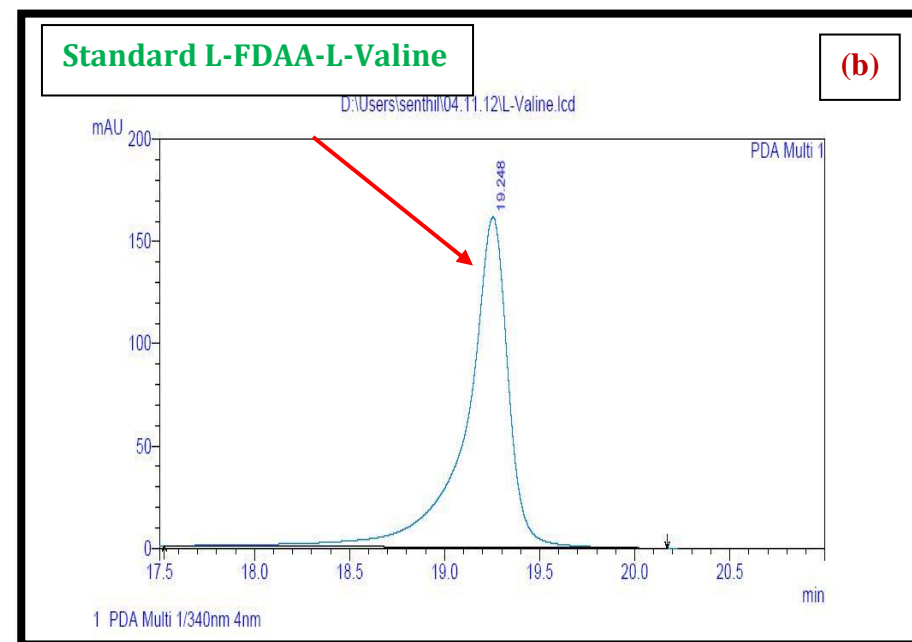


Figure S121c. HPLC Analysis of L-FDAA Derivatives of acid hydrolysates of Transimycin (R1)

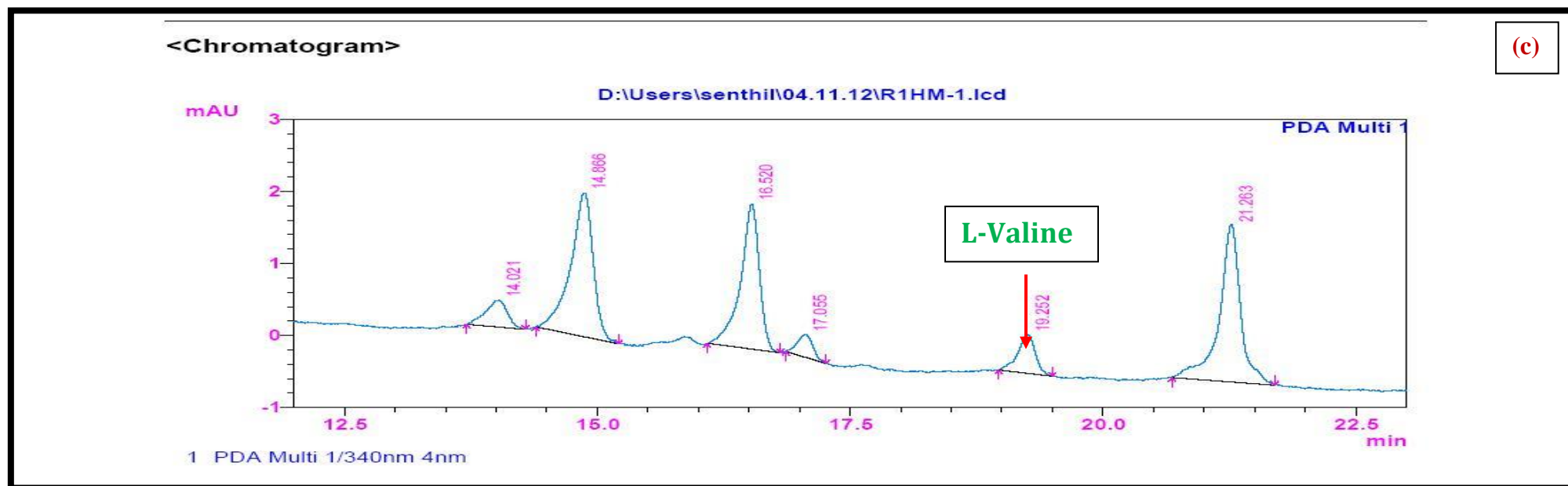


Figure 122a. HPLC analysis of standard L-FDAA-D-Valine

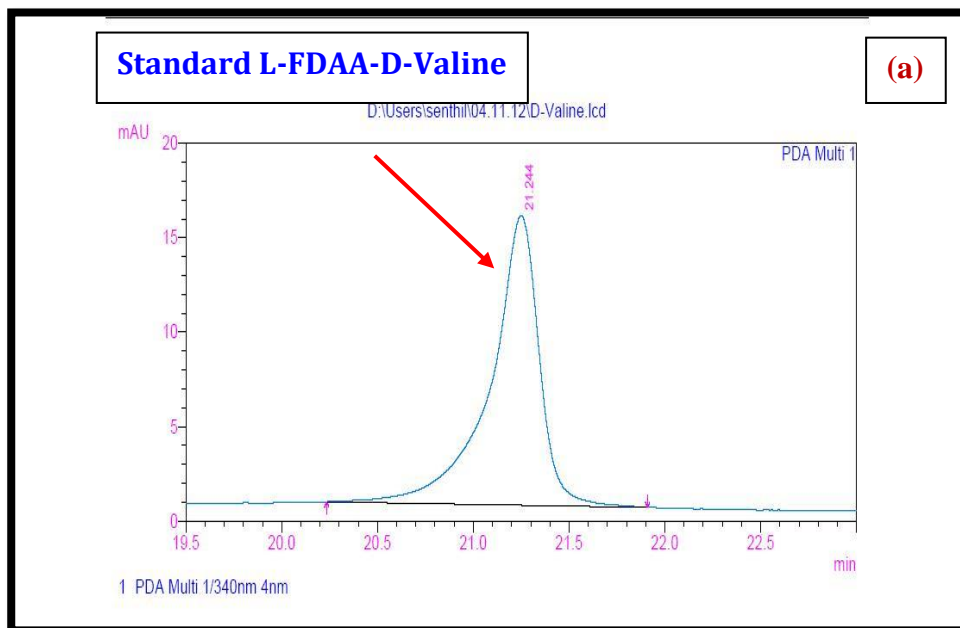


Figure S122b. HPLC analysis of standard L-FDAA-L-Valine

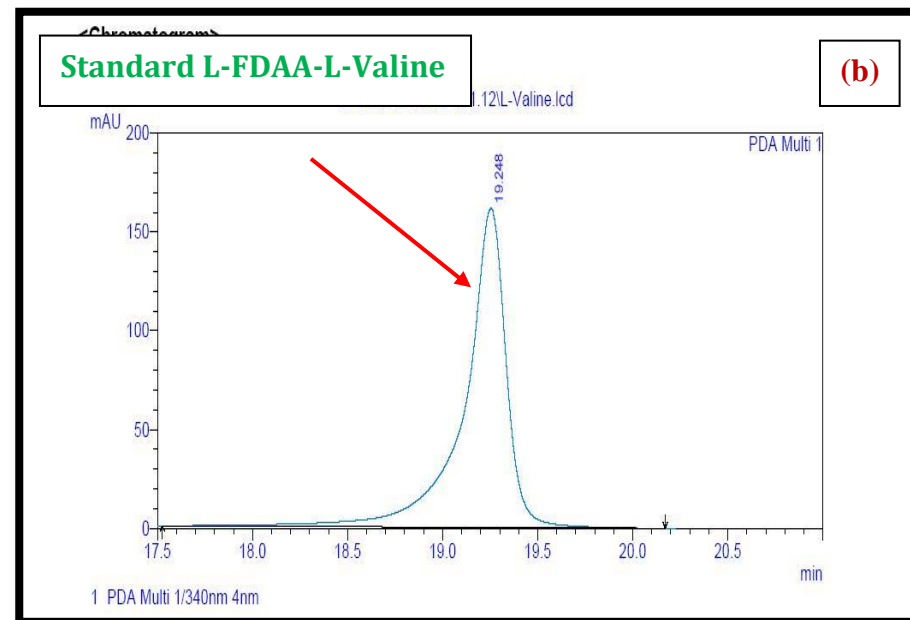


Figure S122c. HPLC Analysis of L-FDAA Derivatives of acid hydrolysates of R2

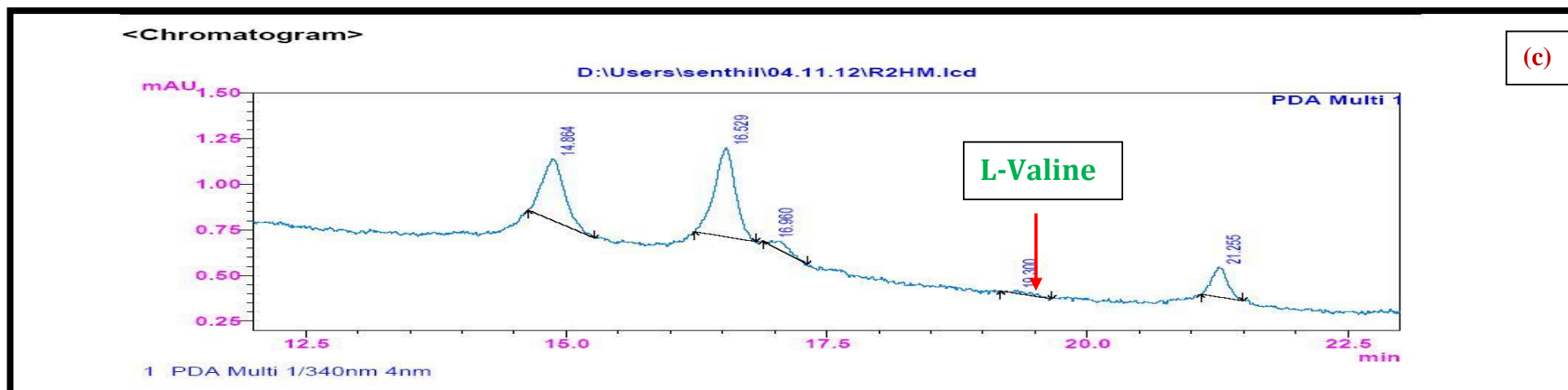


Figure S123a. HPLC analysis of standard L-FDAA-D-Valine

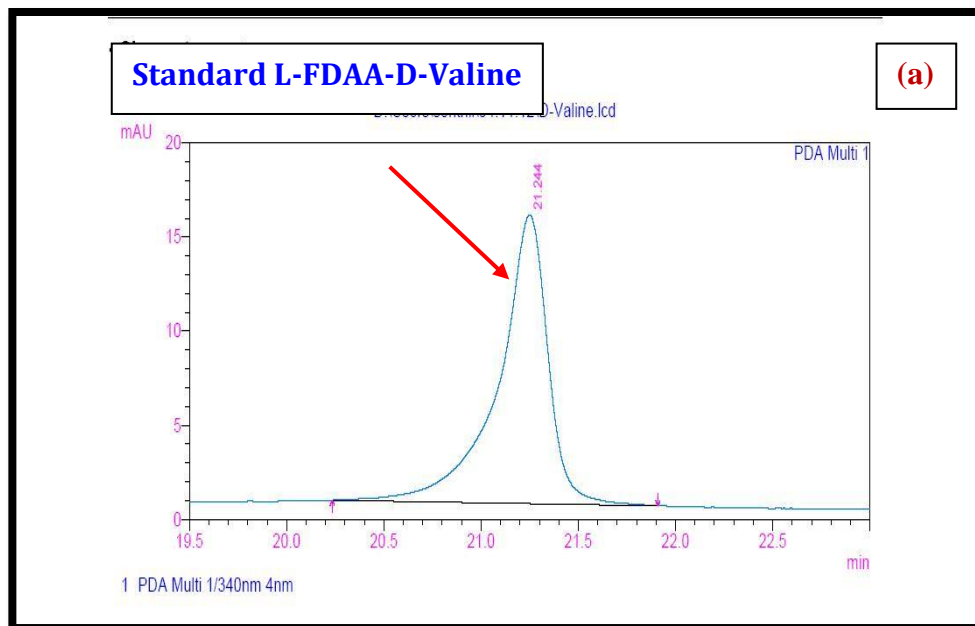


Figure S123b. HPLC analysis of standard L-FDAA-L-Valine

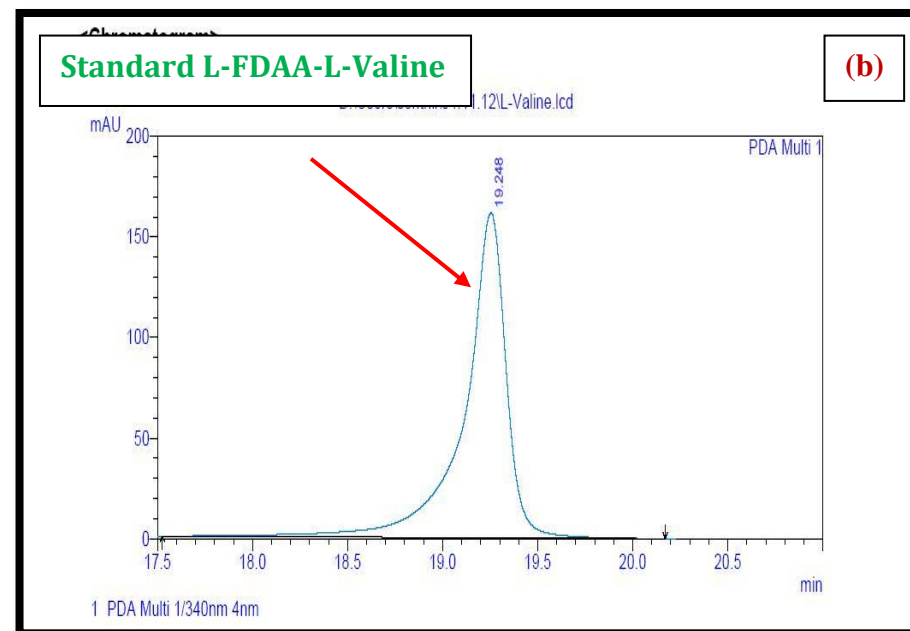


Figure S123c. HPLC Analysis of L-FDAA Derivatives of acid hydrolysates of R3

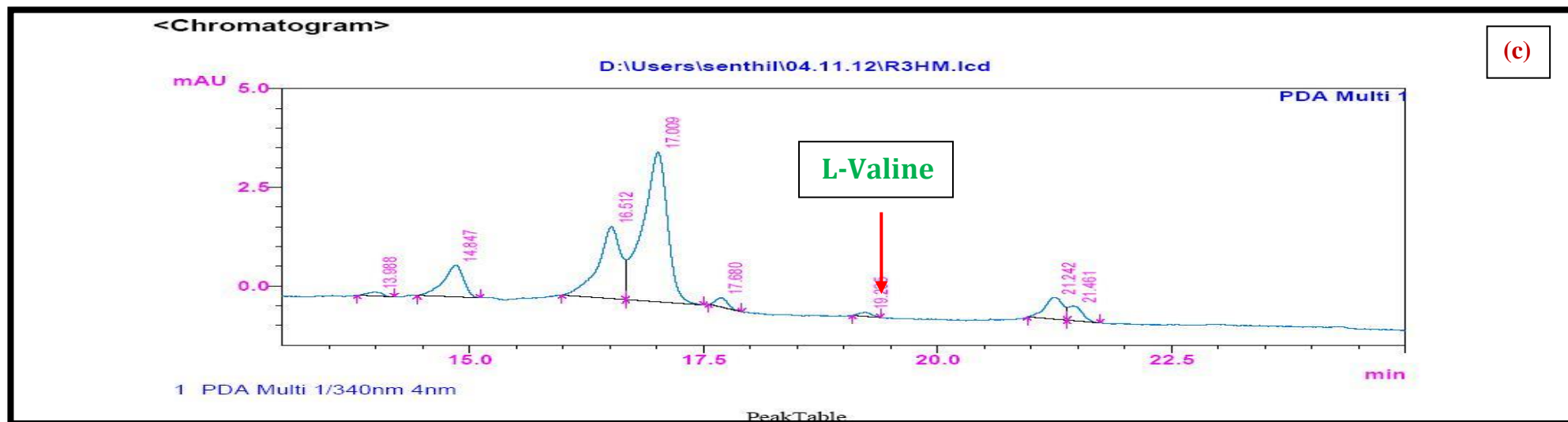


Figure S124. HPLC Analysis of L-FDAA Derivatives of acid hydrolysates of (R2)

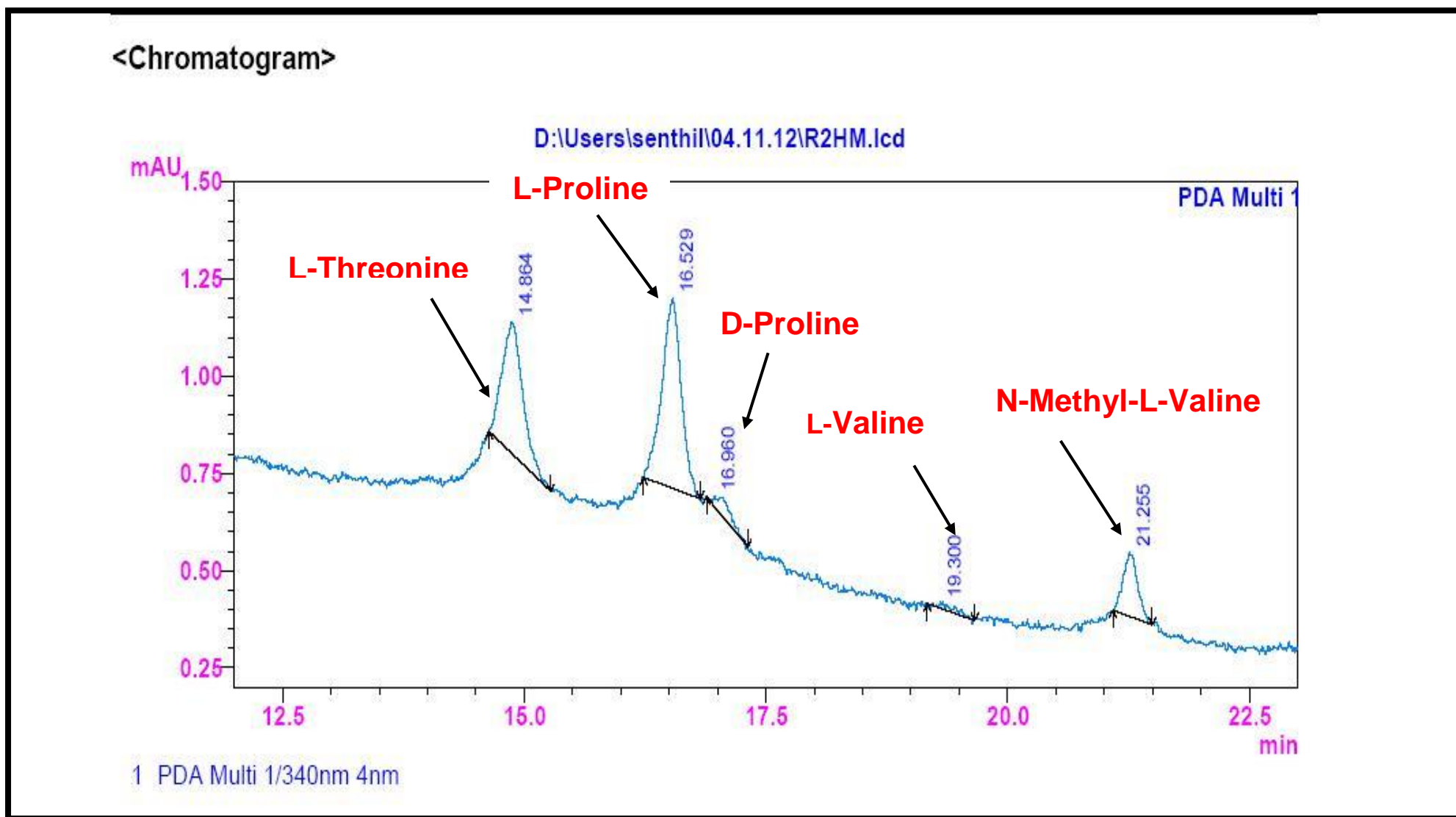


Figure S125. HPLC Analysis of L-FDAA Derivatives of acid hydrolysates of R3

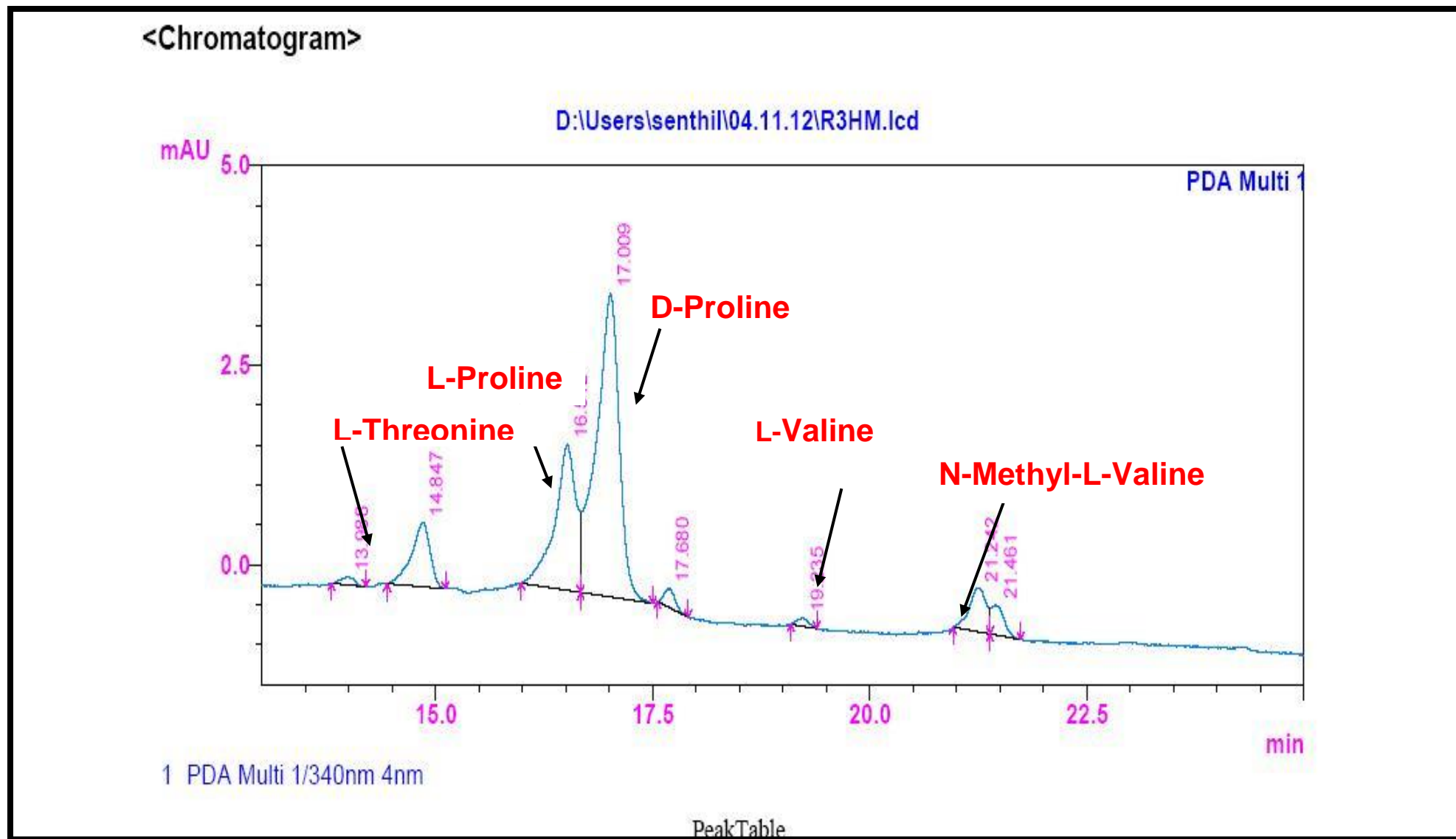


Table 8a. Analysis of L-FDAA derivates of acid hydrolysate of R2 by HPLC

Amino acids	HPLC retention times Marfey's derivatives of standard amino acids		HPLC retention time Marfey derivatives of acid hydrolysate of Transitmycin R2	Assignment
	D	L		
Threonine	15.682	13.987	14.000	L
Proline	17.035	16.519	16.529 & 16.960	D & L
Valine	21.244	19.248	19.300	L
N-methyl valine	22.089	20.814	21.255	L

Table 8b. Analysis of L-FDAA derivatives of acid hydrolysate of R3 by HPLC

Amino acids	HPLC retention times Marfey's derivatives of standard amino acids		HPLC retention time Marfeyderivatives of acid hydrolysate of Transitmycin R3	Assignment
	D	L		
Threonine	15.682	13.987	13.988	L
Proline	17.035	16.519	16.512 & 17.000	D & L
Valine	21.244	19.248	19.235	L
N-methyl valine	22.089	20.814	21.242	L

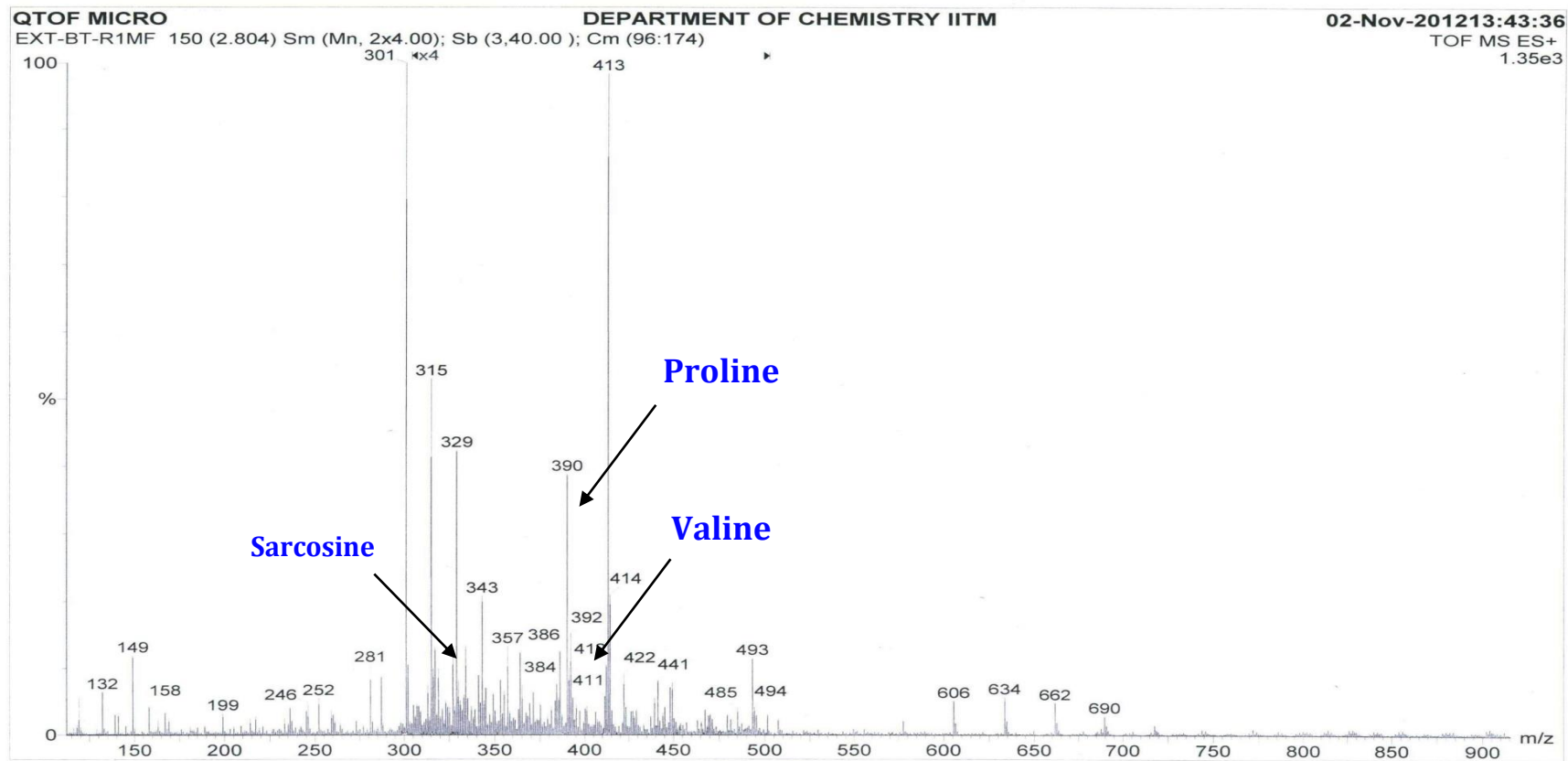


Figure S126. ESI- MS Spectrum of Marfey's Derivatives of Transitmycin (R1) (Positive mode)

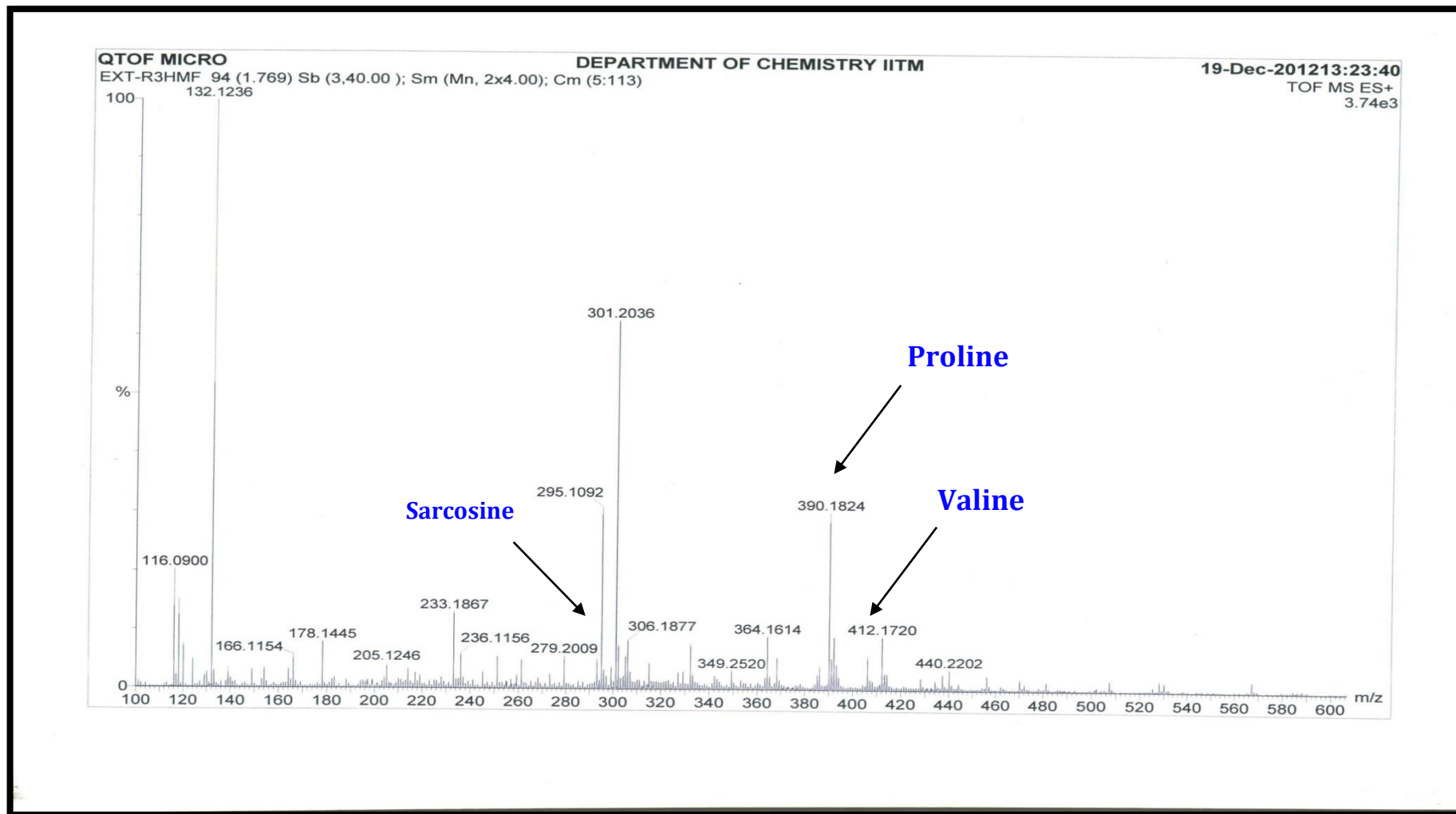


Figure S127. ESI- MS Spectrum of Marfey's Derivatives of Transitmycin (R1) (Positive mode)

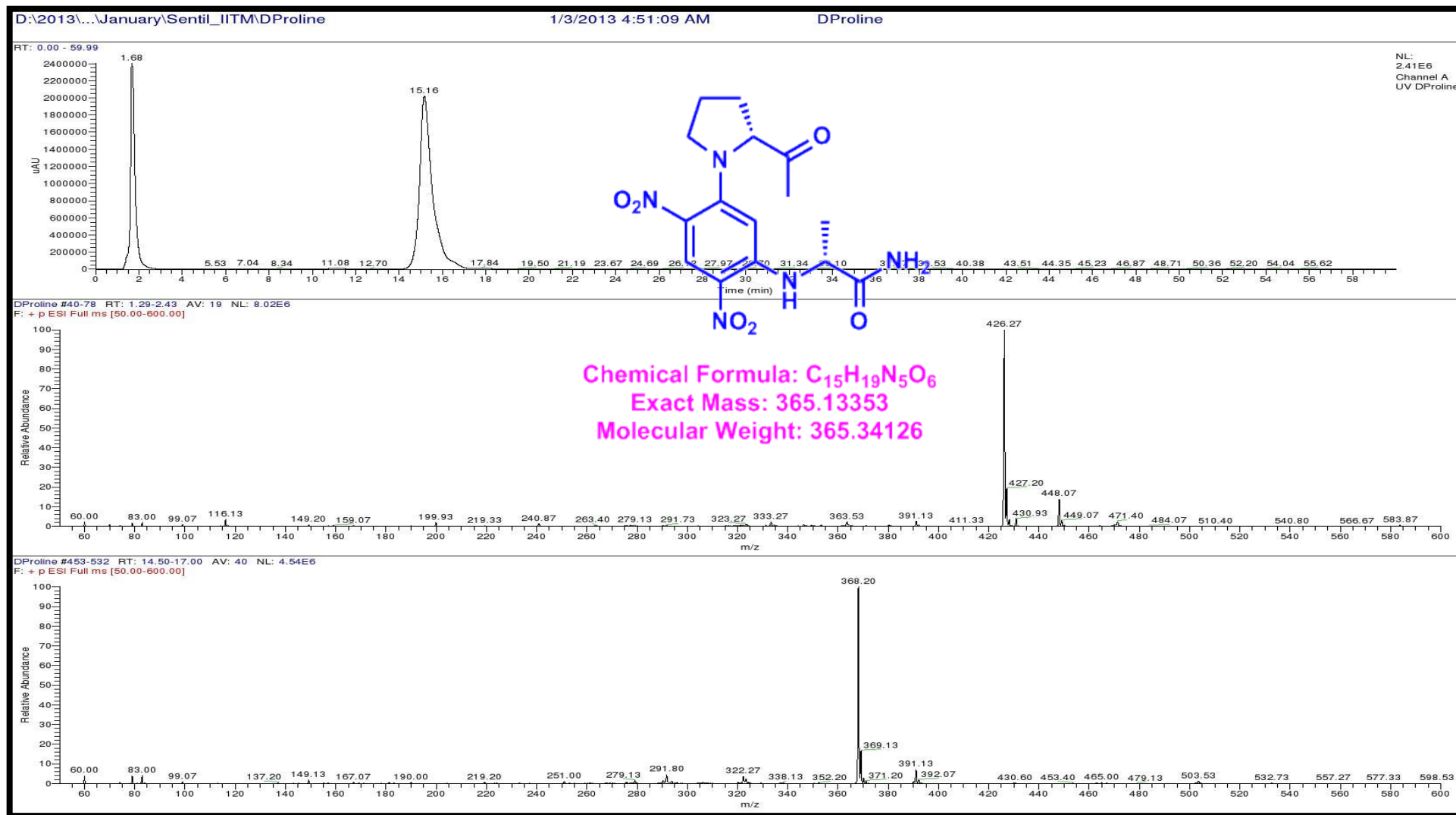


Figure S128. LCMS analysis of Standard L-FDAA-D-Proline (Positive mode)

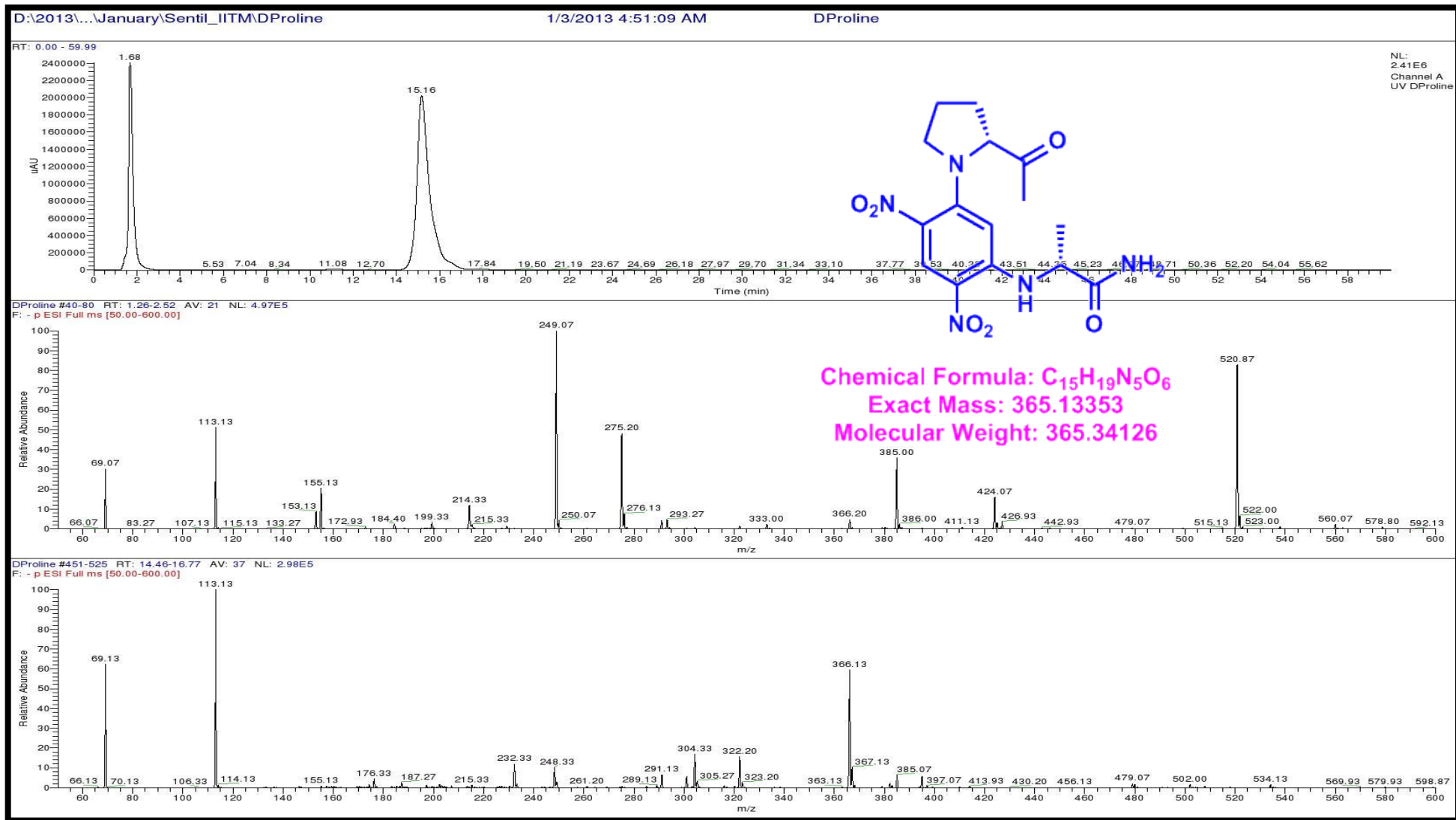


Figure S129. LCMS analysis of Standard L-FDAA-D-Proline (Negative mode)

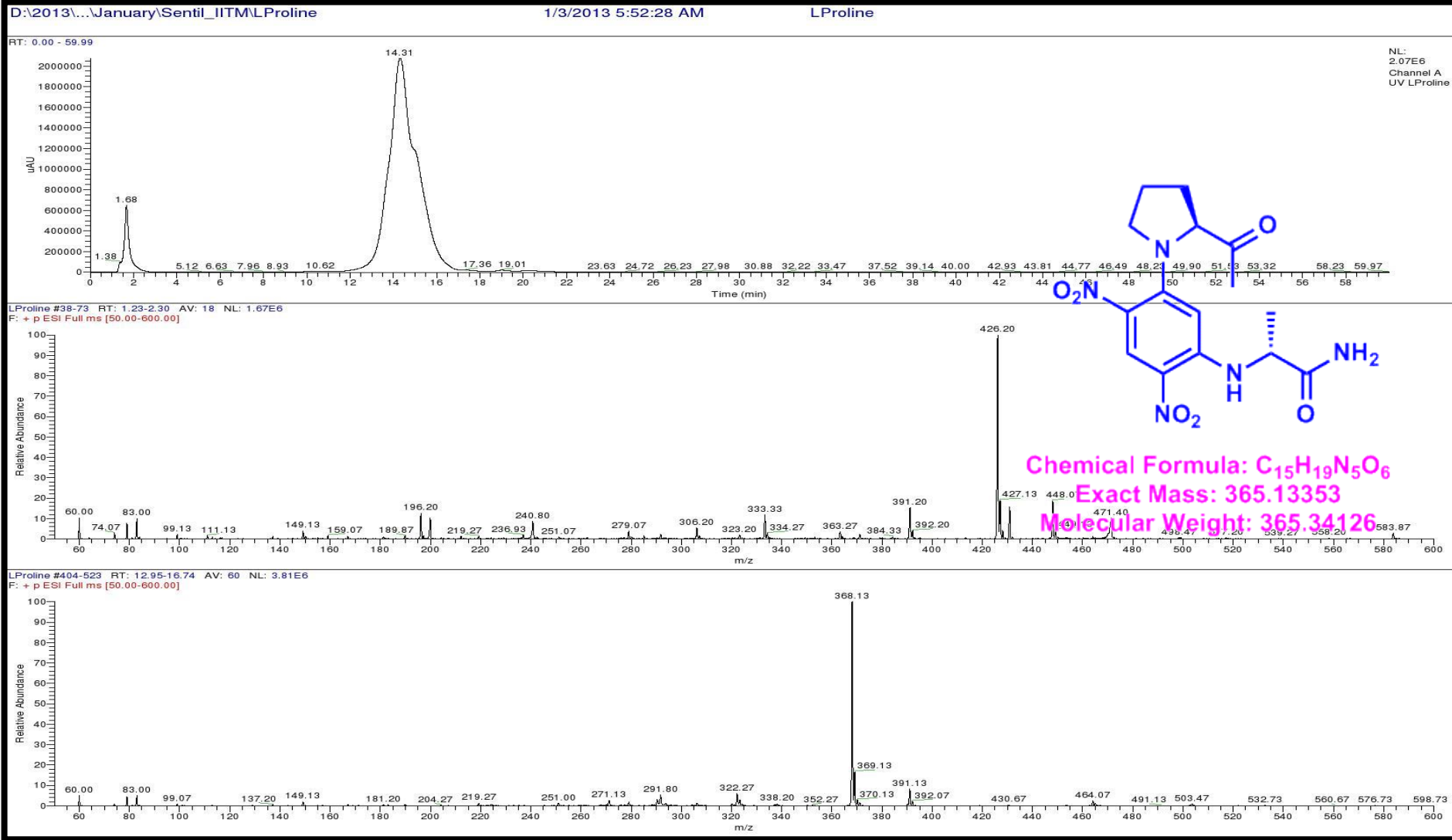


Figure S130 LCMS analysis of Standard L-FDAA-L-Proline (Positive mode)

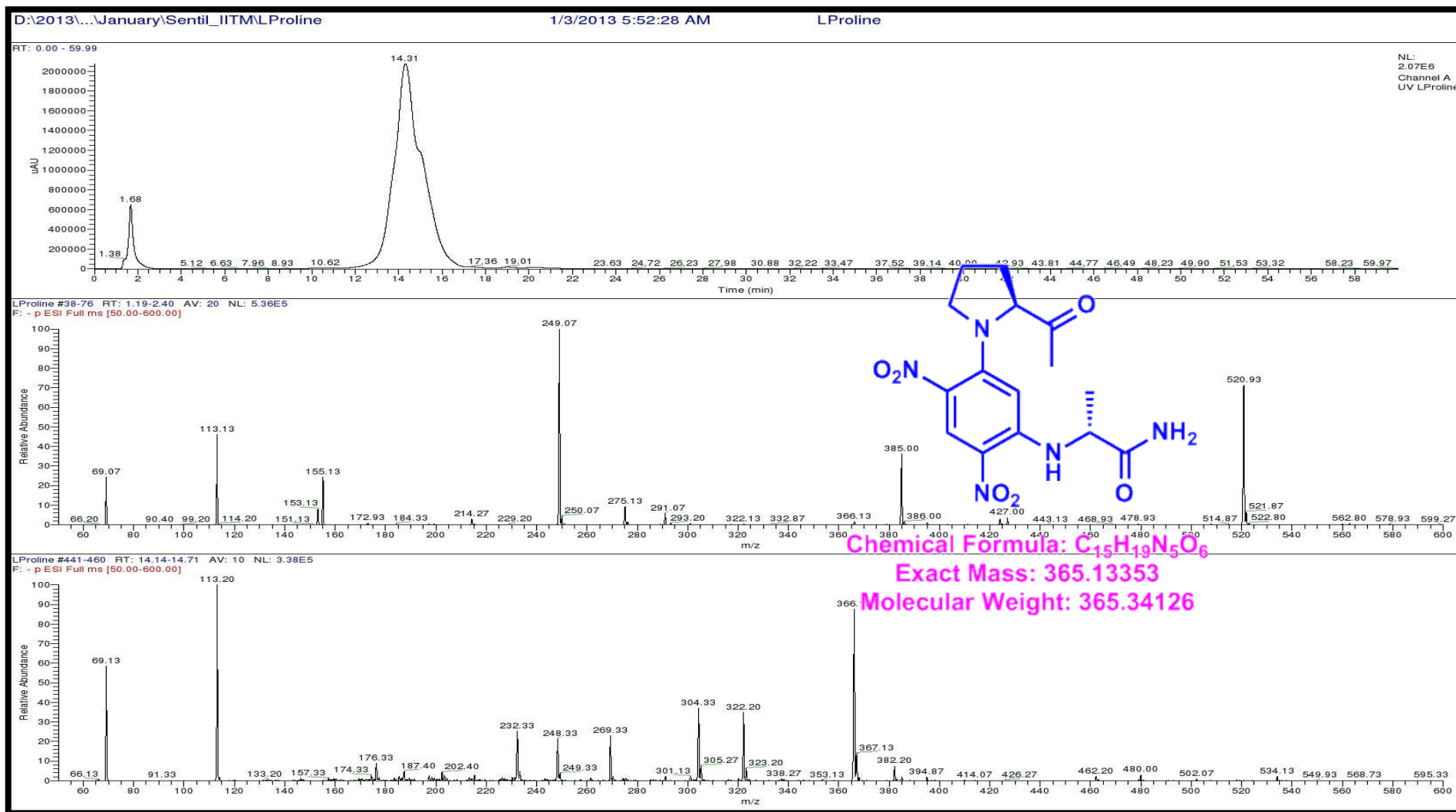


Figure S131. LCMS analysis of Standard L-FDAA-L-Proline (Negative mode)

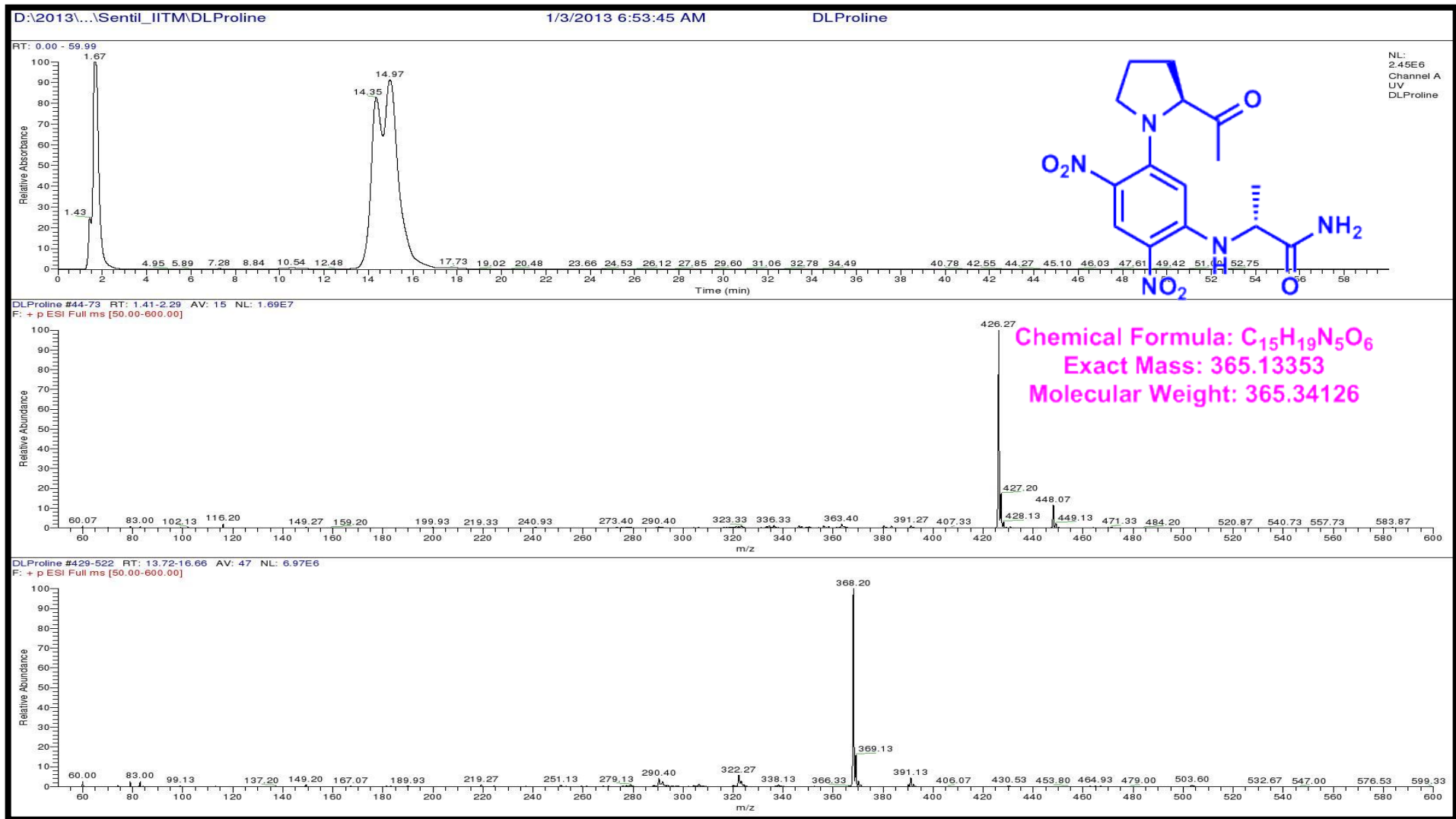


Figure S132. LCMS analysis of Standard L-FDAA-D/L-Proline (Positive mode)

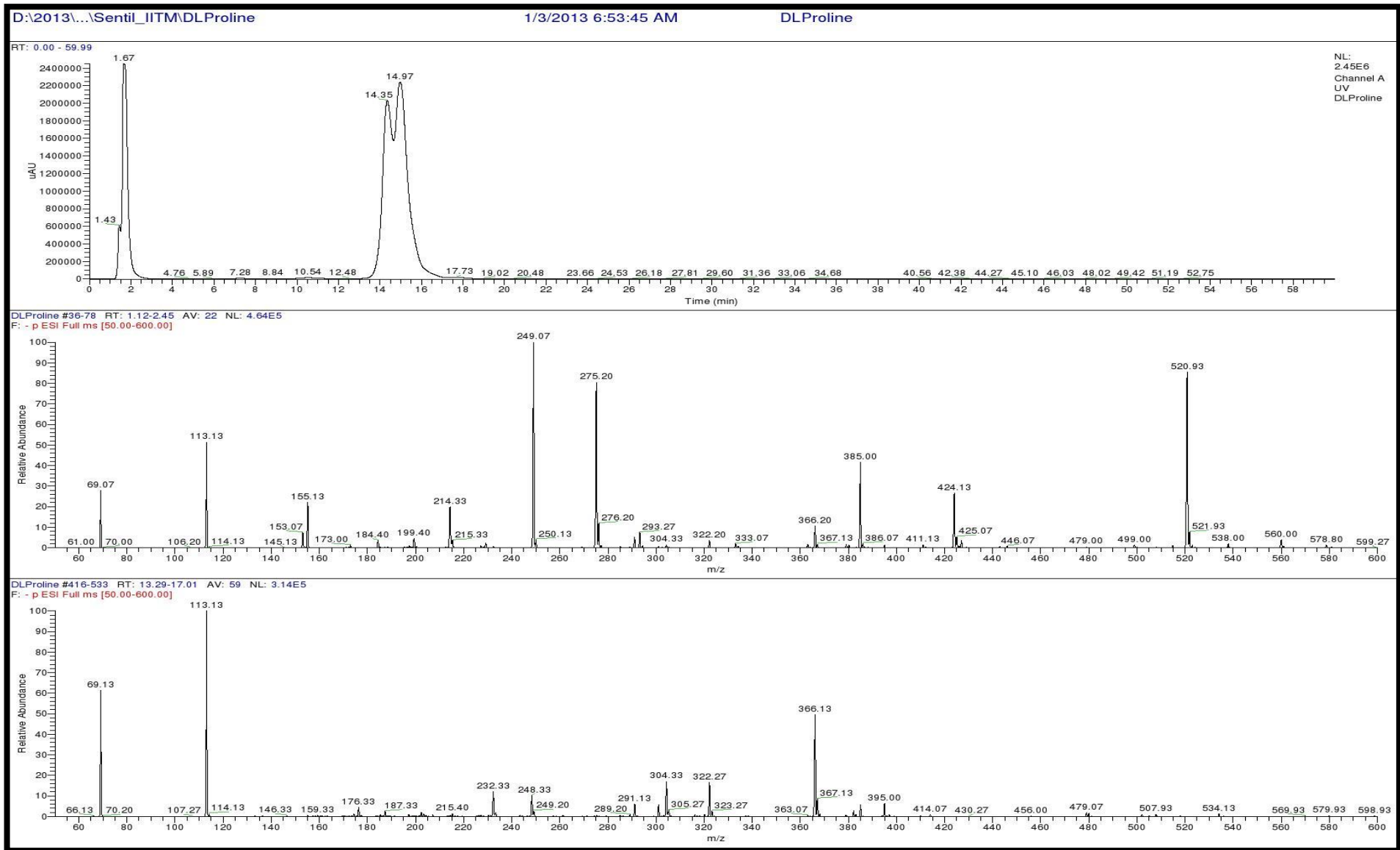


Figure S133. LCMS analysis of Standard L-FDAA-D/L-Proline (Negative mode)

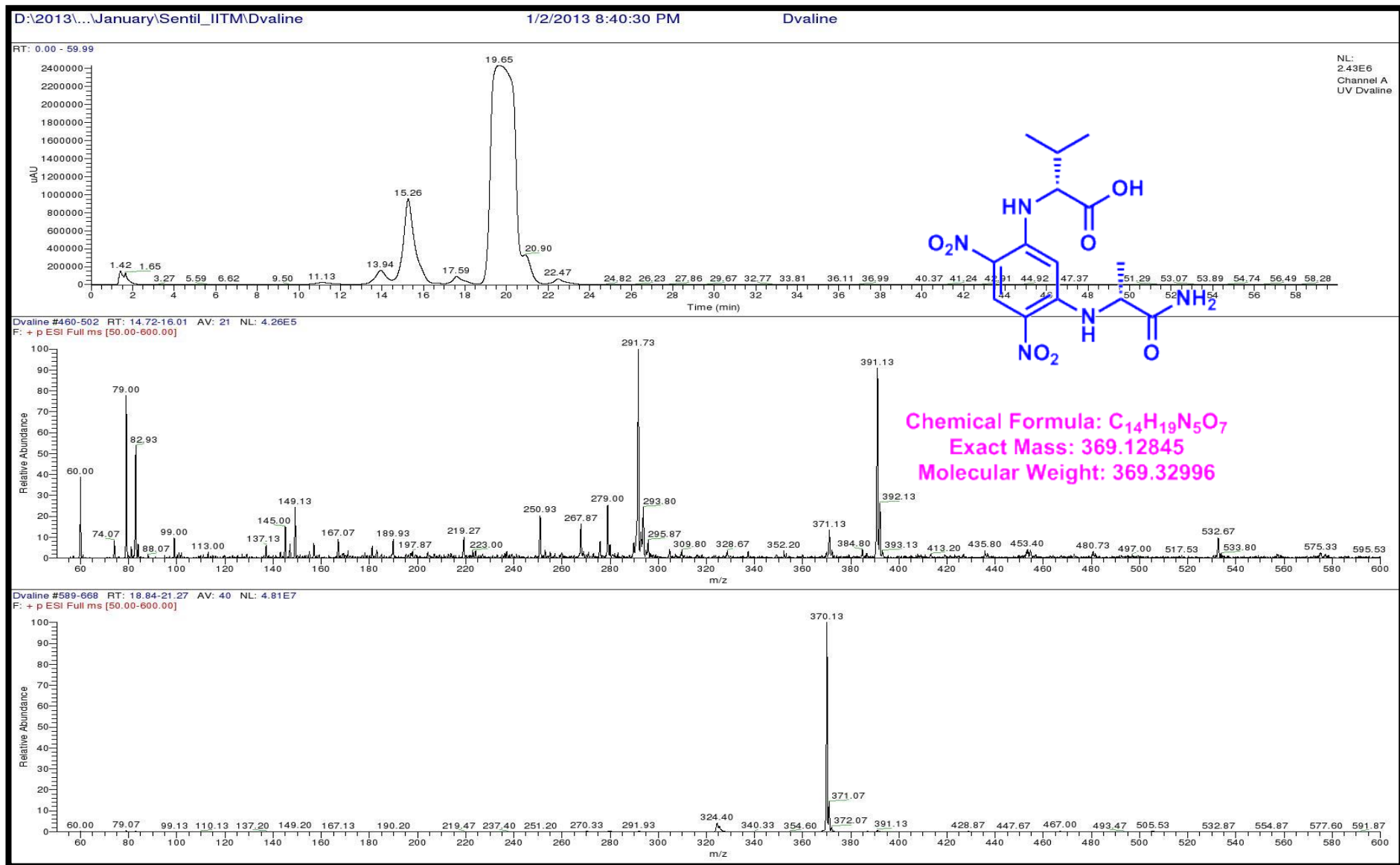


Figure S134.. LCMS analysis of Standard L-FDAA-D-Valine (Positive mode)

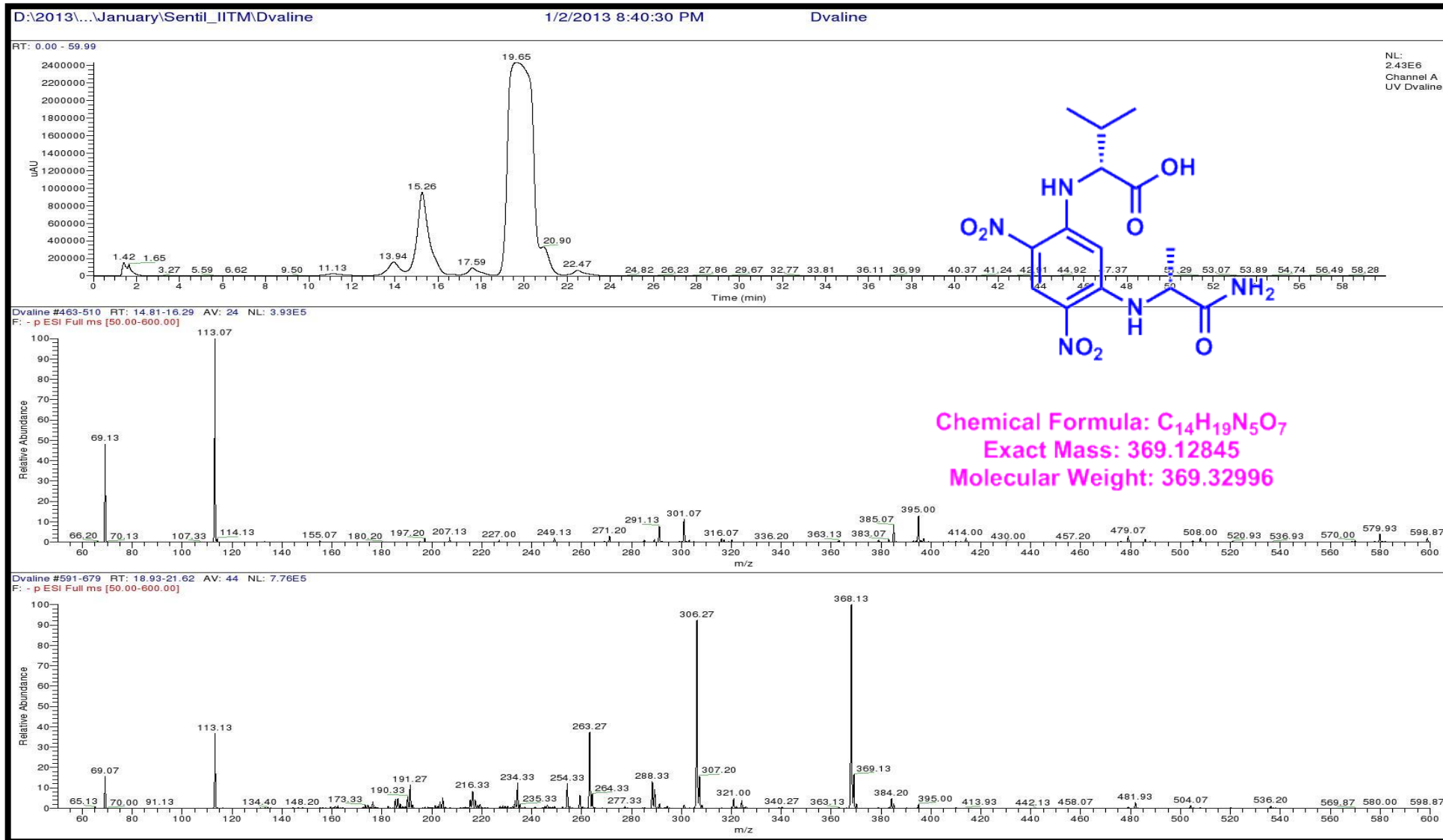


Figure S135. LCMS analysis of Standard L-FDAA-D-Valine (Negative mode)

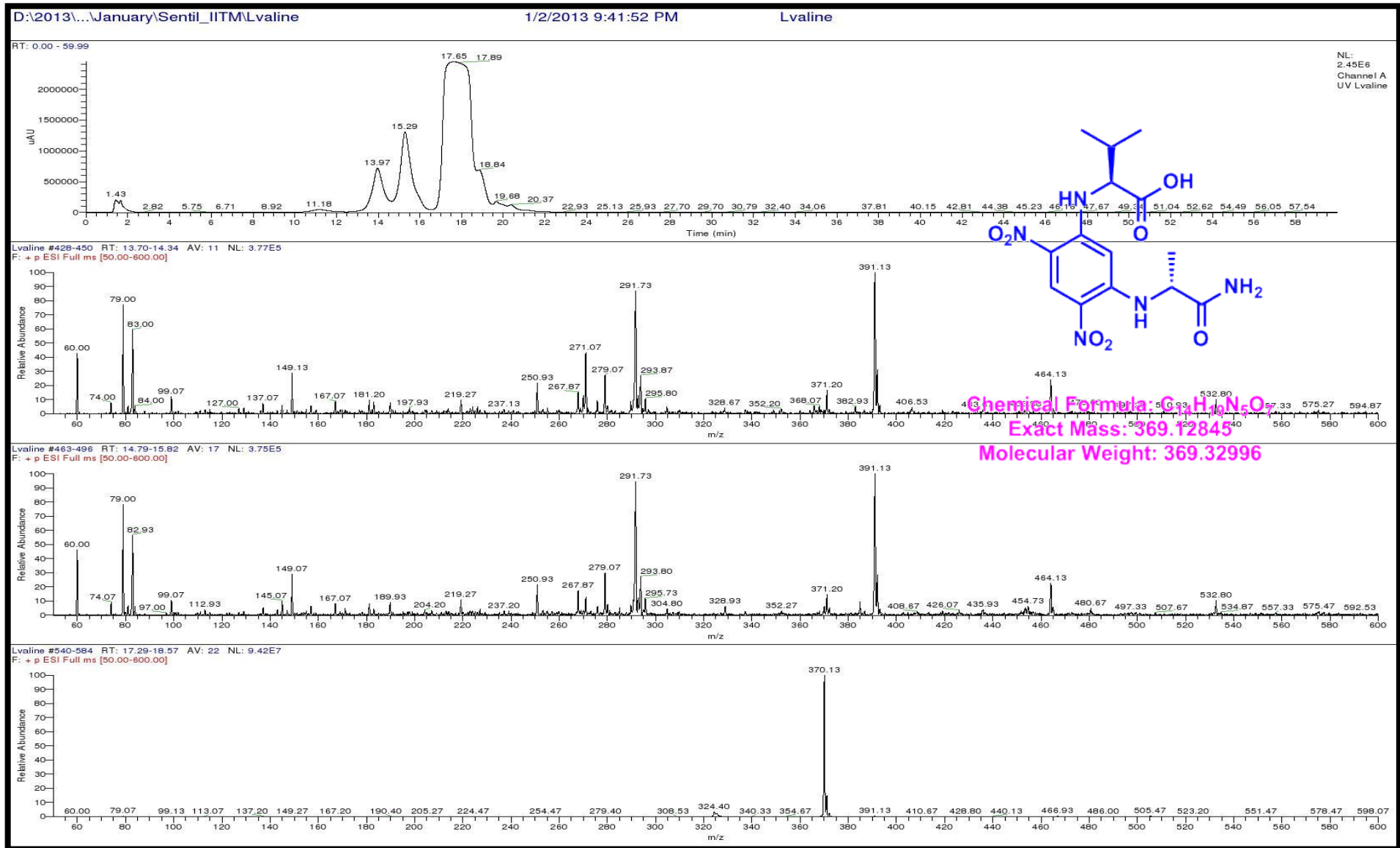


Figure S136. LCMS analysis of Standard L-FDAA-L-Valine (Positive mode)

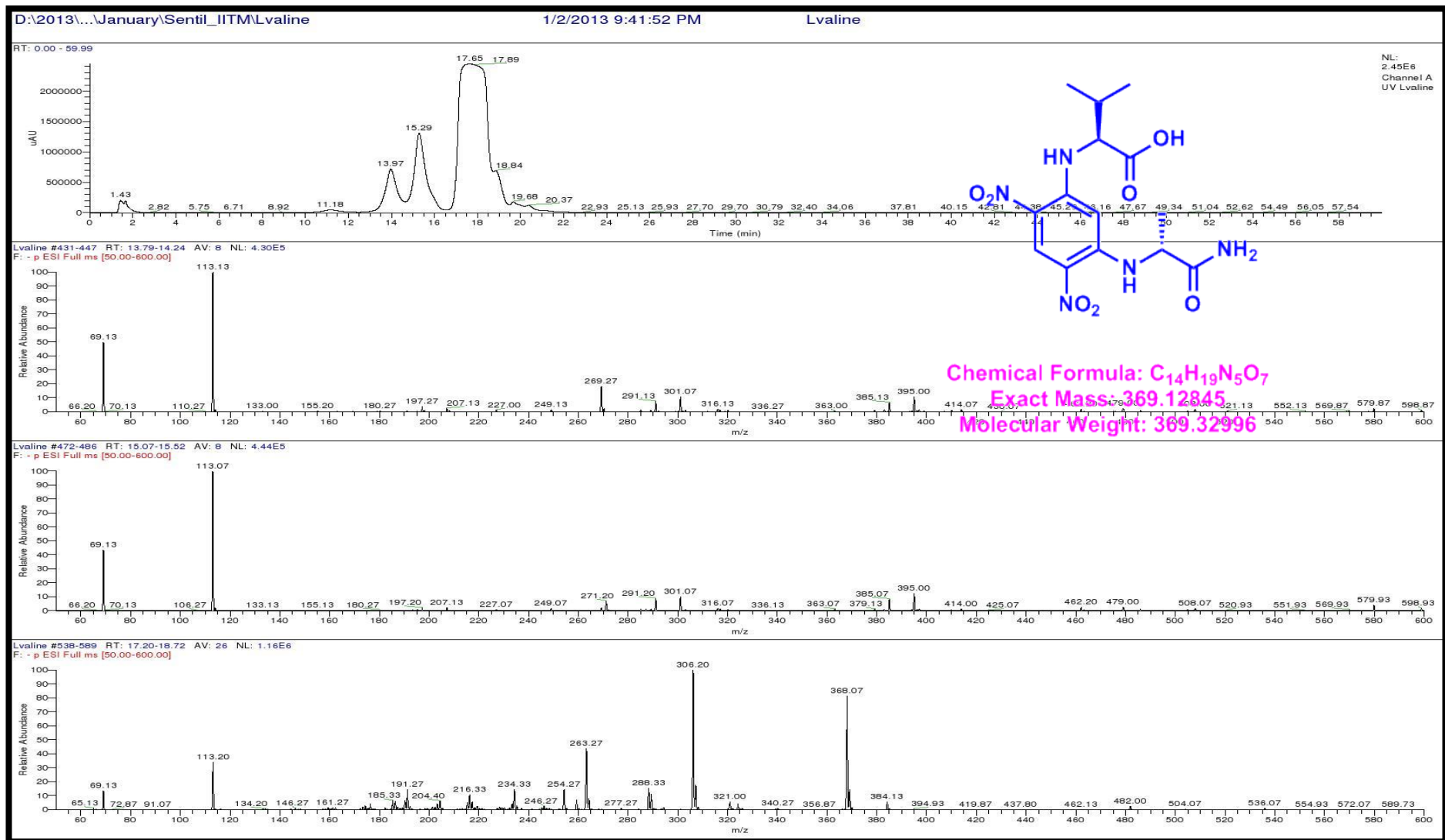


Figure S137. LCMS analysis of Standard L-FDAA-L-Valine (Negative mode)

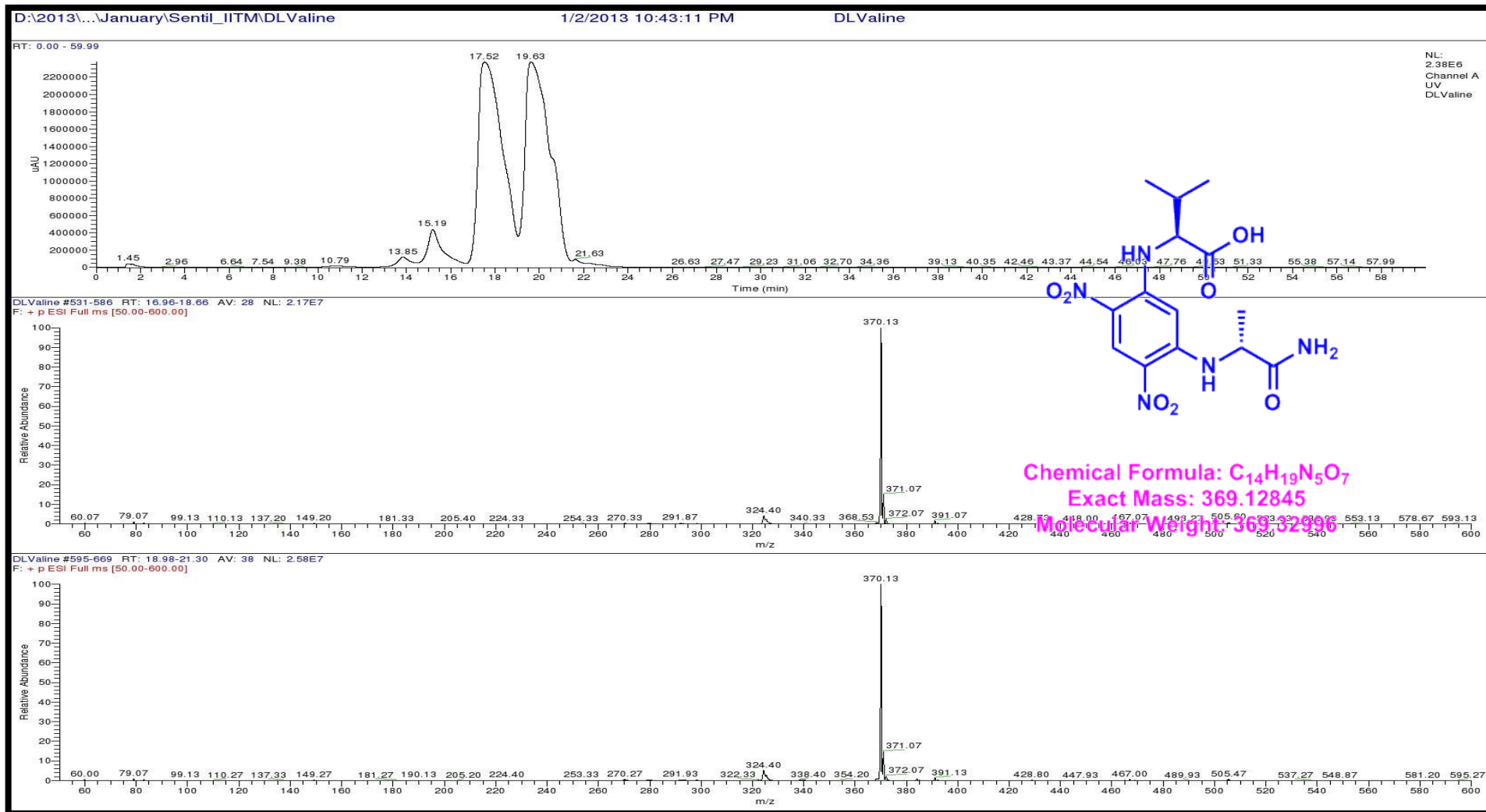


Figure S138. LCMS analysis of Standard L-FDAA-D/L-Valine (Positive mode)

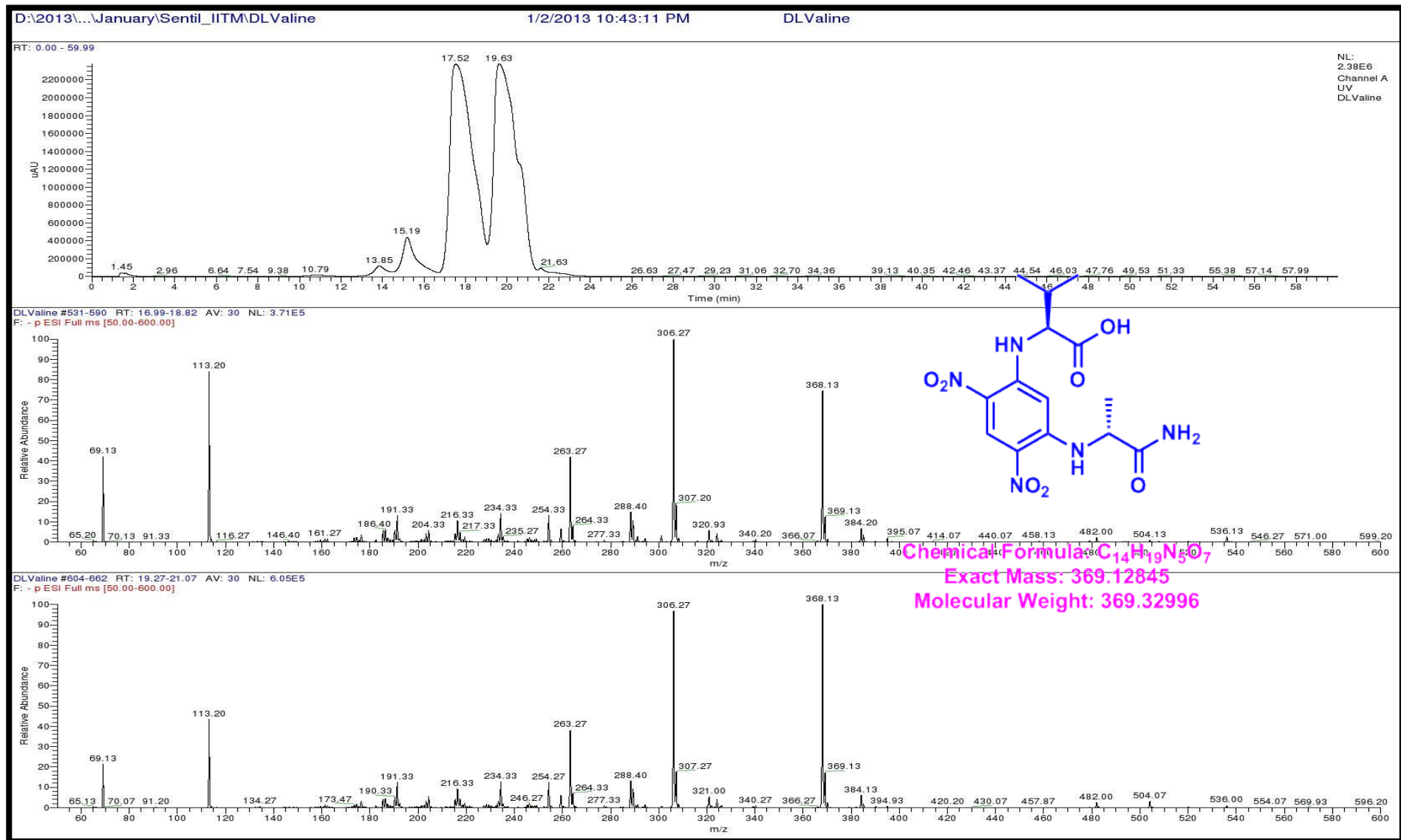


Figure S139. LCMS analysis of Standard L-FDAA-D/L-Valine (Negative mode)

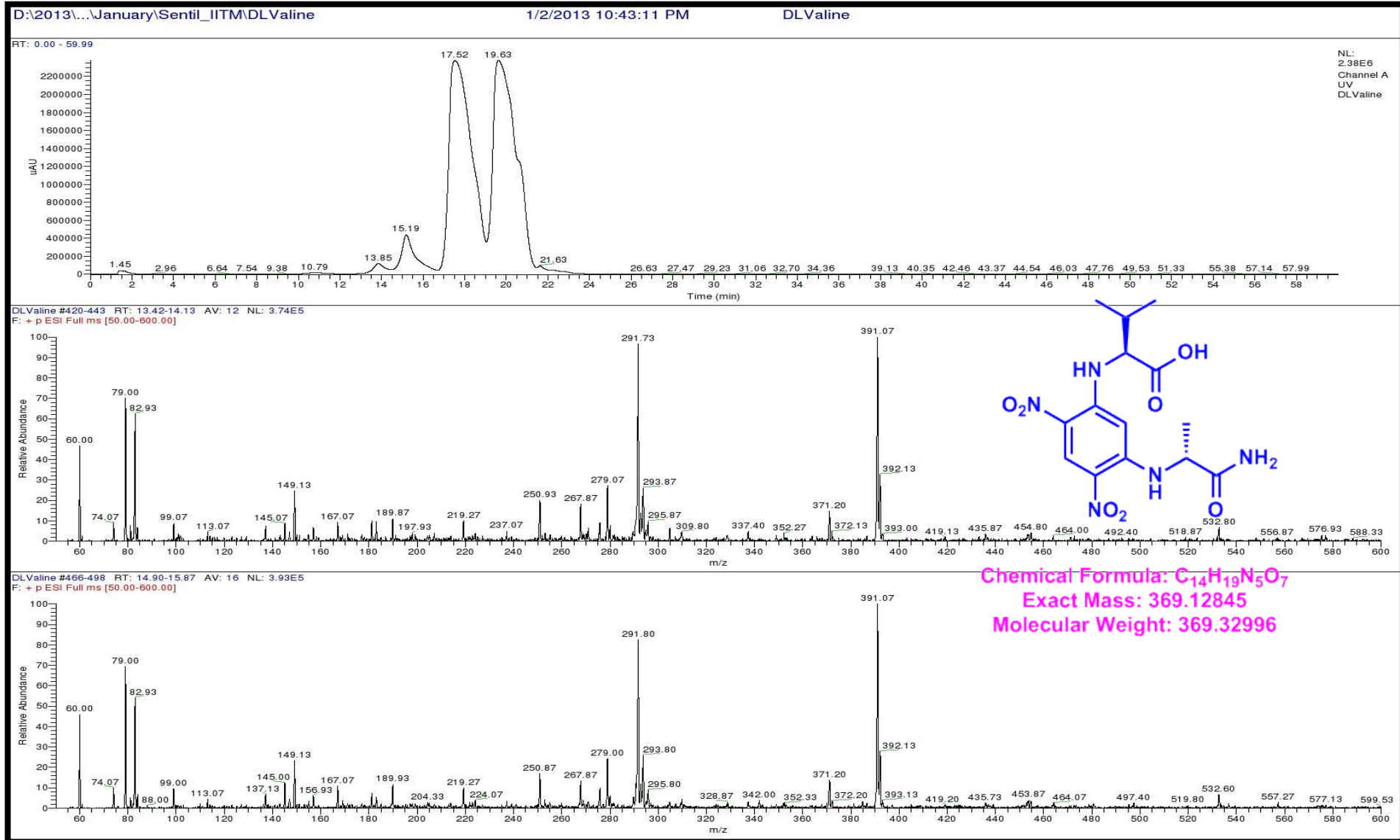


Figure S140. LCMS analysis of Standard L-FDAA-D/L-Valine (Positive mode)

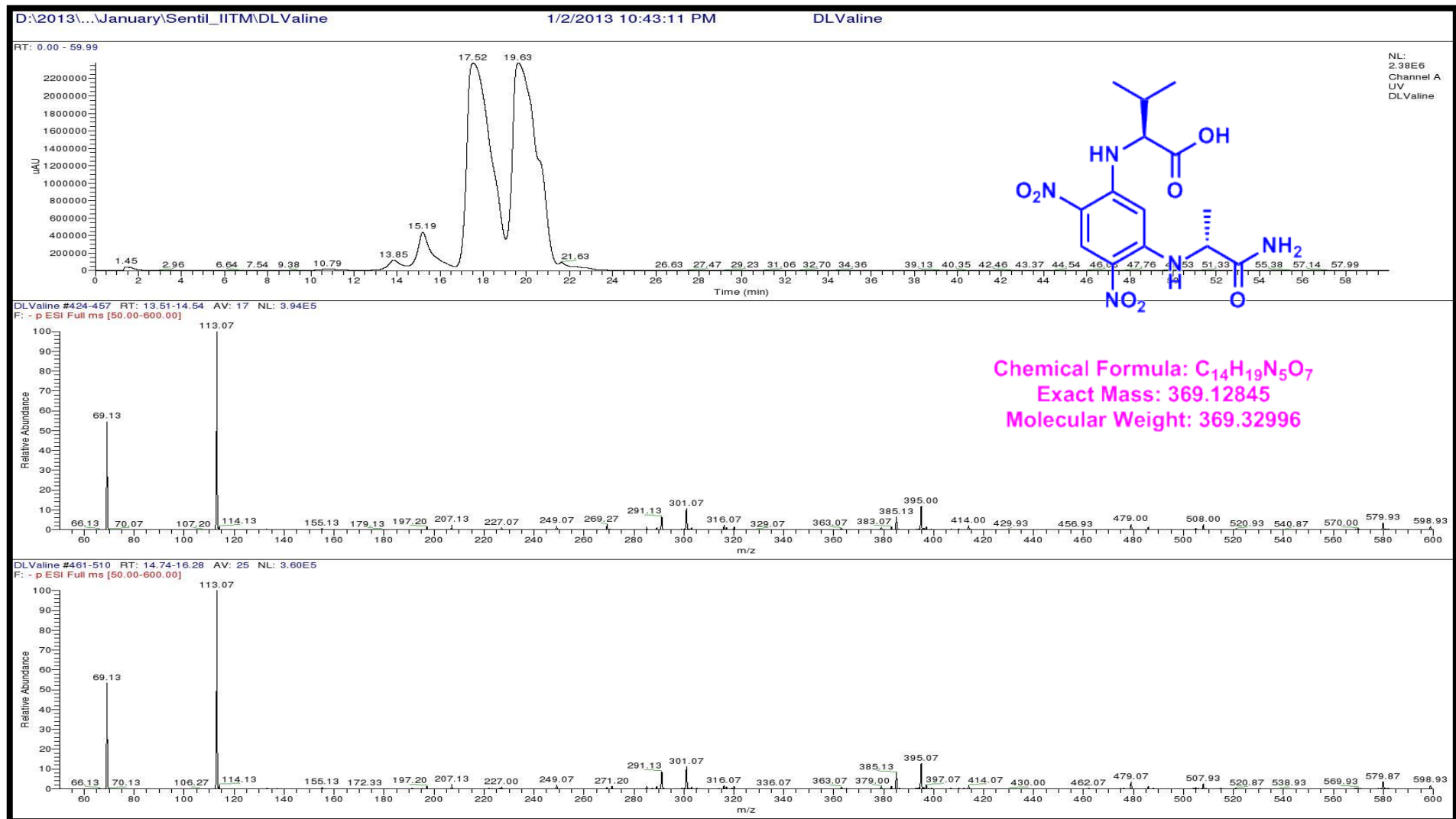


Figure S141. LCMS analysis of Standard L-FDAA-D/L-Valine (Negative mode)

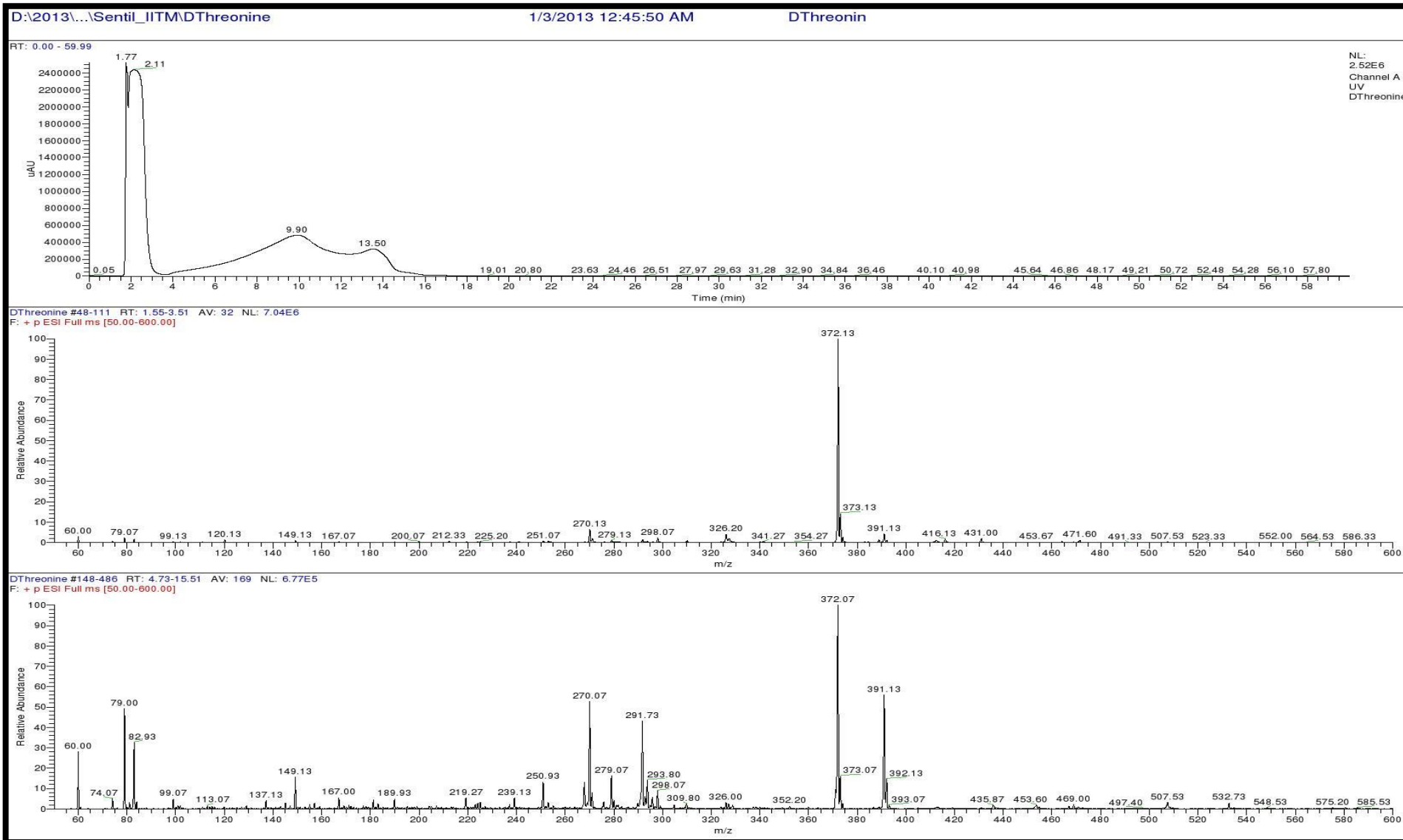


Figure 142. LCMS analysis of Standard L-FDAA-D-Threonine (Positive mode)

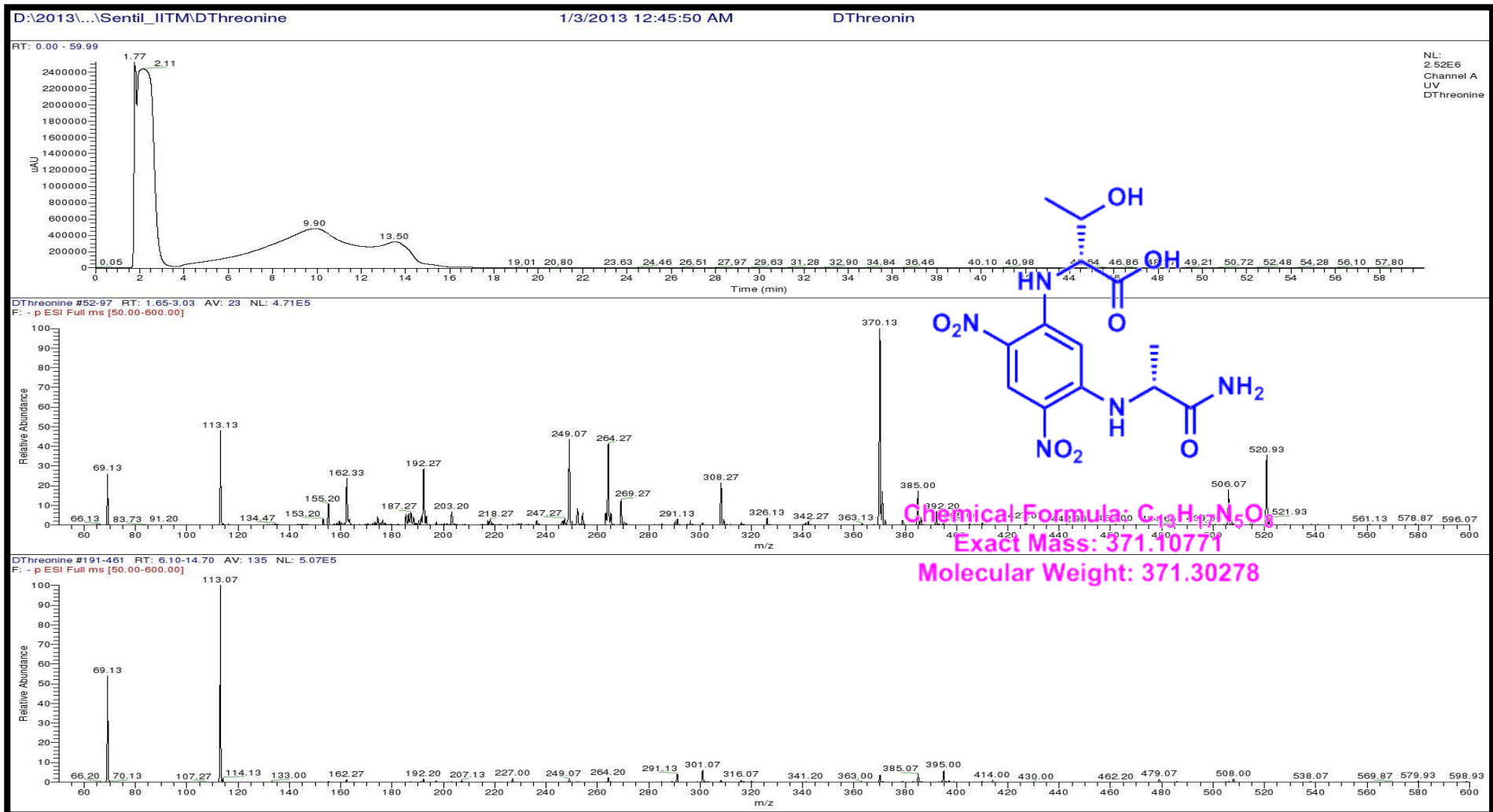


Figure S143. LCMS analysis of Standard L-FDAA-D-Threonine (Negative mode)

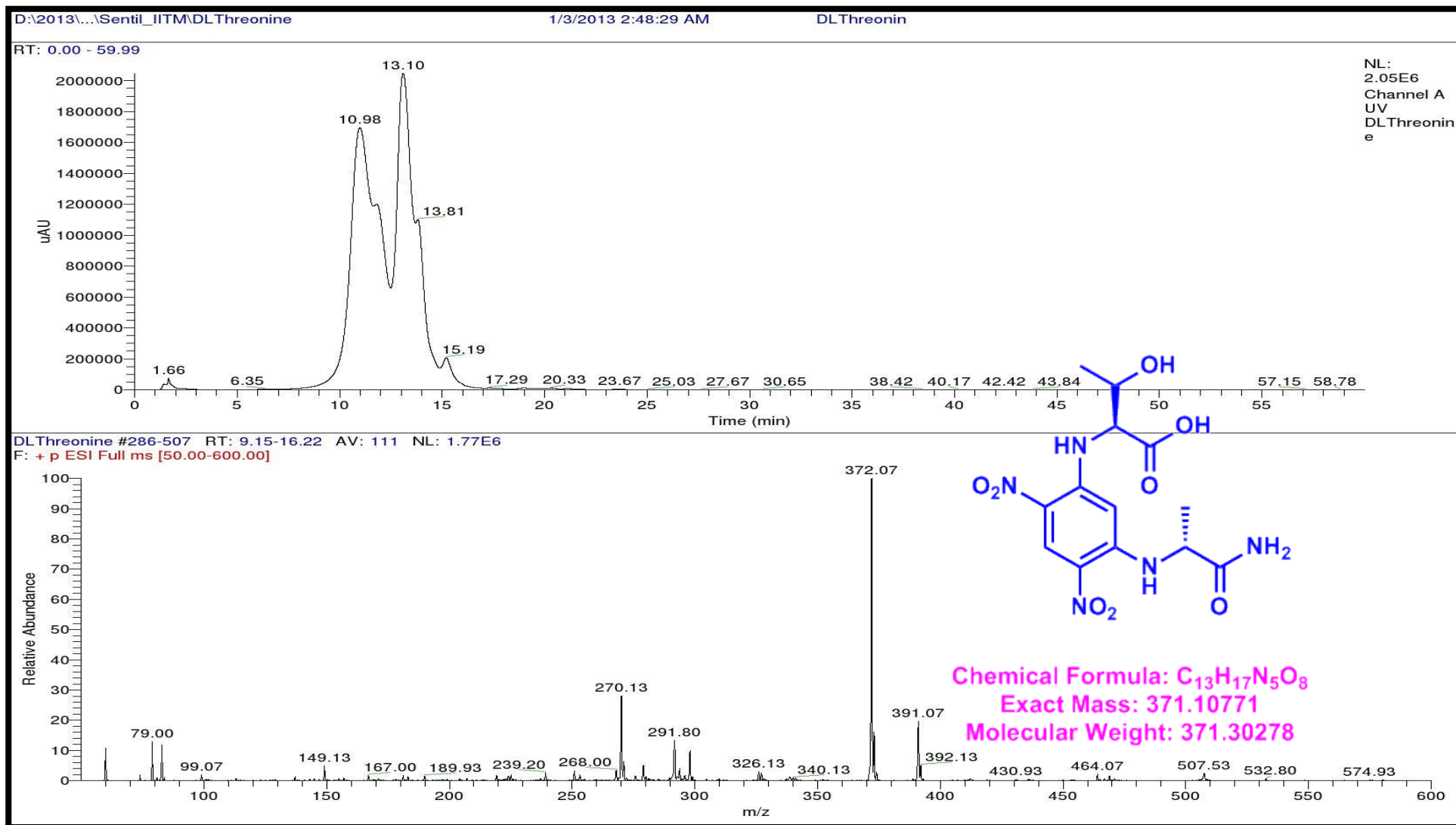


Figure S144. LCMS analysis of Standard L-FDAA-D/L Threonine (Positive mode)

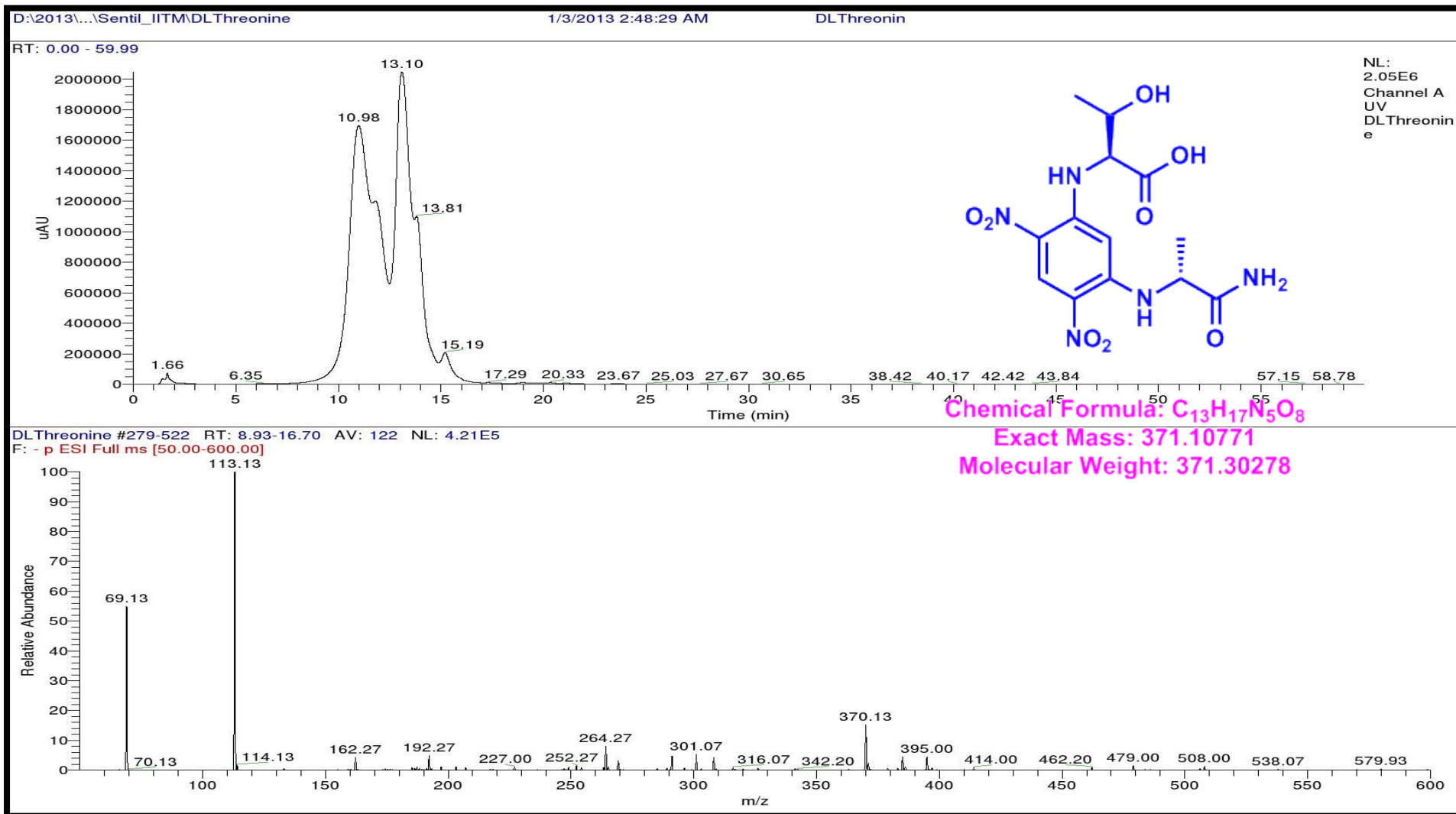


Figure 145. LCMS analysis of Standard L-FDAA-D/L Threonine (Negative mode)

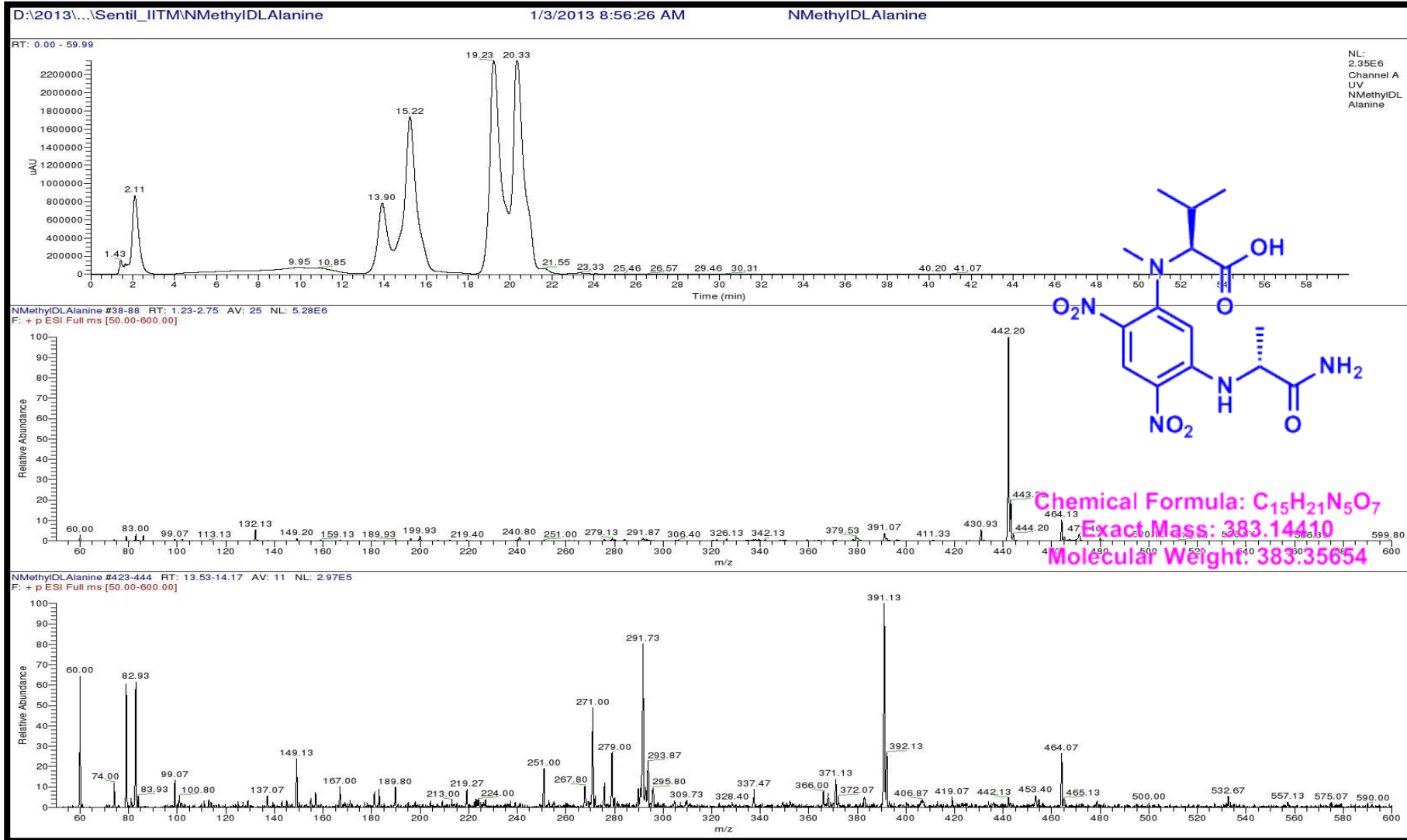


Figure S146. LCMS analysis of Standard L-FDAA-D/L N-Methyl valine (Positive mode)

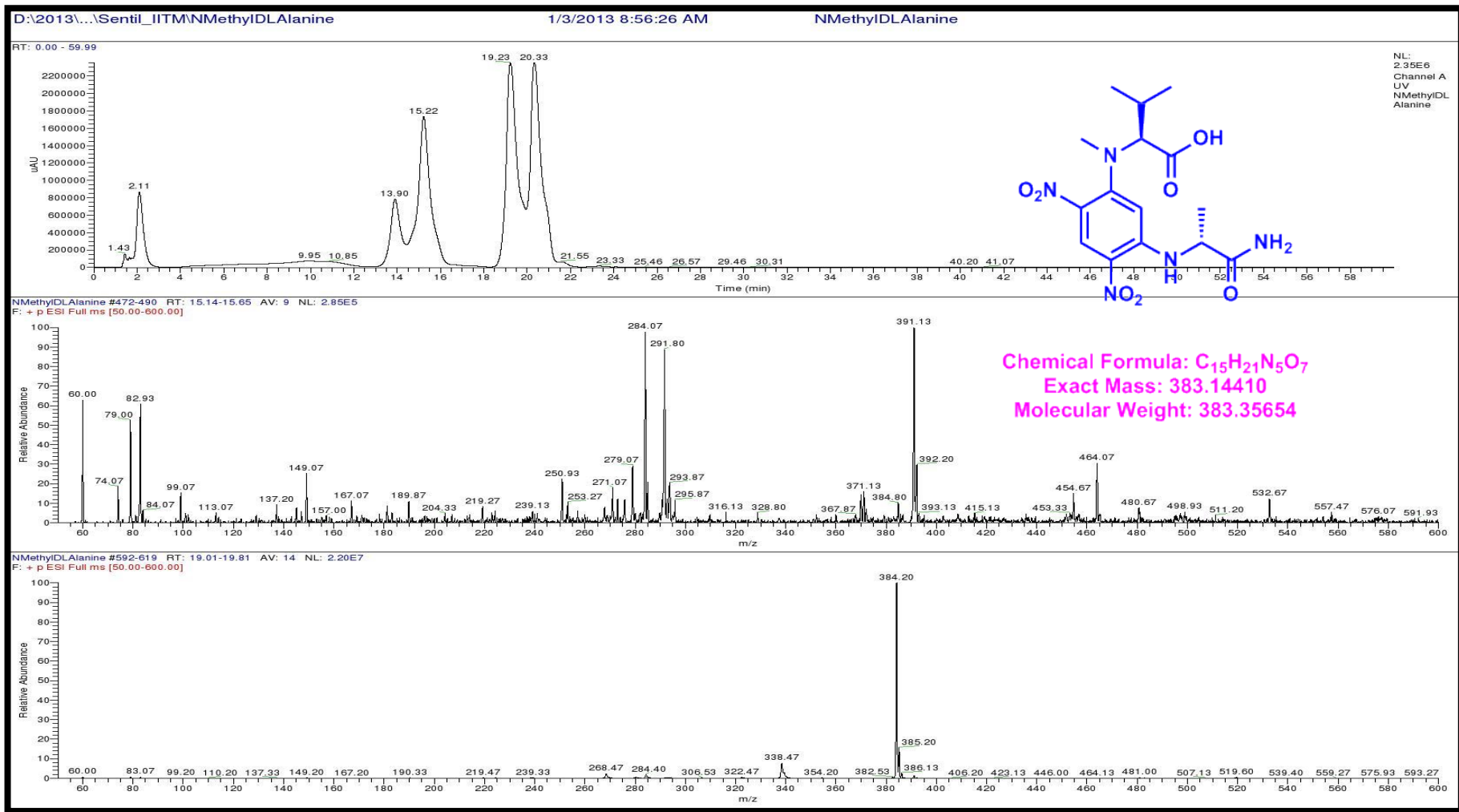


Figure S147. LCMS analysis of Standard L-FDAA-D/L N-Methyl Valine (Positive mode)

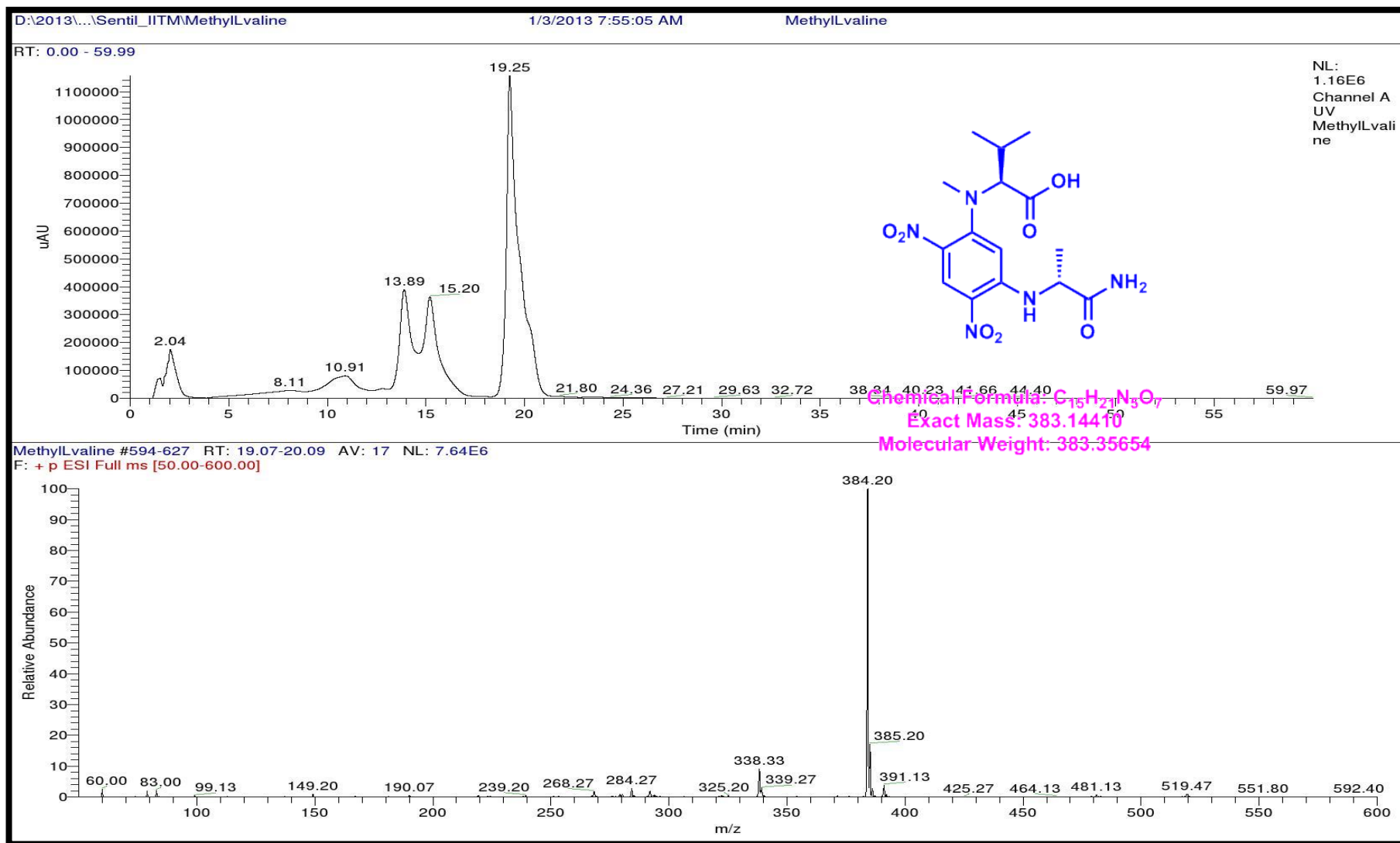


Figure S148. LCMS analysis of Standard L-FDAA-L N-Methyl valine (Positive mode)

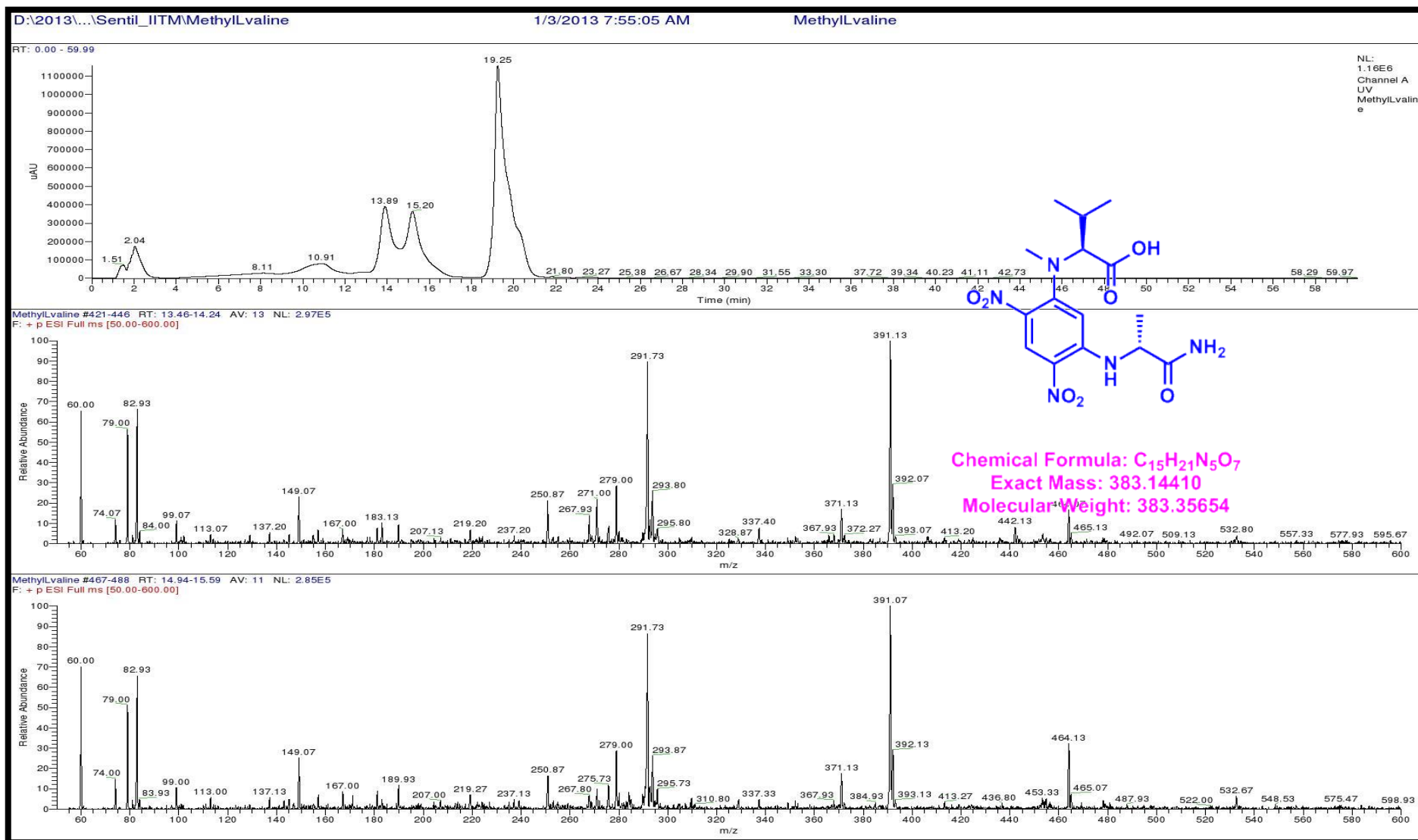


Figure S149. LCMS analysis of Standard L-FDAA-L- N-Methyl valine (Positive mode)

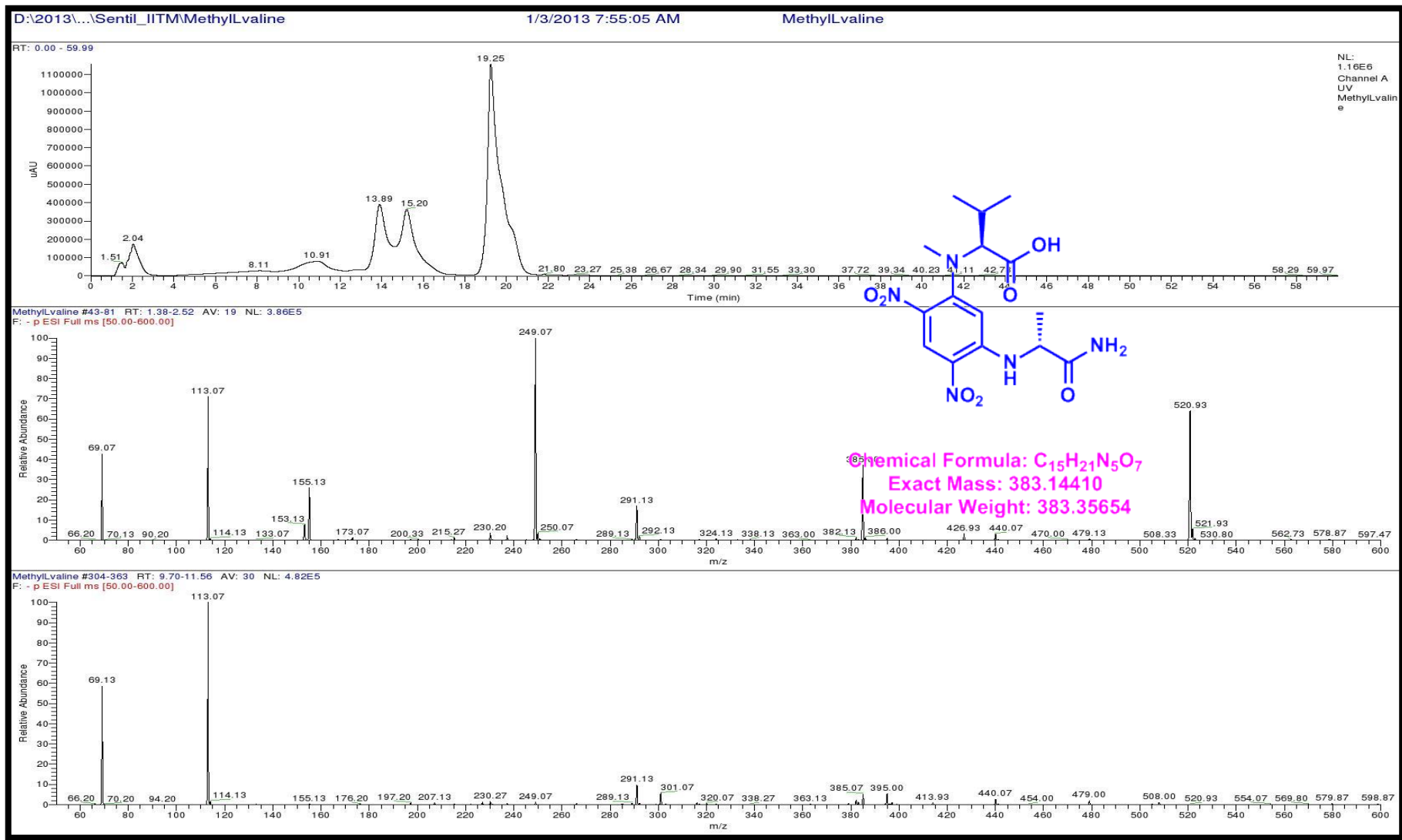


Figure S150. LCMS analysis of Standard L-FDAA-L N-Methyl Valine (Positive mode)

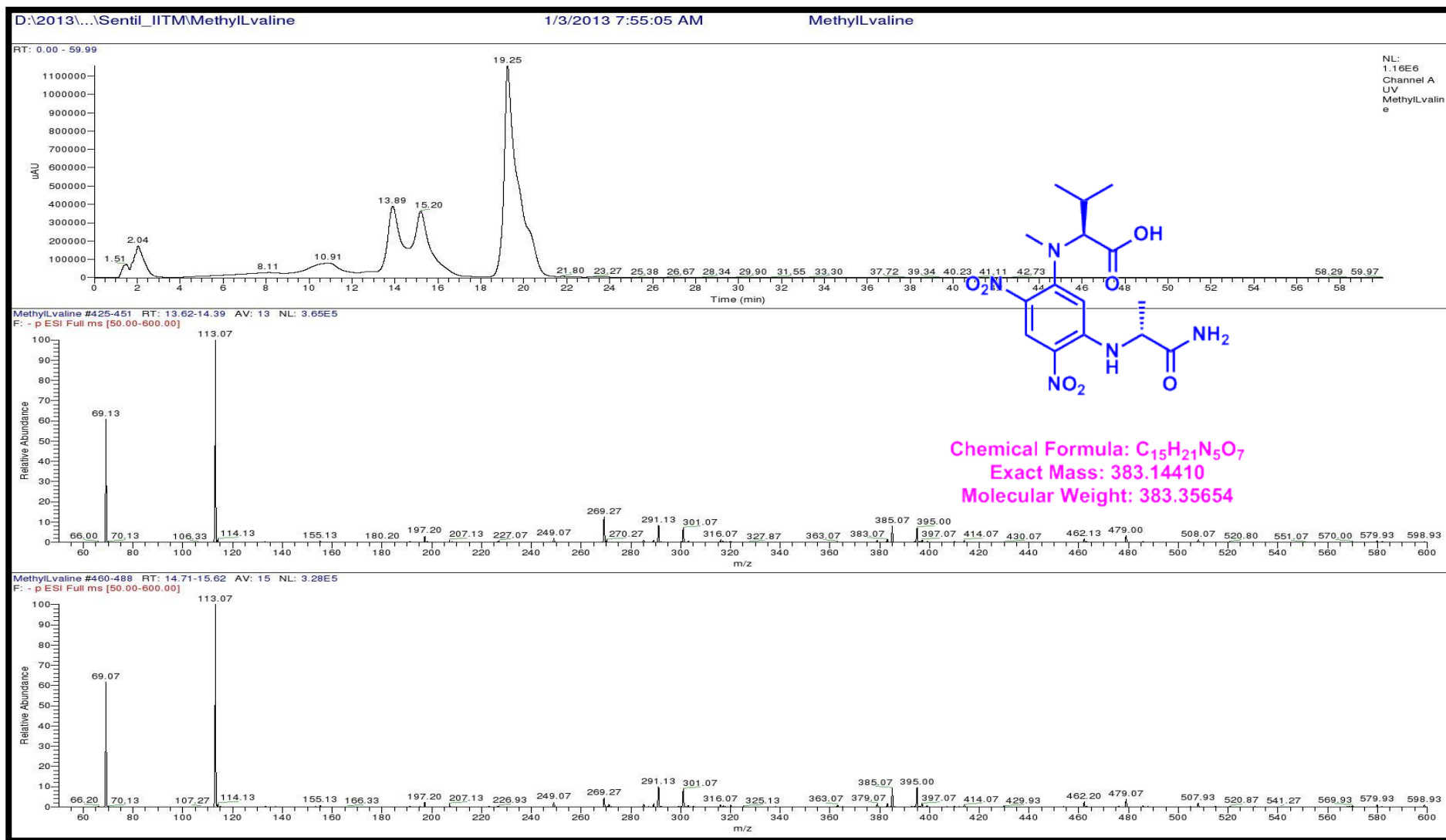


Figure S151. LCMS analysis of Standard L-FDAA-L N-Methyl Valine (Positive mode)

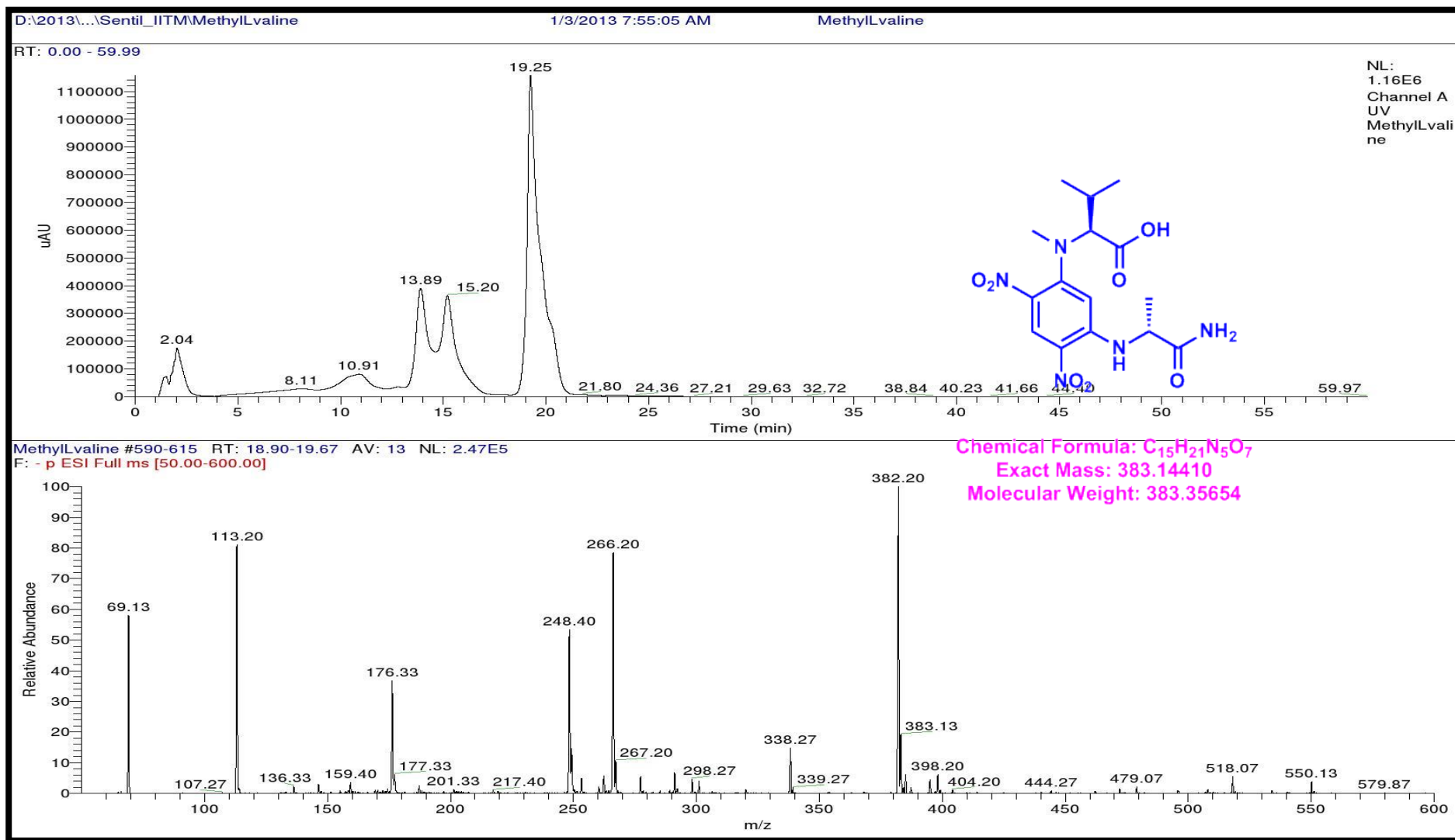


Figure S152. LCMS analysis of Standard L-FDAA-L N-Methyl Valine (Negative mode)

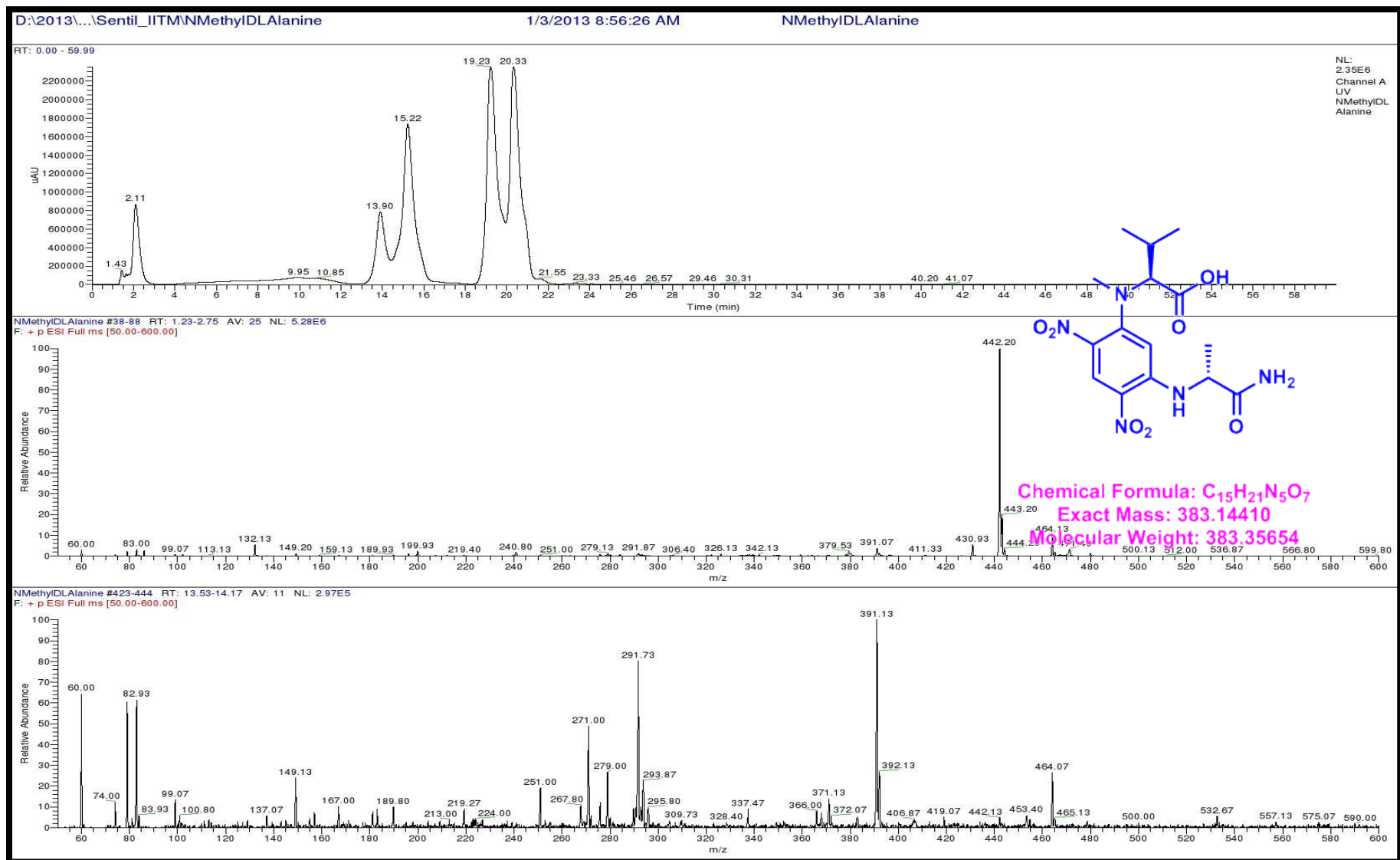


Figure S153. LCMS analysis of Standard L-FDAA-D/L N-Methyl Valine (Positive mode)

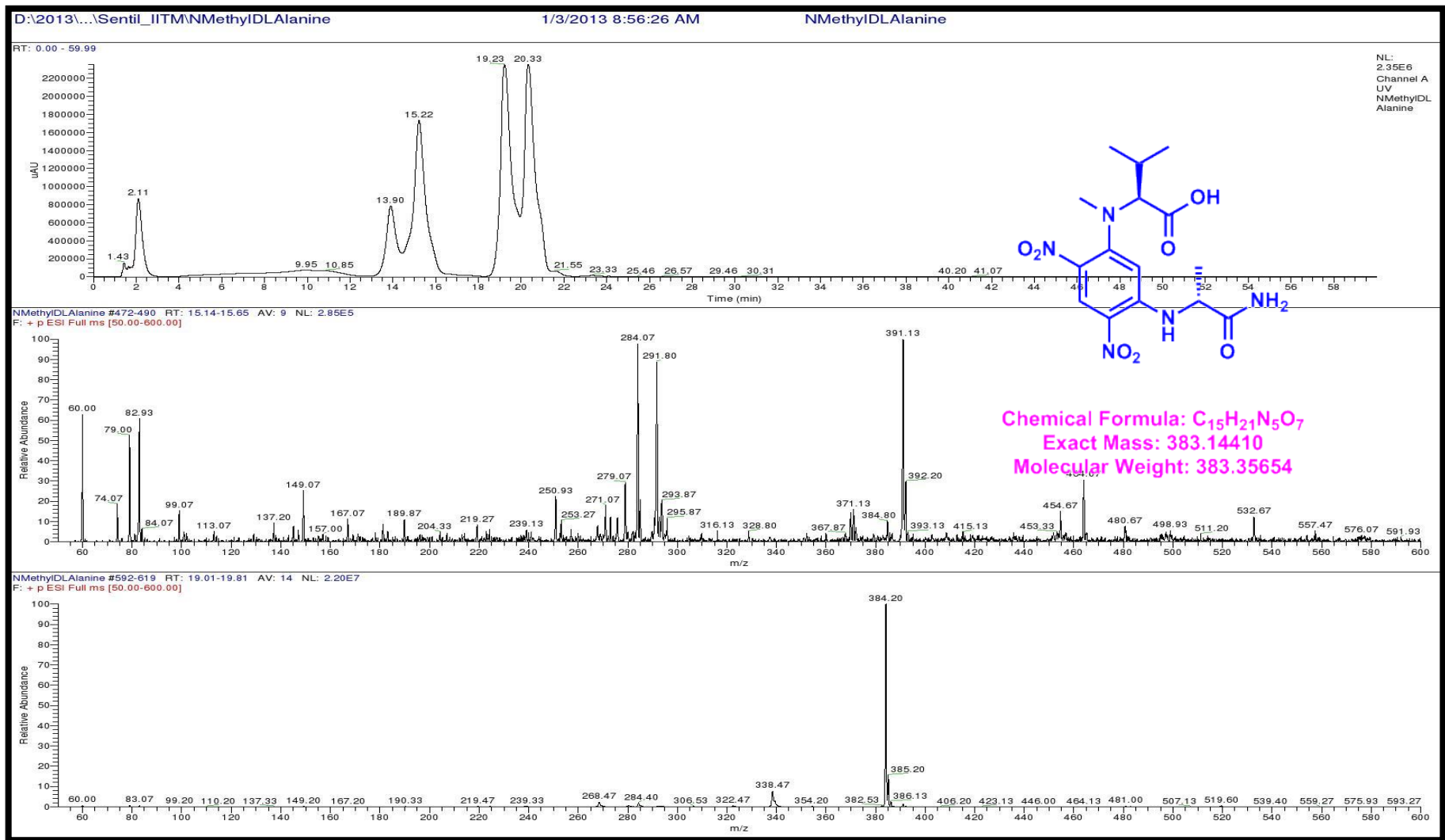


Figure S154. LCMS analysis of Standard L-FDAA-L N-Methyl Valine (Positive mode)

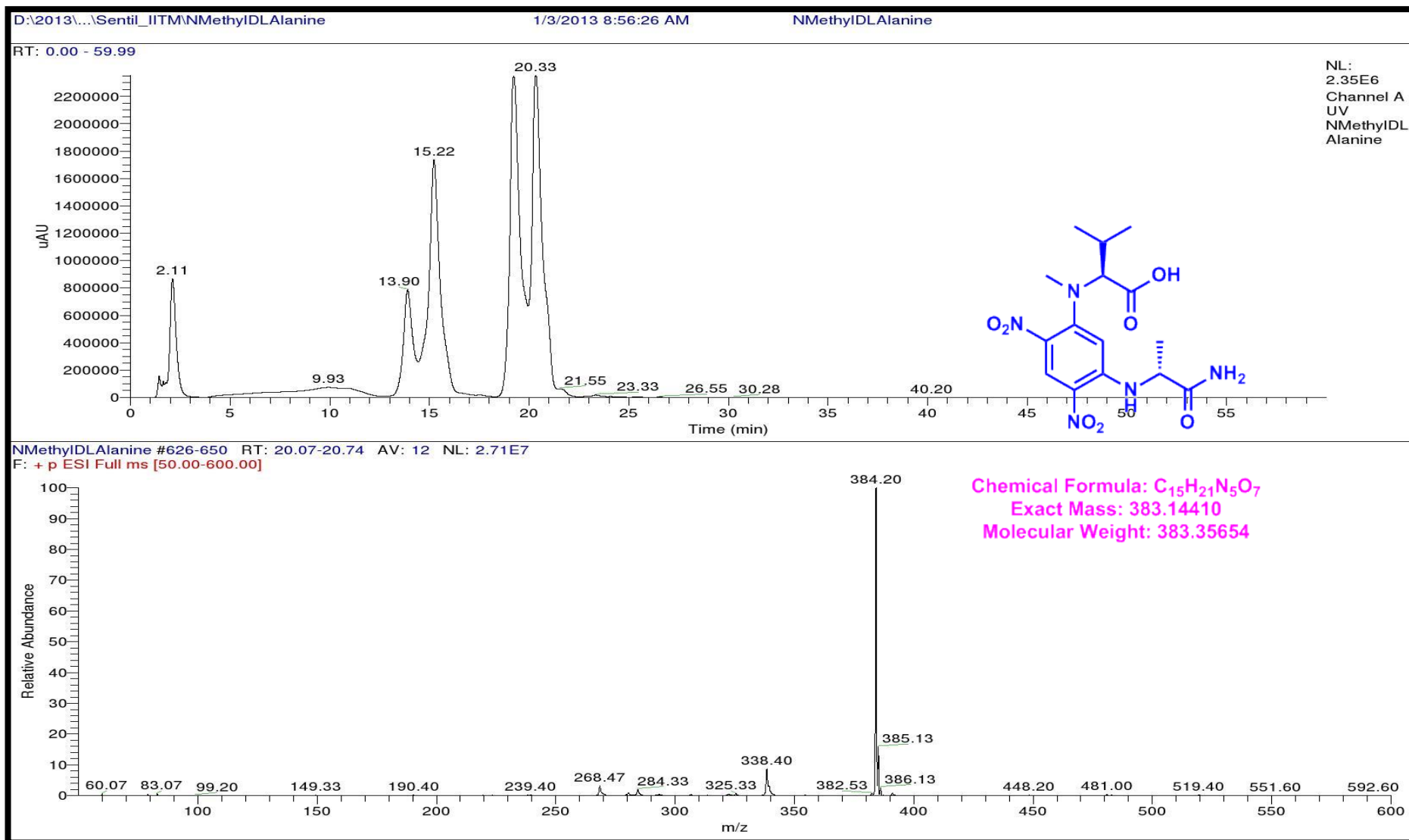


Figure S155. LCMS analysis of Standard L-FDAA-D/L N-Methyl Valine (Positive mode)

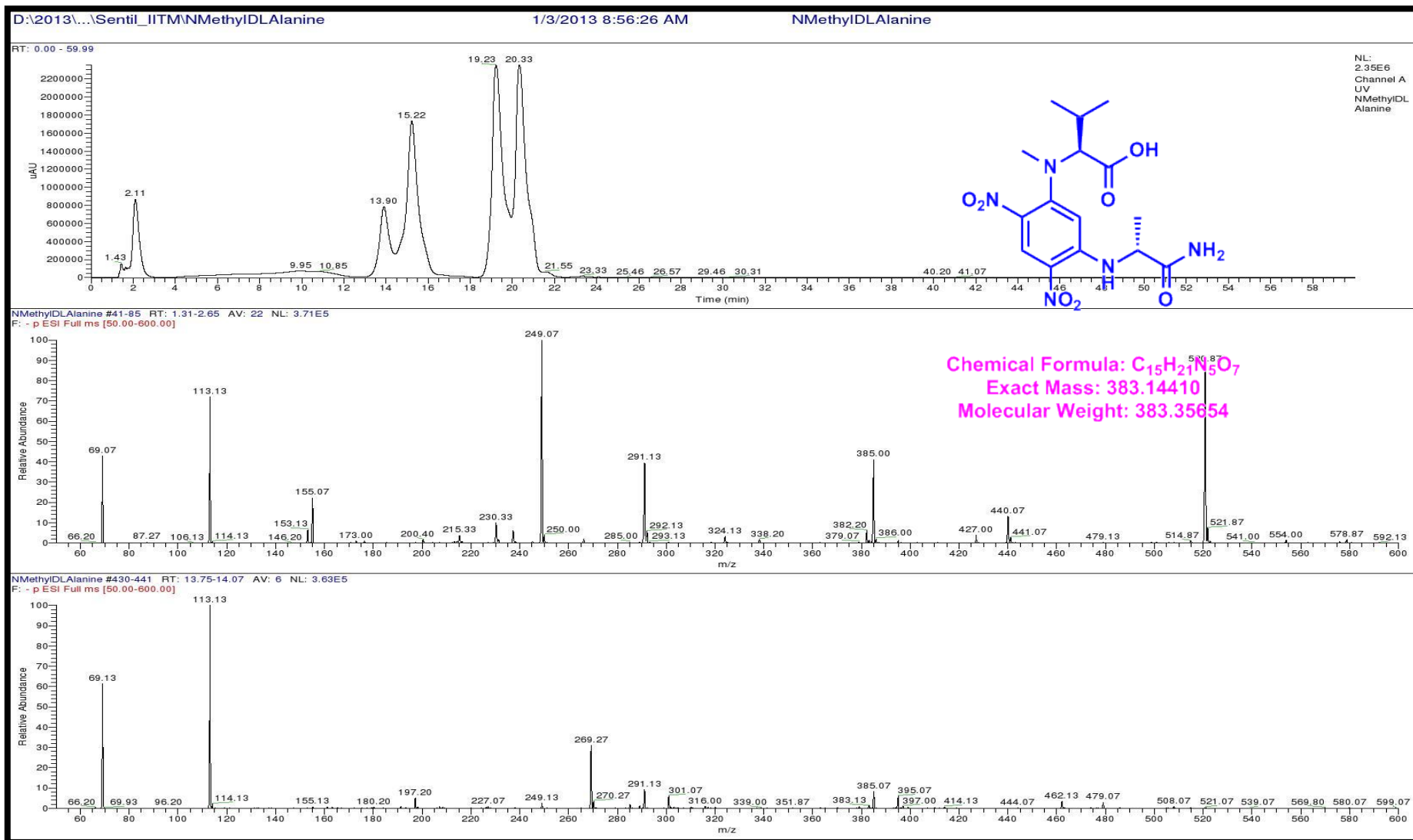


Figure S156. LCMS analysis of Standard L-FDAA-D/L N-Methyl Valine (Negative mode)

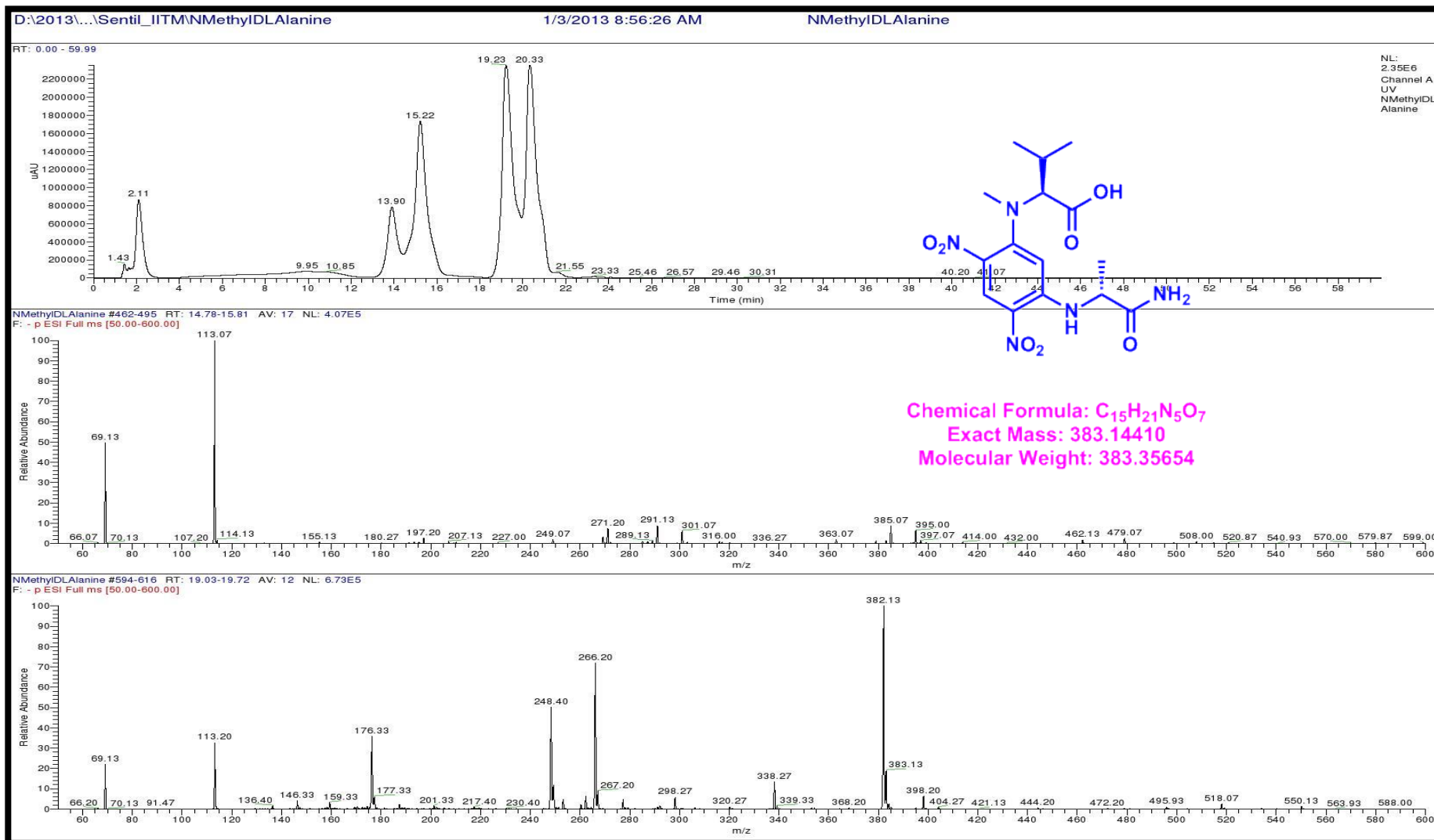


Figure S157. LCMS analysis of Standard L-FDAA-D/L N-Methyl Valine (Negative mode)

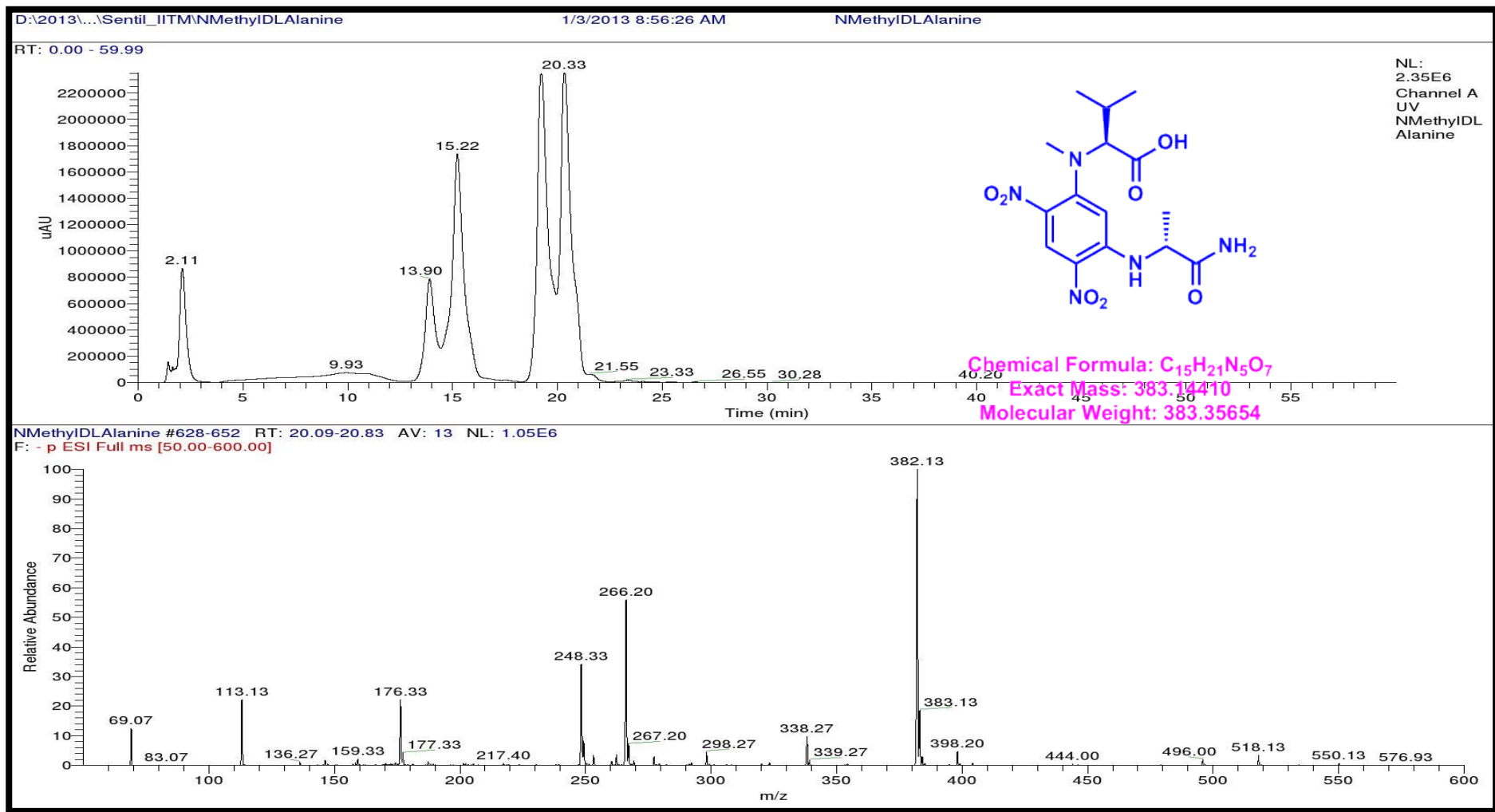


Figure S158. LCMS analysis of Standard L-FDAA-D/L N-Methyl Valine (Negative mode)

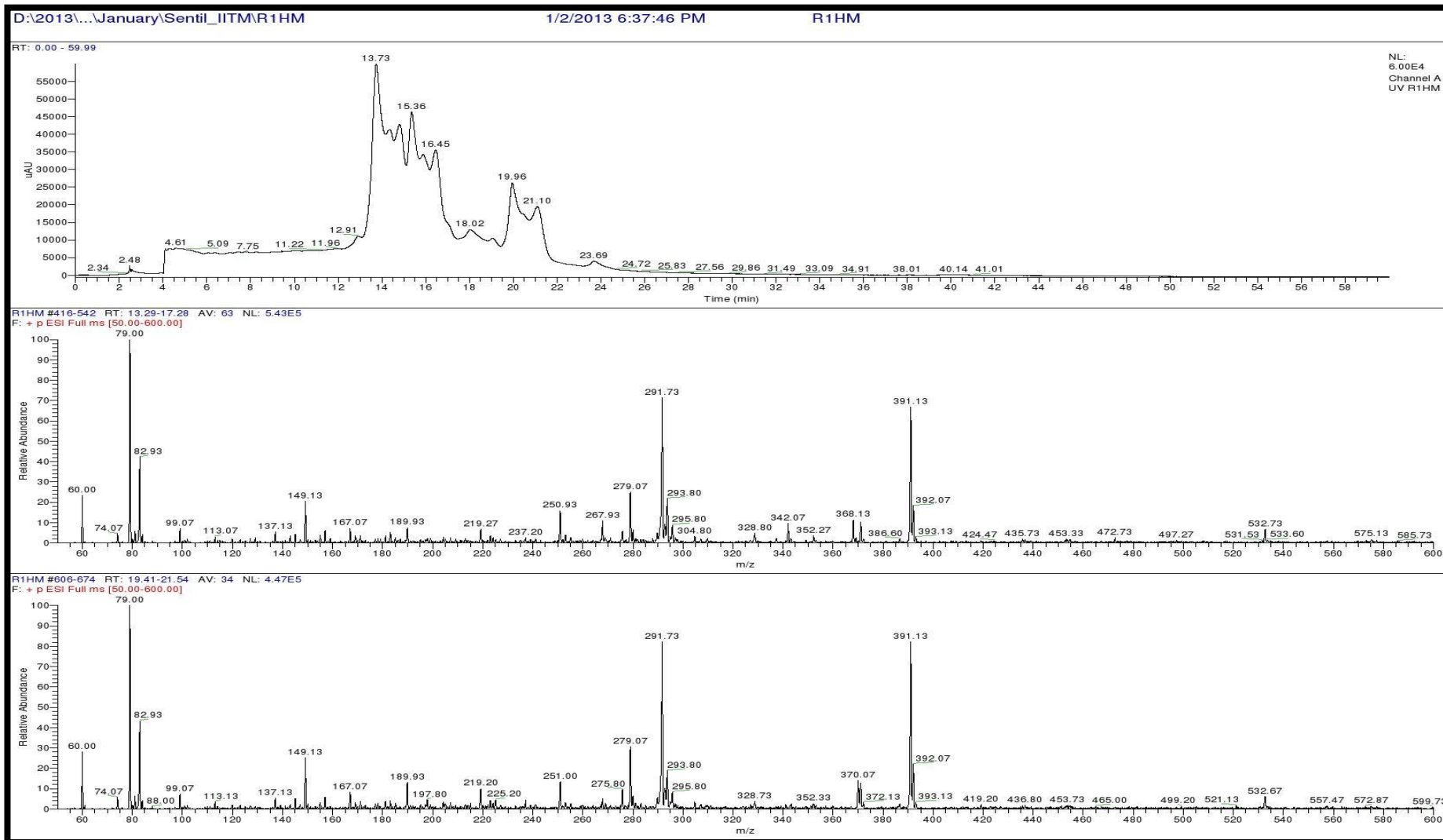


Figure S159. LCMS analysis of L-FDAA derivatives of Transitmycin (R1) (Positive mode)

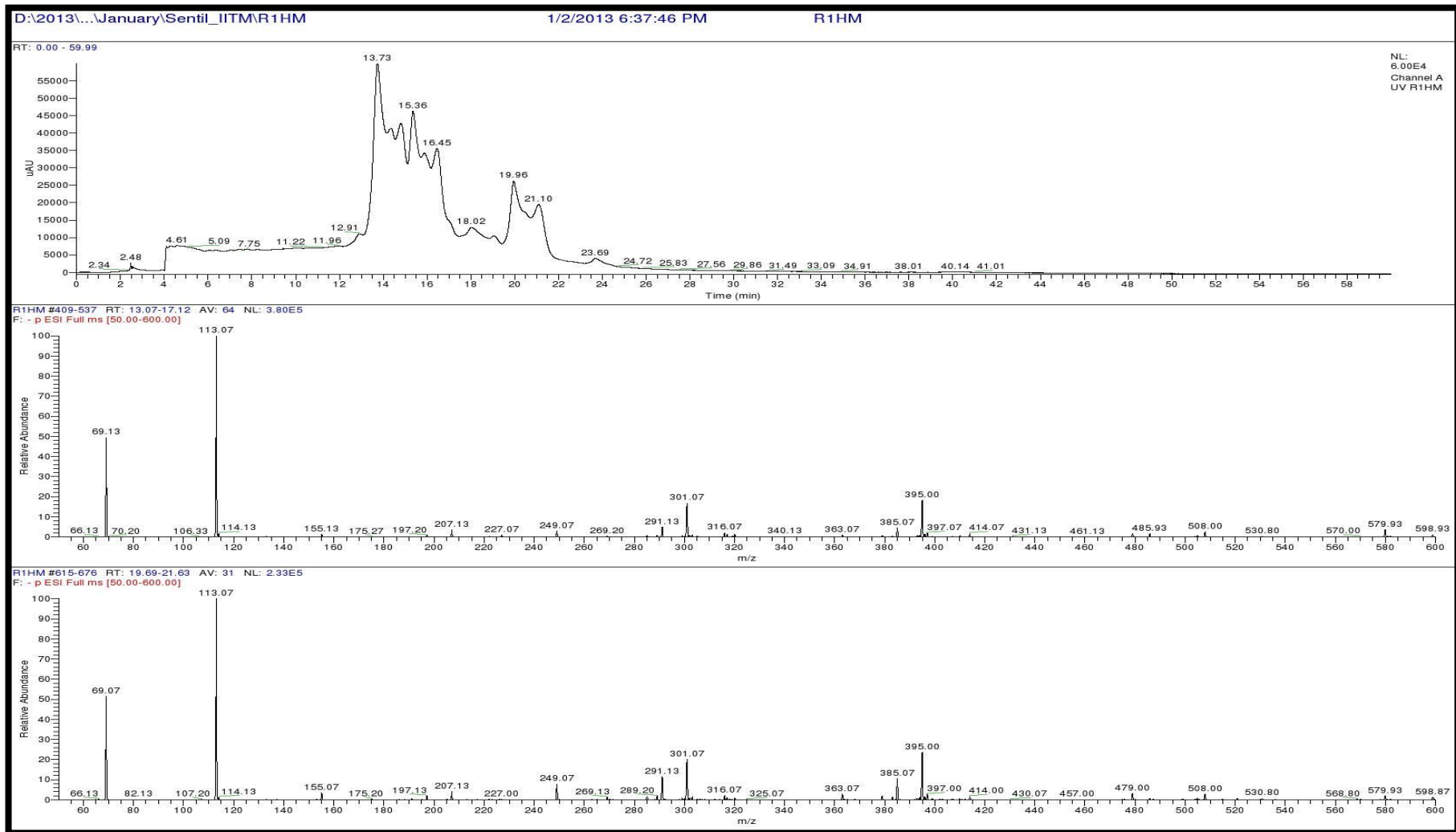


Figure S160. LCMS analysis of L-FDAA derivatives of R1 (Negative mode)

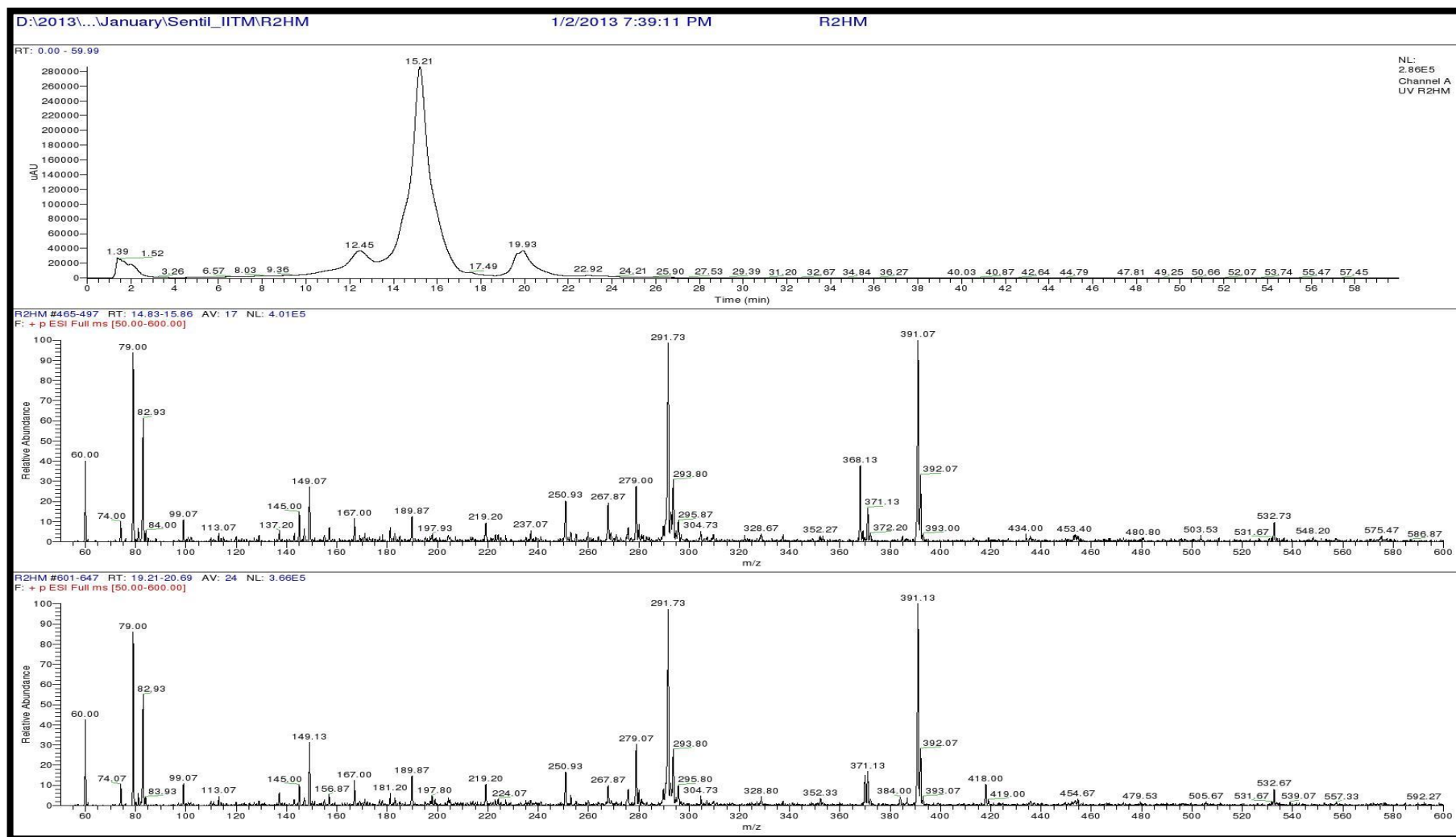


Figure S161. LCMS analysis of L-FDAA derivatives of R3 (Positive mode)

Table S9a. Analysis of L-FDAA derivates of acid hydrolysate of Transitmycin R2 by HPLCMS

Amino acids	LCMS retention times Marfey's derivatives of standard amino acids		HPLC retention time Marfey derivatives of acid hydrolysate of Transitmycin R1	[M+H] ⁺ m/z	[M-H] ⁻ m/z	Assignment
	D	L		Positive mode	Negative mode	
Threonine	9.90	13.50	13.73	372.13	370.13	L
Proline	15.16	14.31	14.23 & 15.36	366.13	363.07	D&L
Valine	19.65	17.65	18.02	370.13	368.07	L
N-methyl valine	20.33	19.25	19.96	384.20	382.20	L

Table S9b. Analysis of L-FDAA derivates of acid hydrolysate of R3 by HPLCMS

Amino acids	LCMS retention times Marfey's derivatives of standard amino acids		HPLC retention time Marfey derivatives of acid hydrolysate of R3 minutes	[M+H] ⁺ m/z	[M-H] ⁻ m/z	Assignment
	D minutes	L minutes		Positive mode	Negative mode	
Threonine	9.90	13.50	12.45	372.13	370.13	L
Proline	15.16	14.31	14.25	366.13	363.07	D & L
Valine	19.65	17.65	17.49	370.13	368.07	L
N-methyl valine	20.33	19.25	19.93	384.20	382.20	L

Table S10. Physico-chemical properties of R2

Colour: Red colour amorphous powder

Yield: 100 mg, 10%

m.p: 250-252°C

TLC: R_f = 0.6 (Ethyl acetate/Methanol, 95:5)

[α]_D²⁵: -24° (c = 0.2, MeOH)

Solubility: Soluble in Chloroform, Dichloromethane, Ethyl acetate, Methanol, Ethanol, Acetonitrile, DMSO, water. Insoluble in Hexane.

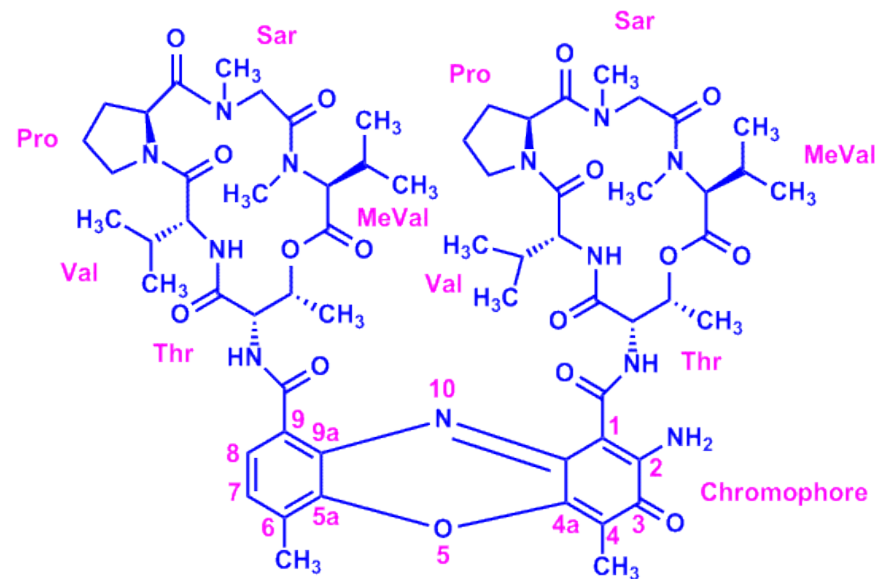
UV: (MeOH) λ_{max}, (log ε) 205, (1.25), 240 (0.63), 425 (0.39), 442 (0.42) nm

CD: [MeOH, [nm], (mdeg)]: λ_{max}, (Δε) 195 (+8.8), 210 (-22.0), 240 (+4.3) nm

IR: (KBr), ν_{max} = 3436, 2961, 2924, 2853, 1744, 1650, 1565, 1415, 1204, 1140, 1045, 1019 cm⁻¹

HRESI-MS: m/z(pos.ions) 650.3413 [M+2H]²⁺, 1277.8245 [M + Na]⁺ 1293.8735 [M + K]⁺

C₆₂H₈₆N₁₂O₁₆Na [M + Na]⁺ calc. 1277.61824, found. 1277.8245



MALDI-TOF-MS: m/z (pos.ions) 1279.94914 $[M + Na+2H]^+$ m/z (neg.ions) 1255.38052 $[M-H]^-$ $[M + Na+2H]^+$ calc. 1279.63424, found. 1279.94914

LCESI-MS: m/z (pos.ions) 1277.8245 $[M + Na]^+$ $C_{62}H_{86}N_{12}O_{16}Na$ $[M + Na]^+$ calc. 1277.61824, found. 1277.8245

EI-MS: (70 ev) m/z (pos.ions): 739.9827, 616.9573, 547.2778, 434.2708, 391.5160, 200.1560, 146.7755, 11.2256

CHN: Anal. calcd for $C_{62}H_{86}N_{12}O_{16}$: C, 59.32; H, 6.90; N, 13.39.
Found: C, 61.05; H, 7.25; N, 11.32.

Table S11. Physico-chemical properties of R3

Colour: Orange colour amorphous powder (50 mg)

Yield: 50 mg, 5%

m.p: 220-222°C

R_f: 0.3 (Ethyl acetate-Methanol 95:5)

Solubility: Soluble in Chloroform, Dichloromethane, Ethyl acetate, Methanol, Ethanol, Acetonitrile, DMSO, water. Insoluble in Hexane

[α]_D²⁵: -27 ° (c = 0.2, MeOH)

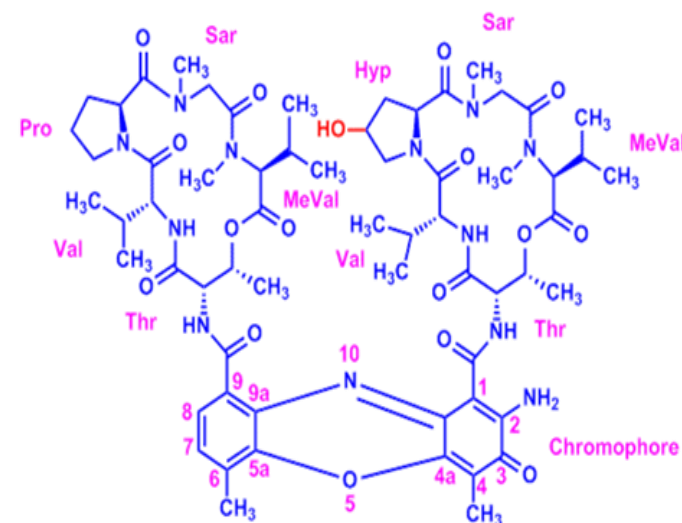
UV (MeOH) λ_{max} (log ε) 206 (1.90), 240 (0.69), 424 (0.191), 442.2 (0.19) nm

CD: [MeOH, [nm], (mdeg)] λ_{max} (Δε) 195 (+24.0), 210 (-21.5), 241 (+1.7)

IR:(KBr), ν_{max} 3415, 2957, 2924, 2853, 1745, 1642, 1583, 1464, 1384, 1193, 1093, 1078 cm⁻¹.

HRESI-MS: m/z (positions) 663.4698 [M+2H]²⁺, 1271.7159 [M + H]⁺

C₆₂H₈₆N₁₂O₁₇ [M + H]⁺ calc. 1277.6312, found. 1271.7159



MALDI-TOF-MS: m/z (pos.ions) 1292.24097 $[M + Na]^+$ m/z (neg.ions) 1268.48582 $[M-H]^-$

$C_{62}H_{86}N_{12}O_{17}Na$ $[M + Na]^+$ calc. 1293.61316 found. 1292.24097

LCESI-MS: m/z (pos.ions) 1277.6149 $[M-OH+Na+H]^+$ $C_{62}H_{85}N_{12}O_{16}$ $[M - OH+Na+H]^+$ calc. 1277.61416, found. 1277.6149

EI-MS: (70 eV) m/z (pos.ions): 98, 956.7713, 900, 9470, 859.8045, 771.227, 708.0386, 562.4686,
515.1946, 446.3967, 351.8868, 1\230.2476, 94.2476

CHN: Anal. calcd for $C_{62}H_{86}N_{12}O_{17}$: C, 58.57; H, 6.82; N, 13.22.

Found: C, 58.75; H, 7.13; N, 11.59.

Supplementary Table 12: Drug resistant profile of the clinical isolates of *Mycobacterium tuberculosis* used to determine the anti TB activity of Transimycin. R: Resistant; S: Susceptible. The drug resistant profile was determined by LJ based Proportion sensitivity method.

Culture No.	Isoniazid	Rifampicin	Kanamycin	Ofloxacin
1-49	S	S	S	S
50	R	S	S	S
51	R	S	S	S
52	S	R	S	S
53	R	S	S	S
54	S	S	S	R
55	R	S	S	S
56	R	S	S	R
57	R	S	S	S
58	R	S	S	S
59	R	S	R	R
60	R	R	R	S
61	S	S	R	S
62	R	S	S	R
63	R	S	S	R
64	R	S	R	R
65	R	S	S	S

66	R	S	S	R
67	R	S	S	R
68	R	S	R	R
69	S	S	S	R
70	S	S	S	R
71	R	S	S	S
72	R	S	S	R
73	R	R	S	S
74	R	S	S	S
75	R	R	S	S
76	R	R	R	S
77	R	R	S	R
78	R	R	S	R
79	R	S	S	S
80	R	S	S	R
81	R	S	S	S
82	R	R	S	S
83	R	R	S	S
84	R	R	S	R
85	R	R	S	S
86	R	R	S	R

87	S	R	S	R
88	R	R	S	S
89	R	R	S	S
90	S	R	S	R
91	S	S	S	R
92	R	R	S	S
93	R	R	S	R
94	S	R	S	R
95	R	S	S	R
96	R	R	S	S
97	R	S	S	R

S - Table 13. Anti-HIV activity of Transitmycin on various HIV-1 subtypes

HIV-1 subtype	IC ₅₀ values at various concentration of Transitmycin (in µg/mL)					EC ₅₀ Value (µM)
	0	0.01	0.1	1	10	
SUB A	4624.7 ± 348.34	2600.31 ± 212.27	1413±84.36	116.00 ± 13.61	133.32 ± 13.33	0.263
SUB B	9123.78 ± 495.29	8419.48 ± 549.73	7470.78 ± 3208.54	4222.52 ± 138.79	1693.95±35.38	2.347
SUB C	11652.5 ± 1339.97	10962.821± 729.96	11005.35±144.9	3435.69 ± 75.80	578.46 ± 65.77	2.167
SUB D	10170.22 ± 1572	10761.7 ± 576.85	7405.783±303.46	1339.49±287.06	306.53± 27.43	0.447
SUB E	3976.34 ± 68.35	3726.96±590.53	2120.49±155.83	970.25 ±38.08	258.84 ± 3.87	0.78
SUB A/C	5871.52 ± 51.10	5562.45±396.06	4654.15 ±262.26	589.52 ± 133.80	154.45 ±30.20	0.685
NEV RES	3325.76 ± 259.01	3636.10 ±743.95	3278.46 ±329.16	627.37 ±69.58	341.00 ±7.88	0.771
AZT RES	3031.83 ± 821.87	3040.03±703.81	2213.102± 48.17	1066.38 ± 17.34	786.32 ±37.46	0.388

Acknowledgements for Characterisation of Transitmycin

The Chairman, NMR Research Centre, IISC, Bangalore

Dr.A.Mohan, Mr.Venkatesan, Department of Chemistry, IIT Madras

Dr.M.S.Moni, Dr.C. Baby, Mr. R. Bhaskar, SAIF IIT Madras for 2D NMR analysis

Prof. T. Pradeep, AnanyaBaksi, DST Unit of Nano science IIT Madras for QTRAP LC/MS/MS

Prof. T. Pradeep, Mr.Kamalesh, Mr. E. Sundaraj, DST Unit of Nano Science IIT Madras for MALDI-TOF

Mrs.Sunita Prakash, Molecular Biophysics Department, IISC Bangalore for ESI-MS/MS, MALDI TOF-MS/MS

Mrs.Santha, Mr.Thankarasu, Department of Chemistry IIT Madras for Q-TOF-ESI-MS

Mr. Sankar, SAIF, IIT Madras for IR, EI-MS

The Head, SAIF CDRI, Luknow for LC-ESI-MS

Mr.Muralidhar, SID IISC Bangalore LC-ESI-MS

Prof.Anju Chanda, Mr. T.Saravanan, Department of Biotech IIT Madras for Optical Rotation measurement

Mrs.S.Srividya, Department of Chemistry, IIT Madras.

Dr. P.M.Sivakumar, Department of Biotechnology, Indian Institute of Technology Madras, Chennai, Tamilnadu , 600036, India

Dr. Veluchamy Prabhawathi Department of Biotechnology, Indian Institute of Technology Madras, Chennai, Tamilnadu, 600036, India

Supplementary References:

1. Xiaoling Wang, Jioji Tabudravu Mostafa Ezzat Rateb, Krystal Joan Annand, Zhiwei Qin, Marcel Jaspars, Zixin Deng, Yi Yband Hai Deng, Identification and characterization of the actinomycin G gene cluster in *Streptomyces iakyrus*, *Mol. BioSyst.*, **9**, 1286—1289. (2013).
2. Rebecca H. Wills, Peter B. O'Connor Structural Characterization of Actinomycin D Using Multiple Ion Isolation and Electron Induced Dissociation *J. Am. Soc. Mass Spectrom.* **25**:186Y19, (2014).
3. Ivana Crnovci c, Siamak Semsary, Joachim Vater and Ullrich Keller, Biosynthetic rivalry of o-aminophenol-carboxylic acids initiates production of hemi-actinomycins in *Streptomyces antibioticus*, *RSC Adv.*, **4**, 5065 (2014).
4. Joachim Vater, Ivana Crnovčić, Siamak Semsary and Ullrich Keller MALDI-TOF mass spectrometry, an efficient technique for in situ detection and characterization of actinomycins, *J. Mass Spectrom.*, **49**, 210–222 (2014).
5. Collisional Activation Decomposition of Actinomycins Using Tandem Mass Spectrometry J. Roboz, E. Nieves and J. F. Holland M. McCamish, C. Smith, *BIOMEDICAL AND ENVIRONMENTAL MASS SPECTROMETRY*, **VOL. 16**, 67-70 (1988).
6. A. B. Mauger, W. A. Thomas, NMR Studies of Actinomycins Varying at the Proline Sites, *ORGANIC MAGNETIC RESONANCE*, **VOL. 17**, NO. 3(1981).
7. Darren Thomas, Michael Morris, Jonathan M. Curtis and Robert K. Boyd, Fragmentation Mechanisms of Protonated Actinomycins and Their Use in Structural Determination of Unknown Analogues, *JOURNAL OF MASS SPECTROMETRY*, **VOL. 30**, 1111-1125 (1995).
8. Jens Bitzer, Martin Streibel, Hans-Jörg Langer, Stephanie Grond, First Y-Type Actinomycins from *Streptomyces* with Divergent Structure-Activity Relationships for Antibacterial and Cytotoxic Properties, *Org. Biomol. Chem.*, **7**, 444–450. (2009).
9. Caixia Chen, Fuhang Song, Qian Wang, Wael M. Abdel-Mageed, Hui Guo, Chengzhang Fu & Weiyuan Hou & Huanqin Dai & Xueting Liu & Na Yang & Feng Xie & Ke Yu & Ruxian Chen & Lixin Zhang, A marine-derived *Streptomyces* sp. MS449 produces high yield of actinomycin X2 and actinomycin D with potent anti-tuberculosis activity, *Appl Microbiol Biotechnol* **95**:919–927, (2012).

10. Shigehiro Kamitori and Fusao Takusagawa' Multiple Binding Modes of Anticancer Drug Actinomycin D: X-ray, Molecular Modeling, and Spectroscopic Studies of d (GAAGCTTC)₂-Actinomycin D Complexes and Its Host DNA, *J. Am. Chem. Soc.*, **116**, 4154-4165, (1994).
11. Jens Bitzer, Victoria Gesheva, and Axel Zeeck, Actinomycins with Altered Threonine Units in the $\hat{\alpha}$ -Peptidolactone, *J. Nat. Prod.*, **69**, 1153-1157, (2006).
12. Xiufang Zhang, Xuewei Ye, Weiyun Chai, Xiao-Yuan Lian, and Zhizhen Zhang, New Metabolites and Bioactive Actinomycins from Marine-Derived *Streptomyces* sp. ZZ338, *Mar. Drugs*, **14**, 181, (2016).
13. Helmut Lackner, Isabel Bahner, Nobuharu Shigematsu, Lewis K. Pannell, and Anthony B. Mauger, Structures of Five Components of the Actinomycin Z Complex from *Streptomyces fradiae*, Two of Which Contain 4-Chlorothreonine, *J. Nat. Prod.*, **63**, 352-356, (2000).
14. F. Conti, P. De Santis Conformation of Actinomycin D Nature, Vol. **227**, 19, (1970).